

The Journal of Refractory Innovations

bulletin

2021



Anniversary Edition

- 12 Circular Economy
in the Refractory Industry
- 16 Reducing the Carbon Footprint
of Raw Material Production
- 106 New Raw Material Source for
Doloma Products in Europe



RHI MAGNESITA



Bulletin

The Journal of Refractory Innovations

2021

| | |
|-------------------------------|---|
| Published by | RHI Magnesita GmbH, Vienna, Austria |
| Chief Editor | Gerald Gelbmann |
| Executive Editors | Thomas Drnek, Christoph Eglsäer, Mateus Vargas Garzon, Thomas Mathew, Felipe Nonaka, Ravikumar Periyasamy, Diane Taylor, Heinz Telser, Karl-Michael Zettl |
| Raw Materials Expert | David Wappel |
| Lingual Proofreader | Clare McFarlane, Janine Pink, Barbara Wrathall-Pohl |
| Proofreaders | Michaela Hall, Janine Pink |
| Project Manager | Michaela Hall |
| Picture Desk | Susanne Steinberger-Steinrisser |
| Design and Typesetting | Universal Druckerei GmbH, Leoben, Austria |
| Contact | Michaela Hall RHI Magnesita GmbH, Technology Center Magnesitstrasse 2 8700 Leoben, Austria |
| E-mail | bulletin@rhimagnesita.com |
| Phone | +43 50213 5300 |
| Website | rhimagnesita.com |

The products, processes, technologies, or tradenames in the Bulletin may be the subject of intellectual property rights held by RHI Magnesita N.V., its affiliates, or other companies. The texts, photographs and graphic design contained in this publication are protected by copyright. Unless indicated otherwise, the related rights of use, especially the rights of reproduction, dissemination, provision and editing, are held exclusively by RHI Magnesita N.V. Usage of this publication shall only be permitted for personal information purposes. Any type of use going beyond that, especially reproduction, editing, other usage or commercial use is subject to explicit prior written approval by RHI Magnesita N.V.

RHI Magnesita Worldwide news

Brazil

New Dead Burned Magnesia (DBM) Rotary Kiln is on the Way to Brumado

Brumado is a key site to support RHI Magnesita's backward integration, producing high-quality DBMs based on extensive magnesite deposits. In 2020, the project to build the largest rotary kiln ever designed for RHI Magnesita was approved. The kiln will be more than 150 m long and will produce annually 170000 tonnes of different DBMs.

The new process will enable the production of four new DBM grades. The kiln will improve the cost-competitiveness of magnesia-based products in the Americas and other regions. Additionally, it will extend the mines' life to more than 120 years and give flexibility to better adapt to the market demands.

Developed in an intensive cooperation between R&D, Technical Excellence and Services, Product Management, and Operations, with lab, pilot and industrial trials as well as a trial run in Breitenau (Austria) for which RHI Magnesita shipped 5000 tonnes from Brazil to Europe, the project is running at full speed.

The predicted startup of the new kiln is Q2 2022, despite a tight schedule due to COVID-19 restrictions. The current challenge only reinforces the importance of this key investment.

Russia

RHI Magnesita and AO Seversky Pipe Plant— A Partnership that Adds Value to the Industry

RHI Magnesita and AO Seversky Pipe Plant (STZ) have been developing the EAF lining design for more than 12 years. In cooperation with one of the leading engineering companies of the Russian Federation, specializing in design and manufacture of metallurgical equipment, STZ performs the modification of gas-oxygen modules. For this it is extremely important that refractory materials and lining maintenance schedules achieve the planned lifetime with the implemented equipment changes.

The first stage, during which basic activities such as optimising the lining design, developing a maintenance schedule, and determining the slag practice, lasted from 2008 to 2011. By the end of this period the lifetime increased from 250 to 1400 heats and the maintenance costs could be reduced almost by half. By 2019, the lifetime could be increased to 1800 heats. According to the latest results, the lifetime reached a record 2502 heats, which makes innovative measures for EAF design and cost reduction of maintenance materials possible.

Achieving a record EAF lining lifetime for the Ural region indirectly influences the increase of environmental friendliness and resource savings in the metallurgical industry as a whole.

The partnership between RHI Magnesita and STZ is mutually beneficial as it is optimising refractory operation as well as reducing the cost of manufactured products. From a scientific perspective, the cooperation achieved one of the highest technical and economic indicators worldwide.

RHI Magnesita Worldwide news (continued)

Brazil

Brazilian Chamottes Produced by RHI Magnesita Approved for Use in the Americas and Europe

One main strategy of RHI Magnesita is to be independent of purchased raw materials. In basic products, RHI Magnesita is strongly backward integrated.

For alumina-based materials, there is still some work to be done. Therefore, RHI Magnesita exploits alumina-based raw material deposits such as refractory clays near Contagem (kaolinitic clay) and in Uberaba (kaolinitic and gibbsite clay), as well as rotary kiln operations in both plants. Furthermore, the production of Chamotte Rosa (45% Al_2O_3) and synthetic bauxite (80–85% Al_2O_3) has long been established.

In August 2020, a new chamotte grade was developed by R&D Americas (CM60 with 60–65% Al_2O_3). The grade was validated in industrial trials, completes the product portfolio, but was only validated for Brazil at first. With further trials from September to December, including a major trial run in Tlalneplanta (Mexico), the new chamotte grades were approved for use in other regions as well. Thereby, the current purchased raw materials have been replaced by the Chamotte Rosa and CM60.

A full characterisation of the bricks showed no major differences of the relevant properties, approving the use in Europe and Mexico. This validation is an important step to ensure the cost competitiveness of RHI Magnesita's products and guarantee the supply of this strategic raw material independent from the market situation.

Brazil

Magnesia-Based Injection Lance Successfully Implemented

A magnesia lance was approved by one of our customers in Brazil. Not only does the lance blow nitrogen into the steel but it can also be used for emergency situations. The performance was doubled, obtaining 4 heats (80 minutes) instead of 2 heats (40 minutes) with the alumina lance. This was achieved due to a higher slag corrosion resistance of the magnesia lance compared to the alumina one. A major concern, which was not observed, was the potentially poor thermal shock resistance.

In addition, this customer has a special product portfolio and produces steels with strong restrictions on alumina inclusions. Based on these results, RHI Magnesita was asked to develop other magnesia precast shapes, ladle covers, argon injection lances, and impact pads. Furthermore, trials with other customers that operate CAS-OBs are planned and will be rolled out soon.

Worldwide

RHI Magnesita Wins Microsoft Intelligent Manufacturing Award in the Category 'Add Value'

RHI Magnesita is one of the winners of the Microsoft Intelligent Manufacturing Award 2020. With this award, Microsoft and Roland Berger honour leading industrial pioneers who drive the change towards Industry 4.0 with innovative ideas and creative approaches. Last autumn, 60 industrial companies applied for the award.

RHI Magnesita impressed the judges with Automated Process Optimization (APO). In its statement of reasons, the jury highlighted the enormous savings potential and the significant increase in efficiency in what has been proven to be a complicated production environment.

"With APO we have created an innovative solution. Our customers benefit from reduced maintenance times and increased safety. Congratulations to the creative minds in our company and the APO team that brought this idea to life. This is how we are taking refractories to the 21st century and beyond," said Stefan Borgas, CEO of RHI Magnesita.

Europe

Rapid Market Recovery: RHI Magnesita Doubles Market Share by Winning Largest Single Tender in Europe

RHI Magnesita is pleased to announce the next European success story: ArcelorMittal, one of the two largest steel producing companies in the world and the largest steel producer in Europe, was looking for refractory linings for its basic oxygen furnace (BOF) plants in Europe.

RHI Magnesita was awarded 36 out of 46 linings, meaning the supply of 17000 tonnes of refractories with a commercial value of approximately €19 million. This corresponds to a market share of 80 percent. "RHI Magnesita not only won this tender against more than 10 competitors, but also doubled its market share while maintaining profitability", said Constantin Beelitz, Regional President of Europe, CIS & Turkey.

"Systematic data-driven market insights and analysis have enabled a better understanding of competitors' moves and capabilities. Implementing a fully customer-centric approach, mapping the customer's decision-making process and considering the requirements of all stakeholders along the entire process, were key factors," explained Matthias Stalzer, Global Key Account Manager. "A dedicated and well-coordinated cross-functional team contributed to this success. They addressed all customer requirements at every stage of the bidding process and demonstrated that together we can deliver on our role and capabilities as market and technology leaders."

Germany

RHI Magnesita to Invest €23 Million in Modernising the Plant in Urmitz

RHI Magnesita plans to invest €23 million in the digitalisation and modernisation of its Urmitz site (Germany) over the next two years. This investment, the group's largest in Germany, will be used to expand and upgrade the plant as a hub for nonbasic refractory products. The comprehensive modernisation measures will increase the plant's production volume while at the same time boosting energy efficiency by 10 percent. In addition, investments will be made in recycling, which will enable RHI Magnesita to increase the share of secondary raw materials.

As part of the investment in Urmitz, RHI Magnesita's pressing capacities will be increased and a new tunnel kiln with an automatic circulation system as well as several climate drying chambers will be installed. The plant will thus become a central hub in Europe for nonbasic refractory products such as bricks, mixes, and prefabricated components.

The investment represents part of RHI Magnesita's approach to optimise its global production network. As a global market leader for refractory products and solutions, RHI Magnesita is focusing on the opportunities regarding automation and digitalisation in order to further strengthen its competitiveness on the world market.

China

Faster and More Accurate: New Unloading Robot with Real-Time Visual Check

The Global Automation team and our colleagues at the Chizhou plant (China) have finished the installation of an unloading robot with visual inspection. This innovation will significantly improve the quality of RHI Magnesita's products and the level of automation.

By using feature screening arithmetics together with a high-resolution camera, RHI Magnesita is now able to detect the smallest cracks in our bricks.

Two robots and four high-resolution cameras were installed in this project, to unload bricks from the tunnel kiln car, check their quality, and load them onto the packing pallet. During this process, the brand-new software collects all suspicious bricks based on high-resolution images with the smallest pixels being 0.02 mm. If any faults are detected, the system instructs the robot to separate the potential defective brick. The cameras are also used to position bricks for the robot and measure the brick dimensions. For quality traceback, the system stores all images for 18 months.

The full load capacity of this system will be 30000 tonnes per year, with a 35 minute interval per tunnel kiln car. With this system, all necessary measurements can be performed efficiently.

RHI Magnesita Worldwide news (continued)

Worldwide

Carbon Disclosure Project (CDP) Awards RHI Magnesita with the Highest Rating in the Refractory Industry

RHI Magnesita's efforts to tackle climate change were rewarded by the Carbon Disclosure Project (CDP), the gold standard for corporate environmental transparency. Building on a C rating (Awareness Level) in 2019, we managed to improve rapidly by getting a B rating (Management Level) this year. Now, RHI Magnesita has the highest rating in the global refractory industry.

Each year, the global non-profit organisation assesses companies on how they are addressing climate risk, tackling carbon emissions, and reporting transparently.

"We are honoured by this recognition," said Stefan Borgas, CEO of RHI Magnesita. "As a technology leader, we are committed to driving the transformation of our business in all areas. Tackling carbon emissions and climate risk as well as identifying low-carbon opportunities are of utmost importance to us."

Worldwide

RHI Magnesita Announces 2020 Results and €50 Million Investment in CO₂ Emission Reduction

On the occasion of the full year results released in March, RHI Magnesita announced a new sustainability programme and reported resilient financial performance despite a challenging market environment. Liquidity was increased and business continuity maintained, while at the same time safe working conditions were ensured for all employees and business partners. In 2021, the company is reinforcing its commitment to sustainability and accelerating plans to become a carbon neutral business.

To expedite sustainability leadership, efforts are being stepped up to achieve the aspiration of becoming CO₂ neutral. For example, a major 4-year R&D programme designed to expand our leading sustainability position within the refractories industry has been introduced. RHI Magnesita will invest €50 million in technology research and pilot plant installations in the next 4 years, including new technology for CO₂ capture.

In the full year results, RHI Magnesita declared a gross profit margin of 24.4% (2019: 24.5%) and adjusted EBITA of 11.5% (2019: 14.0%) despite the volatile market environment. Furthermore, the company achieved a positive adjusted operating cash flow of €290 million (2019: €359 million), supported by a strong working capital management leading to a reduction in net debt to €582 million (2019: €650 million). The Board has recommended a final dividend of €1.00 per share, bringing the total dividend in respect of 2020 to €1.50 per share.

Following a swift and effective response to COVID-19, RHI Magnesita is continuing to supply its customers and addresses their evolving requirements by leveraging digital technology, adapting ways of working, providing flexibility, and maintaining reliability. Despite the disruption caused by the pandemic, RHI Magnesita remained focused on delivering its strategy centred around reducing costs to further improve competitiveness, its business model enhancement, and driving market leadership.



There for you, wherever you need us

The more closely we work with our customers, the greater the difference we can make for them. So having a global network of offices, research centres, and production sites is important to us, and to them. We'll go on extending our global reach, to be nearer to even more customers.

Our exceptional resources and expertise extend far beyond making and selling products. We also provide solutions to customers worldwide for tailored projects, material specifications, thermal studies, numerical simulations, follow-up and technical support for product application, as well as maintenance and electromechanical services for refractory equipment.

Find out more at
rhimagnesita.com

Follow us



RHI MAGNESITA



A warm welcome to the 2021 RHI Magnesita Bulletin. This edition marks the 75th anniversary of our company journal focused on refractory innovations and to celebrate such a special occasion we have compiled the largest number of papers to date. As the global leader in refractories, we aim to drive positive change in this industry and within the 16 articles there are examples of how we are achieving this in combination with delivering the best products and services for our customers.

A letter from our editor



RHI Magnesita is committed to sustainability and it is deeply embedded in our business. Therefore, it was very positive we were recently awarded AA for sustainability achievements and initiatives in the MSCI's ESG ratings. To provide an insight into some of the activities underway to reduce, capture, and utilise CO₂, this edition starts with papers describing the ANKRAL LC series for the cement industry and the approaches to reduce the carbon footprint in refractory raw material production processes. Furthermore, as a company driven by innovation, we have also included many articles detailing our recent advances such as the Spinosphere technology that improves cement rotary kiln brick properties, an unburned zero carbon alumina-magnesia brick which increases the steel ladle performance as well as reducing thermal losses, a novel raw material for slide gate plates, the toolbox for slag modelling and metallurgy, and an advanced technology package for blast furnace runners.

Through our solutions business model, we provide a wide range of services and products to create value for our customers and the articles describing Automated Process Optimization in the RH degasser, ladle and tundish systems ready for robotic handling, the new direct gas purging mononozzle technology for slab casting, and physical and mathematical modelling to optimise tundish refractory design are four examples benefiting the steel industry. Postmortem studies also play a pivotal role in providing tailored refractory solutions for the customer and the next paper details how this approach combined with thermochemical calculations is used to recommend appropriate linings for copper furnaces.

With the customer needs at the heart of RHI Magnesita's culture, it is a pleasure to report some of the success stories such as the fast project realisation and remarkable metallurgical results achieved using BOF gas purging at Severstal Cherepovets (Russia), multiple improvements to the EAF operations in a Brazilian steel plant, and the significant steel productivity increase at Jindal Shadeed (Oman).

The final paper in this edition describes the exciting development of our new state-of-the-art raw material centre at Hochfilzen (Austria). Due to extensive R&D and re-evaluation of the mining opportunities at this site, it has become feasible to cost-efficiently process the previously unused dolomite deposit and secure a high-quality sintered doloma source for our European production plants.

In closing, I would like to express my sincere gratitude to all the authors who provided the plethora of dynamic content and extend a special thanks to the editorial team. As a result of their commitment we are able to highlight how RHI Magnesita is taking innovation to 1200 °C and beyond.

Yours sincerely

Gerald Gelbmann

Head R&D Europe, CIS and Turkey
RHI Magnesita

“ RHI Magnesita is committed to sustainability and it is deeply embedded in our business. Therefore, it was very positive we were recently awarded AA for sustainability achievements and initiatives in the MSCI’s ESG ratings. ”





RHI MAGNESITA

Taking innovation to 1200 °C and beyond

Refractory products withstand extreme temperatures, enabling the production of steel, cement, glass, and many more materials essential to daily life.

Find out more at
rhimagnesita.com

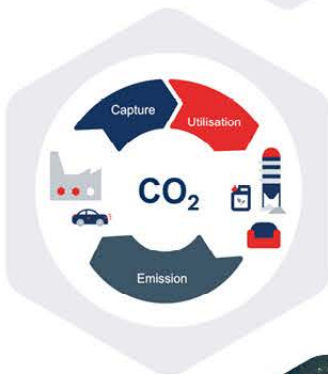
Follow us



Contents



- 12** **Circular Economy in the Refractory Industry**



- 16** **Reducing the Carbon Footprint of Raw Material Production**



- 106** **New Raw Material Source for Doloma Products in Europe**

- 12** **RHI Magnesita is Leading the Way to a Circular Economy in the Refractory Industry**
- 16** **Alternatives to Reduce the Carbon Footprint in Refractory Raw Material Production Processes**
- 22** **Spinosphere Technology— an Advanced Technology to Improve Cement Rotary Kiln Brick Properties**
- 28** **Development of Unburned Zero Carbon Alumina-Magnesia Bricks for Steel Ladle Linings**
- 36** **A Novel Raw Material Developed for Slide Gate Plate Technology**
- 42** **Automated Process Optimization at the RH Degasser in Gerdau Ouro Branco—Results After 2 Years of Operation**
- 48** **Latest INTERSTOP Ladle and Tundish Systems Ready for Robotic Handling**
- 54** **New Direct Purging NC Technology for Slab Casting**
- 60** **Tundish Refractory Design Optimisation Through Mathematical and Physical Modelling**
- 66** **Typical Refractory Wear Phenomena in Copper Vessels and Novel Monitoring Technologies**
- 72** **A Toolbox of Slag Modelling and Metallurgy in Your Pocket**
- 78** **Implementation of BOF Gas Purging Technology and Current Process Results After One Year of Successful Operation at Severstal Cherepovets**
- 84** **Advanced Technology Package for Blast Furnace Runners Focusing on Operational Safety, Availability, and Refractory Performance**
- 90** **Increase of the Internal Volume of an EAF with the Introduction of Hot Heel and Optimisation of the Scrap Melting Process**
- 96** **A Success Story for a Close Cooperation with Jindal Shadeed and RHI Magnesita Since 2016**
- 106** **Development of a New Raw Material Source for RHI Magnesita's Doloma Products in Europe**

Subscriptions Service and Contributions



We encourage you, our customers and interested readers, to relay our comments, feedback, and suggestions to improve the publication quality.

Email
bulletin@rhimagnesita.com

Phone
+43 50213 5300

Michael Klitzsch, Roland Krischanitz and Heinz Telser

RHI Magnesita is Leading the Way to a Circular Economy in the Refractory Industry

Introduction

Today, sustainability plays a key role not only in the cement industry, but also the refractory industry. The cement industry has come under tremendous pressure and is working intensively on emission reduction. One issue that is becoming increasingly important is the reduction of CO₂ in the entire supply chain. In this regard, RHI Magnesita benefits from its global production network with more than 35 sites in over 16 countries and has adapted the production strategy according to local requirements. By producing in close proximity to the customers, the aim is to shorten the transportation routes and thus decrease CO₂ emissions.

However, there are more steps RHI Magnesita is taking to actively contribute to environmental sustainability. In addition to increasing the energy efficiency, reduction of the carbon footprint in raw materials is one of the main efforts.

Geogenic emissions from raw materials represent almost half of RHI Magnesita’s direct emissions (scope 1, 2). CO₂ is released when raw magnesite (MgCO₃) is processed into magnesium oxide (MgO), the basis for many refractory products. These process emissions represent another major focus area of R&D, in particular, increasing recycled content. Due to the progress in R&D, RHI Magnesita is currently in the position to offer many sustainable solutions in the spirit of a circular economy and the goal to drastically reduce CO₂.

Low Carbon Solutions

The ANKRAL LC Series enables production with particularly low emissions of CO₂. These products allow the reuse of recycled materials without compromising technical requirements and specifications. LC stands for low carbon and refers to the significantly lower CO₂ footprint compared to conventional products. This is achieved by using recycled materials from cement rotary kilns. This material was previously considered unsuitable for further use in the production process of magnesia bricks, due to the fact that, in most cases, it contained a high amount of infiltrated salts that have a negative effect on the properties of the bricks. However, the research team developed technical methods for reusing these used linings, which has led to the creation of a sustainable product range—the LC Series.

Introducing a Circular Economy

A circular economy is based on the principles of minimising waste, pollution, carbon emission, and usage of natural resources, keeping products and materials in use, and regenerating natural systems. Based on positive results and experience gained during previous trials between 2016 and 2018, the circular economy for cement customers has been implemented (Figure 1). In the 2019/2020 winter repair season, RHI Magnesita collaborated with cement customers in Austria and Switzerland. Used magnesia spinel bricks from cement rotary kilns were sourced and collected for further processing.

Figure 1.
The circular economy approach of RHI Magnesita for the cement industry.



When breaking out the old lining, the cement plant was required to take the first steps to support the quality of the recycling process. According to the mineralogical composition of the bricks, the used lining was separated into different qualities. RHI Magnesita supported the cement plants in classifying the lining qualities into different categories according to their raw material composition. This differentiation was the basis for proper recycling and use of secondary raw materials. After breaking out, the different brick categories required separate storage on a paved surface under dry conditions (Figure 2). At this stage the cement plant is required to legally classify the waste.

After the legal classification of the waste was completed by the customer, the nonhazardous waste was transported to the recycling hub in Wartberg, (Austria), which is located close to the production plant in Veitsch. At the recycling hub several sorting and cleaning steps occur to increase and ensure the quality of the recycled material. Via a patented reconditioning process, RHI Magnesita is able to remove infiltrations, declare end of waste legally, and then to reintroduce this raw material to the production process at the production plant in Veitsch. The new LC Series was developed by substituting primary sintered magnesite with a specific amount of recycled raw material at the brick production plant (Figure 3).

After the patented reconditioning process, a certain amount of infiltrates remains present in the recycled material. This requires additional measures in the production process, where the remaining infiltrated salts are evaporated during the firing of the LC Series brick.

Figure 2.

Storage location of used lining pile in a Swiss cement plant.



For this reason, an investment in an upgrade to the environmental equipment at the tunnel kiln Veitsch was made in 2019. The environmental equipment ensures an optimal dedusting, desulphurisation, and dechlorination process for the tunnel kiln exhaust gas to meet the required environmental limits. In addition, the firing process in the tunnel kiln ensures that there are no infiltrations remaining in an LC Series brick that uses recycling material. Through this, the composition of LC Series bricks remains essentially the same as that of comparable standard bricks.

Reducing Carbon Footprints

During production of the LC Series, the recycled material substitutes up to 20% of the virgin raw material. This substitution reduces the product carbon footprint (PCF) significantly. Table I shows the PCF of an ANKRAL LC Series and a comparable ANKRAL standard product according to ISO 14044. It shows that the highest impact of the PCF is the burning and dissociation of magnesite. To produce dead burned magnesite (DBM), which is used to produce cement rotary kiln bricks, magnesite is heated to 1750 °C and dissociates to MgO and CO₂. Through the use of recycled material, emissions caused by this process step are avoided. Consequently, the CO₂ emissions that are related to the burning and dissociation of magnesite, depending on the substitution rate, are 17% to 20% lower. This results in a decrease in the PCF of 12–14% for the final product. The calculations of the PCF have been assured by denkstatt, a consulting company for sustainability and environment.

Figure 3.

ANKRAL Q2 LC brick.



Table I.

PCF of standard product and ANKRAL LC brick quality.

| | Traditional | LC Series | Reduction % |
|---|-------------|-----------|-------------|
| Burning and dissociation of MgCO ₃ → MgO + CO ₂ | 1.2 | 1.0 | -17 |
| Production of ANKRAL bricks | 0.1 | 0.1 | 0 |
| Others (PCF external raw material, transportation) | 0.4 | 0.4 | 0 |
| Sum | 1.7 | 1.5 | -12 |

Product Portfolio

The LC Series product portfolio currently consists of three products for application in different operating conditions. ANKRAL RC-LC is a standard grade for application in transition zones of kilns with moderate chemothermal stresses. With ANKRAL Q2-LC, the Q Series concept has also been adapted for the use of alternative raw materials and provides advantages in terms of brick flexibility. ANKRAL Q1-LC represents the top range within the LC Series. Due to the use of top-quality sintered magnesia, ANKRAL Q1-LC can be applied in kilns with high chemothermal loads as occurs with the use of alternative fuels.

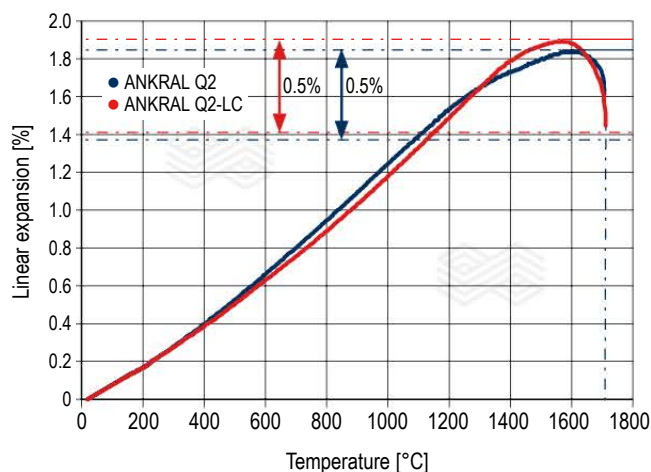
During the development of the LC Series, attention was paid to maintain the key characteristics of the products. This was realised through the selection and treatment of the recycling material, as well as by limiting the recycled content. This ensures brick density is maintained, as well as apparent porosity, cold crushing strength, and refractoriness under load (RUL) at levels comparable to products using primary raw materials. Therefore, the performance of the products is maintained at the same level. Figure 4 compares the RUL measurement results of ANKRAL Q2 based on primary raw materials and ANKRAL Q2-LC. The diagram shows that despite the use of alternative raw materials, the refractoriness can be maintained at the same level with a $T_{0,5}$ of >1700 °C.

The focus of RHI Magnesita for further developments is on continuous optimisation of the sourcing and preparation process in order to achieve higher substitution rates and to obtain an even greater reduction of the carbon footprint. The development of products for the central burning zone based on iron-rich sintered magnesia has also been initiated. This will allow the resource cycle to close in this specific group of products and raw materials.

The cement industry is in the midst of a major transition towards CO₂ reduction and sustainability. RHI Magnesita is dedicated to working closely with customers to help solve these challenges. As a result of years of research and development, RHI Magnesita is able to actively support customers in the cement industry by reducing emissions, shortening supply chains, and enabling a more circular economy.

Figure 4.

RUL test results (acc. to ISO 1893) of ANKRAL Q2-LC (red) and ANKRAL Q2 (blue).



Reprint permission

Reprinted with permission from World Cement.

Authors

Michael Klitzsch, RHI Magnesita, Leoben, Austria.
 Roland Krischanitz, RHI Magnesita, Vienna, Austria.
 Heinz Telser, RHI Magnesita, Vienna, Austria.

Corresponding author: Michael Klitzsch, michael.klitzsch@rhimaginesita.com





We take Leadership seriously

“To maintain our industry leadership, we need best-in-class expertise and world-class leaders. So for us, career and personal development aren't an afterthought.”

RHI Magnesita is the global leader in refractories. Our customers use extremely high temperatures to make materials such as steel and nonferrous metals, cement, lime, glass, energy, and chemicals. They depend on our products and know-how to contain and control those materials at temperatures of 1200 °C and much, much higher.

We're the global leader in tackling these extreme challenges. And to us, leadership is more than just being the biggest. It's about delivering the most innovative, reliable products and services for our customers. It's about constantly being one jump ahead. It comes from finding, retaining, and motivating exceptional people who can do an exceptional job.



RHI MAGNESITA

Tamara Ribeiro, Paschoal Bonadia, Erwan Gueguen, Franz Maier and Thomas Drnek

Alternatives to Reduce the Carbon Footprint in Refractory Raw Material Production Processes

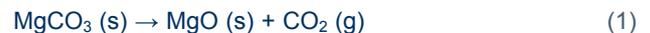
Over the past decades, the world has experienced a significant increase in the volumes of CO₂ released into the atmosphere, mainly due to human activity on the planet. The Paris Agreement on climate change has established that a 45% drop in total emissions would be required by 2030 and reaching carbon-zero would be a must by 2050 to limit global warming to 2 °C above pre-industrial levels—and pursue efforts to keep it below 1.5 °C. Since then, several industrial sectors have been mobilising to minimise their climate impact. In the refractories value chain, the production of dead burned magnesia and dead burned dolomite are the most CO₂-intensive processes, being responsible for around 85% of all RHI Magnesita's scope 1 emissions. Therefore, capturing and managing the CO₂ from raw material production processes is essential to reduce the carbon footprint. The challenge of decreasing the company's geogenic emissions will be overcome by a combination of short- and long-term initiatives, ranging from less complex schemes like changes of fuel and recycling to more disruptive ones such as new kiln technologies, carbon capture, utilisation, and storage (CCUS) as well as new raw material production processes. In the next four years the company will invest €50 million towards technologies to achieve its aspiration to become CO₂ neutral. This paper describes the efforts and alternatives being evaluated by RHI Magnesita to reduce its greenhouse gas emissions.

Introduction

Global warming is a topic of increasing importance for governments, research institutions, companies, and civil society worldwide. The phenomenon has been intensified by the increasing levels of CO₂ in the atmosphere, derived mainly from human activity, leading to many environmental and economic issues. To mitigate the impacts of this phenomenon, in 2016, the Paris Agreement ratified the commitment of the signatory countries to prevent global temperature elevation above 2 °C by 2050 compared to the values of the preindustrial period. Since then, several leading industries have been mobilising to minimise their climate impact [1]. Aware of its role as the world leader in the refractory business, RHI Magnesita announced a review in its climate action strategy in 2019, proposing stricter carbon footprint reduction targets. The company is committed to reducing 15% of its scope 1, 2 and 3 emissions by 2025 [2] and has the aspiration to become CO₂ neutral in future. Many initiatives have been developed to meet these goals, and this article will present an overview of some of them.

Understanding our Carbon Footprint

RHI Magnesita is a vertically integrated company that produces most of its own raw materials. Among them, sintered magnesia or dead burned magnesia (DBM) and sintered dolomite or dead burned dolomite (DBD) have an important role, not only because they are widely used in several refractory formulations, but also because their production is responsible for around 85% of RHI Magnesita's CO₂ emissions. These materials can be obtained either from magnesium-containing ores (magnesite and dolomite) or aqueous sources (seawater and brines). In both cases, production processes are CO₂ intensive, with most emissions related to the decomposition of carbonated materials, which are called geogenic emissions. Magnesite (MgCO₃) and dolomite (CaCO₃.MgCO₃) have a high concentration of CO₂ in their composition, which is released when ore is heated at high temperatures to obtain pure magnesium or calcium-magnesium oxides [3], as shown in equations (1) and (2).



Magnesium oxide can also be obtained from seawater or brine by the synthetic wet route. In this process the aqueous solution containing MgCl₂ reacts with lime (CaO) or dolime (CaO.MgO) to form magnesium hydroxide. Then, this compound is calcined and sintered to produce MgO [3]. Equations (3), (4) and (5) describe the chemistry of the process:



Although the wet route seems to be more ecofriendly at first sight, as lime and dolime are produced from the decomposition of carbonate ores, CO₂ emissions are virtually the same as in the mineral processing route. In fact, depending on the type of kilns and fuel to be used, CO₂-specific emissions can range from around 1.4 to 5.2 kg CO₂eq/kg MgO or CaO.MgO [3,4].

In 2020, RHI Magnesita's DBM and DBD production sites generated in total approximately 1.8 million tonnes of CO₂ scope 1 emissions, of which 60% were geogenic and 40% were fuel-based. Distribution per plant can be seen in Figure 1.

Alternatives for CO₂ Footprint Reduction in DBM and DBD Production Processes

Since the production of dead burned magnesia and dead burned dolomite contributes so significantly to RHI Magnesita’s carbon footprint, the investigation of alternatives to reduce CO₂ associated with these processes is essential to ensure the climate strategy goals are met. To this end, in addition to the short-term carbon footprint reduction measures (linked to increasing recycled content in refractory products, changes in fuel, energy efficiency, and renewable electricity utilisation), there are long-term initiatives for the development of DBM and DBD production process in which less CO₂ is generated and/or geogenic and fuel-based emissions are captured and used/disposed. Three main research lines are being investigated: CO₂ capture technologies, CO₂ utilisation, and value chain and clean process routes (Figure 2).

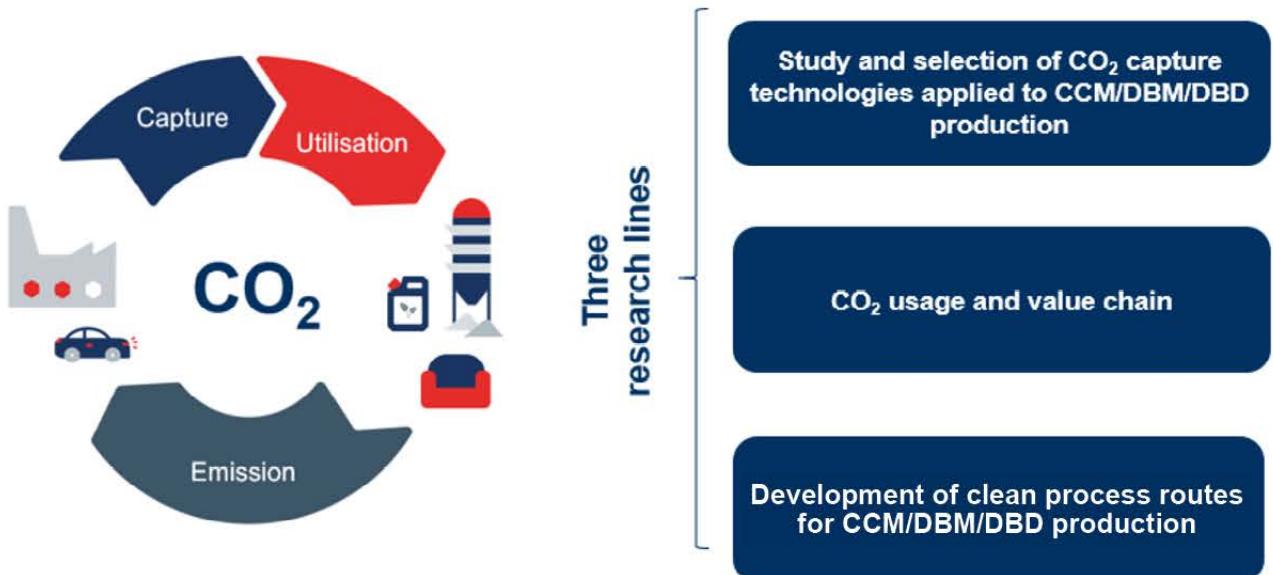
“CO₂ capture technology” is focused on the study and selection of the most appropriate CO₂ capture technologies which can be implemented at RHI Magnesita’s DBM and DBD production plants. “CO₂ clean process routes” comprises the development of new processes, technologies, and equipment to reduce the carbon footprint in DBM and DBD production. “CO₂ usage and value chain” aims to understand the CO₂ value chain (from capture to final users, including infrastructure and logistics required for transportation), in addition to the identification of potential customers and evaluation of technologies, current and emerging, for CO₂ utilisation and/or storage.

From 2021 on, RHI Magnesita will be running a major R&D program designed to expand its leading sustainability position within the refractories industry. The company will invest €50 million towards technology research and pilot plant installations in the next four years, including developments in these three research lines.

Figure 1.
RHI Magnesita DBM and DBD production plants and CO₂ emission distribution in 2020.



Figure 2.
Long-term initiatives for carbon footprint reduction in DBM and DBD production processes.



CO₂ Capture Technologies

CO₂ capture comprises a series of technologies that are increasingly widespread in the global industry and constitute a promising alternative to address process carbon emissions in the medium-term [5]. It consists of the removal of CO₂ from kiln off-gases to obtain a high-purity carbon dioxide gas stream, which can be stored in geological formations or commercialised for different applications.

The main advantage of these processes is that most of them do not require large modifications to the kilns and could be applied to existing facilities [6]. However, current capture technologies are still expensive and, therefore, most of the recent developments are focused on the overall cost reduction of these processes [7]. Table I presents the most relevant existing CO₂ capture technologies.

Technology readiness levels (TRL) is a measurement system developed by NASA in the middle of the 1970s, to assess the maturity level of technologies. It comprises nine levels, where the higher the TRL, the more mature the technology. The TRL scale is as follows: TRL 1: Basic principles observed; TRL 2: Technology concept formulated; TRL 3: Experimental proof of concept; TRL 4: Technology validated in laboratory; TRL 5: Technology validated in relevant environment; TRL 6: Technology demonstrated in relevant environment; TRL 7: System prototype demonstration in operational environment; TRL 8: System complete and qualified; and TRL 9: Actual system proven in operational environment [11,12].

The selection of the most appropriate technology for each process must consider both off-gas flow characteristics (flow rate and purity) and the required final composition [7,8]. The technology readiness level must also be taken into account, depending on the timeline for implementing the technology. Considering these criteria, chemical absorption emerges as one of the technologies with the highest potential to be used in sintered magnesia and sintered doloma production plants.

Among the indicated CO₂ capture alternatives, this has been one of the most studied by RHI Magnesita, which is in interaction with technology suppliers in order to assess the technical-economic feasibility.

Chemical absorption has been used to remove CO₂ from gas flows for years. The classic absorbent for the technology is 20–30 wt% aqueous monoethanolamine (MEA), which enables up to 95% CO₂ capture yields [9,13]. In the process, CO₂ is absorbed from the flue gas at room temperature into the MEA solution, as shown in Figure 3. The amine is regenerated by stripping with steam at 100–120 °C. The steam is then condensed, leaving high-purity CO₂ in the gaseous phase [13]. Using a cement plant as reference, CO₂ capture by MEA absorption costs approximately €80/tonne avoided CO₂, with 55% of the value coming from solvent stripping [14].

Although this is a consolidated technology, extensive research has been conducted in this area, especially in the development of a new generation of absorbents that can either perform better than MEA and/or present lower solvent regeneration costs [9].

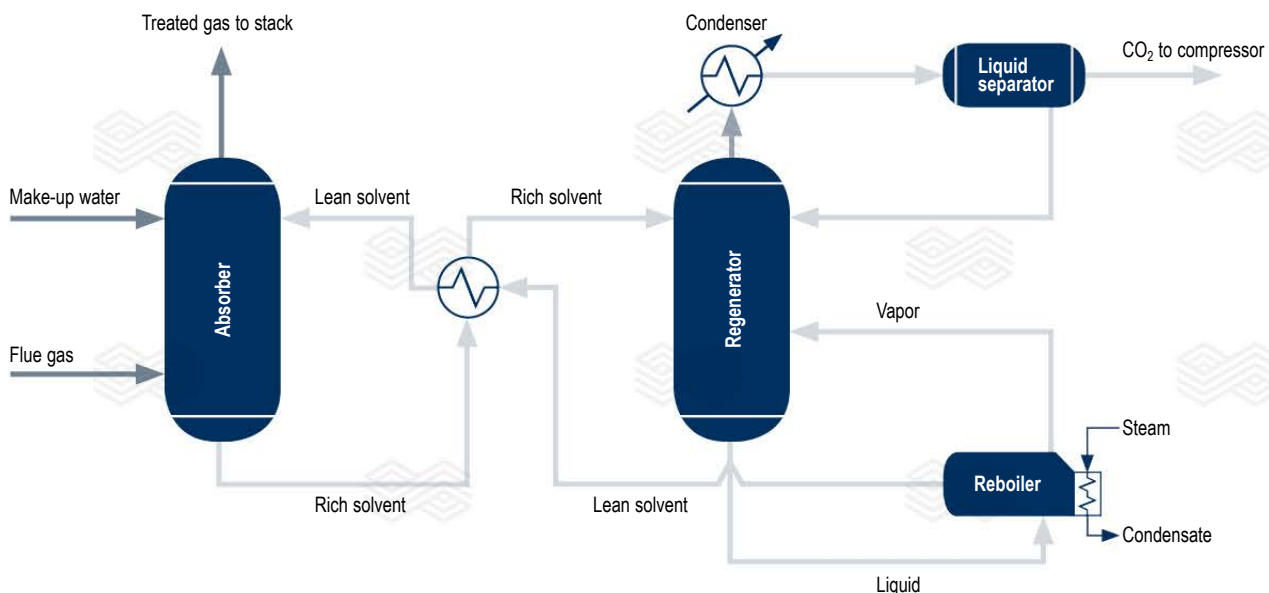
Table I.

Main existing CO₂ capture technologies (based on information provided in the following references [8–10]). High CO₂: >90 wt%; medium CO₂: 90–20 wt%; low CO₂: <20 wt%.

| Main technology | Technology readiness level | CO ₂ purity at source |
|--------------------------|----------------------------|----------------------------------|
| Chemical absorption | 8–9 | Low to medium |
| Physical absorption | 7–8 | Medium to high |
| Adsorption | 6–7 | Low to medium |
| Cryogenics | 8–9 | High |
| Membranes | 5–6 | Medium to high |
| General gas conditioning | 8–9 | High |

Figure 3.

Diagram of chemical absorption CO₂ capture process.



Other CO₂ capture technologies have also been studied in this project; however, due to the low technology readiness level, these are being treated as capture alternatives for the future.

Clean Process Routes for DBM and DBD Production

The projects within this research line correspond to initiatives for the evaluation of new kiln and process technologies that can significantly contribute to reducing the carbon footprint in sintered magnesia and sintered doloma production plants. Regarding new kiln and process technologies, two main alternatives are being considered: Oxyfuel and the direct CO₂ separation furnace. Although these technologies are based on different principles, in both cases the main goal is to obtain, at the end of the carbonate decomposition process, a gas flow rich in CO₂, which can potentially be captured and used at a lower cost compared to current capture technologies. In the oxyfuel process (Figure 4), combustion is performed with oxygen instead of air preventing the dilution of the flue gas with nitrogen. Thus, kiln exhaust gas has a high CO₂ concentration, which makes it easier to purify, dry, compress, and liquefy for further transport and storage or utilisation [15,16]. Although the method presents good technical potential and competitive costs when compared to CO₂ capture technologies (€42/tonne avoided CO₂, with a cement plant as a reference [14]), oxyfuel imposes an additional challenge related to the retrofitability, since it demands the adaptation of existing equipment and processes [15].

The direct CO₂ separation kiln (Figure 5) consists of a technology in which the calcination process is carried out by indirect heating, that is, without any contact between the combustion gases and the gases resulting from the

decomposition of carbonated ores. Thus, as in oxyfuel, the exhaust gas contains a high CO₂ concentration, and can, potentially, easily be processed and disposed of. This technology was developed by the Australian company Calix and is currently being demonstrated at scale in Belgium (LEILAC Project) [17]. In addition to these initiatives, disruptive technologies such as calcination using concentrated solar power (TRL 4–6) and the production of MgO from brines and/or sea water by electrochemical processes (TRL 4–6) are also being studied. Other work fronts comprise the assessment of processes at a lower technology readiness level, including the development of routes for DBM and DBD production using alternative raw materials, renewable energy, and biological systems.

CO₂ Usage and Value Chain

In practical terms, CO₂ capture seems to be a well-established topic from a technical point of view, since there is a range of high-maturity technologies available and many others are in full development. Carbon capture, however, is only the first step in the CO₂ value chain, since the compound needs to be properly disposed of to ensure emissions reduction targets. Thus, technologies for CO₂ capture, use, and storage (CCUS) are key factors to achieve low or neutral carbon scenarios worldwide. Carbon dioxide has several applications, with the possibility of either direct use or conversion to other chemical compounds. Table II presents the current main alternatives for CO₂ utilisation, including demand and gas quality specifications. The volume of CO₂ required for other existing uses, such as horticulture, pulp and paper processing, water treatment, refrigerant gas, metal working, and pharmaceutical processes, is very low.

Table II.

Main current CO₂ utilisation alternatives, including demand and gas quality requirements (with information from [10,18,19]).

| Use for CO ₂ | Current demand [million tonnes/year] | Required purity |
|---|--------------------------------------|-----------------|
| Enhanced oil recovery (EOR) | <30 | High > 95.0% |
| Urea yield boosting | 5 to 30 | High |
| Beverage carbonation | ~8 | High > 99.0% |
| Food processing, preservation and packing | ~8.5 | High > 99.0% |

Figure 4.

Diagram of oxyfuel technology.

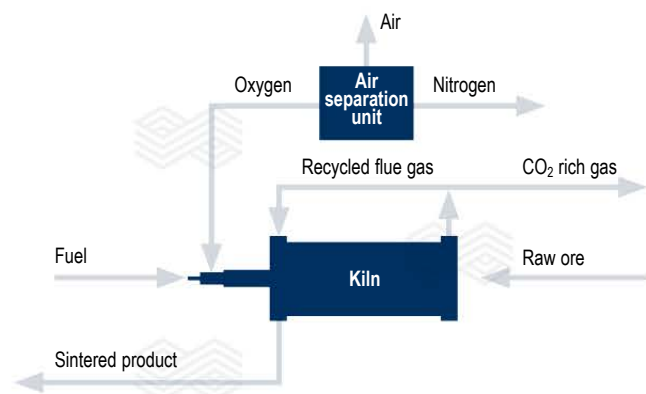
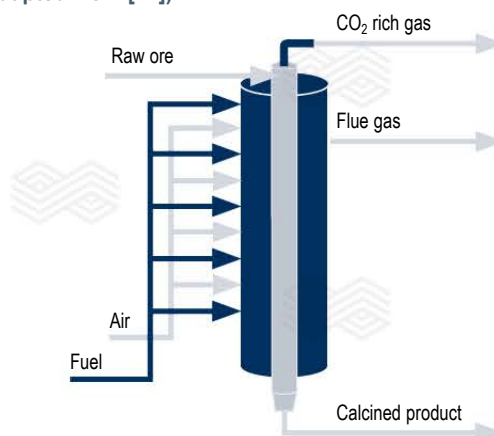


Figure 5.

Diagram of CO₂ direct separation kiln technology (adapted from [17]).



These applications seem to be good options for using the CO₂ that could be captured from kiln off-gases and the feasibility of some of them has been evaluated, to a greater or lesser extent, by RHI Magnesita and with external partners. Many of these markets, however, are facing CO₂ oversupply, while the outlook for demand growth remains stable, which is a hindrance to commercialisation.

In addition, several studies indicate a mismatch between the quantities of CO₂ that are being generated around the globe and the amount of the compound used currently. For reference, in 2019 around 33 giga tonnes of CO₂ from power and industrial facilities was released into the atmosphere [20]. In the same period, world CO₂ consumption was below 250 million tonnes [19]. Taking all this into account, the importance of developing new technologies for CO₂ utilisation is evident.

Four key emerging CO₂ market opportunities have been identified as the most promising alternatives for CO₂ utilisation in the coming years: CO₂ derived fuels; CO₂ derived chemicals; manufacturing of building materials from minerals/waste + CO₂; and crop yield boosting, including algae growth and greenhouses. Although many of these technologies are still in an early stage of development, each one has the potential to increase global CO₂ demand to at least 10 million tonnes of CO₂ per year in the short term [19,20].

From this finding, RHI Magnesita has joined forces with technology suppliers in each of these areas, to identify which

emerging CO₂ utilisation alternatives can be successfully applied to the processes. This work started with a technology landscaping study performed by NineSigma open innovation, which generated a list of more than 130 companies. From the initial screening, a small number of companies were selected as potential partners with which RHI Magnesita has been collaborating, to generate value-added products from CO₂ emissions. In addition to the utilisation alternatives, there is a consensus that CO₂ storage is essential to reach low or zero carbon net emissions goals. It is one of the technologies with the highest CO₂ abatement potential, preventing large quantities of gas from being released in the atmosphere [21]. It consists of the transport and injection of captured CO₂ from stationary sources into deep underground porous rock formations, which can be trapped in these geological reservoirs for millions of years [22]. As building CO₂ storage sites requires high investments and expertise, this type of technology is initially considered only for plants where the location is favourable for CCS implementation. Figure 6 shows a typical CCS scheme.

An important consideration is that far beyond CO₂ capture, storage, and use schemes, it is necessary to understand the entire CO₂ value chain, from source to the final destination, including capture alternatives, intermediate gas treatment stages, compression, and transportation to have a full view of how these technologies can be used to reduce the carbon footprint in the company [10]. Figure 7 presents a summary of these stages and some of the critical parameters in each.

Figure 6.

Typical CO₂ capture and storage scheme.

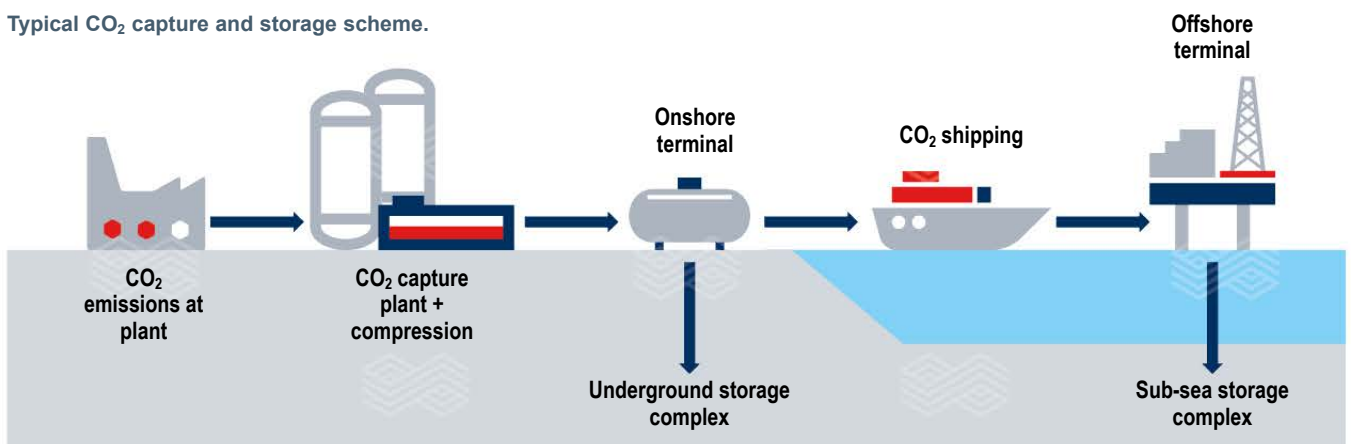
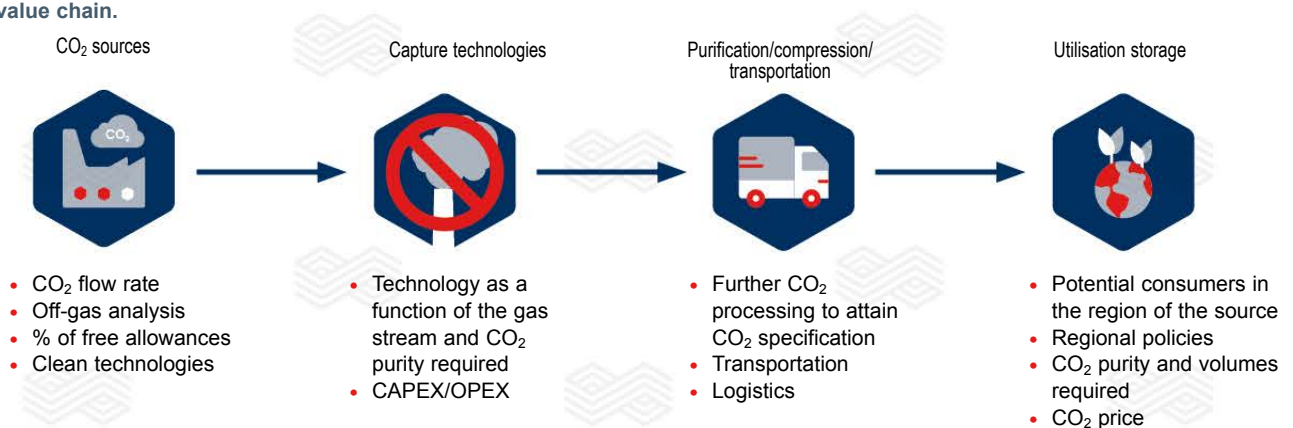


Figure 7.

CO₂ value chain.



To explore the potential to capture and utilise CO₂ containing flue gases from RHI Magnesita plants in Europe, the company developed a comprehensive CO₂ value chain study in partnership with Imperial College Consultants. The project involved:

- The mapping of potential CO₂ consumers in proximity to the plants.
- CO₂ transport infrastructure and logistics assessment.
- The quality of the CO₂ demanded by potential consumers and the capture technologies required.
- Evaluation of local policies that could foster carbon capture and utilisation (CCU).
- Ranking of the most favourable plants for CCU implementation.

References

- [1] Küpper, D., Kuhlmann, K., Pieper, C., Burchardt, J. and Schlageter, J. The Green Factory of the Future. BCG – Boston Consulting Group, 2020.
- [2] <https://www.rhimagnesita.com/energy-and-climate/>; accessed 26.10.2020.
- [3] Drnek, T., Moraes, M. and Bonadia, P. Overview of magnesite. *RHI Magnesita Bulletin*. 2018, 14–22.
- [4] Luong, V., Amal, R., Scott, J., Ehrenberger, S. and Tran, T. A comparison of carbon footprints of magnesium oxide and magnesium hydroxide produced from conventional processes. *Journal of Cleaner Production*. 2018, 202, 1035–1044.
- [5] MacDowell, N., Florin, N., Buchard, A., Hallett, J., Galindo, A., Jackson, G., Adjiman, C., Williams, C., Shahb, N. and Fennell, P. An overview of CO₂ capture technologies. *Energy & Environmental Science*. 2010, 3, 1645–1669.
- [6] IEA – International Energy Agency. Technology roadmap: low-carbon transition in the cement industry, Paris, France, 2018.
- [7] Wilberforce, T., Baroutaji, A., Soudan, B., Al-Alami, A. and Ghani Olabi, A. Outlook of carbon capture technology and challenges. *Science of the Total Environment*. 2018, 657, 56–72.
- [8] Patricio, J., Angelis-Dimakis, A., Castillo-Castillo, A., Kalmykova, Y. and Rosado, L. Region prioritization for the development of carbon capture and utilization technologies. *Journal of CO₂ Utilization*. 2017, 17, 50–59.
- [9] Bui, M. et. al. Carbon capture and storage (CCS): the way forward. *Energy and Environmental Science*. 2018, 11, 1062.
- [10] Pieri, T., Nikitas, A., Castillo-Castillo, A. and Angelis-Dimakis, A. Holistic assessment of carbon capture and utilization value chains. *Environments*, 2018.
- [11] NASA. Technology Readiness Level. https://www.nasa.gov/directorates/heo/scan/engineering/technology/txt_accordion1.html. 2012; accessed in December, 2020.
- [12] European Commission. Technology readiness levels (TRL). Horizon 2020 – work programme 2014–2015. General Annexes G. https://ec.europa.eu/research/participants/data/ref/h2020/wp/2014_2015/annexes/h2020-wp1415-annex-g-trl_en.pdf. 2014; Accessed in December, 2020.
- [13] Stuart Haszeldine, R. Carbon capture and storage: how green can black be? *Science*. 2009, 325, 1647–1652.
- [14] Gardarsdottir, S., De Lena, E., Romano, M., Roussanaly, S., Voldsund, M., Pérez-Calvo, J.-F., Berstad, D., Fu, C., Anantharaman, R., Sutter, D., Gazzani, M., Mazzotti, M. and Cinti, G. Comparison of technologies for CO₂ capture from cement production—Part 2: Cost Analysis. *Energies*. 2019, 12, 3.
- [15] Voldsund, M., Gardarsdottir, S., De Lena, E., Pérez-Calvo, J.-F., Jamali, A., Berstad, D., Fu, C., Romano, M., Roussanaly, S., Anantharaman, R., Hoppe, H., Sutter, D., Mazzotti, M., Gazzani, M., Cinti, G. and Jordal, K. Comparison of technologies for CO₂ capture from cement production— Part 1: Technical evaluation. *Energies*. 2019, 12, 3.
- [16] Ditaranto M. and Bakken J. Study of a full scale oxy-fuel cement rotary kiln. *International Journal of Greenhouse Gas Control*. 2019, 83, 166–175.
- [17] LEILAC. Public LEILAC feed summary report - Version 1.00. July 2017.
- [18] Global CCS Institute. Accelerating the uptake of CCS: industrial use of captured carbon dioxide. March, 2011.
- [19] International Energy Agency. Putting CO₂ to use. IEA Publications, September 2019.
- [20] International Energy Agency. Technology Perspectives: 2020 Special Report on Carbon Capture, Utilization and Storage CCUs in clean energy transitions. IEA Publications, September 2020.
- [21] Global CCS Institute. The Global Status of CCS: 2017. October 2017.
- [22] Ketzner, J.M., Machado, C.X., Rockett, G.C. and Iglesias, R.S. Brazilian atlas of CO₂ capture and geological storage. Porto Alegre, EDIPUCRS, 2014.

Authors:

Tamara Ribeiro, RHI Magnesita, Contagem, Brazil.
 Paschoal Bonadia, RHI Magnesita, Contagem, Brazil.
 Erwan Gueguen, RHI Magnesita, Vienna, Austria.
 Franz Maier, RHI Magnesita, Leoben, Austria.
 Thomas Drnek, RHI Magnesita, Leoben, Austria.

Corresponding author: Tamara Ribeiro, tamara.ribeiro@rhimagnesita.com

Conclusion

To meet RHI Magnesita's commitment to reduce its carbon footprint, several initiatives have been developed within the company over the last years. In 2021 a major R&D program was also started to step up efforts to expand the company's leading sustainability position within the refractories industry. As most of the CO₂ emissions are related to the production of dead burned magnesia and dead burned doloma, many of the medium and long-term developments are focused on carbonate calcination and sintering processes. According to this approach, three main research lines are under investigation: "CO₂ capture technologies", "CO₂ utilisation and value chain", and "Clean process routes for DBM/DBD production". Each of these fields has its own challenges, but they must be addressed in parallel so that it will be possible to have a comprehensive view of the most appropriate alternatives to address RHI Magnesita's carbon emissions and support future decision-making process for technology implementation.



Martin Geith, Susanne Jörg and Roland Krischanitz

Spinosphere Technology— an Advanced Technology to Improve Cement Rotary Kiln Brick Properties

Introduction

After decades of magnesia spinel brick development, compromises still have to be accepted when it comes to optimising flexibility and hot properties. This is because the increased spinel addition, necessary to improve flexibility, inevitably leads to a reduction of hot properties. The alumina contained in all types of spinel reacts with CaO, which is present in the secondary phases of the magnesia and abundant in the clinker, to form low melting phases. The novel Spinosphere technology reduces the alumina content of the flexibiliser by 70% compared to conventional magnesia-alumina spinel (MA-spinel) without reducing the effectiveness in flexibilising the brick structure. This enables the development of products with unique characteristics, combining the seemingly contradictory properties of flexibility and thermal shock resistance (TSR) on one hand and heat resistance on the other hand.

Methodology

For the characterisation of hot strength and flexibility properties, trial bricks were produced on a laboratory scale with a content of 5% MA-spinel, 15% MA-spinel, and 15% Spinosphere as shown in Table I. The unique composition of the Spinosphere concept enables an addition of 15% flexibiliser, resulting in an alumina content of only 3% in the product.

In order to ensure comparability, all bricks were based on the same type of magnesia, grain size distribution, and were produced under the same firing conditions. The samples were tested for hot modulus of rupture (HMOR DIN EN 993-7) and refractoriness under load (RUL DIN EN ISO 1893) to characterise hot strength and refractoriness. For evaluation of flexibility, dynamic Young's modulus measurements and wedge splitting tests were carried out.

Investigation Results Regarding Brick Flexibility

Linear elastic behaviour

To evaluate the linear elastic behaviour of basic refractory material the Young's modulus determined with ultrasound (so-called dynamic Young's modulus) was tested. Figure 1 shows the relative dynamic Young's modulus of the tested samples.

By using conventional MA-spinel (sample T1 5% MA-spinel and T2 15% MA-spinel) it is clear that a reduction of the flexibiliser amount leads to an increase in the dynamic Young's modulus by ~100% and a downgrading of the linear elastic flexibility behaviour. With the use of the newly developed Spinosphere technology the relative Young's Modulus can maintain a similar level as with addition of the same amount of conventional MA-spinel.

Figure 1.

Relative dynamic Young's modulus (reference is a mag-spinel brick containing 15% conventional MA-spinel).

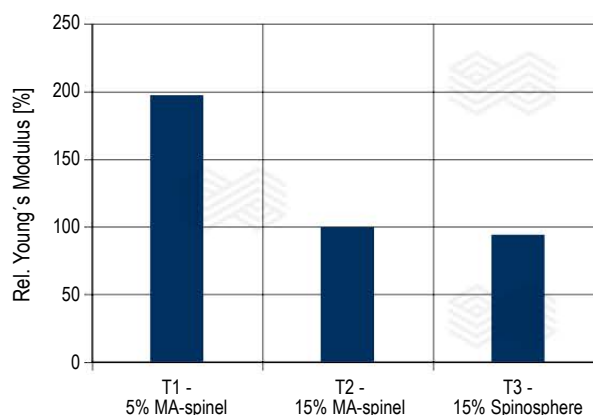


Table I.

Overview of trial bricks and chemical composition.

| | T1 | T2 | T3 |
|---|-----------|-----------|-------------|
| Spinel type | MA-spinel | MA-spinel | Spinosphere |
| Spinel addition [wt.%] | 5.0 | 15.0 | 15.0 |
| MgO content [wt.%] | 94.9 | 87.9 | 95.3 |
| Al ₂ O ₃ content [wt.%] | 3.3 | 10.5 | 3.0 |

Crack propagation behaviour

If the maximum stresses in the lining exceed the material strength, the state of linear elastic material behaviour is left, and subsequently cracks will form. After initiation, the crack propagates through the sample until destruction. The crack propagation behaviour of refractory material can be measured using the wedge splitting test (Figure 2). The detailed test procedure has already been described in [1].

The aim in product development is to achieve high specific fracture energy G_F (total energy required to destroy the sample) combined with a high G_F/G_C ratio (slow crack propagation) [2], which means high flexibility/lowest brittleness.

Figure 3 shows typical wedge splitting test curves of the trial alternatives. The brick containing 5% MA-spinel as flexibiliser showed a wedge splitting test curve that indicated brittle behaviour with crack initiation (G_C) at a high force of ~500 N, followed by a relatively rapid reduction, whereas samples T2 and T3 showed a lower crack initiation force and, most importantly, a much slower fall of the curve, indicating a more flexible behaviour.

Figure 2.
Wedge splitting test curve.

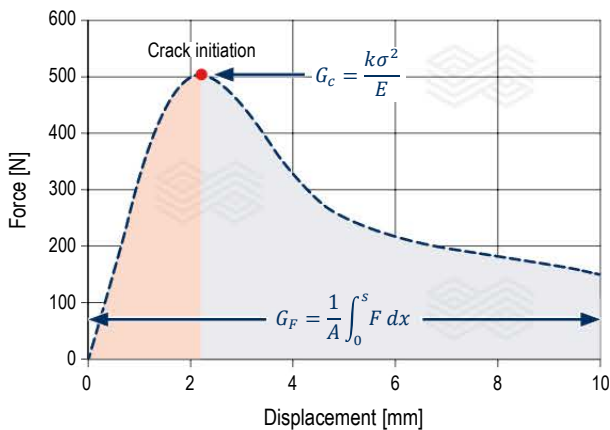
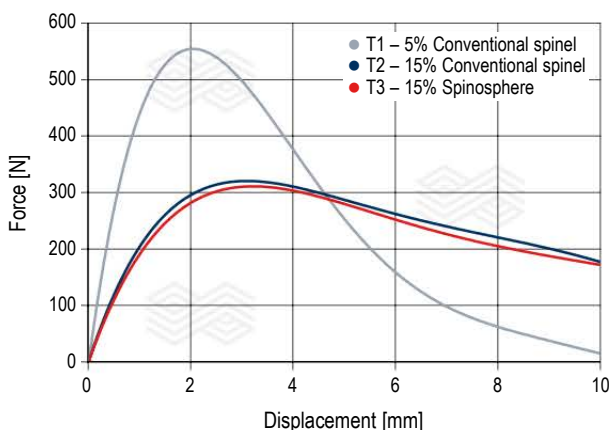


Figure 3.
Wedge splitting test curves of the three tested alternatives.



This is also evident when analysing the numerical wedge splitting test numbers, shown in Figure 4. The bricks containing 15% flexibiliser show an approximately 15% higher consumed specific fracture energy (G_F) compared to 5% MA-spinel. Additionally, the crack initiation energy G_C for T1 (5% MA-spinel) is doubled compared to T2 and T3 with 15% flexibiliser, leading to an unfavourable ratio G_F/G_C . The comparison of a brick containing 15% conventional MA-spinel and 15% Spinospheres shows that both alternatives have a very similar cracking behaviour.

Investigation Results Regarding High Temperature Properties

To evaluate the high temperature properties the refractoriness under load (RUL acc. to DIN EN ISO 1893) and hot modulus of rupture (HMOR acc. to DIN EN 993-7) were determined. Table II displays the results of RUL and HMOR testing. Alternative 3 shows superior properties in both tests in comparison to the 15% MA-spinel alternative, comparable to T1 with only 5% MA-spinel. The T0 values of sample T3 were increased. Comparing the same amount of flexibiliser addition, the use of Spinospheres raises the T0 value by more than 100 °C so that the refractoriness increases to the level of a conventional MA-spinel brick containing only 5% of MA-spinel. This can be related to the significantly lower Al_2O_3 content. Similar results were achieved in the HMOR at 1400 °C. Bricks containing 15% Spinospheres (T3) and 5% spinel (T1) were at the highest level and show clear advantages when compared to bricks containing 15% spinel (T2).

Figure 4.
Numerical wedge splitting test evaluation, calculated values of relative crack initiation energy G_C , relative specific fracture energy G_F and ratio G_F/G_C (reference is a mag-spinel brick containing 15% conventional MA-spinel).

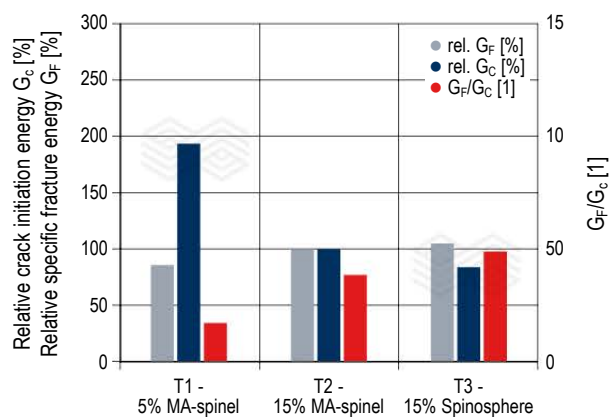


Table II.
RUL (DIN EN ISO 1893) and HMOR (DIN EN 993-7) test results.

| | | RUL T ₀ [°C] | RUL T _{0.5} [°C] | HMOR 1400 °C [MPa] |
|----|------------------|----------------------------|------------------------------|--------------------------|
| T1 | 5% spinel | 1685 | > 1700 | 4.3 |
| T2 | 15% spinel | 1538 | > 1700 | 1.3 |
| T3 | 15% Spinospheres | 1676 | > 1700 | 4.4 |

Investigation Results Regarding Clinker Melt Resistance

For the production of cement clinker a certain amount of liquid phase is required in the production process. The average amount of liquid phase is ~25% and consists mainly of aluminates and ferrites. Moreover, the liquid phase forms a stable coating in the central burning zone, which protects the refractory lining in this highly thermally loaded area. If the process temperature exceeds the standard level (“overheating”) or in the case of an unfavourable composition of the raw meal, the amount of liquid phase increases and the clinker melt easily penetrates deeply into the brick.

The corrosive attack of the supplied clinker melt initially affects the flexibiliser grains, independent of their type, through the dissolution of the alumina and iron components. Therefore, the total amount of soluble components is of major importance regarding the severity of the effects of clinker melt attack. The resistance to clinker melt has been evaluated based on the amount of oxides that contribute to melt formation and are contributed by the flexibiliser. Table III provides an overview of the amount of oxides of the flexibilising additives that can form additional liquid phases in reaction with clinker melt.

The Spinosphere technology (T3) shows superior properties in this regard, as it reduces the amount of oxides contributing to melt formation without reducing the flexibilisation of the brick structure, as does the simple reduction of spinel addition (sample T1). The amount of oxides contributing to melt formation is only 3% using Spinosphere technology compared to 10% with the same amount of conventional MA-spinel.

Case Studies

The new Spinosphere technology has performed impressively in the first references obtained to date.

- Case Study A: In the very first installation, ANKRAL RX was used in the upper transition zone (UTZ) of a rather small but nonetheless challenging kiln due to the use of high amounts of alternative fuels (AF). The kiln was fired with up to 100% AF comprising animal meal, shredded tyres, sewage sludge, wood dust, and plastics. The bricks were installed in the area of 20 to 22 metres, an area usually not protected by stable coating. Figure 5 shows the lining after achieving the expected full campaign of one year, which is usual in this area. The residual thicknesses were between 185–190 mm. The neighbouring lining towards the kiln outlet showed slightly lower residual thicknesses of 170–185 mm. What is significant about this result is the comparison to the adjacent brickwork, which was lined with a brick containing about 16% alumina. This confirms the laboratory results and proves that a brick with such a low alumina content, typical of the Spinosphere technology, behaves mechanically at least as well as bricks containing not only 10% alumina, like standard magnesia MA-spinel bricks, but even equivalent to 16% alumina, which are advertised as being superelastic.

Figure 5.

ANKRAL RX after a full campaign in operation showing slightly higher residual thicknesses compared to the neighbouring lining.

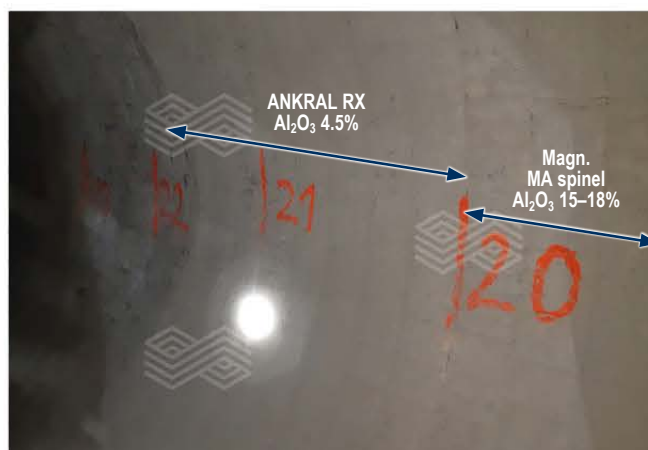


Table III.

Oxide phases contributing to liquid melt of MA-spinel-containing bricks [3] compared to Spinosphere-containing bricks.

| | T1 | T2 | T3 |
|---|-----------|-----------|-------------|
| Spinel type | MA-spinel | MA-spinel | Spinosphere |
| Spinel addition [wt.%] | 5.0 | 15.0 | 15.0 |
| MgO [wt.%] | 33.0 | 33.0 | 79.3 |
| Al ₂ O ₃ [wt.%] | 66.5 | 66.5 | 19.4 |
| Fe ₂ O ₃ [wt.%] | 0.2 | 0.2 | 0.4 |
| CaO [wt.%] | 0.2 | 0.2 | 0.7 |
| SiO ₂ [wt.%] | 0.1 | 0.1 | 0.1 |
| Total Al ₂ O ₃ [wt.%] | 3.3 | 10.0 | 2.9 |
| Total Fe ₂ O ₃ [wt.%] | 0.0 | 0.0 | 0.1 |
| Oxides melt sum | 3.3 | 10.0 | 3.0 |

- Case Study B: In a second installation the targeted lifetime of a year was also achieved. The bricks were installed in the UTZ from metre 27–31 of a 2500 tonne per day kiln with a diameter of 4 metres and a length of 60 metres. This kiln operates at high AF rates of up to 100%. Additionally, the product portfolio also includes the production of sulphate-resistant clinker, which changes a few times a year. Figure 6 shows the lining after 11 months in operation. The hot face groove can still be clearly seen so that the bricks still have the original thickness.

The detailed investigation of a sample reveals deep infiltration of alkali salts up to the cold face of the brick (Figure 7). According to the chemical investigation shown in Table IV, the infiltrate consists mainly of potassium chloride. The most severely infiltrated part of the brick structure shows an intake of up to 9% extrinsic components, which reflects the severity of the chemical attack. The alkali sulphate ratio (ASR) ranges between 15.66 and -2.73. In most sections of the brick there is an alkali overload.

Figure 6.

Lining of ANKRAL RX after a full campaign in operation. The hot face groove of the brick is still visible.



Table IV.

Results of chemical investigation.

| General information | | | | |
|--|-----------------------|---|---------|------------|
| Unit | Cement rotary kiln | | | |
| Position | Upper transition zone | | | |
| Brand | ANKRAL RX | | | ANKRAL RX |
| Sample | 1 | | | |
| Sampling [mm] in distance to the hot face | 50–70 | 120–140 | 180–200 | Data sheet |
| Chemical analyses | Wt. % | Wt. % | Wt. % | Wt. % |
| Loss on ignition (1050 °C) ²⁾ (ISO 26845) | 4.26 | 8.34 | 1.92 | |
| Determination by XRF ¹⁾ (ISO 12677) | | | | |
| MgO | 90.1 | 85.3 | 92.2 | 93.8 |
| Al ₂ O ₃ | 4.38 | 4.01 | 4.38 | 4.5 |
| SiO ₂ | 0.37 | 0.33 | 0.33 | 0.3 |
| CaO | 0.29 | 0.97 | 1.05 | 0.9 |
| MnO | 0.11 | 0.08 | 0.08 | |
| Fe ₂ O ₃ | 0.43 | 0.39 | 0.40 | 0.5 |
| Determination by titration ²⁾ | | | | |
| Chloride | 1.67 | 3.54 | 0.76 | |
| Determination by elemental analysis ^{2) 3)} (DIN 51085) | | | | |
| SO ₃ ⁴⁾ | 0.03 | 0.12 | 0.04 | |
| Determination by ICP-OES ^{2) 5)} (ISO 26845) | | | | |
| Na ₂ O | 0.18 | 0.43 | 0.19 | |
| K ₂ O | 2.49 | 4.83 | 0.59 | |
| Alkali-sulphate ratio, molar ⁶⁾ | | | | |
| $\frac{(K_2O/94) + (Na_2O/62) - (Cl/71)}{(SO_3/80)}$ | 15.66 | 5.64 | -2.73 | |
| ¹⁾ On ignited sample (1050 °C) by X-ray fluorescence analysis | | ⁴⁾ Calculated from the result of the sulphur determination | | |
| ²⁾ On original sample | | ⁵⁾ Optical Emission Spectroscopy by Inductively Coupled Plasma | | |
| ³⁾ High temperature combustion infrared detection technique by LECO | | ⁶⁾ Ideal value 1±0.2 | | |

Microscopic analysis has shown that the Spinospheres have not been corroded by the alkali attack, which is important in order to maintain a certain amount of flexibility when the brick structure is densified with alkali salts.

Conclusion

The new Spinosphere technology enables the development of products with unique characteristics in terms of flexibility and hot properties. Flexibility levels established from standard MA-spinel bricks with an alumina content of 10–12% can be realised in bricks with alumina contents as low as 3%. This opens up completely new possibilities in the development of bricks for cement rotary kilns. This technology not only shows excellent results in laboratory trials but has also proved successful in first applications, in direct comparison to top-grade conventional MA-spinel bricks.

Figure 7.

Cut section of ANKRAL RX sample after one year in service.



References

- [1] Harmuth, H., and Tschegg, E. Fatigue & Fracture of Engineering Materials. *Fatigue & Fracture of Engineering Materials and Structures Ltd.* 1997, 11, 1585–1603.
- [2] Geith, M., Krischanitz, R. and Jörg, S. Influence of Flexibilisers on Basic Cement Rotary Kiln Brick Properties, Proceedings of the 15th Unified International Technical Conference on Refractories, Santiago de Chile, Chile, September 2017, 74–77.
- [3] Geith, M., Krischanitz, R. and Jörg, S. Hybrid Spinel Technology – Basic Refractories for Cement Rotary Kiln Linings with Optimised Flexibility. Proceedings of the 16th Unified International Technical Conference on Refractories, Yokohama, Japan, October 2019, 242–245.

Reprint permission

Reprinted with permission from the *International Cement Review*. Originally printed in June 2020.

Authors

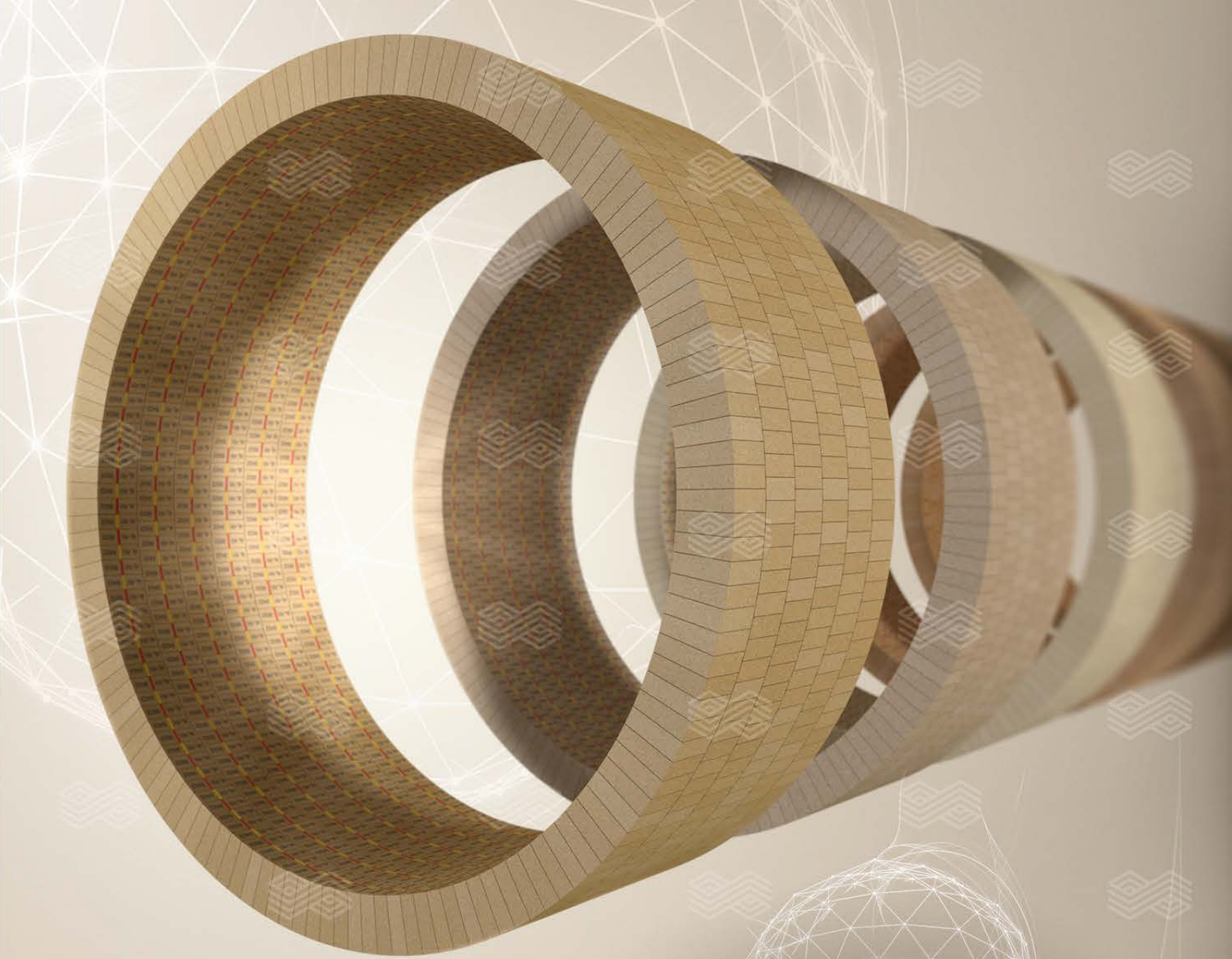
Martin Geith, RHI Magnesita, Leoben, Austria.

Susanne Jörg, RHI Magnesita, Leoben, Austria.

Roland Krischanitz, RHI Magnesita, Vienna, Austria.

Corresponding author: Roland Krischanitz, roland.krischanitz@rhimagnesita.com





ANKRAL X-SERIES

Spinosphere technology by RHI Magnesita

Pushing refractory performance into new spheres

With the new Spinosphere technology you don't have to compromise any longer. Benefit from previously unobtainable brick properties. The novel spinel reduces the alumina content by up to 70%, maximising flexibility without impairing hot properties and clinker melt resistance.

ANKRAL X-Series—improved performance for challenging conditions.

Curious to find out more details?
Visit rhimagresita.com/spinosphere

Follow us



RHI MAGNESITA

Carlos Pagliosa, Haylander Coelho de Avila, Marcelo Borges, Bruno Nery Stoco, Donaldo Silva Orosimbo, Gilvan Nascimento de Souza and Vinicius Teixeira de Morais

Development of Unburned Zero Carbon Alumina–Magnesia Bricks for Steel Ladle Linings

The steel ladle is fundamental to the secondary refining process. The refractories used must be designed to obtain the lowest specific consumption and the lowest possible interaction with the metallic bath. Currently, a lining with carbon (C) in the chemical composition is used in the barrel of the steel ladle. The main goal of this project is to increase the performance potential of the barrel, proposing a tempered alumina-magnesia and C-free brick. This product has superior raw materials compared with the standard one and better compatibility with the current plant production process. The additional benefits of this new concept aim for steel quality, preservation of equipment, and savings in production costs. Another advantage of this product is the formation of the spinel phase at the hot face of the refractory, promoting brick-joint closure and minimising the metallic infiltrations within the lining.

Introduction

The growth of the steel industry in recent years with new technological advances resulted in a more competitive and demanding steel market with consistent product quality and reduced operating costs. Refractories play an important part in the steel industry, enabling steel production with safety and predictability.

Motivation for this work came from the low performance of a steel ladle at Ternium Brazil, directly impacting on an increase in the specific consumption of refractory per tonne of steel produced. One of the main regions with premature wear was the barrel. The main goal of this project was to increase the performance in this zone. The conventional product used was a magnesia-alumina-C brick (MAC) and the proposed solution was an unburned zero-C alumina-magnesia (AM) refractory. Further objectives of this novel product were reducing C-pickup, as well as thermal losses of the metallic bath and shell temperature, as well as eliminating pollutant emissions from the refractory.

Description of the Facilities

Ternium Brazil is a basic oxygen furnace (BOF) steel mill located in Santa Cruz, state of Rio de Janeiro (Brazil), with an average output of 4.5 million tonnes of slabs. The production route consists of two 350 tonne BOF, two ladle treatment stations + bubbling (LTS), two Ruhrstahl-Heraeus (RH) recirculating degassers, one aluminium heating facility (AHF), and finally two continuous casting machines (CCM) with two strands each. All heats go through LTS stations: From there, 50.6% goes to the AHF and the other 49.4% to the RH degasser, before going to the CCM. The flow is shown on Figure 1.

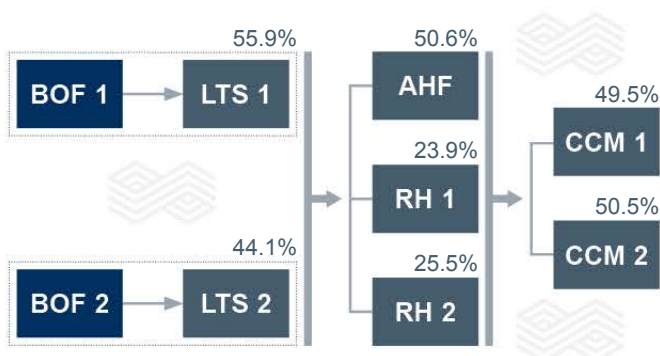
Clean Steel Demand

Clean steel encompasses a multitude of concepts that are based on fulfilling customer requirements. Clean steel can be produced in many ways depending on the existing equipment and detailed customer demands. A common feature of all clean steel production is tight process control along with continuous monitoring. Quality assurance is essential, and it still requires many necessary improvements. There are no specific obstacles to clean steelmaking, as the industrial processes are available, sufficiently understood, and controlled [1].

The major remaining issues to be addressed are disturbances that occur in industrial reality. These require continuous improvements in processes and equipment on the one hand and further development of quality assurance systems for full size control of any possible detrimental effects on the other hand [1].

To meet an increasing demand for cold-rolled (CR) steel sheets of improved mechanical properties, and to cope with the change of the annealing process from a batch-type to a continuous process, it is necessary to establish a technique for making ultra-low carbon (ULC) steel.

Figure 1.
Steel flow at Ternium Brazil.



Particularly, for an economical manufacture of extra deep drawing or high tensile strength CR steel sheet with superior deep drawing properties, it is essential to obtain ULC molten steel with a C-concentration lower than 20 ppm for the steelmaking process. ULC steel is widely used for the automotive industry [1,2].

The composition, quantity, and size distribution of non-metallic inclusions (NMI) in steel determine the quality and performance in application. Over the past decade, ULC steel, also referred to as interstitial free (IF) steel, has been used in automobile parts because of the excellent formability. However, the high quantity of inclusions, especially larger ones, can cause a deterioration of surface properties in ULC steel. In addition to the low C (< 30 ppm) and the low N (< 30 ppm) requirements for obtaining an extraordinary formability and providing a nonaging property, a constraint over the maximum inclusion size (< 100 µm) is also required for ULC steels [3].

The ULC molten steel is produced by two decarburisation steps: 1) in the BOF for reducing the C concentration to approximately 300 ppm, and 2) in the ladle, where vacuum decarburisation in the RH, under reduced partial pressure of CO (carbon monoxide) gas is obtained. Passing the initial quick decarburisation period, when C and O (oxygen) are abundantly available, the decarburisation rate becomes stagnant after a few minutes in the RH degasser. In order to further bring the C down, O must be injected into the liquid steel to speed up the decarburisation reaction. Such O injection contributes to the higher concentration of dissolved O in liquid steel after degassing. Consequently, aluminium addition is necessary for complete deoxidation of the ULC steel. This results in the generation of a large number of indigenous Al₂O₃ (alumina) inclusions after the deoxidation step in the ladle. However, inclusion agglomeration due to Brownian motion, Stokes collision, and liquid steel bath turbulence followed by flotation lead to the inclusion removal [3,4].

The last decarburisation process takes time to reach the desired C-content, which results in a drop in the steel temperature which is offset by increasing the BOF tapping temperature, leading to higher steel cost and placing higher demands on the refractory material [4].

New Refractories for ULC Steel

In order to meet the requirements for the ULC steel quality with strong demand for high-strength and high-toughness plates, some steel customers demand a zero-C brick. Steel ladles are subjected to high temperature effects, aggressive slags, long-lasting metal holding time, and many refining factors that require high-quality refractory products. Usually, the current refractory solution is a fired brick. Standard products such as AMC and MAC bricks are still being used. Natural graphite and the C from the phenolic resin binder have been identified as potential sources for C-pickup [5].

Bricks for ULC steel can be also based on alumina-magnesia compositions and fired over 1500 °C prior to delivery, forming magnesia-alumina (MA) spinel (MgO·Al₂O₃). This new phase presents unique properties as follows: 2135 °C melting point, high mechanical resistance at high temperatures, better corrosion resistance against basic slags than alumina aggregates, low thermal expansion value, similar thermal shock resistance as alumina, high stability under vacuum, and environmentally friendly with no risks of chrome-bearing products [5–7].

MA spinel is the only compound in the MgO-Al₂O₃ system and has a cubic structure. A good combination of physical and chemical properties makes spinel an attractive refractory material for steel. It is important to note that spinel reaction can occur in any proportion between alumina and magnesia and it is temperature and time dependent. Relatively cheap raw materials, such as burned magnesite, sea water magnesia, calcined alumina, or gibbsite can be used [5,6,8].

However, the spinel formation is accompanied by a 5–7% volume expansion, which makes it difficult to develop a dense reaction sintered body. Therefore, a two-step process is usually followed for the sintering of spinel: The first step for spinel formation (900–1200 °C) and the second step for densification (1600–1800 °C). It was found that a partial reaction (55–70% completion) of the oxides was sufficient to overcome the volume expansion barrier, while retaining enough reactivity at sintering temperatures lower than 1640 °C [6,8].

The degree of formation of MgAl₂O₄ secondary spinel governs the expansion behaviour of the brick. This expansion was optimised to achieve sufficient tightening of the brick joints, which prevents liquid metal penetration. Higher expansion may lead to development of stresses, which causes structural spalling. The spinel particles form at the periphery of the periclase grains and play a vital role in determining the refractory property. The formed spinel microstructure minimises the open pores and this densification prevents slag penetration. The structural spalling resistance is increased due to the development of microcracks, due to a mismatch in the coefficient of thermal expansions between MgO (13.5 × 10⁻⁶/°C) and MgAl₂O₄ (7.6 × 10⁻⁶/°C) grains. The higher rate of spinel formation can play a detrimental role because it is associated with substantial volume expansion, which may increase the degree of slag penetration. Thus, careful selection of the MgO quality, the purity and fraction of the aluminous dopant, along with the quantity are of prime importance to improve refractory performance [9].

Unburned alumina-magnesia bricks were developed as a technological alternative for the barrel of the steel ladles for any C-steel with an additional benefit to ULC, for avoiding C-pickup. For all customers, another positive effect is the reduction of the shell temperature due to the low thermal conductivity of the brick. Spinel MgO·Al₂O₃ formation during ladle operation is an expansive reaction that can prevent metal and slag infiltration, better corrosion resistance, closing the joints between the bricks, and operational safety. This paper addresses the development of the unburned AM technology and customer's performance compared to MAC resin bonded bricks.

Unburned Zero-C Alumina-Magnesia (AM) Brick Technology

The unburned AM brick is based on a new binder system for enabling zero C-pickup concerning the production of ULC steel. Instead of using a C-containing binder, the AM product uses a special “K” binder that will be referred to in this paper as “AM-K”. The product was delivered to the customer after tempering at 180 °C, the same as MAC bricks with spinel in situ formation. This expansive reaction inhibits metal infiltration due to coating formation and enables brick-joint closure, promoting better corrosion resistance and operational safety [10].

This new lining project was developed in a steel mill which serves the most sophisticated markets in Brazil and the world, with clients in the segments of civil construction, oil, gas, automobile industry, and others.

In 2018 and 2019 there was a significant reduction in the ladle performance. Figure 2 shows a 13.6% reduction in the average ladle life in 2019 when compared to 2017, due to severe wear in the barrel. After several failure analyses and postmortem studies, the replacement of the MAC product by the AM-K product was indicated due to the new operating conditions at the steel mill.

Methodology

Materials

The conventional product used in the barrel is a magnesia-alumina-carbon refractory brick, resin-bonded and tempered. The product is called MAC. The proposed product for trial in the barrel was an alumina-magnesia refractory brick,

tempered and bonded with a unique C-free binder. The product is called AM-K (1). After the first customer trials, an adjustment was made to the AM-K (1) product, changing some sources of raw material to maximise performance. The adjusted product is also an alumina-magnesia refractory brick, tempered and bonded with a unique C-free binder. This product is called AM-K (2). Table I shows the specification of the three products mentioned in this project.

Methods

Before customer trials, laboratory tests were performed to compare the physical, mechanical, and chemical properties between the MAC and AM-K products. Tests followed internal standards of the Research and Development Center of RHI Magnesita, Contagem (Brazil). For each test, three samples were used. The test result was the arithmetic average. The specimens were produced using new bricks from the production plant. The trials at the customer plant were run in three steps, as shown in Table II. At the end of each ladle campaign, tear-out with technical coverage was carried out with the goal of measuring the remaining refractory thickness and assessing the characteristics of the coating after the campaign end.

Table II.

Trial steps performed with unburned AM bricks.

| Trial Step | Product | Period | # Trials |
|------------|----------|------------------|----------|
| First | AM-K (1) | Dec/18 to Jan/19 | 3 |
| Second | AM-K (2) | Aug/19 to Sep/19 | 2 |
| Third | AM-K (2) | Dec/19 to Jan/20 | 3 |

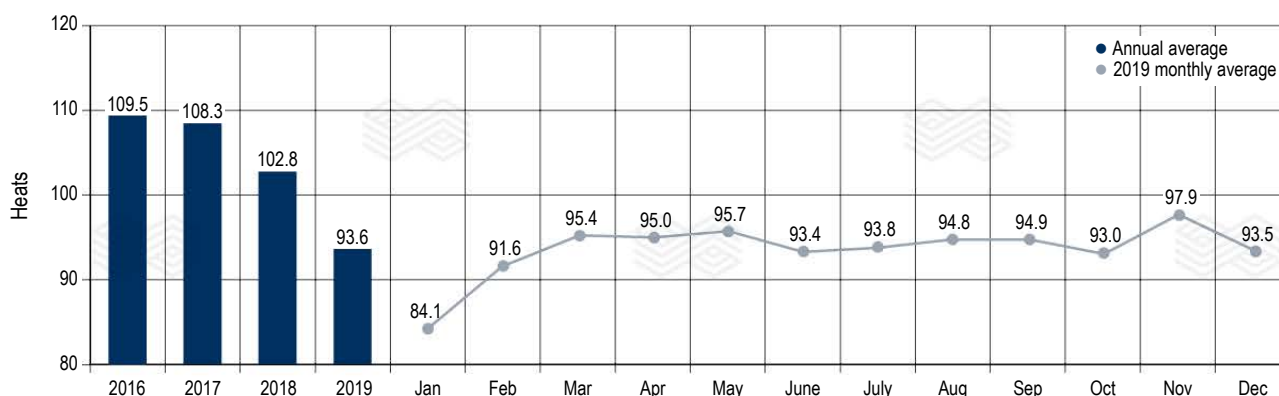
Table I.

Specification of the three products: MAC, AM-K (1) and AM-K (2).

| Product | Al ₂ O ₃ [%] | MgO [%] | Carbon [%] | Binder | Antioxidant |
|----------|------------------------------------|---------|------------|-------------|-------------|
| MAC | 22.8 | 74.8 | 6.7 | Resin | Yes |
| AM-K (1) | 92.2 | 4.7 | No | Special (K) | No |
| AM-K (2) | 94.7 | 4.7 | No | Special (K) | No |

Figure 2.

Steel ladle performance from 2016 to 2019 in a 350 tonne ladle.



The tear-out process with technical coverage took place at the assembly cradle in the steel mill. A pneumatic hammer was used to tear out the barrel in various regions to measure the remaining thickness. Calculations of the wear rate and potential of each layer and region were done.

Results and Discussions

Comparative Evaluation of the Properties Between MAC and AM-K Bricks

The physical and mechanical properties as well as the corrosion resistance are shown in Table III. The density of the AM-K product was higher than the MAC brick at all temperatures due to a higher proportion of raw materials with fewer defects and impurities. The apparent porosity of the AM-K product had a similar behaviour to MAC, mainly after firing at 1400 °C. The main reasons for increasing porosity in MAC were the burning of volatiles and formation of the spinel phase. For the C-free product (AM-K) the predominant factor was only the formation of the expansive spinel phase. Due to differences in the binder system, the AM-K product showed a higher cold crushing strength (CCS) after firing at 1400 °C, while the MAC product had higher CCS after tempering and at 1000 °C. Regarding the elastic modulus, the AM-K product showed an improved behaviour after being exposed to higher temperatures (1400 °C), with a result 3.78 times greater than the MAC product. This can be explained by a smaller number of internal defects in the AM-K.

Table III.

Physical and mechanical properties as well as corrosion resistance of MAC and AM-K.

| Property | MAC | AM-K (1) |
|------------------------------------|-------|----------|
| After tempering at 180 °C/6 h | | |
| Bulk density [g/cm ³] | 2.94 | 3.33 |
| Apparent porosity [%] | 9.97 | 8.41 |
| Cold crushing strength [MPa] | 64.67 | 36.10 |
| Elastic modulus [GPa] | 63.04 | 52.29 |
| After coking at 1000 °C/5 h | | |
| Bulk density [g/cm ³] | 2.88 | 3.27 |
| Apparent porosity [%] | 14.78 | 15.76 |
| Permanent volumetric expansion [%] | -0.54 | 0.15 |
| Cold crushing strength [MPa] | 49.96 | 42.93 |
| Elastic modulus [GPa] | 24.11 | 24.46 |
| After coking at 1400 °C/5 h | | |
| Bulk density [g/cm ³] | 2.79 | 3.16 |
| Apparent porosity [%] | 17.10 | 17.18 |
| Permanent volumetric expansion [%] | 4.16 | 2.19 |
| Cold crushing strength [MPa] | 40.50 | 47.85 |
| Elastic modulus [GPa] | 18.65 | 70.54 |
| Metal corrosion index [%] | 1.6 | 0.5 |
| Slag corrosion index [%] | 82 | 21 |

In the corrosion test, AM-K showed a much better result when compared to MAC. This result was significant for both metal and slag corrosion due the higher sinter ability effect for AM-K that creates a physical barrier for molten slag/metal infiltration.

The AM-K product presented a positive volumetric expansion both at 1000 °C and 1400 °C. Brick-joint closure started earlier than with MAC product during the ladle operation, preventing the penetration of liquid metal. Also, at 1400 °C, the expansion value of the AM-K was lower when compared to the MAC product, with lower stress being generated in the lining.

Figure 3 shows a similar behaviour in the two products when comparing the thermal shock resistance.

Ladle Trial Results

A total of eight linings were tried: Three bricked with the formulation AM-K (1) and five with AM-K (2). During the years that the MAC brand was used, the average ladle life was approximately 96 heats with a remaining safety thickness of 40 mm. The average potential life of the AM-K product was 161 heats, the lowest being 146 heats. Comparing the lowest potential of both brands, the AM-K showed a performance increase of up to 52% higher than the MAC brand, as can be seen in Figure 4.

Figure 3.

Thermal shock resistance for MAC and AM-K (1) bricks

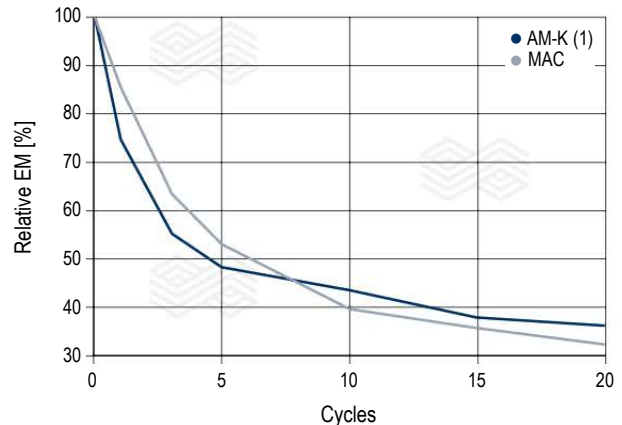
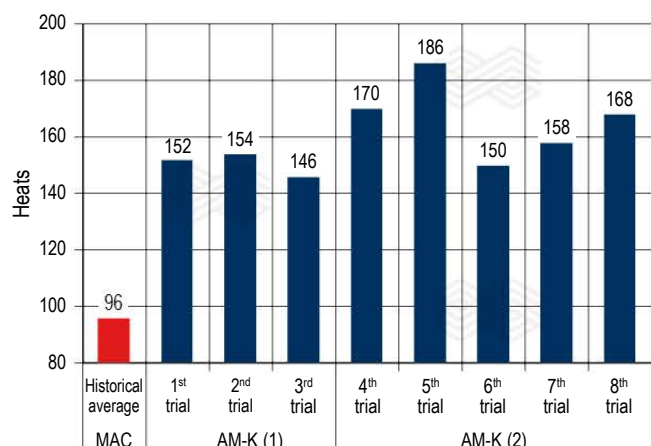


Figure 4.

Comparison of barrel life potential between MAC, AM-K (1), and AM-K (2).



Figures 5 and 6 show the average remaining thickness on the wear profile of linings for MAC and AM-K, respectively. The figures also include the wear rates, considering different end of campaigns limits, 95 heats for MAC and 120 for AM-K, and the potential life for each lining. A noticeable reduction of the wear rate is seen in the AM-K brands, mainly in the south area, where the highest wear was expected. Except for the south area of the ladle, the remaining thickness of the AM-K ladles was vastly higher than 40 mm. This safe remaining thickness could lead to a new design of the barrel to increase the ladle's total internal volume.

Figures 7–9 show a visual inspection of AM-K linings from several stages of the ladle campaign. No drawbacks were noticed at any point.

Figure 10 shows results of the average performance after rolling out of this concept in the operational cycle of this melt shop. The steel ladle with an AM-K lining showed a 23% higher average performance when compared to a MAC lining.

A significant remaining thickness was noticed during tear-out. In the first three trials with the AM-K (1) brand, a parallel crack located 70 mm from the hot face was found. This issue resulted in the development of the second formulation AM-K (2). Field trials certified that the newly designed composition led to a decrease in the distance of this parallel crack to 30 mm.

Figure 5.

MAC ladle thickness profile.

**MAC Average Wear Profile
95 heats**

| Residual [millimeter] | | | | | Wear rate [mm / heat] | | | | | Potential [heat] | | | | |
|--------------------------|-------|------|-------|------|--------------------------|-------|------|-------|------|---------------------|-------|------|-------|------|
| Row | North | West | South | East | Row | North | West | South | East | Row | North | West | South | East |
| 11 | 55 | 50 | 49 | 50 | 11 | 1.02 | 1.07 | 1.29 | 1.07 | 11 | 110 | 105 | 102 | 105 |
| 10 | 47 | 41 | 58 | 47 | 10 | 1.10 | 1.17 | 1.19 | 1.11 | 10 | 102 | 96 | 110 | 101 |
| 9 | 41 | 58 | 50 | 61 | 9 | 1.17 | 0.99 | 1.28 | 0.96 | 9 | 96 | 114 | 103 | 116 |
| 8 | 52 | 84 | 41 | 67 | 8 | 1.05 | 0.71 | 1.37 | 0.90 | 8 | 107 | 157 | 96 | 125 |
| 7 | 59 | 83 | 51 | 66 | 7 | 0.98 | 0.72 | 1.27 | 0.90 | 7 | 114 | 155 | 103 | 124 |
| 6 | 72 | 90 | 52 | 70 | 6 | 0.85 | 0.66 | 1.26 | 0.86 | 6 | 132 | 170 | 104 | 130 |
| 5 | 65 | 85 | | 56 | 5 | 0.92 | 0.71 | | 1.01 | 5 | 122 | 159 | | 111 |
| 4 | 59 | 69 | | 59 | 4 | 0.98 | 0.87 | | 0.98 | 4 | 115 | 128 | | 114 |
| 3 | 50 | 50 | | 62 | 3 | 1.28 | 1.28 | | 1.15 | 3 | 102 | 102 | | 114 |
| 2 | | | | | 2 | | | | | 2 | | | | |
| 1 | | | | | 1 | | | | | 1 | | | | |

Figure 6.

AM-K ladle thickness profile.

**AM-K Average Wear Profile
120 heats**

| Residual [millimeter] | | | | | Wear rate [mm / heat] | | | | | Potential [heat] | | | | |
|--------------------------|-------|------|-------|------|--------------------------|-------|------|-------|------|---------------------|-------|------|-------|------|
| Row | North | West | South | East | Row | North | West | South | East | Row | North | West | South | East |
| 11 | 104 | 108 | 77 | 101 | 11 | 0.40 | 0.37 | 0.78 | 0.43 | 11 | 282 | 307 | 168 | 261 |
| 10 | 107 | 110 | 82 | 105 | 10 | 0.37 | 0.35 | 0.74 | 0.39 | 10 | 299 | 321 | 176 | 286 |
| 9 | 112 | 113 | 80 | 115 | 9 | 0.33 | 0.32 | 0.76 | 0.31 | 9 | 336 | 345 | 173 | 362 |
| 8 | 109 | 115 | 64 | 120 | 8 | 0.35 | 0.31 | 0.89 | 0.27 | 8 | 316 | 364 | 146 | 418 |
| 7 | 110 | 119 | 88 | 121 | 7 | 0.35 | 0.28 | 0.69 | 0.26 | 7 | 321 | 405 | 190 | 429 |
| 6 | 113 | 122 | 80 | 120 | 6 | 0.32 | 0.25 | 0.76 | 0.26 | 6 | 348 | 441 | 173 | 426 |
| 5 | 116 | 122 | 89 | 120 | 5 | 0.30 | 0.25 | 0.68 | 0.27 | 5 | 376 | 442 | 192 | 418 |
| 4 | 115 | 122 | 89 | 122 | 4 | 0.31 | 0.25 | 0.68 | 0.25 | 4 | 365 | 451 | 192 | 442 |
| 3 | 131 | 112 | 106 | 110 | 3 | 0.33 | 0.49 | 0.54 | 0.51 | 3 | 392 | 268 | 241 | 259 |
| 2 | 155 | 141 | 136 | 141 | 2 | 0.62 | 0.73 | 0.77 | 0.73 | 2 | 305 | 258 | 244 | 258 |
| 1 | 156 | 177 | 168 | 169 | 1 | 0.61 | 0.43 | 0.51 | 0.50 | 1 | 311 | 436 | 370 | 375 |

Figure 7.

Visual inspection of two ladles at the beginning of the campaign.

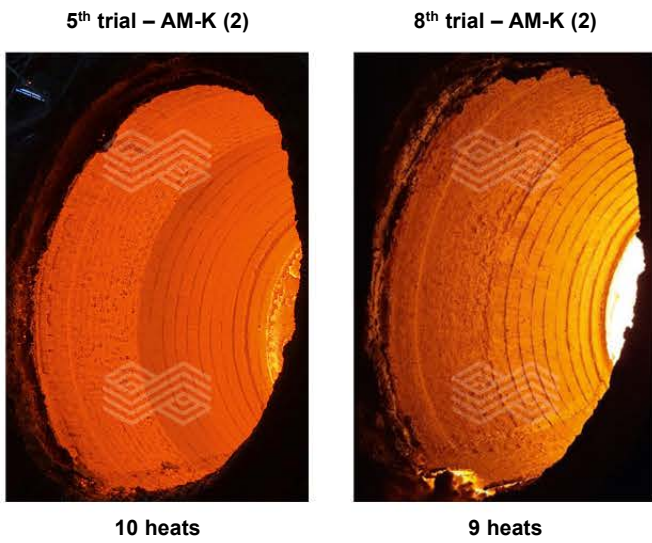


Figure 8.

Visual inspection of two ladles in the middle of the campaign.

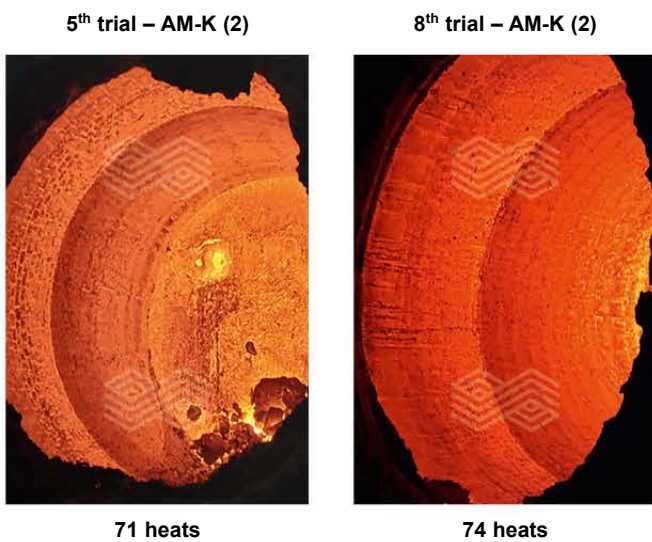


Figure 9.

Visual inspection of two ladles at the end of the campaign.

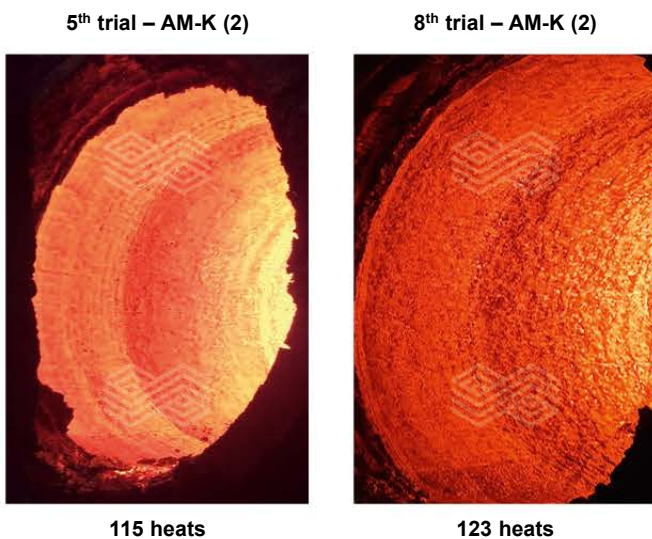


Figure 11 shows the current behaviour. Additional benefits, other than the lower wear rate, were also accomplished with the AM-K lining. One of the most significant was the lower bath temperature loss. More than 220 steel temperature samples were taken just prior to the ladle leaving the first secondary metallurgy station and just after it arrived in the second station. A comparison between both linings was made and the results are shown in Figure 12. A decrease of 8% was achieved in bath temperature loss, which led to a lower consumption of raw materials by the customer for maintaining the desired temperature.

Figure 10.

Average performance comparison between MAC and AM-K lining.

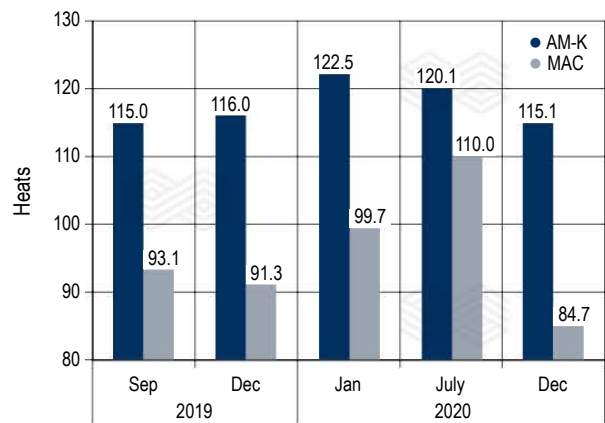
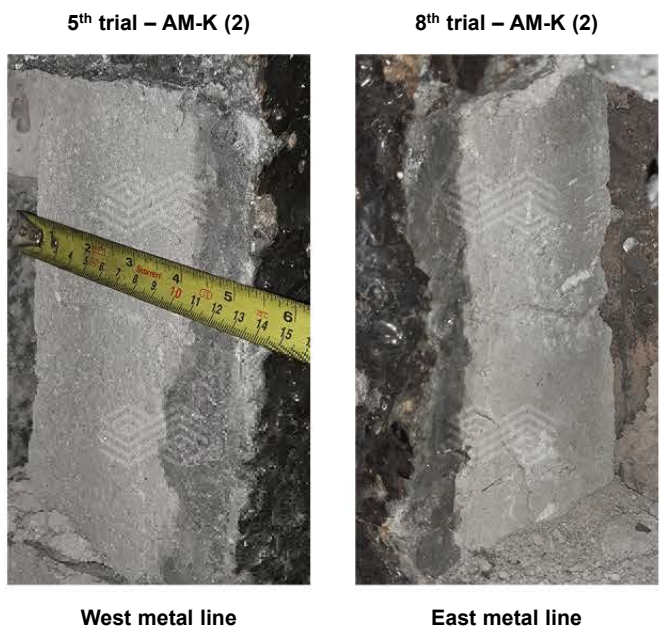


Figure 11.

AM-K bricks after 115 and 123 heats.

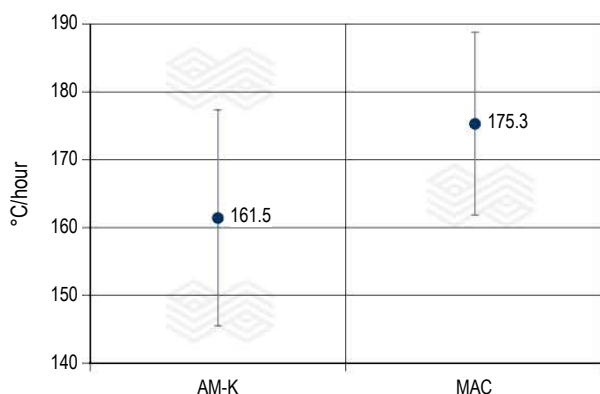


Another expected benefit was a lower steel shell temperature with the AM-K ladles. Customers usually use thermal insulating splits behind the safety lining to decrease the shell temperature, in order to preserve the mechanical properties of the ladle structure and extend the lifetime. AM-K bricks may also contribute to achieving this goal and the insulating thickness could be decreased. It could be an essential contribution to reducing insulation costs. The homogenisation of the temperature distribution throughout the whole lining avoids temperature concentrations, minimising thermomechanical failures and higher wear rates of the barrel.

Shell temperatures were taken using a thermographic camera when ladles arrived at the continuous casting machine. Since the AM-K lining is C-free, with lower thermal conductivity and a lower wear rate, brick thickness was better preserved and may reflect in a better insulating behaviour. The probability of a lower shell temperature is under evaluation.

Figure 12.

Comparison of bath temperature loss in MAC and AM-K linings.



Final Considerations

The AM-K lining demonstrated an outstanding behaviour in severe operational conditions at this Brazilian customer, showing a significant reduction of the wear rate and increasing the potential performance. The minimum campaign expectation was 146 heats, which is 52% higher than the typical MAC lining. Consistent extra remaining thickness may lead to an optimisation of the refractory profile, reducing specific consumption and increasing the internal volume of the ladle. Adjustments applied to the first AM-K (1) concept to the AM-K (2) were extremely positive to boost the lining performance.

In addition to this remarkable performance increase, a lower bath temperature loss of nearly 8% was a noticeable benefit mostly due to the zero-C lining, which can also eliminate any possibility of C-pickup from the refractory. The assessment regarding the shell temperature is currently under way.

References

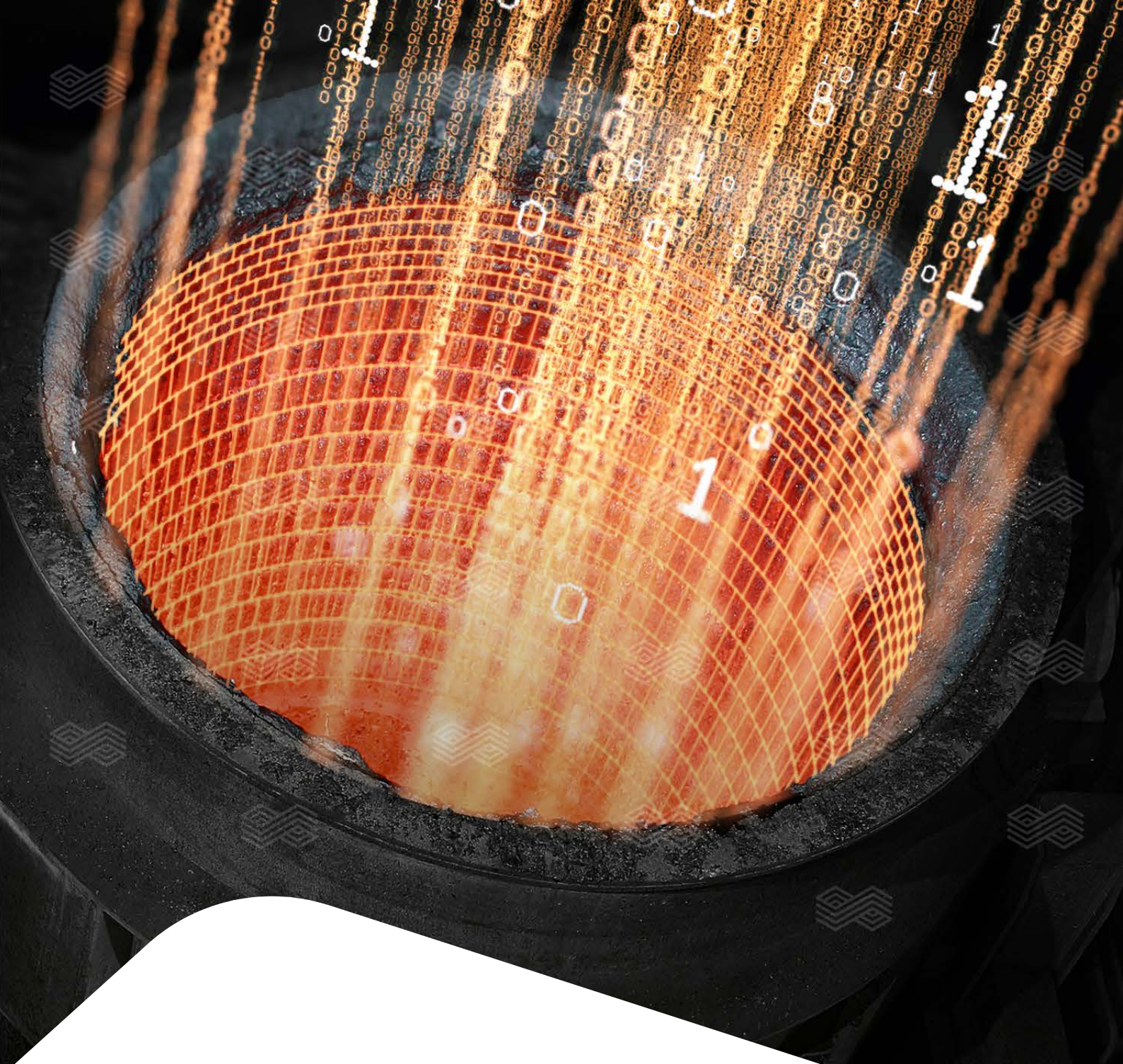
- [1] Wünnenberg, K. IISI study on clean steel. *La Revue de Métallurgie-CIT*. Octobre 2005, 687–692.
- [2] Lee, S., Saito, Y., Park K. and Shin D.H. Microstructure and mechanical properties of ultralow carbon IF steel processed by accumulative roll bonding process. *Material Transaction*. 2002, 43, 9, 2320–2325.
- [3] Pande, M.M., Guo, M., Dumarey, R., Devisscher, S. and Blanpain, B. Determination of steel cleanliness in ultra low carbon steel by pulse discrimination analysis-optical emission spectroscopy technique. *ISIJ International*. 2011, 51, 1778–17871.
- [4] Sumida, N., Fujii, T., Oguchi, Y., Morishita, H., Yoshimura, K. and Sudo, F. Production of ultra low carbon steel by combined process of bottom blow converter and RH degasser. *Kawasaki Technical Report*. 1983, 8, 69–76.
- [5] Pagliosa, C., Campos, A., Freire, N. and Loeffelholz, M. MAC bricks for steel ladle – Novel Technology to Metal Line. Proceedings AISTech 2013, 1, 796–801.
- [6] Sainz, M.A., Mazzoni, A.D., Aglietti, E.F. and Caballero, A. Thermomechanical stability of spinel (MgO-Al₂O₃) under strong reducing conditions. *Materials Chemistry and Physics*. 2004, 86, 399–408.
- [7] Aksel, C., Rand, B., Riley, F. L. and Warren, P. D. Thermal shock behaviour of magnesia-spinel composites. *Journal of the European Ceramic Society*. 2004, 24, 2839–2845.
- [8] Tripathi, H. S., Mukherjee, B., Das, S., Haldar, M. K., Das, S. K. and Ghosh, A. Synthesis and densification of magnesium aluminate spinel – effect of MgO reactivity. *Ceramics International*. 2003, 29, 2, 915–918.
- [9] Mishra, R., Mukhopadhyay, S., and Chatterjee, S. Spinel Bonded MgO-C refractories for steel ladle applications. Proceedings AISTech 2006, 1, 809–813.
- [10] Pagliosa, C. et al. Novel Unburned Alumina-Magnesia Bricks for ULC Steel: Zero-Carbon and Zero-Fume Refractory. Pittsburgh: Proceedings AISTech 2016, 1339–1346.

Authors

Carlos Pagliosa, RHI Magnesita, Contagem, Brazil.
 Haylander Coelho de Avila, RHI Magnesita, Volta Redonda, Brazil.
 Marcelo Borges, RHI Magnesita, Contagem, Brazil.
 Bruno Nery Stoco, Ternium, Rio de Janeiro, Brazil.
 Donald Silva Orosimbo, Ternium, Rio de Janeiro, Brazil.
 Gilvan Nascimento de Souza, Ternium, Rio de Janeiro, Brazil.
 Vinicius Teixeira de Morais, Ternium, Rio de Janeiro, Brazil.

Corresponding author: Haylander Coelho de Avila, Haylander.Avila@rhimagnesita.com





Lifetime prediction with the power of AI Automated Process Optimization (APO)

APO, our unique and patented automated process optimization, uses artificial intelligence to calculate a digital twin of your refractories in order to make refractory lifetime predictable. Meaning: Increased safety, optimized production, and fewer production losses.

Curious to experience APO in more detail?

Then contact us to receive a free online live presentation carried out by our experts.

Visit rhimagresita.com/apo-wear-lifetime-prediction-with-the-power-of-ai/

Follow us



RHI MAGNESITA

Sabine Gschiel, Stefan Eder, Norbert Freiberger and Christoph Bauer

A Novel Raw Material Developed for Slide Gate Plate Technology

Zirconia spinel is a raw material with high potential for the use in slide gate plates. Its application results in an improved thermal shock resistance together with a positive influence on the corrosion resistance. An important aspect is to achieve a microstructure that provides the required effectiveness during application. A modified production technology enables the production of zirconia spinel with finely dispersed ZrO_2 precipitations. Compared to the application of standard zirconia spinel, positive effects of the new material on the thermal shock and corrosion resistance of slide gate plates was demonstrated.

Introduction

Slide gate plates are required to withstand enormous stresses in service. On the one hand, a high thermal shock resistance is required, on the other hand, a high corrosion, erosion, and abrasion resistance is necessary to avoid serious wear by steel and/or slag. These two requirements are usually in conflict with each other. Measures which increase the thermal shock resistance typically have negative influences on the corrosion resistance and vice versa, for example, the application of zirconia corundum or zirconia mullite. However, the use of zirconia spinel has a high potential to fulfil both requirements [1,2]. It provides the ability to induce a high thermal shock resistance, while also providing good corrosion resistance. The raw material's microstructure has a significant influence on the overall effectiveness. An alternative production route was developed to obtain zirconia spinel with an optimised, tailor-made microstructure for targeted applications. The influence of this new zirconia spinel on the properties was studied in detail to prove the effectiveness of the novel raw material for slide gate plates.

Use of Zirconia Spinel in Slide Gate Plates

Slide gate plates containing standard zirconia spinel show very good performance, especially under aggressive conditions. They are characterised by a high strength and excellent corrosion resistance combined with a reasonable thermal shock resistance. The microstructure has an important influence on the effectiveness. The standard zirconia spinel produced by electric arc melting shows partly large, drop-like ZrO_2 precipitations surrounded by MA spinel. In comparison, zirconia corundum contains finely dispersed ZrO_2 precipitations within alumina, leading to a more homogeneous microstructure. Therefore, an improved microstructure for zirconia spinel is required to enable the best possible performance of slide gate plates containing zirconia spinel. Two options were considered to obtain a modified structure for new zirconia spinel. On the one hand, chemical variations would lead to different phase precipitation routes. The other possibility is a modified production procedure where by only fine ZrO_2 precipitations are obtained.

Production and Characterisation of the New Zirconia Spinel

Standard zirconia spinel is produced by melting dead burned magnesia, alumina, and zirconium oxide raw materials in an electric arc furnace. The raw materials have similar grain sizes, ranging from 0 to 1 mm, to prevent demixing due to the varying densities and to ensure good flowability for the continuous feeding system. Before feeding the mixture into the vessel, a safety layer of coarse dead burned magnesia grains is placed on the bottom of the vessel. On top of the first raw material layer, another thin Y-shaped layer of carbon is placed to provide the contact with the electrodes during the ignition phase. After melting, the whole block slowly cools and is then crushed and refined to obtain the required grain size fractions.

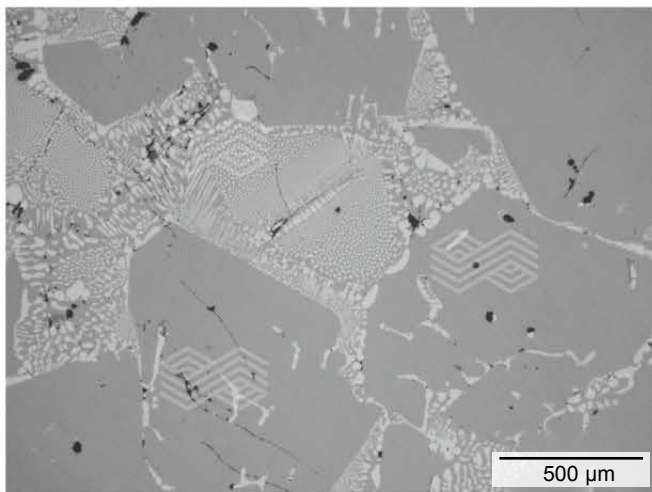
During the cooling process of the ingot, ZrO_2 precipitates in different sizes. On the one hand, fine and crystallographically orientated ZrO_2 segregations form lamellae within MA spinel crystals. On the other hand, large and drop-shaped ZrO_2 precipitates around lamellae-free MA spinel. Common appearance of the large, drop like zirconia precipitations implicate microstructural drawbacks due to an inhomogeneous distribution of crucial material components. The amount of large zirconia drops increases from the top to the bottom of the fused ingot. This is a result of sedimentation of ZrO_2 in the melt and prolonged time for recrystallisation at the bottom of the fused block. The microstructure of the zirconia spinel is shown in Figure 1.

To avoid larger precipitations, an alternative production route was designed. Similar to the standard procedure the solid raw materials consisting of dead burned magnesia, alumina, and zirconium oxide were melted in an electric arc furnace. A rapid cooling sequence was achieved via a spraying process. To achieve this, the vessel was carefully tilted after the mixture reached the liquid state, and the melt stream was subsequently atomised with compressed air mixed with water through a water-cooled channel. A heat resistant curtain placed at the end of the channel collected the rapidly cooled, solidified, white coloured zirconia spinel spheres. The production is currently limited to laboratory scale.

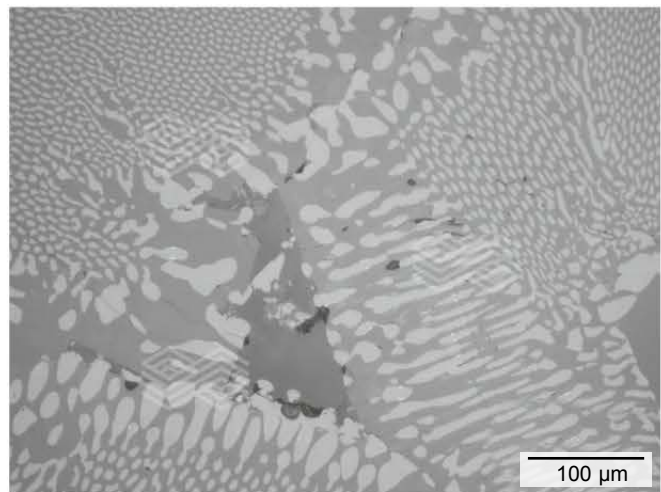
However, the new production route has several advantages. One aspect is the finely dispersed spherical structure, which cannot be obtained by the slow standard cooling procedure of a melting block. A portion of the material can be used without refining. In addition, the crushing and refining of the coarser spheres is easier and less resource intensive, when compared to the processing of the large fused ingot. Figure 2 shows the different zirconia spinel materials after cooling.

Figure 1.

Microscopic images of slowly cooled zirconia spinel (zirconia: bright; spinel: grey; interstitial phase: dark grey).



(a)



(b)

Figure 2.

(a) transverse section through the slowly cooled zirconia spinel block (width approximately 700 mm) and (b) rapidly cooled zirconia spinel spheres resulting from the spray crystallisation method.



(a)



(b)

A more significant impact of the rapid cooling procedure was observed in the size of the zirconia crystal and matrix intergrowth. The initial observation of the general microtexture was similar to the standard material comprised of the two varieties of MA spinel and zirconia intergrowth, however significant differences were observed when comparing the size and homogeneity of the dispersed precipitations. While the minimum thickness of ZrO_2 lamellae in the standard material was $> 1 \mu m$, the rapidly cooled material produced ZrO_2 lamellae at the nanometer scale ($\sim 200 \text{ nm}$). Large, drop-shaped precipitations were insignificant. Figure 3 shows a typical microstructure of the new zirconia spinel.

According to the bulk chemical composition and phase components, significant differences cannot be detected. The spinel is stoichiometric.

Usage of the New Zirconia Spinel in Slide Gate Plates

Production of Slide Gate Plates

The zirconia spinel was crushed and sieved to obtain two grain sizes which were used for the production of test plates. The main raw material was alumina, in addition to further additives, such as carbon carriers and antioxidants. Resin was used as a binder. For comparison, test plates containing zirconia corundum instead of zirconia spinel were prepared in parallel. The following test series were investigated:

- Test series 1: Zirconia corundum
- Test series 2: Zirconia spinel (standard)
- Test series 3: Zirconia spinel (new, rapidly cooled)

The mixing and pressing process was carried out according to the internal standard procedure applied for slide gate production. For each test series the same conditions were maintained with regards to mixing time, mixing sequence, aging, and pressure. The plates were fired under reducing conditions. The samples were tested without impregnation.

Investigation and Results

Standard investigations, including the measurement of bulk density, porosity, cold modulus of rupture (CMOR), thermal expansion, and chemical analysis, were carried out. The results showed minimal differences between test series 2 (standard zirconia spinel) and test series 3 (rapidly cooled zirconia spinel). Test series 1 (zirconia corundum) showed higher bulk density and relative to the raw materials, higher Al_2O_3 and lower MgO and ZrO_2 concentrations. The physical properties are summarised in Table I.

Table I.

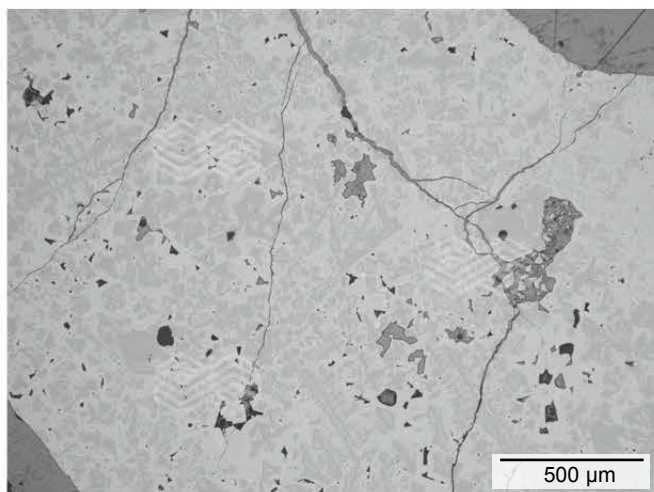
Physical and chemical characterisation of the three-test series.

| Physical properties | 1 | 2 | 3 |
|-------------------------------------|------|------|------|
| Density [g/cm^3] (DIN EN 933-1) | 3.0 | 3.0 | 3.0 |
| Porosity [%] (DIN EN 993-1) | 12.0 | 13.5 | 15.0 |
| CMOR [N/mm^2] (DIN EN 993-6) | 35 | 28 | 26 |
| Young's modulus [kN/mm^2] | 100 | 75 | 70 |
| Thermal expansion [%] (DIN 51045-1) | 1.2 | 1.0 | 1.2 |

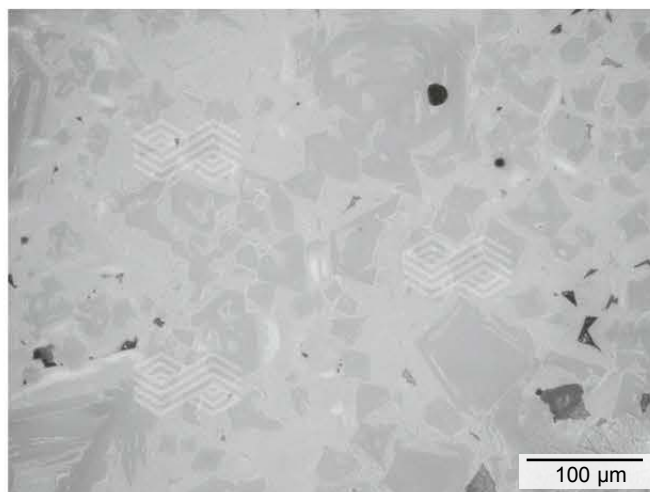
Thermal shock resistance and corrosion resistance were investigated to provide further information. The thermal shock resistance was measured by a dipping test where the specimens were dipped ten times into a steel bath at a temperature of $1600 \text{ }^\circ C$. After each dipping, the specimens were checked for cracks and spalling. After the tenth cycle, the test was stopped and the specimens were compared. The most impressive results were achieved with test series 3, containing the new zirconia spinel, fine cracks had formed after four thermal cycles and minor modifications could be detected. Test series 2 showed several broken edges and earlier crack formation. The thermal shock resistance of test series 1 was the lowest, when compared to both specimens containing zirconia spinel, due to large pieces that broke off. The results are summarised in Table II and shown Figure 4.

Figure 3.

Microscopic images of rapidly cooled zirconia spinel (zirconia: bright; spinel: grey).



(a)



(b)

Table II.

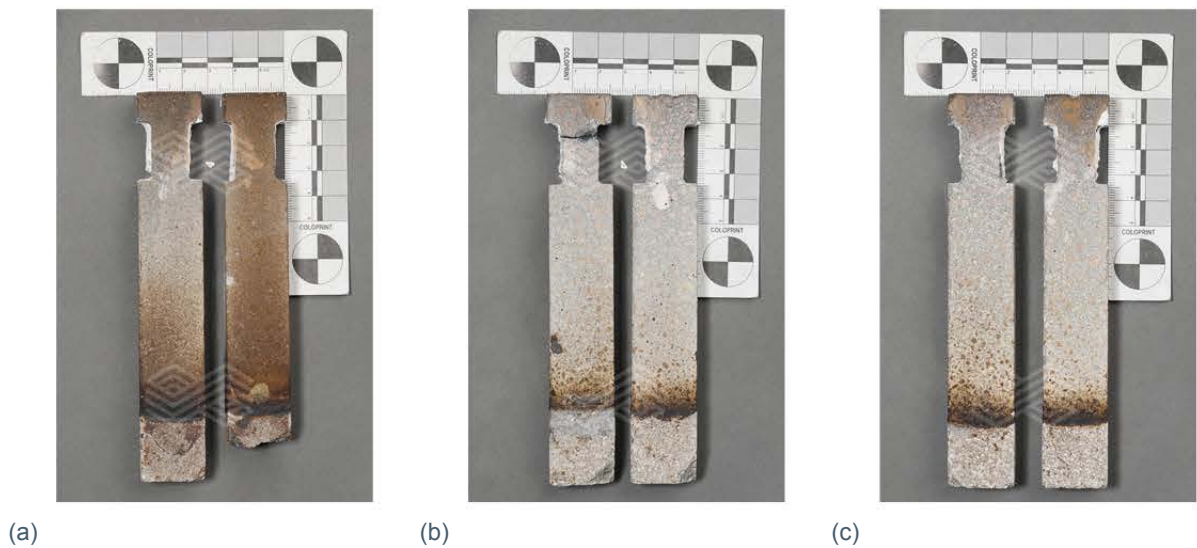
Results of thermal shock test; the lower the number of thermal cycles the specimen undergo prior to showing alteration, the lower the thermal shock resistance is assumed be.

| Test series | 1 | 2 | 3 |
|--------------------------------|------------------------|--------------|-------------------|
| Cycle of first crack formation | 2 | 3 | 4 |
| Appearance after test | Large pieces broke off | Broken edges | Minor alterations |

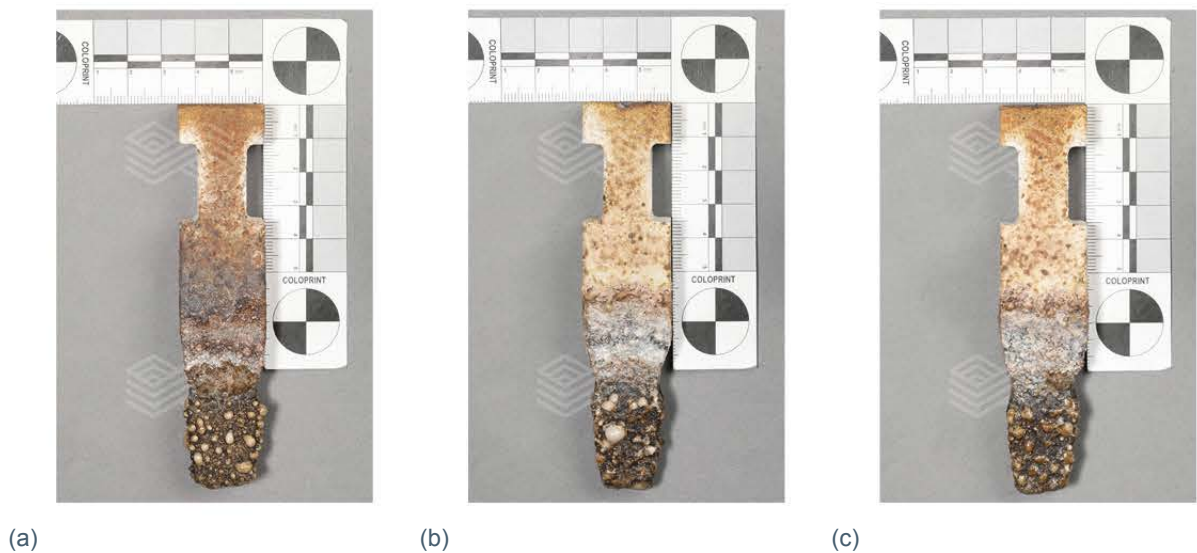
Corrosion resistance was tested with an in-house developed, comparative method where the finger-shaped test specimen were dipped into a crucible filled with an aggressive basic slag containing a high content of manganese oxide at a temperature of 1600 °C under argon purging. The specimen holder was rotated to simulate slag movement and to obtain a more aggressive environment. After two hours the samples were removed from the slag to be evaluated. Although not impregnated (as standard products are), all test series showed a desirable corrosion resistance. As expected, the sample containing zirconia corundum showed a slightly lower wear. Macroscopically, the two chemically equivalent materials containing standard and rapidly cooled zirconia spinel had a comparable corrosion rate. The results are shown in Figure 5.

Figure 4.

Test specimens after thermal shock test: (a) zirconia corundum, (b) zirconia spinel standard, and (c) rapidly cooled zirconia spinel (scale bar division 1 cm).

**Figure 5.**

Test specimens after corrosion test: (a) zirconia corundum, (b) zirconia spinel standard, and (c) rapidly cooled zirconia spinel (scale bar division 1cm).



Detailed investigations showed a slightly better corrosion resistance for test specimen 3 with rapidly cooled zirconia spinel.

The cyclic softening under load was tested for test series 2 and 3 and showed comparable results, indicating that both materials can generally withstand the high stresses of cyclic loading up to 1500 °C. Maximum expansion was slightly higher for test series 2 at 2.3 %, compared to test series 3 with a maximum expansion of 2.2 % (Figure 6). Test series 3 containing the new zirconia spinel indicated a slightly increased absorbance of thermomechanical stresses due

Figure 6.

Softening under load: Linear expansion (Lin%) dependence on time and temperature.

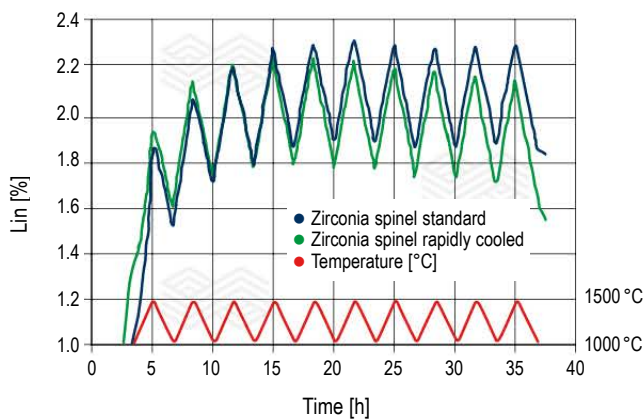
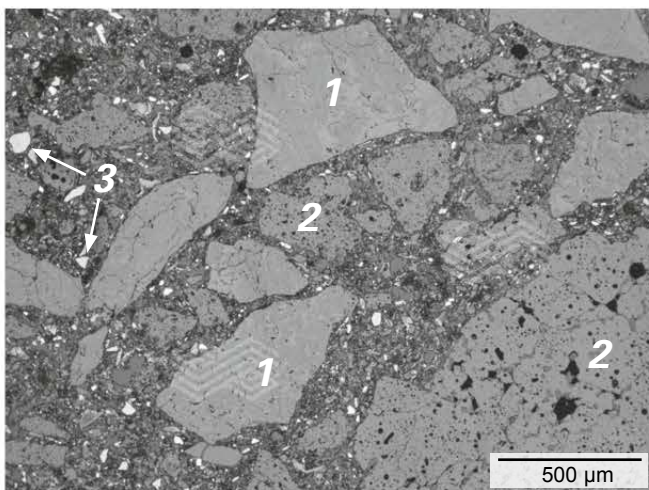
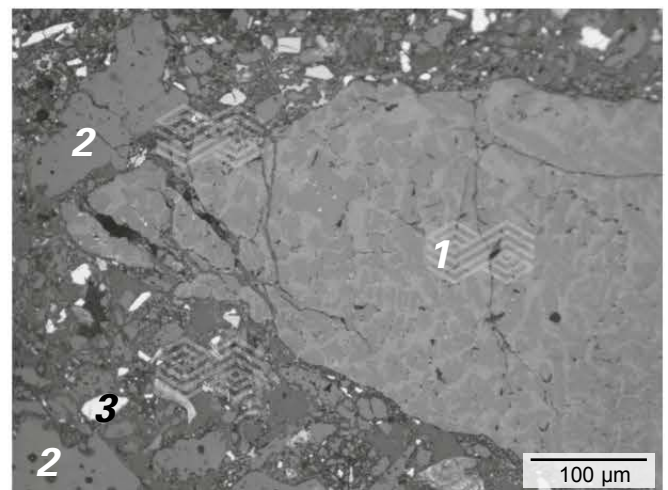


Figure 7.

Microstructure of test series 1 with zirconia corundum: Zirconia corundum (1), tabular alumina (2), and antioxidants (3).



(a)



(b)

to softening, whereas peak maxima of test series 2 show negligible fluctuation. Accordingly, sample 2 showed fine cracks at the surface whereas test sample 3 with rapidly cooled zirconia spinel did not show any defects after testing.

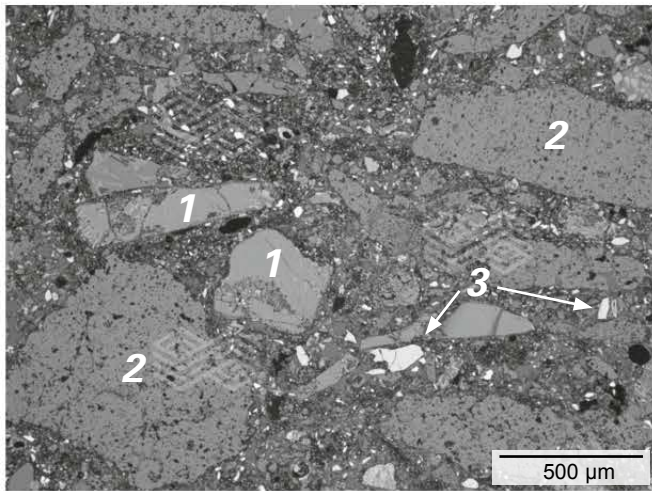
The microscopical investigation of the plates after firing revealed a dense and homogeneous microstructure for all tested samples. Zirconium corundum grains of test series 1 showed a compact structure with minimal flaws (Figure 7), while the standard zirconia spinel grains in the refractory matrix partly showed cracks and large ZrO_2 precipitations (Figure 8). The spherical structure of the new, rapidly cooled zirconia spinel could be detected in the microscopic images of test specimen 3 (Figure 9). A compact structure could be detected for this new zirconia spinel. This might be an explanation for the improved corrosion resistance compared to standard zirconia spinel.

Results/Conclusion

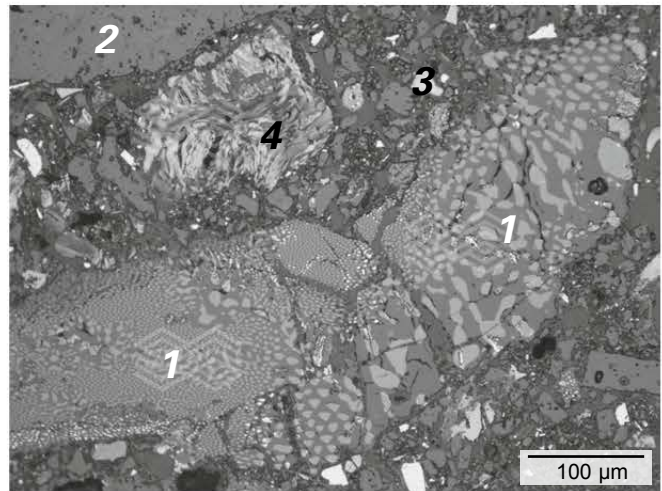
It has been demonstrated that the application of rapidly cooled zirconia spinel leads to elevated thermal shock resistance while the physical properties and corrosion resistance remain on a high level. This was achieved by an alternative zirconia spinel production process leading to a more homogeneous distribution of sub- μm ZrO_2 segregations. Subsequent studies will evaluate the potential of modified zirconia spinel bulk compositions.

Figure 8.

Microstructure of test series 2 with zirconia spinel—standard. Large ZrO_2 precipitations: Zirconia spinel (1), tabular alumina (2), antioxidants (3), and carbon (4).



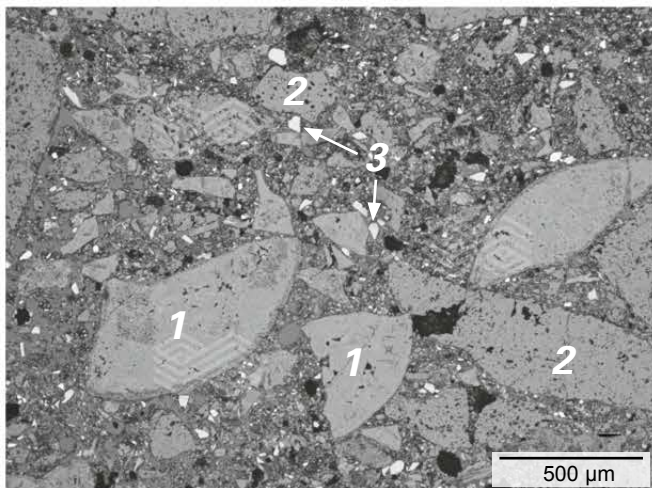
(a)



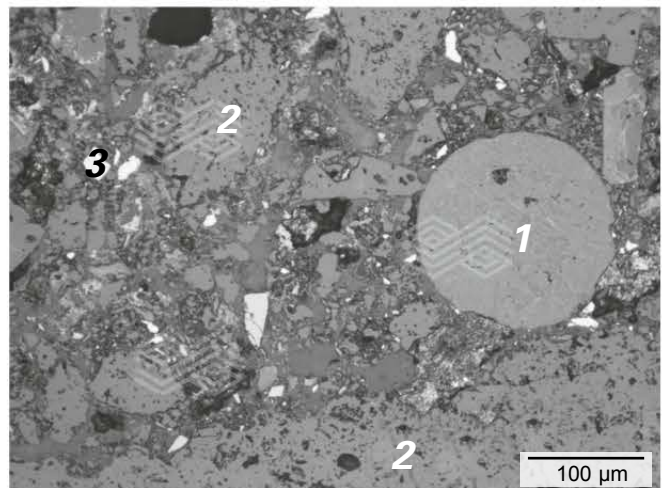
(b)

Figure 9.

Microstructure of test series 3 with zirconia spinel—fast cooled: Zirconia spinel (1), tabular alumina (2), and antioxidants (3).



(a)



(b)

References

- [1] Müller, M.A., Nilica, R., Wiesel, M., Mühlhäußer, J. and Grasset-Bourdel, R. Versatz zur Herstellung eines kohlenstoffgebundenen oder harzgebundenen geformten feuerfesten Erzeugnisses, ein Verfahren zur Herstellung eines solchen Erzeugnisses, ein solches Erzeugnis sowie eine Verwendung von Magnesiaspinell-Zirkonoxid. EP 2 848 598 A1, 2013.
- [2] Coes, L. Jr. Fused zirconia-spinel abrasives and articles made therewith. US 3 498 769 A.

Authors

Christoph Bauer, RHI Magnesita, Leoben, Austria.
 Stefan Eder, RHI Magnesita, Leoben, Austria.
 Norbert Freiberger, RHI Magnesita, Leoben, Austria.
 Sabine Gschiel, RHI Magnesita, Leoben, Austria.

Corresponding author: Sabine Gschiel, sabine.gschiel@rhimaginesita.com



Paulo Souza, Samuel Oliveira, Eric Almeida, Marina Campos, Anderson de Paula, Tito Hugo, Gabriel Gomes, Gregor Lammer, Romulo Batista Baitz and Joao Berganholi

Automated Process Optimization at the RH Degasser in Gerdau Ouro Branco—Results After 2 Years of Operation

Gerdau Ouro Branco (GOB) is the largest plant facility of the Gerdau Group with an annual production of 3.8 million tonnes of steel and the only producer of slabs, blooms, and billets in Brazil. Following the group's vision of providing the market with more added value finished products, a major investment in a new heavy plate rolling mill facility was made a few years ago. More than ever, secondary metallurgy is playing a very important role, specifically the RH degasser facility. With oxygen top blown capabilities, this equipment is the only one capable of achieving the very challenging steel specifications where minimum hydrogen, nitrogen, and carbon contents are required for the oil/gas and automobile industries. Due to the intense flow of different phases (gas, liquid slag, liquid steel, and solid phases), refractory erosion/corrosion is very high in RH degasser vessels, which decreases productivity, consequently increasing the steelmaking costs. Furthermore, the vessel operates under very low pressure and the geometry prevents hot inspection between heats. In alignment with customer requirements, RHI Magnesita developed an online refractory wear prediction model: Automated Process Optimization (APO) for the lower RH degasser vessel. APO helped the process and operational engineers over the past two years to make data-driven decisions when it came to refractory cost, operational productivity, and safety. This paper describes the development of APO for the RH degasser and shows the technical and financial results achieved.

Introduction

In recent years, the steel industry has recorded a very strong increase in demand, with the production levels on par with that only previously experienced in the early fifties when the world steel outputs increased by around 5–7% yearly [1]. Along with the increased demand, the requirement for a cleaner steel increases every year, forcing the industry to rapidly adapt to new requirements and specifications [2].

The term clean steel means a low or ultra-low level of impurity elements such as nitrogen, hydrogen, sulphur, phosphorus, and even carbon. Also, a very controlled level of inclusions is required when it comes to size distribution, morphology, and composition [2]. Table I summarises the maximum impurity fractions and the maximum inclusion size for different end users. Highlighted in light blue are specifications only achievable when using a vacuum degasser facility.

Table I.

Typical steel cleanliness requirements for various steel grades [2].

| Steel product | Maximum impurity fraction | Maximum inclusion size |
|--------------------------------------|---|--|
| IF steel | [C]≤30ppm, [N]≤40ppm, T.O.≤40ppm, [C]≤10ppm, [N]≤50ppm | |
| Automotive & deep-drawing sheet | [C]≤30ppm, [N]≤30ppm | 100 µm |
| Drawn and ironed cans | [C]≤30ppm, [N]≤30ppm, T.O.≤20ppm | 20 µm |
| Alloy steel for pressure vessels | [P]≤70ppm | |
| Alloy steel bars | [H]≤2ppm, [N]≤10-20ppm, T.O.≤10ppm | |
| HIC resistant steel (sour gas tubes) | [P]≤50ppm, [S]≤10ppm | |
| Line pipe | [S]≤30ppm, [N]≤35ppm, T.O.≤30ppm, [N]≤50ppm | 100 µm |
| Sheet for continuous annealing | [N]≤20ppm | |
| Plate for welding | [H]≤1.5ppm | |
| Ball bearings | T.O.≤10ppm | 15 µm |
| Tyre cord | [H]≤2ppm, [N]≤40ppm, T.O.≤15ppm | 10 µm |
| Non-grain orientated magnetic sheet | [N]≤30ppm | |
| Heavy plate steel | [H]≤2ppm, [N]≤30–40ppm, T.O.≤20ppm | Single inclusion 13 µm Cluster 200 µm |
| Wire | [N]≤60ppm, T.O.≤30ppm | 20 µm |

When it comes to clean steel production, the vacuum degasser facilities are the most important reactor in secondary metallurgy. This is due to their unique capabilities to reach very low levels of C, N, and H in the steel in addition to heating and desulphurisation capabilities, which other reactors can also do. Therefore, it is unsurprising that the installation of vacuum facilities worldwide has inevitably increased tremendously in the last two decades as can be seen in Figure 1 [3].

In line with this developing trend within the steel industry, Gerda Group, the 30th largest steel producer in 2019 with 13.13 million tonnes [4], has invested in a hot rolling mill facility during the past years to produce plates for the oil and gas industry at the integrated steel shop unit in Ouro Branco (Brazil). RHI Magnesita has a long-term partnership with the Gerda Group globally. Since 2010, RHI Magnesita has had a cost per performance (CPP) contract that ranges from refractory products to installation services and therefore, the main refractory solutions partner from blast furnace to continuous casting.

Closely engaged with the customer needs, an intensive project to increase the RH degasser vessel availability started in 2013. The most important achievements are listed below:

- Several refractory design changes (quality and project).
- Reviewing SOP for refractory installation.
- Reviewing SOP for gunning application.

- Several process improvements such as reduction of total oxygen consumption and vacuum treatment time per heat.
- Reviewing SOP for heating and preheating practices.
- Reducing nonscheduled shutdowns.
- Optimization of lining performance and prediction—APO.

This paper will only detail the development of APO.

Challenges

Laser scans are a very common technology in the steel industry to measure refractory wear in basic oxygen furnaces and ladles. However, with RH degassers, there is currently no technology available that can measure the refractory thickness inside the lower vessel or in the snorkels during operation. Additionally, unlike other equipment such as ladles [5], there is still no technology that can measure the shell temperature as a method to indirectly correlate the remaining refractory thickness inside the vessel. Infrared cameras are being investigated in a steel mill in Austria [6] and more conclusive results will follow in the near future. Finally, the RH degasser vessel is a reactor where refractory hot inspections and maintenance between heats are either impossible or very limited. Therefore, there was no systematic and reliable way to judge if the refractory lining is in a good condition to perform the next treatment sequence. Figure 2 summarises the above.

Figure 1.
Vacuum facility installations worldwide from 1990–2010.

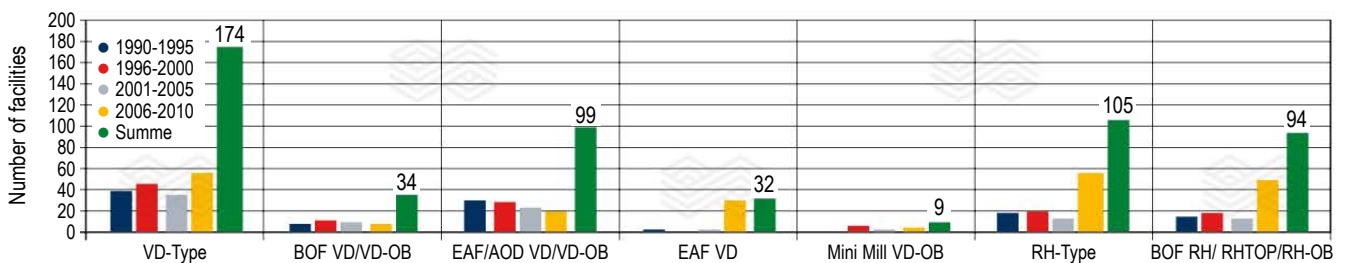


Figure 2.
Refractory monitoring and maintenance for different equipment being investigated.

| | Hot inspection | Laser | Infrared | Hot repair |
|-------------|----------------|-------------------------|---|------------|
| BOF | | | Not common. Fixed thermocouples in few steel plants to monitor shell temperature. | |
| Ladle | | | | |
| RH Degasser | | No technology available | | |

In addition to this, because of the wide range of steel grades GOB produces every month, the process parameters vary greatly at the RH2, which leads to a completely different refractory wear pattern from one degasser campaign to another. Figure 3 shows a variation of the process parameters (average per campaign) of up to 400%.

One example of the impact of different process variables in the refractory wear profile can be seen in Figure 4: For the campaign (a) the left average heats per day were 0.75, total oxygen 0.74, and vacuum time 0.71. For the campaign (b) the average heats per day were 0.50, total oxygen 0.81, and vacuum time 0.67.

Increasing refractory performance under such conditions is extremely challenging and can lead to unpredicted events such as a lower vessel hot spot, requiring an unscheduled shutdown and consequently production loss (Figure 5). It became obvious that a data-based decision would be the only option available to address the ambitious targets of performance increase at GOB.

Figure 5.
Hot spot on lower vessel RH2.



Figure 3.
Relative average of main process parameters for RH degasser.

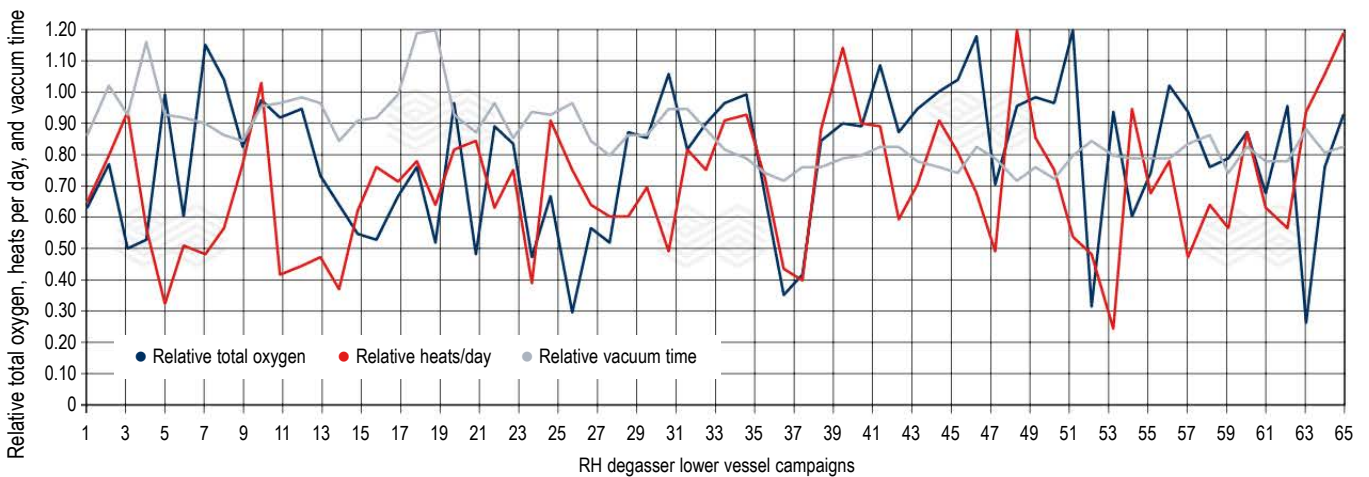
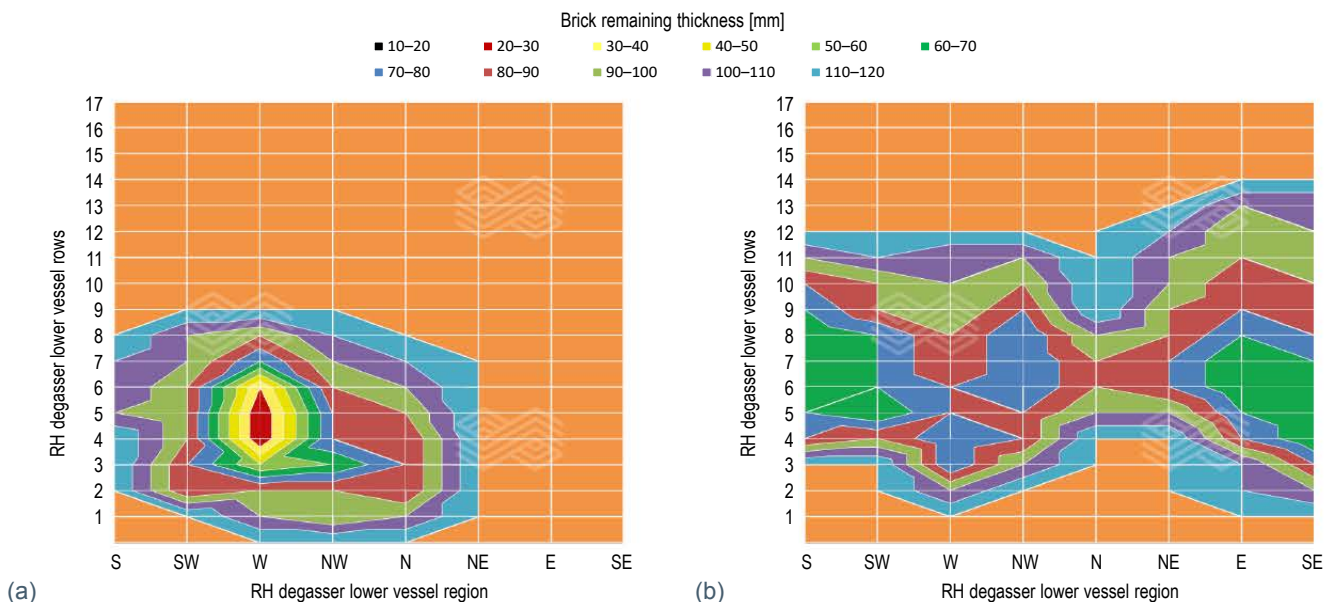


Figure 4.
(a) Lower vessel wear profile in April 2020 (279 heats) and (b) lower vessel wear profile in May 2020 (226 heats).



APO—Automated Process Optimization

APO is a service developed and provided by RHI Magnesita. During the development, sets of historical data of a specific plant were combined to generate and train a model to predict refractory wear [7–9]. For this work, two data sets were used:

- Process data: In a RH degasser treatment, a large amount of sensor data can be recorded. It is common to store, for example, temperatures, consumptions, intervals, chemical additions, and blown gas volumes.
- Refractory wear measurements: At the end of a campaign, the residual lining of the lower vessel is measured and recorded. A minimum residual value is registered for each of the predefined regions and rows of the lower vessel.

A data set was built combining the lining measurements and the process parameters of an entire campaign. To provide a prognosis of the RH degasser life, the maximum wear rate of the vessel predicted by the model was used to calculate the minimum residual thickness of the lining. The difference between this theoretical prediction and the safety residual thickness defined by GOB was then used to calculate the potential life of the vessel.

Classical Linear Regression Model Approaches

In multivariate regression analysis, a vector of variables x is used to fit a function $f(x)$, where $f(x)$ gives an estimated value of a target variable t . This function $f(x)$ is possibly nonlinear. To determine if a vector of parameters has a linear relation with the target value, a pairwise correlation between each variable of x and t can determine whether any of the parameters have a linear influence on the target value. One method to measure it is calculating the Pearson correlation value [10]. The Pearson correlation coefficient between two variables x and y ranges from -1 to 1. This value represents the strength of the relation. A value of 1 implies a perfect positive linear correlation between x and y . A value of -1 implies a perfect negative linear correlation between x and y . A value of 0 implies no linear correlation. A value closer to 1 implies a stronger linear correlation than a value closer to 0. Also, a value closer to -1 implies a stronger linear correlation than a value closer to 0. Figure 6 describes the correlation between some process data, for example, average treatments per day (ATD), average vacuum duration (AVD), average total oxygen (AO), and average oxygen blown (AOB).

Since no obvious linear relation could be found between wear rate and one process parameter, different approaches to linear multivariate linear regression were used to construct a nonlinear regression model with better results.

Machine Learning Methods for Regression

Machine learning algorithms are widely used as an alternative method to construct a model with acceptable accuracy in cases where no easy correlations have been established.

Since machine learning methods are more complex, it was necessary to have a larger amount of data compared to classical statistical approaches. Due to this, and to the model's complexity, machine learning methods have a drawback of low interpretability compared to the classical linear multivariate approach [11]. There are a large set of machine learning methods; in this work decision-tree-based methods were used to build a regression model. These methods are often efficient for many data sets of tabular structured data [12]. Three methods were used: XGBoost, Gradient Boosting, and AdaBoost [13–15].

Train and Test Models

In this study, data from 38 RH2 degasser campaigns were used to develop APO, where 37 campaigns were used to train the machine learning models while the remaining campaign was used to evaluate the performance.

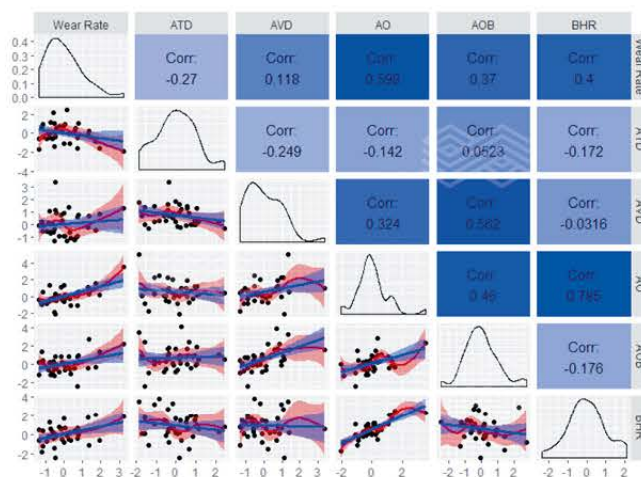
Results and Discussion

Figure 7 shows a representation of the wear rate predicted by APO and the real measurements after the vessel campaign. The maximum absolute difference between the predicted wear rate and the measured value was 0.22 mm per treatment during campaign 1. The maximum residual thickness error reported was 45 mm. The mean absolute thickness error was approximately 17 mm.

After the APO model was developed the results were initially shared with GOB via email on a daily basis after receiving the required process data. The information sent to GOB was essentially a summary of the main process parameter conditions as well as the predicted lifetime for the vessel, as calculated by the machine learning model. During the early stages the decision to take the vessel out of operation was a combination of historical experience of the melt shop engineers and the result of the model prediction. Eventually, a combination of intense work of the melt shop team and with increasing confidence in the APO's prediction, GOB achieved the historic record of 330 heats on the lower vessel and snorkels.

Figure 6.

Correlations between process data. Values are average per campaign, normalised. ATD, AVD, AO, and AOB.



The wear profile was compared with the APO prediction, and an error rate below 4% was observed. This correlation of the predicted and actual wear enabled the process engineers to take the vessel out of operation only considering data-driven information—APO. It is clearly evident in Figure 8 that the green line (true vessel life) became much more aligned to the blue line (predicted by APO). Calculating this difference in the before and after record, there was a saving of 43 heats per vessel campaign on average, which represents savings of 18% of the entire refractory cost for the lower vessel. The difference today remains approximately 19 heats because the decision to stop the vessel production needs to be very well coordinated, both upstream and downstream, as well as with the refractory installation team.

The overall results regarding refractory performance can be seen in Figure 9.

Through the increase in performance, the steel plant saved on average one RH2 vessel change per month from 2017 onwards, which represents 24 hours of production per month or 12 days of operation per year. In order to have an online prediction model easily accessible to the people involved in the RH process, especially via smartphone, a cloud-based solution was developed to automatically receive raw process parameters from the GOB Level 2 system. This data was processed; then relevant features and the current prediction was presented in a web-based APO Tool. A few snapshots are presented in Figure 10. It is important to state that the solution provided, complies with both companies' IT privacy policies.

Figure 7.

Wear rate prediction for each campaign.

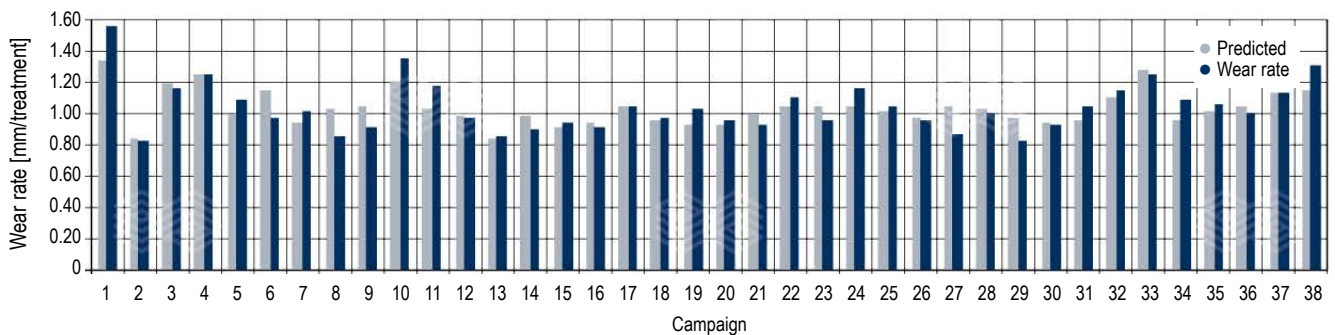


Figure 8.

Potential life calculated via postmortem (wear profile), predicted life via APO, and actual life of the RH2 lower vessel.

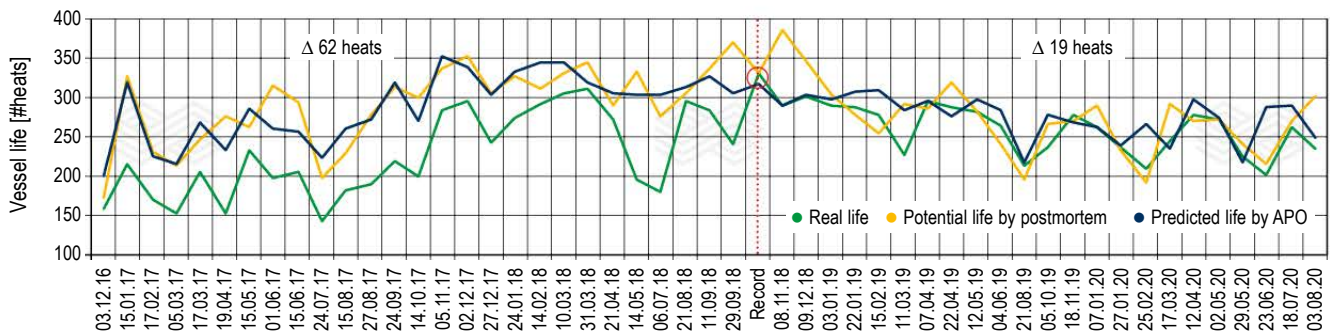
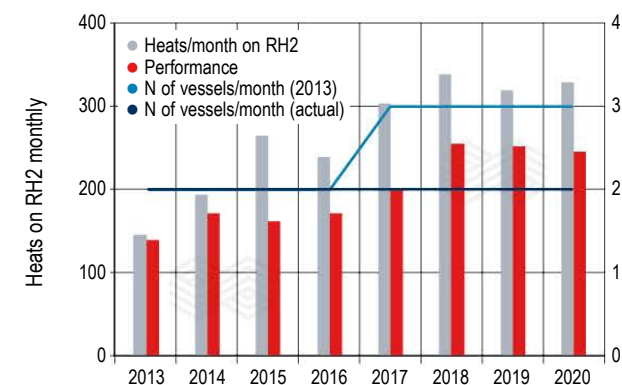
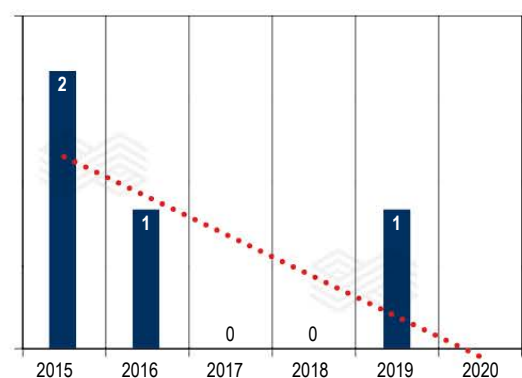


Figure 9.

(a) RH degasser lower vessel performance 2013–2020 and (b) unpredicted events in the lower vessel. *In 2019 there were two refractory related events, however as one was predicted by APO it was not considered in the chart.



(a)



(b)

Number of lower RH degasser vessel unpredicted events

Figure 10.

Original example of APO cloud solution for automatic data upload and report.



Conclusion

The development of a data-based algorithm that can predict refractory wear based on process data and wear data history has been successfully implemented in GOB. This solution is currently in use to ensure that data driven decisions provide a reduction in the overall cost to the steel plant and enable the melt shop to better schedule refractory maintenance.

Acknowledgment

This state-of-the-art work would not have been possible without a seamless collaboration between RHI Magnesita and Gerdau Ouro Branco. Our special thanks go to those who believed in this innovative project from the beginning and never gave up, even in the most difficult times.

References

- [1] <https://www.worldsteel.org>; accessed 13.10.2020.
- [2] Zang, L. and Thomas, B. State of the Art in Evaluation and Control of Steel Cleanliness. *ISIJ International*. 2003, 43, 3, 271–291.
- [3] Tembergen, D. Verbesserte Stahlumlafsimulation beim RH-Prozess. *Stahl und Eisen*. 2009, 129, 10, 41–52.
- [4] <https://www.worldsteel.org/steel-by-topic/statistics/top-producers.html>; accessed 13.10.2020.
- [5] [www.rhimagnesita.com/agellis/steel-making-solutions/Visir FurnaceSafe](http://www.rhimagnesita.com/agellis/steel-making-solutions/Visir-FurnaceSafe); accessed 03.02.2020.
- [6] Viertauer, A. Refractory Lifetime Prognosis for RH Degassers. *bulletin, The Journal of Refractory Innovations*. 2020, 36–41.
- [7] Steiner, R., Lammer, G., Spiel, C. and Jandl, C. Refractories 4.0. *BHM*. 2017, 162, 11, 514–520.
- [8] Lammer, G., Lanzenberger, R., Rom, A., Hanna, A., Forrer, M., Feuerstein, M., Pernkopf, F. and Mutsam, N. Advanced Data Mining for Process Optimizations and Use of A.I. to Predict Refractory Wear and to Analyze Refractory Behaviour. Presented at AISTech 2017, Nashville, USA, May 2017, 1195–1207.
- [9] Viertauer, A., Mutsam, N., Pernkopf, F., Gantner, A., Grimm, G., Winkler, W., Lammer, G. and Ratz, A. Refractory Condition Monitoring and Lifetime Prognosis for RH degasser. Presented at AISTech 2019, Pittsburgh, USA, May 2019, 1081–1087.
- [10] Dixon, W.J. and Massey F.J. Jr. Introduction to Statistical Analysis. 1951.
- [11] Doshi-Velez, F. and Kim B. Towards a Rigorous Science of Interpretable Machine Learning. arXiv preprint arXiv:1702.08608, 2017.
- [12] Breiman, L. Classification and Regression Trees. Routledge, 2017.
- [13] Chen, T. and Guestrin, C. Xgboost: A Scalable Tree Boosting System. Proceedings of the 22nd ACM SIGKDD International Conference on Knowledge Discovery and Data Mining, San Francisco, California, USA, August 2016.
- [14] Friedman, J.H. Greedy Function Approximation: a Gradient Boosting Machine. *The Annals of Statistics*. 2001, 29, 5, 1189–1232.
- [15] Freund, Y. and Schapire, R.E. A Decision-Theoretic Generalization of On-line Learning and an Application to Boosting. *Journal of computer and system sciences*. 1997, 55, 1, 119–139.

Authors

Paulo Souza, RHI Magnesita, Vienna, Austria.

Samuel Oliveira, RHI Magnesita, Contagem, Brazil.

Eric Almeida, Gerdau Group, Ouro Branco, Brazil.

Marina Campos, Gerdau Group, Ouro Branco, Brazil.

Anderson de Paula, Gerdau Group, Ouro Branco, Brazil.

Tito Hugo, Gerdau Group, Ouro Branco, Brazil.

Gabriel Gomes, RHI Magnesita, Ouro Branco, Brazil.

Gregor Lammer, RHI Magnesita, Vienna, Austria.

Romulo Baitz, RHI Magnesita, Contagem, Brazil.

Joao Berganholi, RHI Magnesita, Contagem, Brazil.

Corresponding author: Paulo Souza, paulo.souza@rhimagnesita.com



Reinhard Ehrenguber, Guido Baumgartner, Achim Steins and Raphael Renggli

Latest INTERSTOP Ladle and Tundish Systems Ready for Robotic Handling

Since the introduction of slide gate technology by INTERSTOP more than 50 years ago, improvement of existing and development of new flow control systems has always been strongly interacting with the market situation and trends in the steel industry. Currently, the dominating system requirements are addressing health and safety for operators, process control and reliability, operating costs, contribution to clean steel casting, and robotic handling support. This paper focuses on the latest system developments in the area of ladle slide gates and tundish slide gates. The design and the complementary robotic handling support set new standards in regards to future research and development.

Introduction

Flow control systems play a crucial role on the continuous casting floor, as they ensure an uninterrupted and highly precise flow regulation from the ladle to the tundish and from the tundish to the mould. In addition to flow regulation, these systems and the related refractories further secure that the steel quality during transfer from the ladle to the tundish and from the tundish to the mould is shielded from the atmosphere and therefore prevented from downgrades of the steel quality. The new INTERSTOP systems for ladle and tundish applications are designed for economic and precise clean steel casting.

To operate these flow control systems, up to now the physical presence of personnel was necessary on the continuous casting floor or on the preparation area. For example, the casting cylinder had to be manually connected to the slide gate, the inner nozzle broken out at the ladle preparation area, or the monotube manually handled to carry out a monotube exchange. On one hand, the working environment for the operators is dangerous near the vessels full of liquid steel with exposure to radiant heat, and on the other hand, the physical loads that had to be handled were extremely exhausting. Under these conditions, the personnel had to perform on the highest level, as small deviations from the required instructions could result in serious events like a breakout.

The new systems and the applied design principle for no-man operation during the development enable these risks to be overcome. Robots take over the safety concerns or physically exhaustive tasks, enabling in several cases a shift of the physical presence of the personnel from the exposed areas to the operator room. From this safe place, they can trigger and supervise the robotic systems carrying out the required actions. In line with the systems described in this article, examples for available robotic solutions are presented.

New INTERSTOP SX Ladle Gate

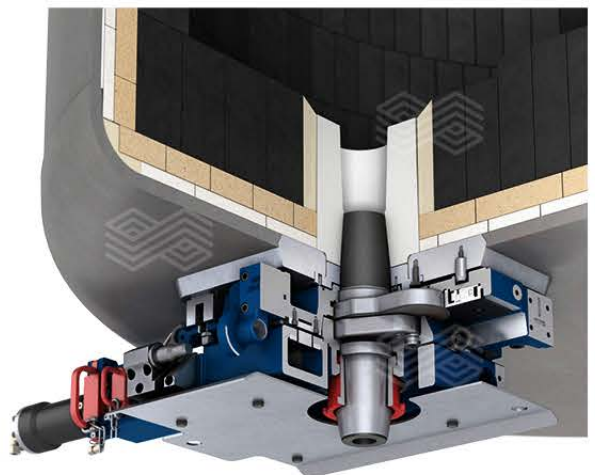
The market introduction of the new INTERSTOP SX ladle gate began recently (Figure 1). Customers who already use the new INTERSTOP SX ladle gate benefit from the following main advantages:

- User-friendly design for fast, safe, and simple operation.
- Easy and quick handling at the preparation area.
- Size selection according to specific customer requirements.
- Low operational costs.
- Readiness for automation and robotic operation.

Figure 1.
INTERSTOP ladle gate type SX.



(a)



(b)

User-Friendly Design for Low Operational Costs

The new INTERSTOP ladle gate Type SX is a high-performance ladle gate system focused on optimising total cost of ownership (TCO) as well as safe and easy operation. The advanced refractory concept leads to higher efficiency. The smart handling characteristics enable easy and safe operation and are incorporated within a maintenance-friendly design. The new development has a positive impact on the overall operating costs and increases the safety standard during handling and operation. Moreover, the new SX type gate provides the possibility to perform an “open check”, a feature allowing the personnel in the ladle preparation area to assess the refractory plates more reliably.

System reliability and availability are the most important objectives in operating a ladle slide gate system. When this is achieved, improved safety is the consequence. In addition to this, optimising operating costs and the focus to improve the TCO is a continuing demand.

INTERSTOP Robotics Ladle to Mould Solutions for Ladle Gates

The mission of RHI Magnesita is to best support customers in making steel production safe and economic while complying with the highest quality standards. In order to achieve this goal RHI Magnesita is following a modular scope of supply, centred around our core business of system engineering. For ladle gate systems, INTERSTOP offers solutions at the ladle preparation area and on the continuous casting machine (CCM) floor that allow for manual and robotic operation. The full package contains the latest slide gate technology, fully equipped with casting cylinder and media coupling, all being operated by our customised robotic system.

In order to automate processes, the systems or subsystems are required to permit an automated operation as well. Currently, an important contributor considered in the development of new slide gate systems for the steel industry, is the swift and easy manual operation and handling. However, an easy manual operation does not necessarily result in an easy to automate operation. For that reason, in new developments specific emphasis has been placed on defining concepts and interfaces that can be adequately operated in automatic mode whilst still allowing manual operation in, for example an emergency. Among the new systems recently developed which enable robotic operation, two are presented in the following sections in more detail.

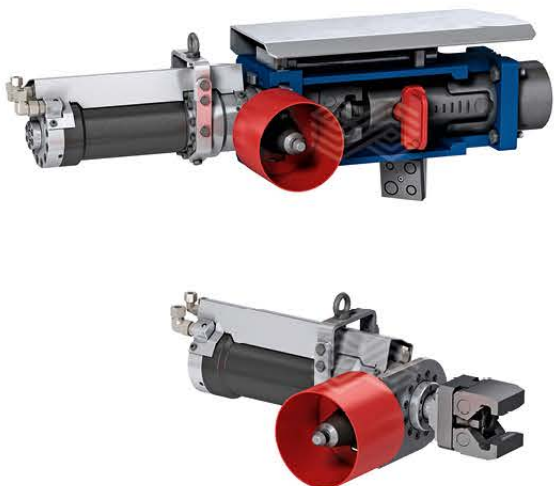
Robotic Casting Cylinder Handling on the Continuous Casting Floor

The casting floor is one of the areas in a steel plant with a high safety concern for operators. Removing people from dangerous areas is the goal. For this reason, a special automated casting cylinder has been developed that is designed to be handled by a robot (Figure 2). The operator is only required to monitor the process from the operating room. The automated casting cylinder can be installed on INTERSTOP slide gates by simply replacing the drive unit. A special built-in safety anti-opening device locks the slide gate during the transfer process without external intervention.

The drive unit has been specifically designed to allow, in the event of an emergency, a manual mounting of the casting cylinder instead of the automated cylinder. An integrated locking/unlocking mechanism prevents the cylinder from disengaging during the casting operation. The system also offers the incorporation of an automated slag detection connector and gate air cooling. With this development, in a single movement, the cylinder and all the utilities are connected and ready to use, reducing the handling time.

Figure 2.

(a) design of slide gate drive unit including automated handled cylinder and (b) reference example of automated cylinder handling in use.



(a)



(b)

Automation at the Ladle Preparation Area

The ladle preparation area is a place in steel plants where critical tasks are carried out by operators under very harsh conditions. Heat, dust, and time pressure can influence the performance quality, in addition to a constant issue with safety. INTERSTOP provides technology with the target of a fully automated ladle preparation area (Figure 3).

In order to master the complexity of such a task, INTERSTOP currently is commissioning a real-life robotic cell, where more than 25 individual processes and combinations are thoroughly developed and tested. They are then combined so they work together in perfection in a steel plant worthy fashion. Furthermore, our mock-up enables us to simulate individual customer requirements and thereby show tangible results early on in the customer project phase.

As a striking example, the newly designed oxygen cleaning tool, which cleans the casting channel and removes any residual steel or slag, is noteworthy (Figure 4). This cleaning process goes hand in hand with the process of “inner nozzle repair”.

Figure 3.

Layout of the automated ladle preparation area.

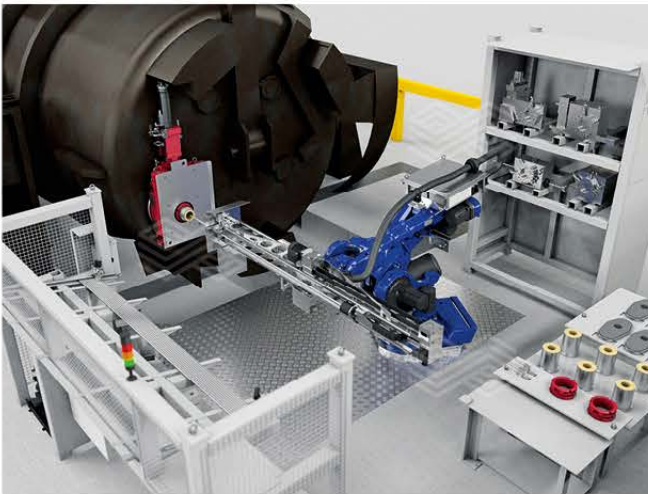


Figure 4.

INTERSTOP's oxygen lancing at the laboratory.



Inner Nozzle Repair

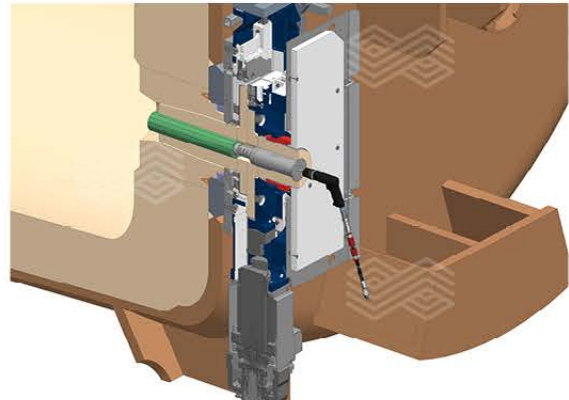
The primary target of the “inner nozzle repair” process is to match the lifetime of the inner nozzle with the lifetime of the entire ladle lining, which makes the manual online inner nozzle exchange obsolete. The fact that the inner diameter and the overall shape of the casting channel is kept constant over the entire ladle refractory life bears further operational advantages, such as:

- Oxygen cleaning is more efficient as constant geometries are always being dealt with.
- Increased self-opening rate since sharp edges or agglomerations are avoided.
- Constant casting conditions due to a constant diameter of the casting channel while reducing heat impact on the slide gate refractory plates.

A very positive feedback from colleagues and customers was received when the “inner nozzle repair” was tested and verified in various steel plants, as a manual, stand-alone process. The concept with a tailored ready-to-use single-serving mortar-cartridge, which can be mounted to the manual or robot tool just by one click, completes the entire process (Figure 5). The current steps of the mortar cartridge development are optimising the mortar cartridges for serial production and introduction into the product portfolio.

Figure 5.

(a) manual tool and mortar filled cartridge and (b) manual application of “inner nozzle repair” at a hot ladle.



(a)



(b)

New INTERSTOP STG 33 Tundish Slide Gate Including Monotube Changer

The INTERSTOP sealed tundish gate with monotube changer type STG 33 is a three-plate linear gate with the advantages of a tundish gate and the possibility of changing the monotube without interruption of the casting process (Figure 6).

This enables the sequence length to be increased and optimised. The play-free drive and plate clamping systems ensure a precise and fast reacting mould level control. In the sealed and gas floated housing, the refractory plates and consequently the steel flow is protected against any reoxidation. This is illustrated in Figure 7.

Both cylinders, one for the flow control and the second for changing the monotube, are hydraulically actuated and permanently connected to the hydraulic circuit. The flow control cylinder is additionally equipped with an integrated stroke measuring system. Tensioning of the plates is carried

out with four long-life and cooled spiral disc springs to ensure tightness during the whole casting sequence. Any refractory expansion is compensated for by a flexible supporting plate of the lower plate. The monotube is pressed against the lower plate with eight spring-loaded tilting levers. Both tensioning systems work independently. Figure 8 shows the easy accessibility of all three refractory plates. A sturdy and self-adjusting plate clamping system holds the three plates play-free in the mechanism. The engineers achieved the goal to simplify the cleaning, setup, and maintenance of the inner area of the tundish gate. Only a few tools are necessary to carry out the plate exchange. A customer-tailored brand range for the refractory components is available to optimise the sequence lengths and the operation costs.

As previously described, the STG 33 features the integrated monotube changer (MTC). The MTC is designed according to the automation-ready principle. In the next section, the corresponding robotic cell is explained to ensure an automatic monotube exchange, and with the same robotic cell the mould powder addition is managed.

Figure 6.
STG 33 with integrated monotube changer.

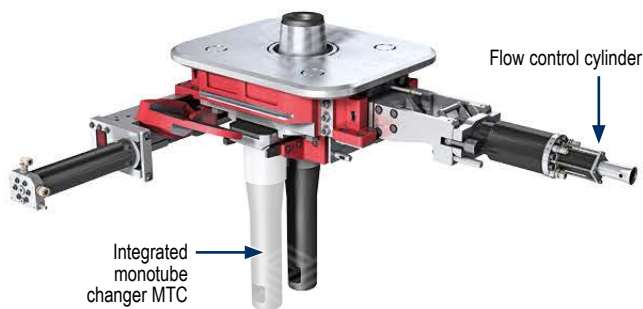


Figure 7.
Housing completely sealed against reoxidation.

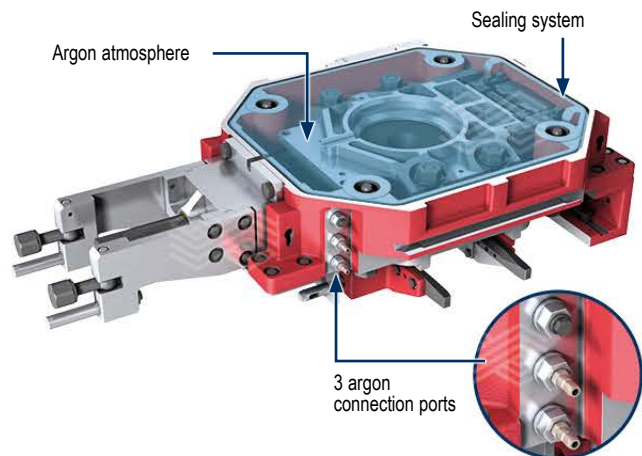
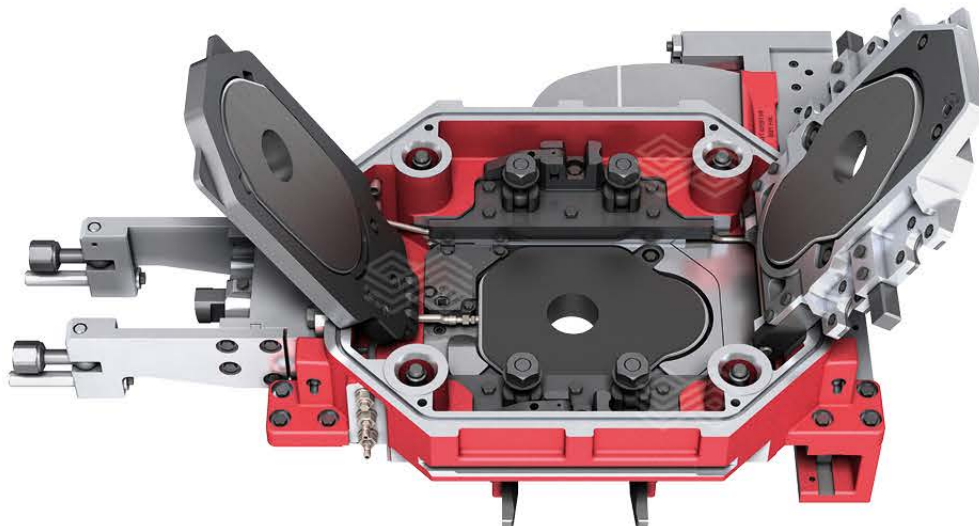


Figure 8.
Plate insertion and fast clamping system.



INTERSTOP Robotics Ladle to Mould Solutions for a Monotube Changer

Apart from the solutions for the ladle slide gate, the product range in robotics to tundish and mould operations has been extended. The monotube change, being one of the more dangerous tasks in this regard, lead to the underlying design-concepts of both the latest models of monotube changer as well as tundish gates.

Following the philosophy of providing tangible and reliable solutions early on in any customer project and being able to simulate customer specific requirements we have commissioned a mock-up for monotube changing at the facilities in Switzerland.

The concept minimises civil works and space requirements at the customer plants through the installation of a ceiling robot onto the backside of the tundish car. At the same time the front side of the mould remains accessible at all times, which in combination is the unique selling point for this solution (Figure 9).

Our MTC mock-up was developed and implemented together with a well-known partner for mechatronic systems in the area of casting. The mock-up is modular, which features the integrated modules of “monotube preheating and disposal” and “mould powder feeding and dosing”.

As of this year, customers are invited to visit our facilities at Hünenberg (Switzerland) to become familiar with the robotic solutions, make an individual choice of modules, and to finally lead the workforce of the global steelmakers into a safer and more efficient future.

Figure 9.

Layout of the robotic cell for monotube change and mould powder feeding.



Results/Conclusion

With the newly developed INTERSTOP flow control systems and the parallel development focus on enabling robotic operation, a new era begins. Operators are released from risky and exhausting work, taking over more and more supervision of the robotic cells that physically carry out the tasks. In addition to the advantage of providing a much more attractive and safer workplace, the robotic operation enables a significantly higher level of repeated precision of the tasks performed. The robotic operation further enables a constant optimisation of the equipment handling, connecting human intelligence with the physical power of robots. The roll-out of the new systems has successfully started and the robotic cells are available for commissioning.

Authors

Reinhard Ehrenguber, RHI Magnesita Interstop AG, Hünenberg, Switzerland.

Guido Baumgartner, RHI Magnesita Interstop AG, Hünenberg, Switzerland.

Achim Steins, RHI Magnesita Interstop AG, Hünenberg, Switzerland.

Raphael Renggli, RHI Magnesita Interstop AG, Hünenberg, Switzerland.

Corresponding author: Reinhard Ehrenguber, reinhard.ehrenguber@rhimagnesita.com





Tailor-made tundish-to-mould solutions INTERSTOP Robotics

The operation of Flow Control related products in the steel industry is still very challenging in terms of people's safety and process reliability. The interaction with the production facilities exposes the operator to significant risks.

For this reason, we developed a fully automated solution for a monotube change designed to be handled by a robot. The robot enables the monotube to be changed automatically during casting. Furthermore, a preheating station as well as a powder lance tool ensure a reliable and holistic solution for our customers.

Curious to find out more details?
Visit rhimagnesia.com/automation-and-robotics

Follow us



RHI MAGNESITA

Patrick-Paul Seitz, Gerald Nitzl, Markus Fauhl and Olena Botvinikova

New Direct Purging NC Technology for Slab Casting

It is state-of-the-art to supply argon into the casting channel to reduce the amount of clogging on the refractory wall to allow long sequence casting of aluminium-killed steel grades. The key to further minimising surface defects on the final product is to establish the optimum quantity of argon by optimising the gas distribution in the casting channel combined with erosion-resistant refractories in the control area of the molten steel flow from tundish to mould. This is achieved via new direct purging technology which supports low gas quantities with homogeneous gas and bubble distributions to float non-metallic inclusions (NMI) in the continuous casting mould. Production trials of mononozzles (NCs) have been accomplished at the pilot plant in Trieben (Austria) and the new product has been trialled successfully by ArcelorMittal in Bremen (Germany).

Introduction

The so-called clogging is caused by precipitation of alumina particles on a refractory surface. This phenomenon is commonly observed when steel flows through the refractory tubes from the tundish into the continuous casting mould [1,2]. During this very short time period of 1–2 seconds the liquid steel's fluid dynamic boundary conditions change rapidly in terms of pressure, flow velocity, turbulence, and heat balance. Argon addition in the casting channel reduces unfavourable occurrence of clogging, since the NMI can be captured and isolated in the argon bubbles [3,4]. These particle-loaded bubbles are removed downstream in the continuous casting mould. There they are transferred smoothly into the meniscus, releasing the particle load into the molten mould flux at the meniscus level. Hence major bubble bursting effects can be avoided and less slag entrapment at the meniscus level is consequently observed. Modern slab casters which produce aluminium-killed grades, ultra-low carbon (ULC), and interstitial-free (IF) grades for automotive applications pay great attention on maintaining steel quality flowing from the ladle to mould. In addition, processes are improved to avoid new steel contaminations in the mould.

One key area of optimisation is to operate the caster at the lowest possible argon quantities, to avoid sliver defects in the mould [5], but high enough to be able to cast long sequences on a stable and consistent quality level with acceptable clogging and wear rates in the nozzle. Another focus at ArcelorMittal Bremen is refractory wear in the upper area of the mononozzle (NC), which can reduce the total casting time. The demand on casting higher aggressive calcium treated steels is increasing. Conventional NCs with permeable materials show severe corrosion when casting calcium-treated steel grades, causing a stopper drop of nearly 20 mm during a ten-heat sequence. Also, the argon pressure in the purging line is negatively impacted by refractory corrosion in the inlet area. Stable backpressure and argon flow are mandatory to achieve stable mould level performance, which will directly contribute to low inclusion entrapment in the solidified steel. The new direct purging NC technology (DP-NC), with corrosion resistant inlet material, is designed exactly for these customer requirements.

Refractory Performance and Process Stability is Key

In order to achieve the highest yield of prime quality products, very tight control of casting boundary conditions and refractory performance is required. The new design is characterised by the fact that the point of argon injection into the downwards flowing stream of molten metal is located above the throttle area from stopper to the nozzle.

Figure 1 illustrates the argon flow from above the stopper throttling point all along the refractory surface of the mononozzle to avoid alumina deposition (clogging). Furthermore, it is possible to purge the argon through the monoblock stopper which is illustrated via the blue vertical lines in the middle of the casting channel. Another requirement for argon purging NCs is positive backpressure at the requested flow rate in the argon line to avoid suction of air into the gas line and channel.

As shown in the Figure 2, the injection point of the DP-NC is at the highest possible static pressure level in the casting channel in the “overpressure” region of the tundish. To avoid any steel infiltration into the refractory gas channel structure, the pressure at the gas outlet of the NC always needs to be higher than the ferrostatic head pressure deriving from the steel level of the tundish. In contrast, it has been observed during a ladle change, that the level drop in the tundish correlates with the backpressure signal of the argon line to the NC.

The exit of the argon line is located in the tundish and not in the “negative pressure” region below the throttle point. Therefore, backpressure has become completely independent from the flow regime of the liquid steel in the nozzle which can change, depending on the casting conditions from bubbly to slug flow and vice versa.

At ArcelorMittal Bremen, ULC steels have an argon purging flow rate in the range of 3–5 l/min depending on the steel throughput. Beyond the observed pressure drop during the ladle change, the backpressure signal at 3 l/min is very stable compared to a conventional purged NC (gas purging via a permeable material), where the gas injection is in the “negative pressure” region.

The improved mould level and stopper performance is expected to contribute to enhanced quality for ULC steels (Figure 3), however more data is required to confirm the observation. ArcelorMittal Bremen has experienced that the amount of argon is relevant when ULC steel grades are cast. In this particular case, the quantity of argon on the stopper to avoid clogging is more important than the argon quantity on the nozzle [6,7].

Product Design

Conventional gas purging NCs are typically comprised of a gas permeable liner in the inner bore and/or throat with a gas feeding channel system connected to a metal connector. The exit of the liner is in the “negative pressure” area of the casting channel (Figure 2). This pressure fluctuates during casting between approximately -600 and -100 mbar depending on the flow regime and the throughput of the caster. This pressure variability can lead to unfavourable air ingress resulting in refractory wear and clogging during casting. These disadvantages are eliminated with the new DP-NC design.

Figure 1.

Cross section of a monoblock stopper and mononozzle. (a) without argon purging and (b) argon injection (blue) in steel (red) above the throttle for the new NC design.

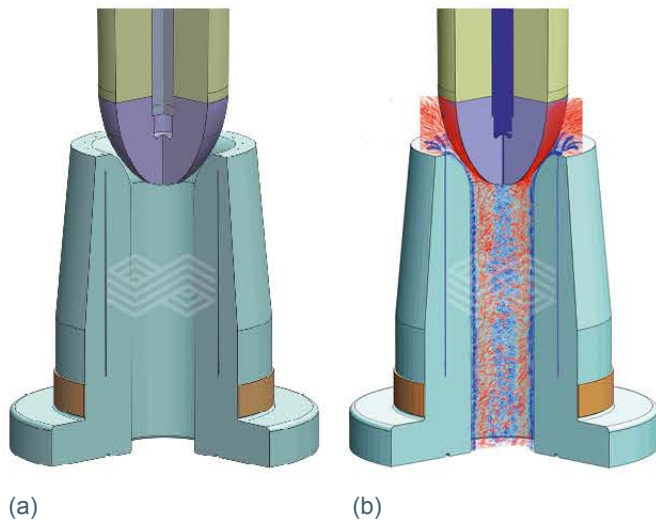


Figure 2.

Static pressure: Colour coded, pressure regions from tundish to mould marked with arrows. Injection point indicated by black arrows.

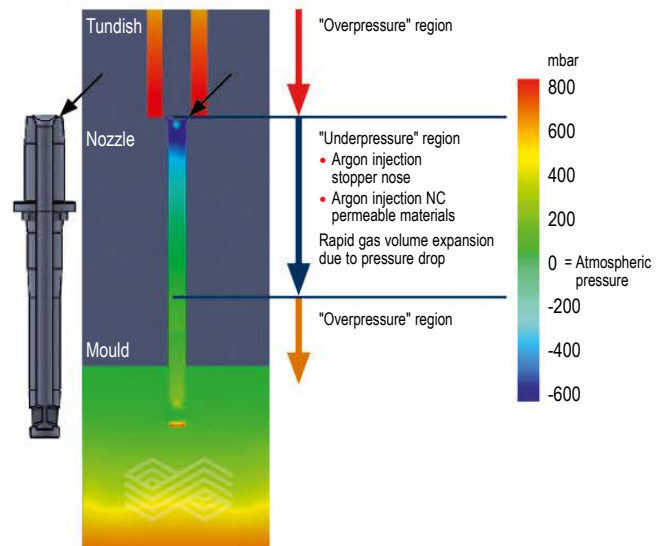
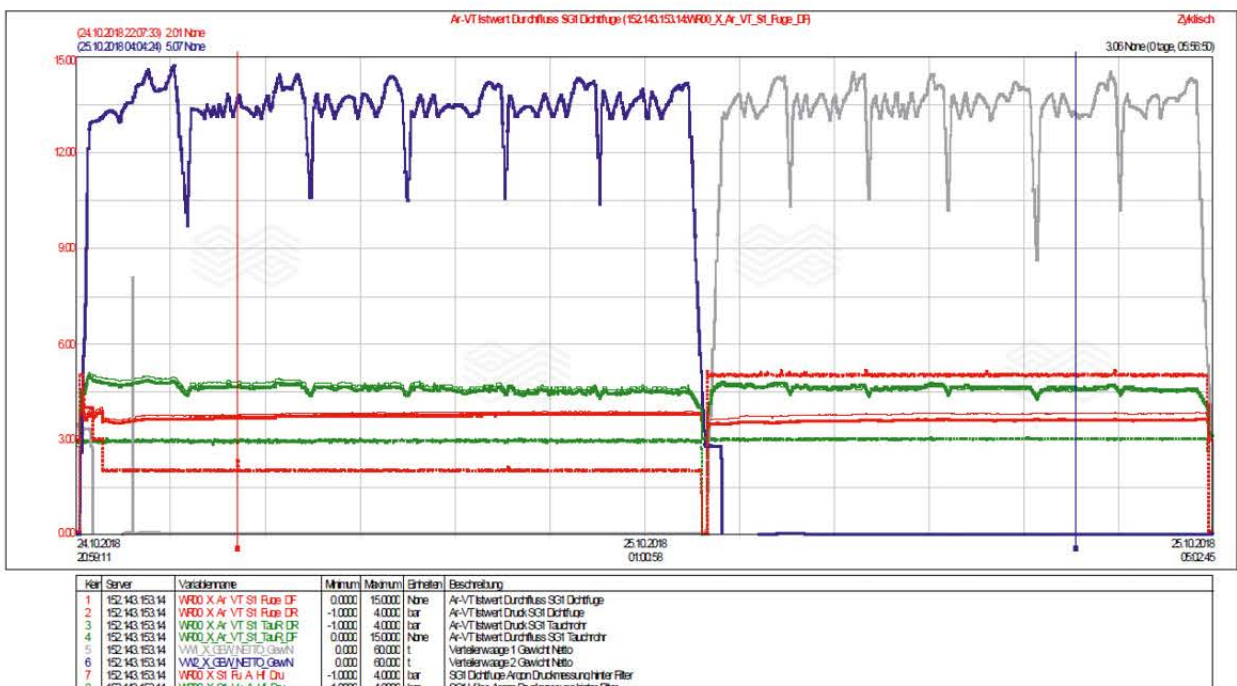


Figure 3.

Schematic graphs of a casting sequence, tundish weight, and argon flow data (pressure and argon flow) from top and bottom plate area of NC for ULC steel over time.



The main advantages of the DP-NC design are:

- Solid refractory material with high corrosion resistance for the throat area.
- The bore of the NC can be reinforced with special refractory coatings, such as anti-clogging or thermally insulating liners.

The new product, as shown in Figure 4, was developed and optimised over a time period of approximately two years at the pilot plant in Trieben (Austria). Within the project several new tooling and manufacturing concepts were trialled and tested in the steel plant.

The main challenges were:

- New tooling development.
- Slot geometry optimisation.
- Filling and pressing technology improvements.
- Tighter argon flow tolerances on the finished product.

The development process was supported by simulation and modelling to optimise dimensions, pressure, and flow performance [8,9].

Process Improvements in the Steel Plant

Within the time period of approximately five years, the operational performance of the slab caster in ArcelorMittal Bremen has been improved to fulfil the latest end-customer quality requirements. This improvement program consisted of a variety of changes along the complete metallurgical and casting process.

The main objectives for improvements at ArcelorMittal Bremen were:

- Gastight argon connections of the NC in the tube changer mechanic for plate and purging line (Figure 5).
- Refractory corrosion resistance in the throttle area.
- Improved and consistent argon distribution by achieving an improved mould level control during casting.
- Stable backpressure at low argon flow rates of 3 l/min.

Figure 4.

Innovative DP-NC design.



From the operational side on the slab caster, the following actions were undertaken as shown in Figure 6:

- New piping and flow control devices.
- Flow testing and sealing before installation and casting.
- Metallurgical improvements in secondary steel treatment.
- Regular maintenance.
- Operator awareness, training, and quality control.
- Throughput-dependent argon management.

Field Performance

Figure 7 shows a typical graph of the new DP-NC for an eight-heat sequence at 4.2–4.6 tonnes/min. The backpressure of the argon line correlates with the tundish level at a constant argon flow rate of 3 l/min. Between the ladle changes the backpressure signal is very stable compared to a conventional purged NC.

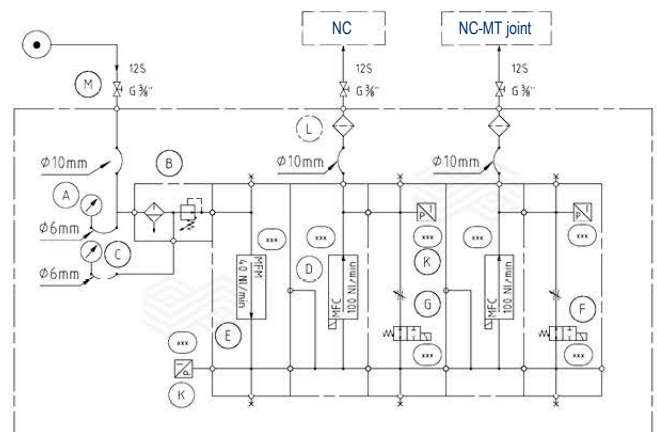
Figure 5.

RHI Magnesita DP-NC installed in INTERSTOP Tube-Changer SNC System. At lower end of image: Argon connector pipes for direct purging to the top surface and to the bottom plate of the NC. This Tube-Changer System enables a change of the refractory tube underneath the mononozzle, the so-called monotube (MT).



Figure 6.

Example of a flow circuit of argon system. Gas purging to the top surface (NC) and to the bottom plate (NC-MT joint).



After casting, the wear on the purging surface of the RHI Magnesita NC was significantly less, when compared to the porous NCs with a permeable refractory, as shown in Figures 8 and 9. For the DP-NC it is not required to use a permeable material at the inlet area of the NC, which relates to an increased refractory performance. Generally, the wear of the refractories, including the mononozzle, influence the casting time and so the performance of the steel plant. Also, the corrosion resistant alumina/graphite ceramic shows very little clogging in the inlet area, which will result in a more stable mould level with less perturbations during the casting process.

Benefits

Within the time period of five years of continuous improvement and product development, the following benefits were observed:

- Less clogging on the:
 - > Stopper nose.
 - > Inlet area of the NC.
 - > Bore of the monotube.
- Improved corrosion resistance.
- Stable backpressure and mould level performance.
- Surface quality improvements with fewer sliver defects on IF and Al-killed steel grades as expected due to better mould level performance.

After the development and trial period, the refractory manufacturing technology was transferred from the pilot plant in Trieben to the plants in Scotland (Bonnybridge) and China (Dalian) to supply the European and Asian markets with this new technology.

Figure 7.

Data recording during cast at ArcelorMittal Bremen. Mould length 2630 mm; casting speed 1.0–1.1 m/min; argon flow at 3 l/min.

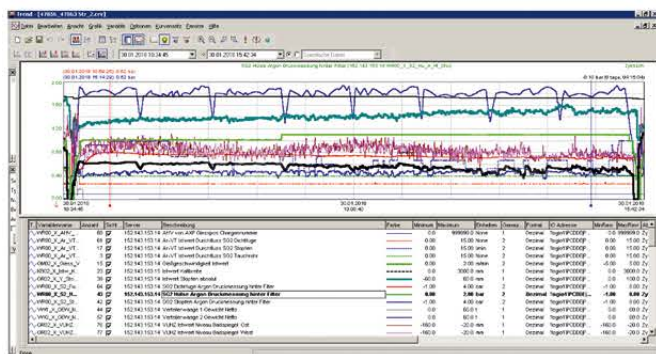


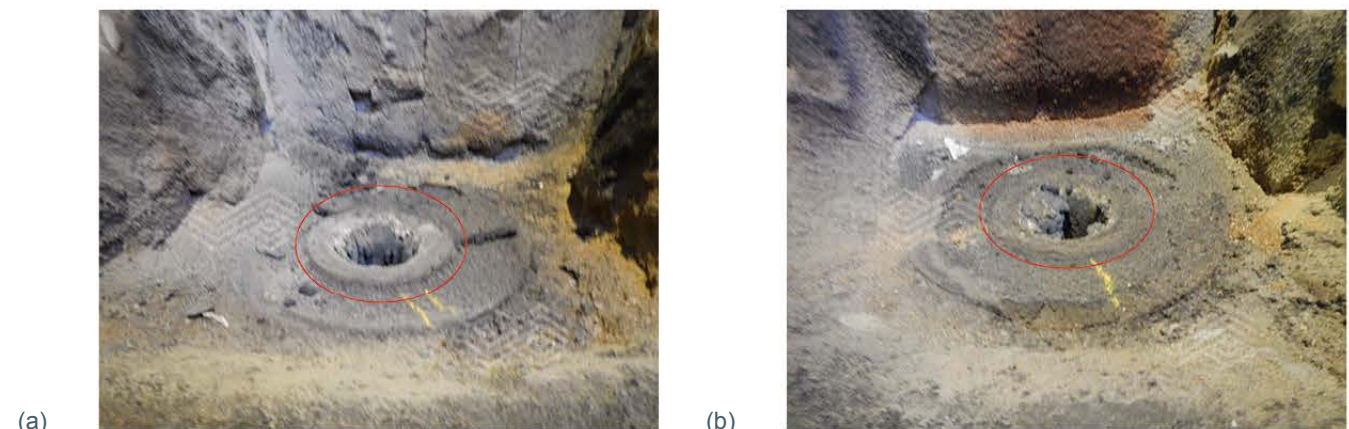
Figure 9.

Comparison of used and dismantled purged NCs after ten heats, Ca-treated steel grade, showing (a) RHI Magnesita DP-NC showing less wear at top surface and (b) conventional purged NC showing worn top surface.



Figure 8.

Nozzle inlet area after eight heats cast with (a) RHI Magnesita DP-NC showing less wear compared to (b) conventional purged NC with purging through a porous material which is showing a worn and clogged top surface.



Conclusion and Outlook

Clear measurable improvements have been achieved for the customer ArcelorMittal Bremen. The new direct purging technology for mononozzles enabled a better monitoring of argon management. In addition, a decreased clogging and corrosion appearance at the inlet area of the NC has been observed.

On this basis, a solid technology platform has been created with the potential for further improvements in the future.

The expected potential for further developments are with:

- Carbon-free liners to reduce clogging.
- Insulating liners to reduce heat losses in the casting channel.
- Higher corrosion resistant materials for the inlet.

New refractory developments contribute actively towards quality improvements for customers in the future and will strengthen the market position of RHI Magnesita.

References

- [1] Pretorius, E.B., Oltmann, H.G. and Schart, B.T. An Overview of Steel Cleanliness from an Industry Perspective. Presented at AISTech, Pittsburgh, USA, May 2013.
- [2] Naveau, P., Visser, H.H., Galpin, J.M. and Sussek, G. An Investigation on the Mechanism of Gas Bubbles/Inclusions Entrapment in the Solidified Steel Shell. Report European Coal and Steel Community.
- [3] Thomas, B.G., Dennisov, A. and Bai, H. Behavior of Argon Bubbles during Continuous Casting of Steel. Presented at the ISS 80th Steelmaking Conference, Chicago, USA, April 1997.
- [4] Ramirez Lopez, P.E., Jalali, P.N. and Nilsson, Ch. Adding Argon Injection to an Advanced Model for Continuous Casting of Steel; Presented at the 8th European Continuous Casting Conference, Graz, Austria, June 2014.
- [5] L. Zhang, B. Thomas, Inclusions in Continuous Casting of Steel, XXIV National Steelmaking Symposium, Morelia, Mich, Mexico, 26-28, Nov. 2003, pp. 138-183.
- [6] Tang Y., Nitzl G. and Hackl G., Novel Stopper Designs to Improve Argon Purging Efficiency in Slab Casting; Presented at the 7th International Symposium on Refractories, Xi'an, China, September 2016.
- [7] Liisanantti, V., Pirinen, J., Makala, J. and Nevala, H. Benefits Of Stopper Rod Argon Injection at Ruuki Production Raahe Works; Presented at the 6th European Continuous Casting Conference, Riccione, Italy, June 2008.
- [8] Qin, X., Cheng, C., Li, Y., Zhang, C., Zhang, J. and Jin, Y. Simulation Study on the Flow Behavior of Liquid Steel in Tundish with Annular Argon Blowing in the Upper Nozzle. *Metals* 2019, 9(2), 225.
- [9] Hackl G., Tang, Y., Nitzl, G., Chalmers, D., Dorricott, J.D. and Heaslip, L.J. Flow Control Refractory Design Optimization of Submerged-Entry Nozzles by Simulation Technology; Presented at AISTech, Pittsburgh, USA, May 2013.

Authors

Patrick-Paul Seitz, RHI Magnesita, Leoben, Austria.

Gerald Nitzl, RHI Magnesita, Vienna, Austria.

Markus Fauhl, RHI Magnesita, Vienna, Austria.

Olena Botvinikova, ArcelorMittal Bremen, Germany.

Corresponding author: Patrick Seitz, Patrick-paul.seitz@rhimagnesita.com





Exceptional opportunities for exceptional people

Tackling extreme challenges with calm efficiency is our business.

To continue being one jump ahead we count on exceptional colleagues who can do an exceptional job.

Discover our worldwide vacancies at rhimagresita.com/career



RHI MAGNESITA

Alexandre Dolabella Resende, Gernot Lukesch, Gernot Hackl and Daniel Meurer

Tundish Refractory Design Optimisation Through Mathematical and Physical Modelling

The development and improvement of flow control devices have been an extensive topic of research in the steel industry. Modelling techniques, such as physical and numerical simulation, are commonly adopted as tools to support these developments. However, there is room for improvement in the process of designing these components, which is generally based on trial and error until a design that meets selected (or predefined) criteria is obtained. In this work, the application of numerical optimisation tools in the tundish refractory design are presented. The optimisations are based on the results of computational fluid dynamics (CFD) simulations, which feed adaptive algorithms based on response surface generation. Through this approach, it is possible to obtain optimum designs for the tundish refractories with respect to key performance indicators of the flow, such as higher values for steel residence time. The superior performance of the optimised designs has been validated through water modelling experiments, confirming that significant improvements in the flow residence time were obtained compared to the previously existing designs.

Introduction

In the past decades, new solutions to improve steel cleanliness in the tundish have emerged in the steel industry. Many alternatives for impact pots and furniture were developed, evidencing the high practical interest in optimising the continuous casting process through better refractory designs [1]. Nevertheless, the commonly observed process of “optimising” the designs consists of trying different alternatives until a specific improvement is obtained, according to a preexisting expectation [2–4]. Such procedures rely on trial and error and do not ensure that the best possible solution according to a given set of constraints is obtained.

In order to truly determine the optimal solution for a given process condition and design constraints, RHI Magnesita performs design optimisation studies based on mathematical modelling. CFD simulations are performed driven by an adaptive optimisation algorithm that finds the optimal design according to the desired result, given a set of constraints.

Optimisation Model Description

The optimisation model is based on the results of CFD simulations. The CFD model solves the Navier-Stokes equations for continuity and momentum (equations 1 and 2):

$$\frac{\partial \rho}{\partial t} + \frac{\partial}{\partial x_j} (\rho U_j) = 0 \quad (1)$$

$$\frac{\partial \rho U_i}{\partial t} + \frac{\partial}{\partial x_j} (\rho U_i U_j) = -\frac{\partial P}{\partial x_i} + \frac{\partial}{\partial x_j} \left[\mu_{eff} \left(\frac{\partial U_i}{\partial x_j} + \frac{\partial U_j}{\partial x_i} \right) \right] + S_M \quad (2)$$

Where ρ is the fluid’s density, t is the time, x_j is the coordinate in the j -direction, U_j is the velocity component in the j -direction, P is the pressure field, S_M is the sum of the body forces, and μ_{eff} is the effective viscosity accounting for turbulence, given by equation 3:

$$\mu_{eff} = \mu + C_\mu \rho \frac{k^2}{\varepsilon} \quad (3)$$

Where μ is the fluid’s molecular viscosity, C_μ is a constant, k is the turbulent kinetic energy, and ε is the dissipation rate of turbulence.

Equations 4 and 5 represent the transport equations for turbulent kinetic energy and dissipation rate of turbulence:

$$\frac{\partial \rho k}{\partial t} + \frac{\partial}{\partial x_j} (\rho U_j k) = \frac{\partial}{\partial x_j} \left[\left(\mu + \frac{\mu_t}{\sigma_k} \right) \frac{\partial k}{\partial x_j} \right] + P_k - \rho \varepsilon \quad (4)$$

$$\frac{\partial \rho \varepsilon}{\partial t} + \frac{\partial}{\partial x_j} (\rho U_j \varepsilon) = \frac{\partial}{\partial x_j} \left[\left(\mu + \frac{\mu_t}{\sigma_\varepsilon} \right) \frac{\partial \varepsilon}{\partial x_j} \right] + \frac{\varepsilon}{k} (C_{\varepsilon 1} P_k - C_{\varepsilon 2} \rho \varepsilon) \quad (5)$$

Once the flow field is calculated, a residence time distribution (RTD) analysis is performed to characterise the flow according to the definitions of plug volume, dead volume, and mix volume [5]. To perform the RTD study, a numerical simulation of tracer transport in the calculated flow field is performed. The transport equation for the tracer is given by equation 6:

$$\frac{\partial (\rho \phi)}{\partial t} + \nabla \cdot (\rho \mathbf{U} \phi) = \nabla \cdot \left(\left(\rho D_\phi + \frac{\mu_t}{Sc_t} \right) \nabla \phi \right) + S_\phi \quad (6)$$

Where ϕ is the tracer concentration, Sc_t is the turbulent Schmidt number, S_ϕ is a source term for the concentration, μ_t is the eddy viscosity, and D_ϕ is the kinematic diffusivity of the tracer.

The equations above describe the mathematical modelling procedure for the CFD simulations. The process of optimising the design parameters of refractories such as the impact pot or other tundish furniture consists of coupling the results of the CFD calculations with an adaptive optimisation algorithm, which determines the next designs to be simulated based on the results obtained so far by the previous simulations. The optimisation algorithm converges when the result of interest ceases to improve with subsequent simulation rounds.

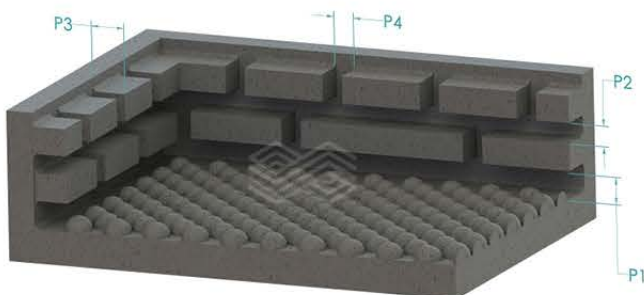
The procedure can be summarised as the following:

- Each different combination of design parameters (e.g., length of and gap between the internal ribs of the impact pot) defines one design point.
- For each design point, a CFD run is performed and the relevant results are extracted (e.g., minimum residence time).
- These results are used to feed the optimisation algorithm and new design points are created automatically by the process based on the results of the previous calculations.
- The process is repeated until the optimisation algorithm converges.

A more detailed explanation about the optimisation algorithm is given by dividing it in three steps. Firstly, a design of experiments (DOE) matrix is generated with several different combinations of the design parameters to cover the whole range of admissible parameters with the fewest number of simulations possible. Secondly, a response surface is adjusted in the obtained data from the CFD model and extra refinement points (represented as additional combinations of the design parameters) are computed and added to the response surface calculation to increase the accuracy. Finally, a verification algorithm is run with the goal of assessing the accuracy of the response surface and searching for the global maximum and minimum of the desired outputs.

Figure 1.

Design parameters of the impact pot geometry to be optimised.



Impact Pot Design Optimisation—Water Modelling

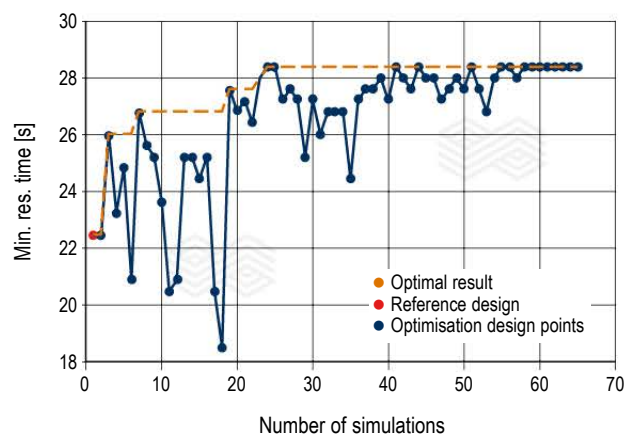
An impact pot design optimisation was performed representing a 1:3 scale water model, in order to validate the technique presented in this publication.

Figure 1 shows the parameters included in the optimisation study. The focus of the study was on finding the optimal setup of the horizontal breakers in the interior of the impact pot geometry, without significantly changing the overall dimensions or features. The chosen criterion for the optimality of the design was to have the maximum value for the time taken by the earlier flow fractions to reach the strands (also known as minimum residence time). Higher values for the minimum residence time allow more time for non-metallic inclusions flotation and thus enhanced steel cleanliness. It is also correlated to lower volumes of stagnant flow in the tundish, which is a major cause for issues such as strand freezing, poor mixing, and premature steel solidification in the vessel. Thus, by maximising the value of the minimum residence time, several practical benefits can be obtained [5].

Figure 2 shows the results obtained by the optimisation algorithm. The first point on the left represents the result for reference configuration. Then, different combinations of the design parameters were simulated, and the results represented as new points in the chart. The adaptive nature of the optimisation algorithm can be seen from the trend of the curve of showing increasing values for the variable of interest as the number of simulations increases. In other words, the optimisation algorithm learns the ranges of values for each design variable that have a positive influence on the result of interest and, as more simulations are performed, each design point has a higher probability of returning a higher value for the result of interest. This behaviour is illustrated, for example, by the fact that after 20 simulations had been performed, all subsequent design evaluations have shown superior results compared to the reference design.

Figure 2.

Curve showing the evolution of the result of interest (minimum residence time) as each new design is simulated within the optimisation procedure.



The optimum design returned by the optimisation study is shown in Figure 3 compared to the initial reference design prior to the model application. Although the optimisation algorithm selects the design parameters purely from statistical and numerical standpoints, the final design proposed by the model must have an explanation, based on the physics, as to why it performs better.

In this study, the modifications suggested by the optimisation algorithm acted in the direction of increasing the spacing between the horizontal breakers (increasing P2 and P4, while P1 and P3 were maintained), in order to allow a larger fraction of the flow to pass through this region and dissipate more energy. Therefore, the velocity of the upward jet is lower, as can be seen in Figure 4, which is a positive perspective in terms of residence time and steel cleanliness.

The reference and the optimised impact pot designs were compared by water modelling experiments. The experiments were carried out on a model representing a twin strand slab casting tundish without any additional flow modifiers except an impact pot. As previously described, the water model was operated on a scale of 1:3, fulfilling Froude similarity.

According to literature [6], this approach is most likely to simulate flow phenomena of the corresponding full-scale system fairly accurately. The Froude number, which is the ratio between inertial and gravitational forces, is defined by Equation 7:

$$Fr = \frac{u^2}{g \cdot l} \quad (7)$$

Where u is the flow velocity [m/s], g the gravitational acceleration [m/s²] and l a characteristic length of the system [m].

Table I provides information about the considered operating conditions in the model and the converted values for the real application.

Table I.

Operating conditions for the water model and corresponding values for the real application.

| | Water model | Real application |
|------------------------|-----------------------|------------------|
| Throughput | 2.5 m ³ /h | 4.5 t/min/strand |
| Bath level | 380 mm | 1150 mm |
| Ladle shroud immersion | 70 mm | 210 mm |

Figure 3.

(a) reference impact pot design and (b) optimum design proposed by the model. The spacing between the horizontal breakers has been increased in the optimum configuration.

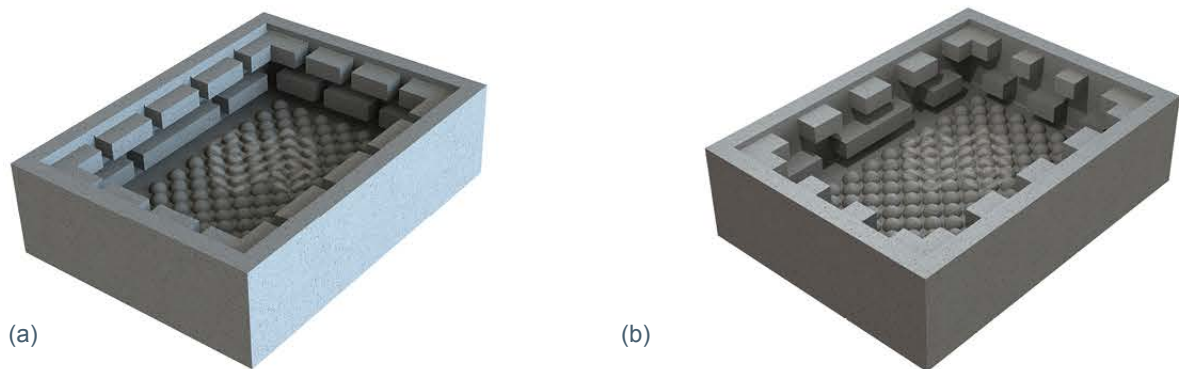
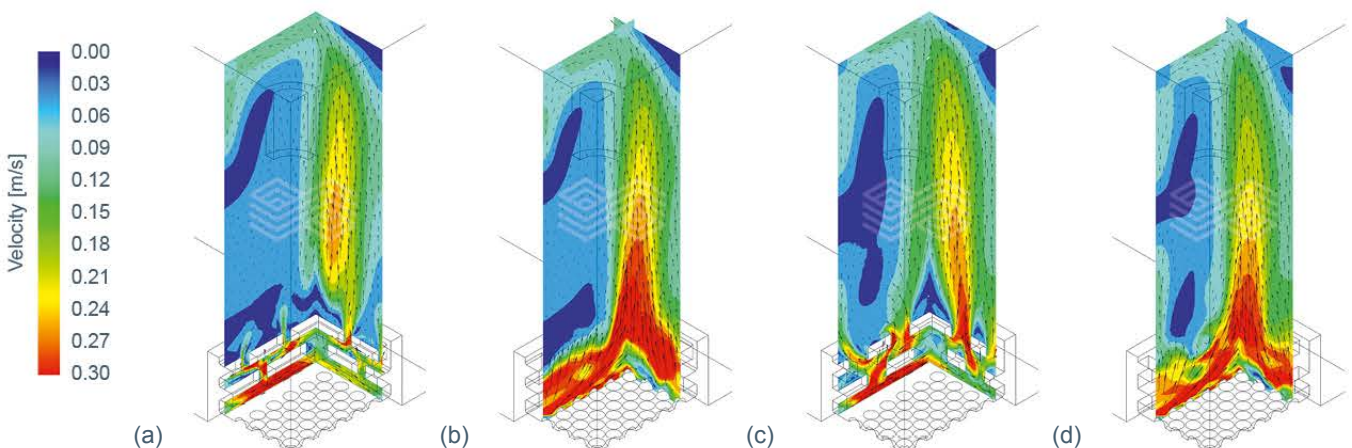


Figure 4.

Comparison between the flow behaviour in the region of the horizontal breakers. (a) reference design outer planes, (b) reference design inner planes, (c) optimum design outer planes, and (d) optimum design inner planes.



To characterise the flow performance of the given tundish set-up, the stimulus response technique, where the concentration of an injected tracer fluid (e.g., dye) is recorded at the outlets, was applied. Analysis of the measured curve provides key information about the flow characteristics in the tundish, like the minimum residence time and other parameters. Besides those dye concentration measurements, a video was recorded synchronously to get an impression of the general flow characteristics. The results of the physical simulation have shown an improvement of similar magnitude compared to the CFD in the residence time for the optimised design: An approximately 20% higher minimum residence time. While the tracer starts to be detected at $t = 25$ seconds for the reference design, the detection is delayed until $t = 30$ seconds for the optimum design, as shown in Figure 5.

Figure 6 shows a snapshot of the ink dispersion profile after 25 seconds after the instant of injection. The ink travels more slowly in the optimised configuration and takes longer to reach the strands, illustrating the increase in flow minimum residence time with the optimised design.

Figure 5.

Tracer concentration curves obtained in the water modelling experiments, showing a minimum residence time of 25 s for the reference configuration and 30 s for the optimum configuration.

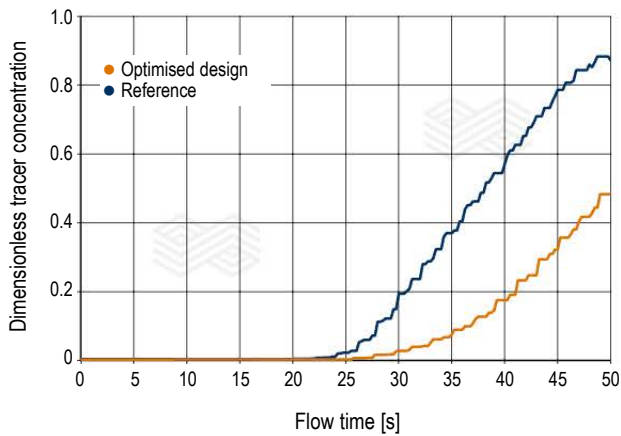
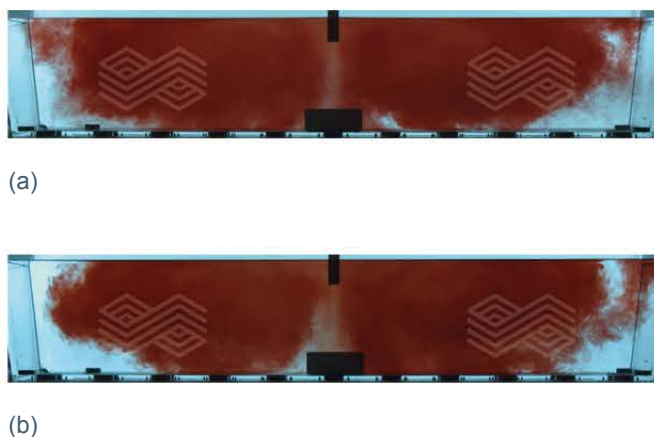


Figure 6.

Water modelling results after 25 s. (a) reference and (b) optimised.



The experimental results confirm the potential of mathematical optimisation tools. A 20% improvement in performance was obtained with an impact pot of comparable size and features, with no additional furniture being necessary, just by applying the optimisation technique to the design parameters of the product. In the reduced scale model, the result under evaluation was the flow minimum residence time, which is strongly correlated to the steel cleanliness. The design parameters to be optimised were the dimensions and positioning of the internal horizontal flow breakers of the impact pot. However, the mathematical optimisation model can also be adopted with the goal of influencing other results of interest and of optimising other design variables.

Impact Pot and Tundish Furniture Optimisation—Steel Caster

The model was also applied to an existing tundish on an industrial scale, representing the full size and the properties of the molten steel. The vessel studied was a 40 tonne slab tundish with two strands located symmetrically with respect to the impact zone. The tundish had a preexisting configuration of weirs and dams and the simulations were carried out to evaluate this arrangement as a reference configuration.

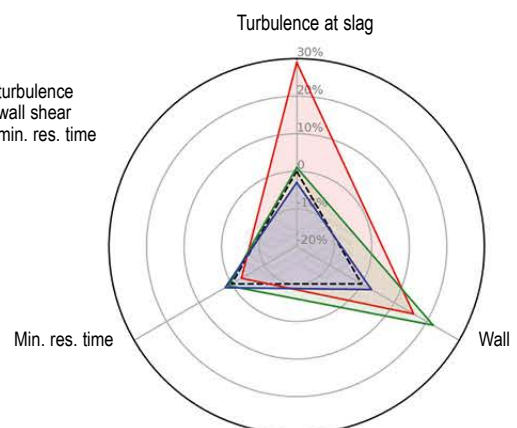
The impact pot design optimisation study for the full scale tundish was performed according to multiple results of practical interest such as:

- Minimise turbulence at the slag layer.
- Minimise refractory wear by flow shear stresses.
- Maximise the steel cleanliness by increasing the minimum residence time.

Figure 7 shows a visualisation of the improvements that could be obtained through the optimisation process with respect to each of the results of interest. In this graphic, the improvements are shown as positive variations in the chart (even if a lower value for the variable is desired, such as for turbulence, this is represented as a positive variation in the curve, for the sake of visualisation), which means that the larger the area of a curve, the better is its overall performance.

Figure 7.

Optimum designs obtained when multiple results of interest are considered. There is no single global optimum solution and trade-offs must be made.



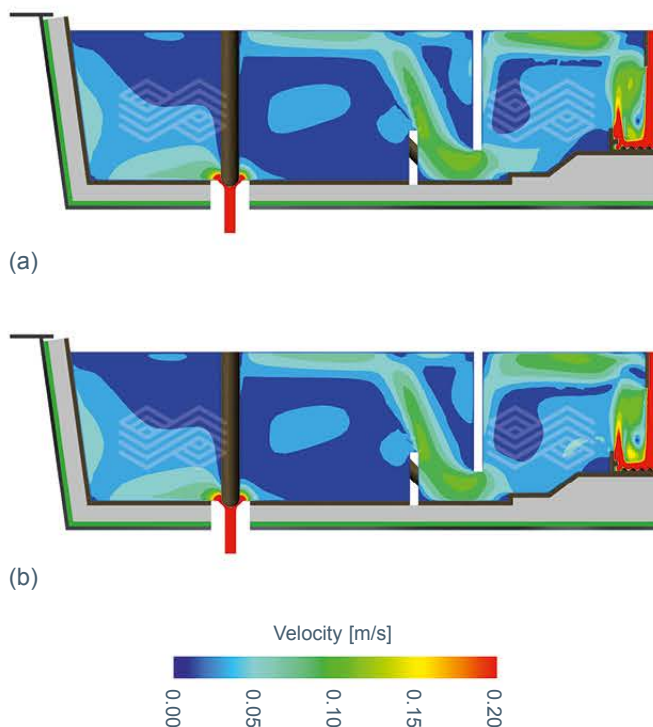
When multiple objectives are considered in the optimisation model, it is often not possible to obtain a single global optimal design. The results of interest are not independent and one design which satisfies the optimum value for one of the objectives may achieve that at the expense of the others (e.g., a minimum value of turbulence at the slag layer may be obtained by redirecting a fraction of the steel flow to the tundish walls, which negatively impacts the wall shear stresses.) Therefore, it is crucial that the specific goals of such studies are established and that the relative importance of each variable of interest is clear, so that an optimum choice can be made weighing the combination of the results.

Figure 8 illustrates the results of turbulence at the slag layer for the optimum design with respect to this variable. Significant improvements can be obtained both in lowering the maximum value and in reducing the size of the affected region.

At this point, one might ask: Why has the model not been able to significantly improve the minimum residence time, as was achieved in the water modelling experiments? The optimum designs proposed both for minimising turbulence and wall shear stresses showed improvements greater than 20%. However, there was not a significant improvement in the minimum residence time for this case. The answer to this question can be seen in the velocity contours of the flow in the tundish, shown in Figure 9. The existing tundish furniture, composed of a weir and dam arrangement, was governing the flow pattern in the vessel, limiting the effect of any modifications in the impact pot design to the impact region alone.

Figure 9.

Comparison of flow pattern in the tundish between the reference (a) impact pot and (b) optimum. The flow pattern is almost identical, due to the effect of the weir and dam.



Since the minimum residence time depends on the flow pattern in the entire tundish, if the weir and dam have a strong influence on the flow and their arrangement remains unchanged, it is unlikely that changing only the impact pot design will significantly affect the flow residence time.

Figure 8.

Comparison between the results of (a) turbulence in the slag layer for the reference configuration and (b) for the optimum impact pot design with respect to minimising this value.

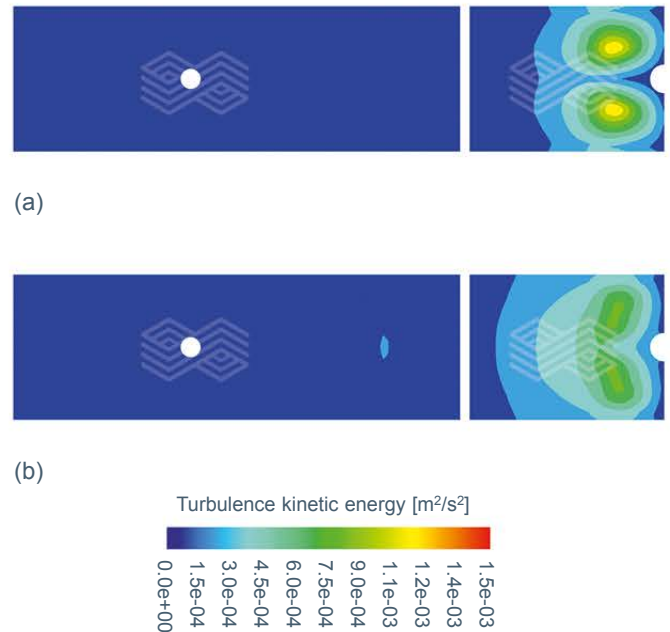
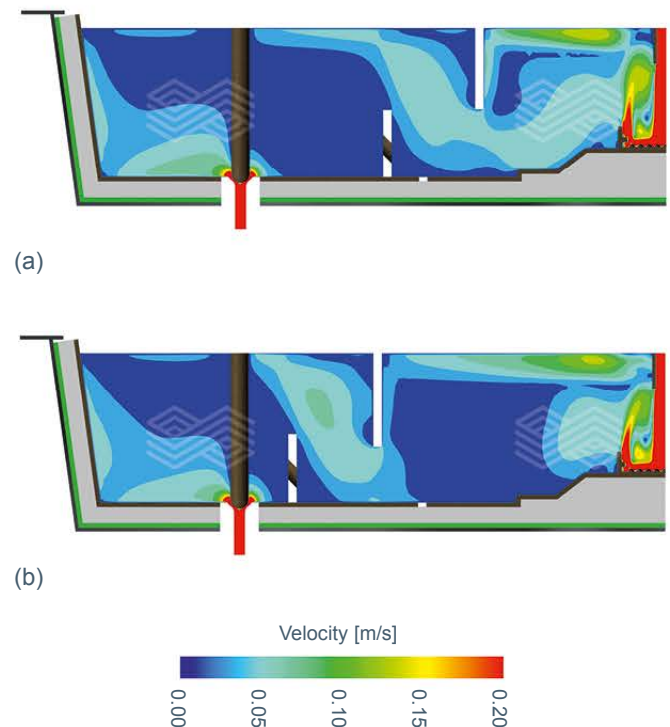


Figure 10.

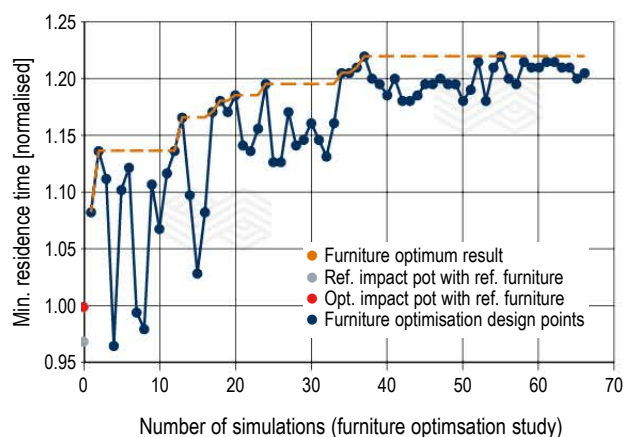
Comparison of flow patterns in the tundish for the reference (a) impact pot configuration and (b) optimum impact pot configuration when both are used in tandem with the respective optimised weir and dam configurations. The weir and dam arrangement has a significant influence in the overall flow pattern.



In scenarios such as these, the mathematical model can be applied to optimise the dimensions and position of the barriers, rather than focusing on the impact pot alone. By acting on the weir and dam arrangement, when such furniture is used, significant improvements can be obtained in the flow pattern and in the minimum residence time. Figure 10 illustrates the lower flow velocities obtained in the gap between the weir and the dam when the size and position is optimised. Comparing the flow patterns obtained for the optimised weir and dam arrangements shown in Figure 10 with the results seen for the reference weir and dam configuration shown in Figure 9, a reduction of approximately 50% in the flow velocities at the gap can be seen (from approximately 0.1 m/s shown in Figure 9 to about 0.05 m/s shown in Figure 10).

Figure 11.

Curve showing the evolution of the result of interest (minimum residence time, normalised) as each new design is simulated within the optimisation procedure. The reference furniture results are also shown in comparison.



The improvement, of approximately 20%, in the minimum residence time obtained between the reference weir and dam configuration and the optimised design proposed by the model can be seen in Figure 11.

It should be noted, the optimisation studies shown in this publication illustrate where possible interventions in the tundish refractory design can have the highest effect in terms of steel cleanliness:

- When no other furniture is adopted, small changes in the impact pot design can have a significant effect in the steel residence time in the tundish.
- However, weirs, dams, and other furniture have a significant influence on the flow, and should they be adopted, it is crucial to find their optimum configuration with the mathematical model in order to obtain the best outcome in steel cleanliness.

Results/Conclusion

Optimal designs of tundish refractories can provide significant benefits in the continuous casting process. Several results of interest can be significantly improved such as:

- Minimum turbulence at the slag layer.
- Minimum shear stresses.
- Highest minimum residence time.

The outcomes above can be achieved through more efficient choices of design parameters for the impact pot and for the tundish furniture. These optimum configurations are suggested by the mathematical model and show superior results without increasing the quantity or size of the refractory pieces.

References

- [1] Hackl, G., Tang Y., Lukesch, G., Meurer, D., Shivaram, P. and Resende, A. Impact Zone Solutions for an Improved Flow Performance in the Tundish. Presented at the AISTech 2019 Conference and Exhibition, Pittsburg, USA, 6–8 May 2019, 2851–2858.
- [2] Espino-Zárate, A., Morales, R., Nájera-Bastida, A., Macías-Hernández, M. and Sandoval-Ramos, A. Fluid Flow and Mechanisms of Momentum Transfer in a Six-Strand Tundish. *Metallurgical and Materials Transactions B*. 2010, 41B, 962–975.
- [3] Chattopadhyay, K., Isac, M. and Guthrie, R.I.L. Effect of Flow Modifiers on Liquid Metal Cleanliness in Four-Strand Delta Shaped Billet Caster Tundish. *Ironmaking and Steelmaking*. 2012, 39, 6, 454–462.
- [4] Fan, C.M., Shie, R.J. and Hwang, W.S. Studies by Mathematical and Physical Modelling of Fluid Flow and Inclusion Removal Phenomena in Slab Tundish for Casting Stainless Steel Using Various Flow Control Device Designs. *Ironmaking and Steelmaking*. 2003, 30, 5, 341–347.
- [5] Sahai, Y. and Emi, T. Melt Flow Characterization in Continuous Casting Tundishes. *ISIJ International*. 1996, 36, 6, 667–672.
- [6] Mazumdar, D. and Guthrie, R.I.L. The Physical and Mathematical Modelling of Continuous Casting Tundish Systems. *ISIJ International*. 1999, 39, 6, 524–547.

Authors

Alexandre Dolabella Resende, RHI Magnesita, Contagem, Brazil.

Gernot Lukesch, RHI Magnesita, Leoben, Austria.

Gernot Hackl, RHI Magnesita, Leoben, Austria.

Daniel Meurer, RHI Magnesita, Leoben, Austria.

Corresponding author: Alexandre Dolabella Resende, alexandre.resende@rhimagnesita.com



Dean Gregurek, Katja Reinharter, Jürgen Schmidl, Christine Wenzl and Alfred Sparring

Typical Refractory Wear Phenomena in Copper Vessels and Novel Monitoring Technologies

Copper smelting furnaces are typically lined with magnesia-chromite refractories, which are exposed to multiple and complex stresses. The selection of the processing route, furnace type, and slag system is dictated by the specific ore type available; which will determine the individual refractory wear. This paper evaluates the common refractory wear mechanisms as observed in the copper Peirce-Smith converter and in the copper anode furnace. The chemical factors include corrosion caused by fayalite type slag and sulphur supply, as well as by Cu-oxide attack. Changes in the temperature during the furnace operation (thermal shock) create stresses in the brick lining which can only be absorbed to a limited extent. Mechanical factors include erosion, caused primarily by the movement of the metal bath, slag and charging material, as well as stresses in the brickwork due to punching. Finally, improper lining procedures can also affect the service life. All these wear parameters lead to severe degeneration of the brick microstructure and a decreased lining life, and in the worst case overheated furnace structures and possibly dangerous hot spots or even breakouts. Therefore, a detailed investigation and understanding of the wear mechanisms through “postmortem studies” together with thermochemical calculations by FactSage software is an important prerequisite for the refractory producer. Based on these research results, combined with specific process knowledge, appropriate brick lining solutions for copper processing furnaces can be recommended. In addition to the described efforts to investigate refractory wear and optimise lining qualities, it is also essential to monitor the process and the effect on the refractories to further improve both safety and process. For this purpose, technologies using sensors and novel digital solutions can be applied.

Introduction

The refining of copper includes converting matte or black copper into blister copper for the final fire refining process in the anode section. Typically, Peirce-Smith (PS) converters are used. Other technologies include the Hoboken converter, top blown rotary converter (TBRC) but also flash converting furnaces and bath smelting furnaces (ISA, Ausmelt) [1]. For fire refining two types of furnaces are used: The rotary furnace type is dominantly used in the primary production route while secondary smelters tend to use hearth refining furnaces, which are more suitable for scrap melting.

Installed working linings are based on magnesia-chromite bricks but especially in the anode refining section the application of alumina-chromia bricks has become more popular in recent years. It goes without saying that, to some extent, large variations in the slag composition can be observed from the data provided to RHI Magnesita during postmortem studies of used refractory samples and this needs to be addressed properly during the selection process of refractory linings.

To be able to provide the best possible understanding of the brick wear mechanisms occurring during operation, a close cooperation between operating plant and refractory supplier is essential for achieving improvements in the service life of refractory linings. This paper presents various factors which affect the brick lining in the PS converter and copper anode furnaces, and shows how different refractory types behave under various conditions and how the process and furnace operation can be stabilised and further optimised by sensors and digital technologies. The wear phenomena discussed include corrosion caused by slag and sulphur supply, as well as by copper oxide attack, copper infiltration, and refractory damage by (thermo)-mechanical load. In addition to mineralogical investigations, thermochemical calculations using FactSage software were performed.

Analytical Procedure

Generally, each postmortem study begins with a visual inspection of the brick cross section. This is followed by a selection of samples from this cross section for chemical analyses and mineralogical investigation. Then, chemical analyses are carried out using X-ray fluorescence analysis (Bruker S8 TIGER). The subsequent mineralogical investigation is performed on polished sections using a reflected light microscope, X-ray diffraction (Bruker D8 ADVANCE), and a scanning electron microscope (SEM) (JEOL JSM-6460) combined with an energy-dispersive and wavelength-dispersive X-ray analyser.

Postmortem Investigations—General Overview

The observed wear phenomena can generally be subdivided into continuous and discontinuous wear [2]. The continuous wear is characterised by continuous mass loss as a function of time. It is caused by chemical, thermal, and mechanical load that can occur as single or interrelated wear factors [3]. In most cases, particularly for magnesia-chromite bricks, the most frequent continuous wear is corrosion of the refractory by dissolution in melts/slugs with additional hot erosion. Nevertheless, in industrial furnaces dissolution in melts/slugs occurs at the direct refractory hot face, whereas hot erosion of corroded refractory material by fluid motion predominates [4]. Increased temperatures, as well as the copper metal infiltration into the brick microstructure, are further phenomena on the thermal side. Mechanical load includes the above-mentioned hot erosion, which is primarily caused by the movement of the metal bath, slag, and charging material. Discontinuous wear is mainly characterised by mechanical failure initiated by thermal/chemical load occurring discontinuously over time. It is associated with mass loss. Further discontinuous wear phenomena include (structural) spalling, thermal shock failure, and bursting reactions (e.g., alkali, carbon, and forsterite). Thermal shock is mainly due to changes in the temperature and partial pressure during the furnace operation. Proper temperature control and avoidance of overheating is an essential factor to prolong refractory life, as well as minimise energy losses and avoid damage to the furnace steel structure. Stresses in the brickwork due to improper lining procedures additionally contribute to damage of the refractory by mechanical load.

Postmortem Investigations—Wear Phenomena

Corrosion of the refractory by acidic slag

The most common chemical attack in the PS converter is corrosion by fayalite slag. In anode refining operations the slag chemistry is different (Table I).

As a result of infiltration by the fayalite slag, degeneration of the brick's microstructure takes place. Generally, the corrosion of the refractories, particularly magnesia-chromite bricks, by slag attack manifests in three ways [4]:

- Dissolution reaction occurring at the immediate brick hot face: The driving force here is the lower activity of the refractory oxides such as MgO in the slag. The dissolution process, at least in the closed system, will continue until the liquid slag has reached saturation. However, in practice, the point of saturation is never reached, and dissolution continues until the entire refractory has been consumed. However, in practice (industrial furnace), the equilibrium conditions are never reached due to residence time, homogenisation, and bath convection for example.
- Dissolution and chemical reaction within the refractory microstructure: Infiltrating slag will dissolve MgO especially from the fines and from silicates according to the respective phase equilibria. At service temperature a liquid phase will remain, which is then saturated in MgO. This will not directly contribute to corrosive wear which takes place at the refractory hot face. Nevertheless it will contribute to wear by preparing hot erosion due to a loss of brick bonding. The latter is caused by dissolution of fines in the liquid due to the grain size dependency of the solubility limit and following precipitation on the surface of coarse particles. This represents so-called Ostwald ripening [4].
- Kinetics of slag infiltration: Kinetics of slag infiltration causing processes mentioned above depend on several parameters such as viscosity, pore size distribution, and wetting angle. It is assumed that these kinetic considerations can be neglected here as the ratio of the wear rate to the infiltration velocity is much smaller than one. As a consequence, microscopic investigations of used bricks always showed a total infiltration of the porosity in some cases up to the cold face. This moreover means that the invariant point of the respective mineral phase assemblages is below the cold face temperature in cases where the infiltrate is observed up to the cold face.

Table I.

Typical slag composition in copper smelting operations [5,6,7].

| Slag type | Cu [%] | Fe [%] | Pb [%] | Zn [%] | SiO ₂ [%] | CaO [%] | Al ₂ O ₃ [%] | η _{1200-1250 °C} [poise] |
|--------------------|-----------|-----------|-----------|-----------|-------------------------|------------|---------------------------------------|--------------------------------------|
| Smelting slag | 0–5 | 38–45 | 0–1 | 1–3 | 28–35 | 2–4 | 3–6 | 2–10 |
| PS-converting slag | 3–7 | 40–45 | 1–10 | 0–7 | 20–25 | 0–3 | 1–4 | 1–3 |
| Refining slag | 30–40 | 15–25 | 0–2 | 1–3 | 10–15 | 0–2 | <1 | <1 |

Based on the mineralogical investigation, several zones can be distinguished. Below the slag coating, covering the immediate brick hot face, there is usually a thin reaction zone followed by an infiltrated and corroded brick microstructure (Figure 1a). As can be seen in Figure 1a, within the reaction zone there was severe dissolution of the magnesia brick component frequently leaving relics of primary and secondary chromite precipitations. In the adjacent infiltrated and corroded brick microstructure, due to corrosion of the brick-inherent magnesia (coarse grains and matrix fines), the main reaction products were (calcium)-magnesium silicates, namely monticellite (CaMgSiO_4) and forsterite (Mg_2SiO_4).

Additionally, the interstitial phase of the magnesia component, especially dicalcium silicate (Ca_2SiO_4), was corroded. Chromite in general shows higher corrosion resistance in comparison to magnesia. The reason for this is the fact that periclase (MgO) is more basic than chromite and therefore more susceptible to acidic corrosion [3]. Due to infiltration and diffusion between slag and chromite the chemical composition of chromite was changed; usually the chromite rims were enriched with iron oxide.

In addition, the alumina-chromia bricks lined in the PS converter or anode furnace showed microstructural degeneration due to infiltration and slag corrosion. The main corrosion phenomena were similar to those previously observed for the magnesia-chromite bricks. The hot face was frequently covered with a thin slag coating (Figure 1b). Below the slag coating in the infiltrated brick microstructure severe corrosion of fused alumina was frequently observed. There was formation of zinc-enriched Fe-Cr-Al-oxide of spinel type, copper-containing Mg-Fe-Al-Cr-oxide (chromite spinel), and Cu-(Cr)-Al-oxide of type cuprous aluminate delafossite ($\text{Cu}_2\text{Al}_2\text{O}_4$). In the infiltrated brick microstructure Zr-mullite was also heavily corroded. Particularly at the rims of zirconium-oxide—within the Zr-mullite—zirconium-silicate was formed.

In addition to the mineralogical investigation, thermochemical calculations were performed with FactSage software and the databases FactPS, FToxide, and FTmisc [8].

For the calculation, an average composition of the two different slags present in the PS converter operation, the iron and copper blowing slags, was used to determine the Al_2O_3 , MgO , as well as the Cr_2O_3 solubility of refractory components into the slag. For the iron blowing slag, the sensitivity of changed Fe/SiO_2 ratio to the solubility behaviour was varied from 1.6 to 2.1. The results are illustrated in Figure 2.

Figure 2.

Solubility of the refractory components Al_2O_3 , MgO , and Cr_2O_3 in iron blowing slag from PS converter operation as a function of Fe/SiO_2 ratio, temperature, and fixed oxygen partial pressure of $p_{\text{O}_2} = 10^{-8}$ atm.

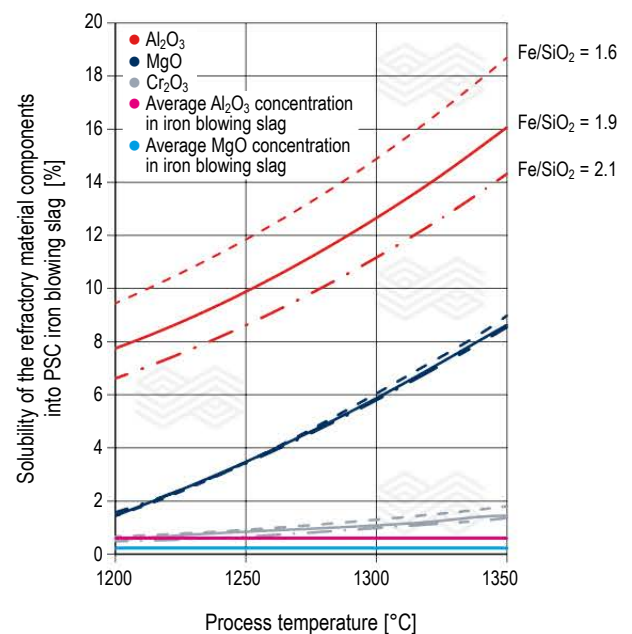
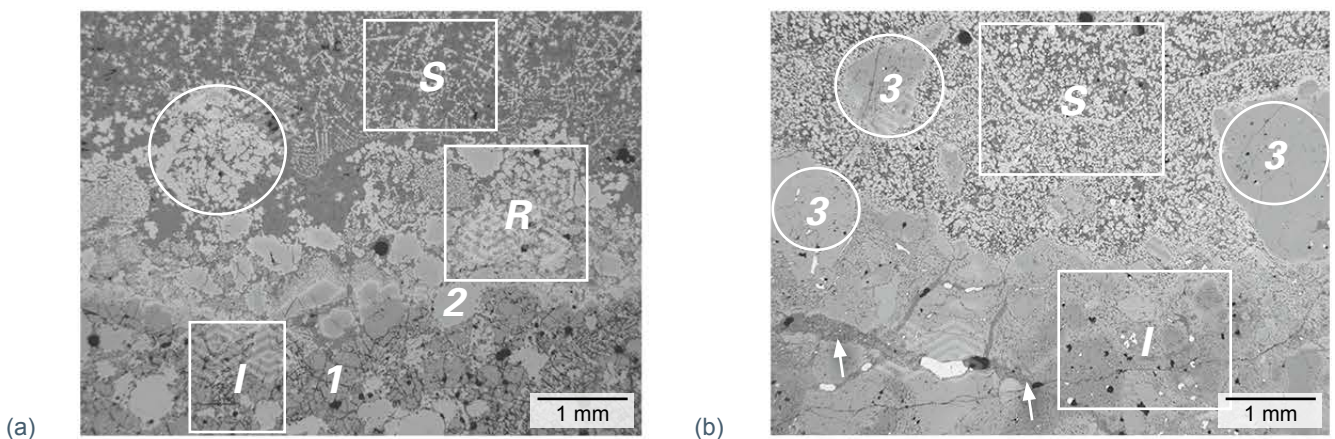


Figure 1.

Photomicrograph of the immediate brick hot face taken with reflected light microscopy showing (a) microstructural overview of a used magnesia-chromite brick and (b) used alumina-chromia brick. Slag coating (S), reaction zone (R), and infiltrated and corroded brick microstructure (I). Chromite precipitations (circle) after corrosion of the magnesia brick component (1). Chromite relics (2). Corroded fused alumina (3). Crack formation (arrows).



- The solubility of refractory components increases in the order of $\text{Cr}_2\text{O}_3 \rightarrow \text{MgO} \rightarrow \text{Al}_2\text{O}_3$.
- MgO and Al_2O_3 are sensitive to temperature increases while the Cr_2O_3 solubility is rather stable.
- Solubilities of Cr_2O_3 and MgO are not sensitive to any changes in the Fe/SiO_2 ratio.
- With increasing Fe/SiO_2 , the Al_2O_3 solubility decreases.

In a second step, the composition of the copper blowing slag was used to calculate the Al_2O_3 , MgO , as well as the Cr_2O_3 solubility in the Cu_2O -rich slag system (copper blowing slag). The results are illustrated in Figure 3.

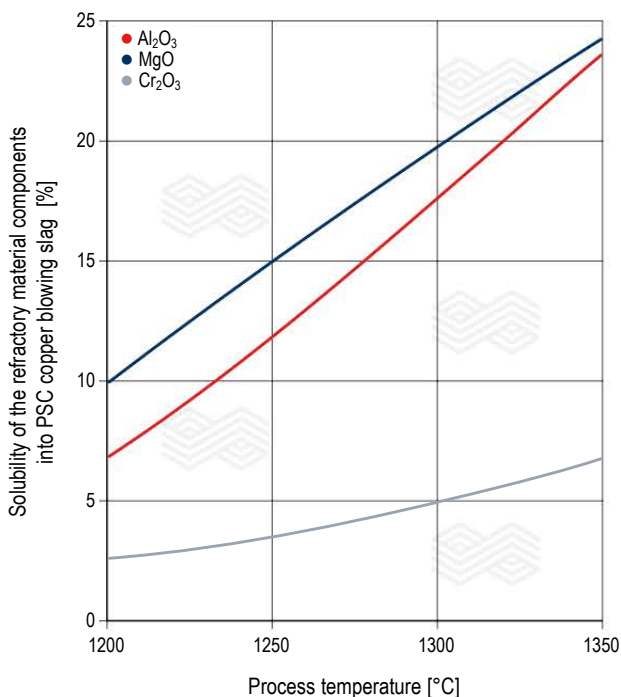
- In contrast to the iron blowing slag, the solubility of refractory components increases in the order of $\text{Cr}_2\text{O}_3 \rightarrow \text{Al}_2\text{O}_3 \rightarrow \text{MgO}$.
- With increasing temperature, the difference between MgO and Al_2O_3 solubility decreases and at 1350 °C is almost equal.
- Generally, the Cu_2O -rich slag is more aggressive in terms of solubility towards the refractory components MgO and Al_2O_3 than for the iron blowing slag. Also the Cr_2O_3 solubility is more than doubled compared to the iron blowing slag.

Based on the thermochemical calculations, the magnesia-chromite bricks appear to be more corrosion-resistant (i.e., lower solubility) against the iron blowing slag, whereas the alumina-chromia bricks shows lower solubility when used with copper blowing slag.

The temperature dependence of the refractory component dissolution clearly indicates the importance of proper

Figure 3.

Solubility of the refractory components Al_2O_3 , MgO , and Cr_2O_3 in copper blowing slag from PS converter operation at fixed Fe/SiO_2 ratio of 1.5, fixed oxygen partial pressure of $p_{\text{O}_2} = 10^{-6}$ atm, and as function of temperature.



process temperature control (e.g., using continuous temperature measurement) and monitoring of furnace conditions (e.g., using continuous monitoring and/or digital technologies for lining status prediction).

Chemical Attack by Sulphur

Another very common type of chemical attack is corrosion by high sulphur supply when processing sulphidic ores. The penetration of gaseous SO_2 from the oxidation of sulphidic matte creates the prerequisite for SO_3 to react with basic oxides of the magnesia-chromite brick at temperatures below approximately 1100 °C, leading to formation of earth alkaline sulphates in the system MgSO_4 and CaSO_4 (Figure 4).

Although the oxidation of SO_2 to SO_3 rapidly decreases above 760 °C, a certain partial pressure of SO_3 can be assumed in the temperature range between 760 °C and 1100 °C that would allow the formation of basic sulphates.

The intensity of the sulphate corrosion depends, on one hand, on the amount of supplied SO_2 , surplus of acidic SO_2 versus the basic components of the infiltrate such as alkaline compounds, reaction temperature, and time, and on the other hand on brick properties such as porosity, bonding strength, type of bonding, and brick composition. [9].

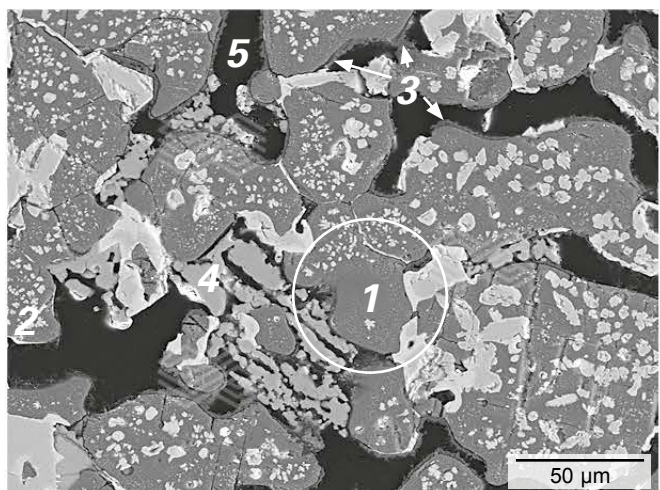
In the case of magnesia-chromite bricks with a high CaO/SiO_2 ratio, the interstitial phase such as dicalcium silicate is also massively corroded. The latter resulted in the formation of Ca sulphate (Figure 4). The possible reaction is schematically represented in equation 1:



This means that the CaO/SiO_2 ratio of the silicate phases is shifted to a lower value, and this similarly proceeds until forsterite is formed. The alumina-chromia bricks show generally higher corrosion resistance against sulphur attack.

Figure 4.

Photomicrograph taken by scanning electron microscopy showing microstructural details of a used magnesia-chromite brick: Corroded magnesia (1), chromite (2), Mg sulphate (3), Ca sulphate (4), and pore (5).



Nonoxide Infiltration and Copper Oxide Attack

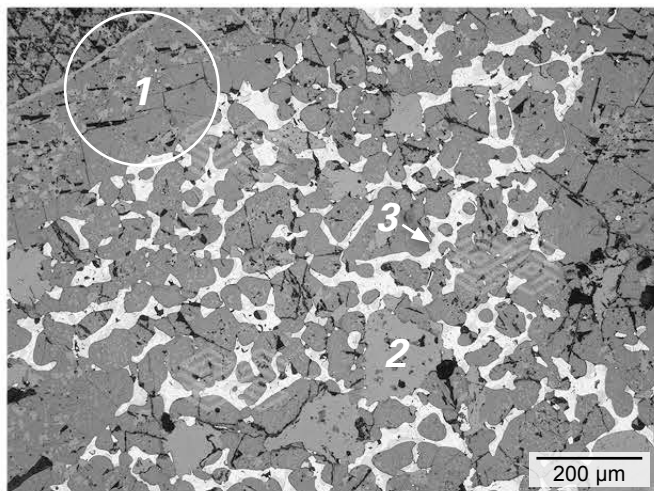
The nonoxide infiltration described in this section reveals infiltration of the refractory microstructure with copper and matte (Figure 5). Both copper and matte infiltration result in an increase in the brick brittleness, which is mainly caused by changed thermomechanical properties. Similar to the slag, the degree of infiltration depends on the surface tension, the boundary angle in contact with the refractory oxides, the metal density, the bath height, and the size as well as distribution of the brick pores [2].

Due to the high wetting and mobility properties of Cu-oxide (low viscosity, Table I, e.g., refining slag) Cu-oxide was able to penetrate up to the cold face of the refractory causing pore-filling densification by cuprite (Cu_2O). Within this brick area particularly the magnesia component was highly enriched with Cu-oxide. Divalent copper oxide (e.g., tenorite (CuO)) was also rarely observed.

The infiltrated copper oxide reacted with the brick's inherent periclase (MgO) to form a (Mg,Cu,Ni)O solid solution. Additionally, güggenite (Cu_2MgO_3) formation at the rims of the (Mg,Cu,Ni)O solid solution particles was frequently observed.

Figure 5.

Photomicrograph taken by reflected light microscopy showing the brick microstructure of a used magnesia-chromite brick, which is completely infiltrated with matte: Magnesia (1), chromite (2), and matte (3).



Thermo-(Mechanical) Load

Particularly in the tuyere zone of the PS converter, the refractory lining suffers from high thermomechanical load. Temperature changes due to discontinuous converter operation create stresses in the brick lining which can only be absorbed to a limited extent, thus leading to crack formation as soon as microstructural strength was exceeded.

The mechanical load includes mechanical fatigue, impact by charging material (e.g., blister copper), static stresses, and hot erosion [2]. Mechanical fatigue is typical of the drum type anode furnace. Static tension which arises through inadequate brick lining or failure in the heating procedure leads to serious deformation of the brick lining and crack formation.

Conclusions

The wear mechanisms observed in the postmortem analyses and discussed in this paper demonstrate that a combination of slag attack, infiltration, and corrosion of the brick's inherent components lead to a softening of the brick's microstructure and a loss of flexibility and brick strength. This weakened microstructure is then susceptible to continuous wear by hot erosion. Additionally, due to the changes in the thermomechanical properties of the refractory, thermal shock leads to crack formation, primarily at the interface between the infiltrated and noninfiltrated brick areas, and finally, to discontinuous wear by spalling. Monitoring of both process and furnace, as well as digital technologies to predict the lining status are valuable tools for metal producers. All these technologies need to be closely coupled to refractory material data and experience of refractory behaviour in metallurgical vessels to provide maximum benefit to the customer.

The acidic fayalite slag mainly corrodes the MgO component in the magnesia-chromite brick. In addition, alumina-chromia bricks suffer from severe chemical slag attack. In the infiltrated brick microstructure, particularly fused alumina and Zr-mullite are severely corroded. Cr-corundum shows higher corrosion resistance. The results from FactSage calculations proved to be in good accordance with the results of postmortem studies and operational experience. Based on the practical experience and thermochemical calculations, the magnesia-chromite bricks should provide higher performance than alumina-chromia bricks for the application in the PS converter operation. For applications in anode furnaces for example, the alumina-chromia bricks can be an alternative which confirms the experience that RHI Magnesita has already obtained with these types of refractories.

The high sulphur supply, typically occurring when processing sulphidic materials under oxidising conditions, leads to corrosion of the brick-inherent magnesia and of the interstitial CaO-containing secondary phase like dicalcium silicate within the magnesia. Chromite generally shows a higher corrosion resistance against both fayalite slag and sulphur attack. The alumina-chromia bricks generally show higher corrosion resistance against sulphur attack.

Noncorrosive infiltration of the brick microstructure by copper or matte dramatically changes the thermal conductivity of the brick, thus increasing the susceptibility to crack formation and spalling, which is intensified by thermal shocks. In comparison to copper metal or matte, copper oxide reacts with the refractory components.

Additionally, mechanical load results in a continuous abrasion of the infiltrated and corroded brick material at the hot face.

A detailed investigation of wear mechanisms is an important prerequisite for the refractory producer as it provides the basis for both product recommendations and innovative product development. Such postmortem investigations can clearly highlight which specific stresses affect the refractory products in the copper processing furnaces such as the PS converter and anode furnace. On the basis of the investigation results, combined with long-term service experience, a refractory producer can recommend the most appropriate choice of furnace brick lining for the client's specific operational parameters. This is frequently enhanced through active collaborations with the customer.

For further optimisation of lining life, monitoring technologies and digital prediction tools need to be implemented. A possible solution package for the cases described in the present paper could be: Continuous process temperature measurement to avoid overheating, continuous level measurement to track level changes and bath movement (process efficiency), continuous monitoring of the furnace and lining conditions to minimise energy losses and avoid hot spots, as well as using digital technologies to predict the lining status dependent on the actual process conditions. These technologies and use in metallurgical vessels will be discussed in more detail in an upcoming paper.

References

- [1] Davenport, W. G., King, M., Schlesinger, M., and Biswas, A. K. Extractive Metallurgy of Copper. Elsevier Science Ltd., 2002, 1–10.
- [2] Barthel, H. Wear of Chrome Magnesite Bricks in Copper Smelting Furnaces. *InterCeram*. 1981, 30, 250–255.
- [3] Routschka, G., and Wuthnow, H. (2012). Handbook of Refractory Materials (4th ed.). Vulkan-Verlag, Essen, 2012.
- [4] Harmuth, H., and Vollmann, S. Refractory Corrosion by Dissolution in Slags – Challenges and Trends of Present Fundamental Research. *Iron and Steel Review*. 2014, 58 (4), 157–170.
- [5] Mackey, P. The Physical Chemistry of Copper Smelting Slags – A Review. *Canadian Metallurgical Quarterly*. 1982, 21, 221–260.
- [6] Sarhadi, M., Niknejad, E., and Yoozbashizadeh, H. Fire refining of copper- As, Sb and Bi removal by basic oxidation with decreased refractory wear. Presented at Copper 2013, Santiago, Chile, December 2013.
- [7] Yamauchi C., Application of sodium carbonate slag to copper refining. Presented at TMS 2003, San Diego, USA.
- [8] Bale, C. W., Chartrand, P., Deckerov, S. A., Eriksson, G., Hack, K., Ben Mahfoud, K. R., Melançon, J., Pelton, A. D., and Petersen, S. FactSage thermochemical software and databases. *Calphad*. 2002, 62, 189–228.
- [9] Gregurek, D., Reinharter, K., Majcenovic, C., Wenzl, C., and Spanring, A. Overview of Wear Phenomena in Lead Processing Furnaces. *Journal of European Ceramic Society*. 2015, 35, 1683–1698.

Authors

Dean Gregurek, RHI Magnesita, Leoben, Austria.

Katja Reinharter, RHI Magnesita, Leoben, Austria.

Jürgen Schmidl, RHI Magnesita, Vienna, Austria.

Christine Wenzl, RHI Magnesita, Vienna, Austria.

Alfred Spanring, RHI Magnesita, Vienna, Austria.

Corresponding author: Dean Gregurek, dean.gregurek@rhimagnesita.com



Dickson Souza, Francisco López, Herman Moggee and Carlos Lamare

A Toolbox of Slag Modelling and Metallurgy in Your Pocket

Thermodynamic modelling is an important tool for understanding the various factors that contribute to phenomena observed in steelmaking. Factors such as temperature, composition, and basicity are frequently discussed when dealing with slags and the proper tuning of these variables is required for good metallurgical results (desulphurisation and inclusion removal) and to obtain a refractory compatible slag. Savings on energy and material costs are also possible when a model indicates that an imbalance exists in added raw materials or when enough slag is generated so as to cover the arc in an electric arc furnace—just enough, no excess. A toolbox containing several thermodynamic models is offered by RHI Magnesita and the development is rooted in several years of research and development and application: The guiding principle is the easy application of scientific principles to the melt shop, enabling control and even increased performance of refractory linings as well as good metallurgical results. This paper will illustrate some practical cases where a model contributes to diagnostics and improvement of the melt shop operation.

Introduction

The importance of slag engineering has been growing in the past decades. Slag is more than a by-product and it is being recognised that proper slag management benefits steel quality and refractory linings and more research is carried out each year to uncover new aspects and properties of slags. Slag management includes optimisation of the chemistry and other relevant aspects such as phase composition, viscosity, density, and surface tension.

The functions of slags in metallurgical processing are summarised below, according to Mills [1]:

- It seals off the metal from oxygen and prevents oxidation.
- It removes undesirable elements (e.g., S, P) from the metal.
- It helps to remove non-metallic inclusions (e.g., by flotation).
- It reduces the heat losses from the metal surface and prevents “skull formation”.
- In the continuous casting of steel, liquid slag infiltrates continuously between the metal and mould and it provides both lubrication and control of the heat extraction.

There are two other important functions of slags: Firstly, to cover the arc and prevent arc flare and damage to electric arc furnace and ladle refractories and secondly to be fully compatible with the refractory lining and avoid chemical corrosion that reduces equipment availability and safety [2,3].

The complex nature of slag structure requires the use of a combination of physical and computational methods for a deep comprehension of the specific role and effects in steelmaking. Simplified models are usually derived from these high-level models to be applied in the melt shop. The simplification can either be present in the modelling itself, stripping out finer details, or in the computational aspect, in order to enable calculations to be useful at the melt shop floor.

The e-tech website is a toolbox of such models, including slag and steel models, developed by RHI Magnesita and offered as an additional service to customers, with a network of experts in metallurgy around the world that use these tools to provide advice to customers to optimise the steelmaking process with a dual goal: Improve refractory performance and enable the production of high-quality steels.

Fundamental Concepts

Slags can be defined as ionic solutions consisting of molten metal oxides and fluorides that float on top of the steel (completely liquid or partially liquid) [3]. They can be classified according to the process they belong to: Ladle slags and blast furnace slags are based on the system CaO-Al₂O₃-MgO-SiO₂ (CAMS) while EAF and BOF slags belong to the system CaO-FeO_x-MgO-SiO₂. Slags formed from mould powders usually contain Na₂O and CaF₂ and, belong to the system CaO-Al₂O₃-SiO₂-Na₂O-CaF₂ [4].

Slags can be classified as basic or acidic and as oxidised or reduced slags depending on the specific chemistry. Basic slags are rich in CaO and MgO while acid slags are rich in SiO₂ and Al₂O₃; oxidised slags have high amounts of so-called reducible oxides (R₂O₃ = FeO, MnO and Cr₂O₃), and therefore a high O potential, due to the oxidative environment in which they are formed (either in electric arc furnaces or in basic oxygen furnaces); reduced slags, on the other hand, are present in ladle metallurgy and in later stages of stainless steelmaking in argon oxygen decarburisation (AOD). They are characterised by a low content of reducible oxides, which is ideal for desulphurisation and for higher metallic yield.

Given the multiple roles performed by slag in metallurgical processes, it is unsurprising that conflicting goals may sometimes arise. Fortunately, there are recurrent cases where metallurgical functions and refractory compatibility can be optimised at the same time by proper tuning of slag chemistry. A useful measurement of refractory compatibility is the saturation of the main refractory oxides in slag. Magnesia-based refractories, for example, are well suited to work with slags saturated in MgO. Thermodynamically speaking, the chemical wear of refractories will be as high as the slag is far from the saturation point, since the driving force will favour the dissolution of the refractory until the slag reaches the saturation point. The wear rate, if dissolution is the only mechanism active [5], can be expressed by the Nernst equation (1):

$$\frac{dC^A}{dt} = h \cdot (C_s^A - C^A) \quad (1)$$

Where C^A is the concentration of A in the liquid phase outside the boundary layer, C_s^A is the saturation solubility of A in the liquid phase, and h is the mass transport constant.

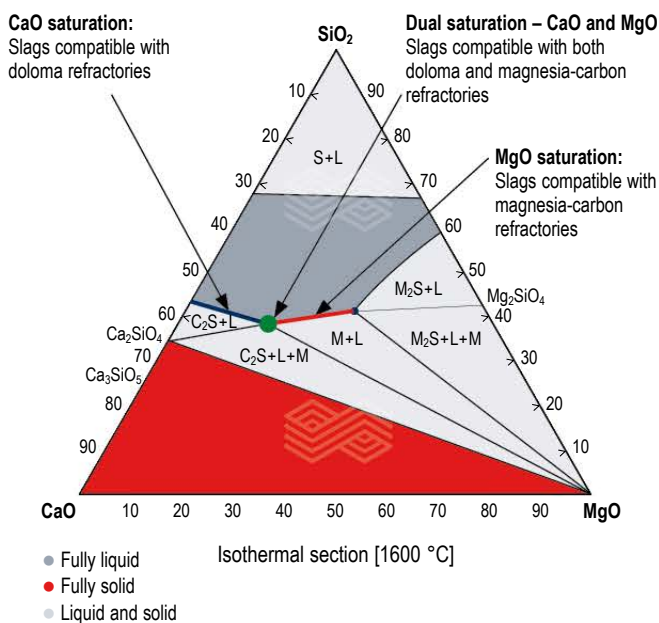
As slag lines in steelmaking are mostly made of MgO-based or CaO-based materials, three main types of saturation calculations can be identified:

- MgO saturation: Typically used with oxidised slags with MgO-C linings (EAF, BOF).
- CaO saturation: Typically used with doloma linings. As the matrix phase in dolomitic refractories is predominantly lime, it is crucial to have slag saturated with CaO.
- Dual saturation: Typically used with ladle slags and MgO-C slag lines. Slag in this condition has a maximum amount of CaO and MgO dissolved at the same time.

Figure 1 shows these three types of saturations for a simple CaO-MgO-SiO₂ slag.

Figure 1.

CaO-MgO-SiO₂ isothermal section at 1600 °C, showing saturation boundaries [8, adapted].



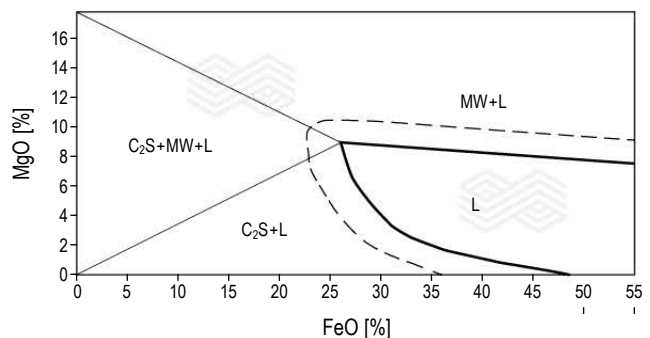
Electric Arc Furnaces

In 2019, electric arc furnaces (EAF) accounted for 27.7% of the world crude steel production, according to the World Steel Association (2020), with an even greater share in some regions (76.5% in Africa and 94.5% in the Middle East). The operation of the refining process in EAF is improved if a good foaming slag practice is established. Foaming slag ensures better refractory performance and other benefits to the process such as lower electrode consumption, higher thermal efficiency and, consequently, lower melting time [6]. Two basic requirements are needed for a slag to foam: Sustained generation of gas bubbles and a suitable consistency, neither completely liquid or crusty.

The Foamy Slag application is designed to provide some insights into the slag chemistry. Before delving into an example calculation, let us see the typical phase distribution in EAF slags according to the specific chemistry. That goal is fulfilled using the so-called isothermal stability diagram (ISD). ISD allows the representation of a given slag, displaying MgO content on the vertical axis, FeO (and MnO) on the horizontal axis and is drawn for a fixed basicity (B3) and temperature and can be thought as a 6-oxides phase diagram. Slags in the region marked with an L are completely liquid and are therefore not good for foaming, since viscosity is too low to sustain a stable foam [3]. Outside fully liquid regions, ISD displays the existence of three partially liquid regions: Magnesio-wustite + liquid in high MgO area, C₂S + liquid in low MgO, low FeO area and, finally, magnesio-wustite + C₂S + liquid in the intermediary region. Research and empirical evidence [3,9] support that the presence of a small percentage of solid particles provides a foamy behaviour, as it increases the viscosity and that is the reason for a dotted line along the liquid region boundary in ISD. It is an indication for the target one should have for their EAF slags.

Figure 2.

Isothermal stability diagram (ISD) for a basicity (B3) of 2.0 and 1600 °C [3].



Using e-tech’s Foamy Slag application, one can run calculations that evaluate slags with respect to foamy behaviour. Figure 3 presents a screenshot of input data required to perform the assessment. Data from slag analysis, raw material chemistry, temperature, supersaturation, and targets (FeO +MnO and basicity) is required. In this example, we see a typical EAF slag chemistry [3] at 1600 °C, weighing 10000 kg. The target content of % FeO + % MnO is set to 30% and the supersaturation of MgO (excess of MgO after the saturation line) is defined to be 1%—needed to create a small percentage of precipitated magnesio-wustite particles. No change in basicity is expected—the calculation should consider that the current basicity (B3 = 1.70) will be the goal.

Figure 3.
Input data to make an assessment of slags for EAF [7].



Figure 4.
Results of the assessment of slag presented [7].



The output for this scenario is shown in Figure 4. Saturation is reached for MgO at 9.68% and due to the specified supersaturation value, the target slag contains 10.68% MgO. In order to reach the target slag chemistry, an additional 188 kg of doloma is required and the amount of original lime added should be decreased by 114 kg. Through a simple manual calculation, it can be found that, using lime and doloma, the initial slag was created by adding 1384 kg of doloma and 2068 kg of lime. The results therefore indicate that, for the next heat, the charges should be changed to 1582 kg (+ 14%) of doloma and to 1954 kg (- 9%) of lime. Depending on the actual initial slag, the changes in operational practice might be even more profound than this example, requiring larger changes in the charge amounts.

Figure 5 presents an analysed slag and target slag plotted on the same ISD, showing that the analysed slag was liquid and may therefore not show ideal foaming characteristics, while the target slag lies in the region containing magnesio-wustite and liquid. The amount of solid particles in the target slag must be sufficient to improve the foamy behaviour. Figure 6 presents another case to illustrate that slag may be even farther from the saturation boundaries—straight red lines—and then adjustment may require larger additions of fluxes, in this case 572 kg of magnesia for a scenario of lime and magnesia addition.

Figure 5.
ISD for the example shown in Figures 3 and 4 [7].

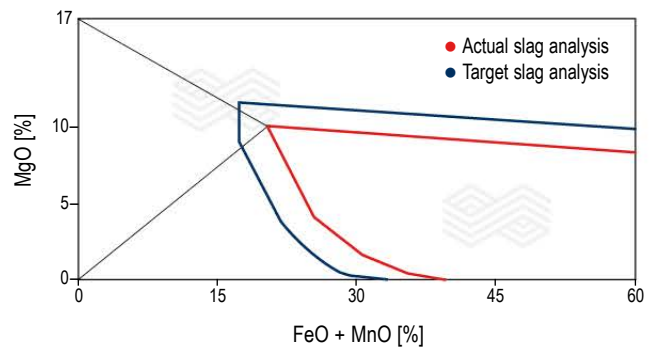
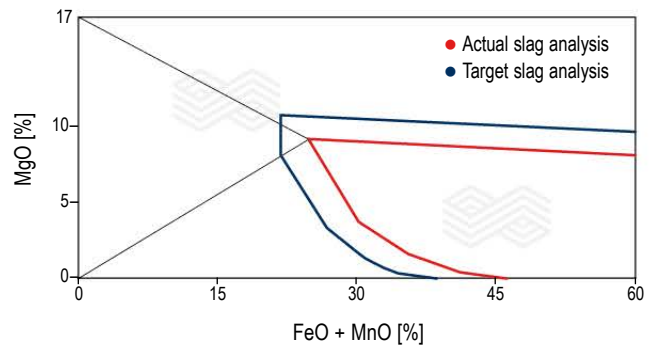


Figure 6.
ISD showing a slag farther in the liquid region that requires larger additions of magnesia to correct the MgO content [7].



Ladles

Ladle metallurgy has a central place in today's steelmaking. The crude steel from primary refining stages (basic oxygen furnace or electric arc furnace) can undergo further refining in ladles through operations like degassing, desulphurisation, inclusion flotation, and inclusion modification.

Ladles can also function as a buffer and enable sequential operation of continuous casting and allow intermittent operation of primary furnaces. In this situation, it is sometimes required to reheat steel to the temperature specified for continuous casting to compensate for the loss in temperature due to prolonged hold times in the ladle. When no ladle furnace station is available, chemical reheating is the method used to adjust the final temperature before casting.

Chemical reheating uses the energy released in oxidation reactions. Pure aluminium and ferrosilicon alloys are commonly used for this purpose as they have a strong affinity for oxygen. Oxygen required for the reaction is provided using a lance or a bottom plug. It is recommended to add lime in chemical reheating operations to compensate the increase in Al_2O_3 and/or SiO_2 content in the slag as a consequence of the reaction of Al and Si with dissolved O.

Figure 7.

Inputs of Al-Si reheat application. Alloys, oxygen, and lime additions to be calculated for a 50 °C increase in steel and slag temperature. Steel and slag are assumed to be at the same initial temperature [8].

| INITIAL CONDITIONS AND TEMPERATURES | | | | | |
|-------------------------------------|---------------------|--------------------------|---------------------------|------------------------|--|
| Steel weight (tonne) | Slag weight (tonne) | Initial Temperature (°C) | Temperature increase (°C) | Final Temperature (°C) | |
| 55 | 2 | 1600 | 50 | 1650 | |

| ADDITIONAL INFORMATION | | Lime Addition Factor | | Chemistry of additions | |
|------------------------|-----------------------------|-----------------------------|--------------|------------------------|--|
| Heating efficiency (%) | Al reheating (default: 3.5) | Si reheating (default: 3.2) | % Si in FeSi | % CaO in lime | |
| 85 | 3.5 | 3.2 | 75 | 90 | |

Figure 8.

Results of Al-Si reheat calculation [8].

| HEATING WITH ALUMINUM | | HEATING WITH FERROSILICON | |
|--|--------|--|--------|
| Variable | Result | Variable | Result |
| Aluminum Required (kg) | 187 | Silicon Required (kg) | 152 |
| O ₂ Required (Nm ³) | 117 | FeSi Required (kg) | 202 |
| Pure CaO Required (kg) | 655 | O ₂ Required (Nm ³) | 121 |
| Lime Required (kg) | 690 | Pure CaO Required (kg) | 485 |
| | | Lime Required (kg) | 511 |

The Al-Si Reheat application, available on the e-tech website, is a simple yet useful calculation model that enables the estimation of Al or Fe-Si weight and oxygen volume required to increase the temperature of steel and slag. The amount of lime to adjust the slag chemistry is also provided as part of the calculation. The inputs required (Figure 7) are the steel and slag weight, the initial temperature (assumed to be identical for steel and slag), and the desired temperature increase to achieve the casting temperature, for example. The heat losses via conduction, convection, and radiation are accounted for in the heating efficiency parameter. Figure 7 also shows the lime addition factor and chemistry of additions as other input parameters. Lime addition factors are calculated to obtain slags with a CaO/SiO_2 ratio close to 1.5 and $\text{CaO}/\text{Al}_2\text{O}_3$ ratio close to 1.85 and, assuming the oxide/metal stoichiometric ratio ($\text{Al}_2\text{O}_3/\text{Al} = 1.88$ and $\text{SiO}_2/\text{Si} = 2.14$), default values of 3.5 and 3.2 were finally obtained.

The results, shown in Figure 8, indicate that 187 kg of aluminium are required or 202 kg of FeSi (75% Si) to increase the temperature of 55 tonnes of steel and 2 tonnes of slag to 1650 °C. 690 kg of lime are required to counteract formation of alumina; if ferrosilicon is used, 511 kg of lime are required. A complete analysis of consequences of chemical heating is out of the application's scope; however, a careful consideration of phenomena like alloy fading and fine inclusion formation should be included before process changes are made.

Stainless Steelmaking

One of the processing steps of stainless steelmaking is the refining in the argon oxygen decarburisation converter (AOD). Primary steel is produced in either EAFs or BOFs and then transferred to AODs to follow the steps to produce the final stainless steel [2]. Primary steel (also known as transfer steel) contains high amounts of carbon and silicon and the removal of these two elements is among the main goals for AOD. AOD operation is based on lowering the carbon monoxide partial pressure via the use of a diluting gas (argon) so that the decarburisation reaction takes greater precedence than the chromium oxidation, which is harmful to the process (as it affects steel composition and production cost). A heat in an AOD is processed in two steps. Step 1 consists of decarburisation, where the oxygen to inert gas ratio is high at the beginning and may gradually decrease as carbon is removed to obtain low pCO in the gas bubbles. The oxygen to inert gas ratio is controlled to keep a high carbon removal efficiency (CRE) where CRE is defined by equation 2 [10]:

$$CRE = \frac{O_2 \text{ used in removing } [C]}{\text{Total } O_2 \text{ added}} \quad (2)$$

After reaching the desired carbon level, the Cr and Mn oxides formed need to be reduced from the slag. These oxides were formed during the decarburisation stage step 1 as a side effect of the reactivity of these metals towards oxygen and an unbalanced gas composition with instantaneous pCO; this is the reason why an optimised blowing regime is so important: It allows high CRE without too much oxidation. Cr and Mn oxides are reduced by addition of FeSi in step 2, the reduction stage. While in step 1 slag was predominantly solid, slags in step 2 need to be liquid to allow quick reduction reactions. Step 3, the desulphurisation and/or reheating stage, also requires liquid slag to perform its function.

Taking into account details of the steel and slag transfer and raw materials charged (Figure 9), Stainless Mass Balance, another application of the e-tech website, enables the user to perform a full mass balance of AOD slags in all 3 stages, providing recommendations of fluxes and alloys charges. The recommendations aim to optimise slags to fulfil their functions in each step and make them compatible with doloma refractories, commonly used in AOD vessels.

The first output of this application addresses the changes required to adjust slags to the desired target. The results shown in Figure 10 are the recommendations when magnesia is selected as the MgO source and dual saturation is chosen for the reduction stage. In Figure 11, the slag analysis for the reduction and desulphurisation stages is displayed. Actual and target slag chemistries are compared side by side and the required additions are shown in the last two rows.

Figure 9. An overview of input parameters required to run Stainless Mass Balance calculation. For conciseness, some tables were not displayed completely [11].

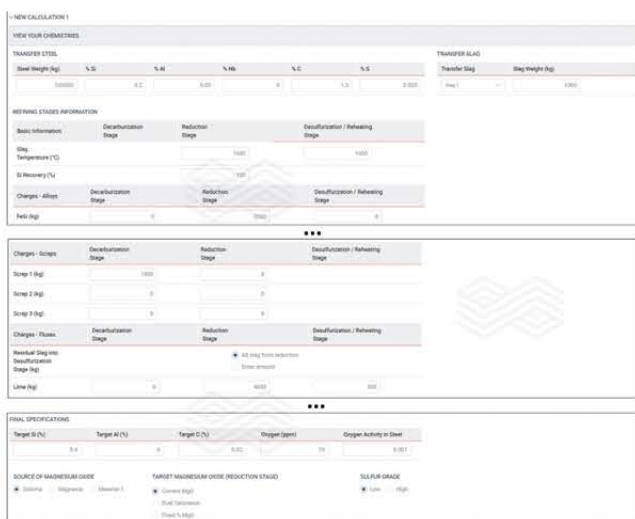


Figure 10. Flux additions for each stage of the AOD process [11].

| Decarb Slag | | Reduction Slag | | Desulf/Reheat Slag | |
|-------------|-------------------|----------------|-------------------|--------------------|-------------------|
| Lime | Magnesia Required | Lime | Magnesia Required | Lime | Magnesia Required |
| 1215 kg | 0 kg | 3604 kg | 2364 kg | 2143 kg | -0 kg |

Casting

The last example of the toolbox available at the e-tech website is the calculation of ferrite potential for carbon steels, a value that indicates the solidification mode of steels. $F_p > 1$ are indicative of steels that solidify as ferrite δ while values below 0 indicate a fully austenitic structure. This concept was introduced by Manfred Wolf [7] and is useful to determine the potential (or tendency) for cracking or surface defects that might occur during casting as shown schematically in Figure 12.

The calculations in this case are based on steel chemistry and involve calculating the carbon equivalent and then use it to calculate the ferrite potential using the following equations:

$$F_p = 2.5 \cdot (0.5 - [C_{eq}]) \tag{3}$$

$$C_{eq} = [\%C] + 0.04[\%Mn] + 0.1[\%Ni] + 0.7[\%N] - 0.14[\%Si] - 0.04[\%Cr] - 0.1[\%Mo] - 0.24[\%Ti] - 0.7[\%S] \tag{4}$$

Figure 11. Calculated slag analysis for reduction and desulphurisation slags. The last two rows show the required flux addition to adjust actual slag to the target slag [11].

| | Reduction Slag | | Desulf Slag | |
|---------------------------------|----------------|--------|-------------|--------|
| | Actual | Target | Actual | Target |
| %MgO | 0.88 | 14.12 | 0.83 | 0.80 |
| %CaO | 46.25 | 51.54 | 47.83 | 55.93 |
| %Al ₂ O ₃ | 11.07 | 7.20 | 10.41 | 8.79 |
| %SiO ₂ | 37.41 | 24.34 | 35.18 | 29.72 |
| %CaF ₂ | 4.29 | 2.79 | 5.63 | 4.76 |
| %CaCrSiO ₆ | 1.24 | 2.12 | 1.36 | 1.89 |
| Ch-MgSiA | 0.97 | 2.68 | 1.97 | 1.47 |
| Lime Required (kg) | | 3604 | | 2143 |
| Magnesia Required (kg) | | 2364 | | -0 |

Figure 12. Schematic representation of the tendency for stickers, depressions, and crack type according to Wolf [7].

- | | | |
|--|---|--|
| <p>0.005 [%C] Primary δ</p> <ul style="list-style-type: none"> • Some shell distortion at mould surface. • Short freezing range. • Low shell strength. | <p>0.10 [%C] Primary $\delta + \gamma$</p> <ul style="list-style-type: none"> • Rapid transformation to γ. • Large shell distortion. • Small ($T_s^* - T_s$) range. • High shell strength. | <p>1.0 [%C] Primary γ</p> <ul style="list-style-type: none"> • Little shell distortion. • Long freezing range. • Lower shell strength (liquid microsegregation). |
|--|---|--|

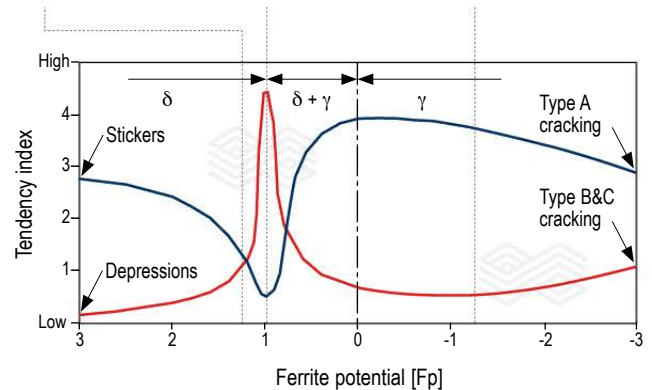


Figure 13 shows the Ferrite Potential application and the results obtained for this steel chemistry. The chart in Figure 14 shows that this steel solidifies as ferrite δ and it is more prone to stickers than to depressions.

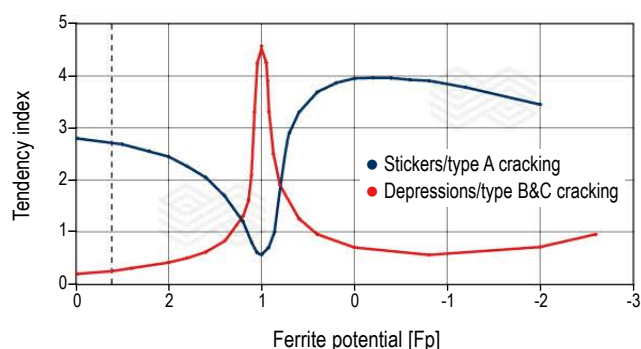
Figure 13.

Ferrite potential and carbon equivalent calculated values based on input steel chemistry [13].



Figure 14.

Plotting of ferrite potential for input steel chemistry and tendency index for defects [13].



References

- [1] Mills, K.C. The estimation of slag properties. Short course presented as part of Southern African Pyrometallurgy 2011.
- [2] Asth, H.G. Desenvolvimento de escórias de refino secundário para o forno panela da V&M do Brasil. Dissertação Universidade Federal de Minas Gerais, Brazil, 2011.
- [3] Pretorius, E.B. Fundamentals of EAF and ladle slags and ladle refining principles. Course Notes Baker Refractories. York, 2000.
- [4] Lehman, J., Jung, I.-H. and Zhang, L. The main thermo-statistical models of metallurgical slags: theory and applications. Proceedings of the International Conference Of Molten Slags, Fluxes And Salts, Beijing, China, 2012.
- [5] Poirier, J. et al. An overview of refractory corrosion: observations, mechanisms and thermodynamic modeling. *Refractories Applications Transactions*, 2007, 3, 2.
- [6] Pretorius, E.B. and Carlisle, R.C. Foamy slag fundamentals and their practical application to Electric Furnace steelmaking. *Electric Furnace And Process Technology*. 1998.
- [7] <https://etech.rhimagnesita.com/furnace/FoamySlag>; accessed on 30.10.2020.
- [8] <https://etech.rhimagnesita.com/ladle/Al-SiReheat>; accessed on 30.10.2020.
- [9] Kho, T.S. et al. Understanding stainless steelmaking through computational thermodynamics Part 1: electric arc furnace melting. *Mineral Processing and Extractive Metallurgy*. 2020, 119, 1.
- [10] Nunnington, R.C. Fundamentals of Stainless Steel Refining. Course Notes. LWB Refractories: York, 2003.
- [11] <https://etech.rhimagnesita.com/stainless/StainlessMassBalance>; accessed on 30.10.2020.
- [12] Nunnington, R.C. Ferrite potential (Fp) and ferrite share (Fs) calculations for casting carbon and stainless steels. Course Notes. LWB Refractories, York, 2004.
- [13] <https://etech.rhimagnesita.com/caster/FerritePotential>; accessed on 30.10.2020.
- [14] Pretorius, E.B. and Marr, R. Computer modeling of refractory/slag/metal interactions. Proceedings of the International Conference On Molten Slags, Fluxes And Salts, Sydney, Australia, 1997, p. 281–288.
- [15] World Steel Association. World Steel in Figures 2020. Available at <https://www.worldsteel.org/en/dam/jcr:f7982217-cfde-4fdc-8ba0-795ed807f513/World%2520Steel%2520in%2520Figures%25202020i.pdf>, accessed on 30.10.2020.

Authors

Dickson Alves de Souza, RHI Magnesita, Contagem, Brazil.

Francisco José López Gonzalez, RHI Magnesita, Contagem, Brazil.

Herman Moggee, RHI Magnesita, York (PA), USA.

Carlos Lamare, RHI Magnesita, Rotterdam, Netherlands.

Corresponding author: Dickson Alves de Souza, dickson.souza@rhimagnesita.com

Conclusion

Some calculation models, available at the e-tech website, were presented briefly in this paper to show the potential benefits in the day-to-day life of a metallurgist or a refractory engineer. As models based on sound science and engineering, they provide insights on aspects of slags and steels that can help with the optimisation and correction of processes with a strong focus on the improvement of refractory lining life by fine tuning the slag chemistry. Caution and understanding of adopted assumptions are essential to evaluate if the model is valid for the situation under investigation. RHI Magnesita has a team of engineers that has proven records of applying these models in close cooperation with customers, making the necessary adjustments and helping to modify process conditions. Moreover, these applications are part of the digital solutions portfolio of RHI Magnesita and they are in constant evolution.

Acknowledgements

This work was based on a coordinated effort to modernise the e-tech website and improve user experience when performing calculations. The website is also a platform for learning, given the diversity and depth of content presented. The authors would like to acknowledge all colleagues involved in the modernisation of e-tech, based on a shared understanding that modelling is an important tool to assist customers in their processes. Special thanks go to Eugene Pretorius, Helmut Oltmann and Robert Nunnington, who developed and promoted the use of these models, founded on decades of research and empirical experience in several plants around the world.



Andreas Viertauer, Michael Schacher, Stanislav Ulitsky, Matthias Scheibmayr, Erich Röllin, Reinhard Ehrenguber, Matthias Stalzer, Oswin Dolzer, Teodor Staicu, Thomas Kollmann, Bernd Trummer, Alexander F. Orlov, Alexander Papushev, Sergey Razgulyaev, Marcus Kirschen and Sergey G. Zhuravlev

Implementation of BOF Gas Purging Technology and Current Process Results After One Year of Successful Operation at Severstal Cherepovets

The paper describes the milestones for the project realisation, dealing with inert gas purging in the BOF converter and provides an insight into the results achieved during and after one year of operation with inert gas bottom stirring. In addition to the fast project realisation, the metallurgical results were remarkable and have been achieved in two major steps. Three significant key performance indicators (KPIs) are used to describe the performance improvement. These are the oxygen activity $a[\text{O}]$, the product $[\text{C}]$ in % multiplied by $a[\text{O}]$ in ppm, and the content of (FeO) in % in the slag determined at the end of the blowing process.

Introduction

The steelmaking company Severstal, located at Cherepovets, is the 4th largest steel producer in the Russian Federation and number 37 globally with a crude steel production of 11.85 million tonnes in 2019 [1]. Severstal's approach, as leading steel producer, is to continuously upgrade the production facilities along the process chain. In 2018, the decision was made to upgrade the existing three basic oxygen furnaces each with a nominal heat size of 380 tonnes with RHI Magnesita INTERSTOP converter inert gas purging (CIP) technology. The contract to implement the complete CIP technology system together with installation of eight multi hole plugs (MHP) and the complete lining from RHI Magnesita was signed in September 2018. The final acceptance certificate (FAC) was received in November 2019.

Initial Situation

Severstal decided in 2018 to equip all three BOFs with bottom stirring technology to gain metallurgical benefits thereby improving production efficiency. Corresponding literature and background information can be found in the cited literature [2–5].

Project Realisation

It was decided to implement the complete CIP technology system together with installation of eight multi hole plugs (MHP) together with the BOF lining from RHI Magnesita. The contract was signed on September 19, 2018. The first commissioning at BOF No. 3 was carried out during a complete relining and the hot test followed only two months later in November 2018. The completion of the performance tests occurred an additional two months later in December 2018. The same procedure was followed for the two remaining BOFs.

The commissioning and hot tests of BOF No. 2 and 1 occurred in January 2019 and March 2019, respectively. The final performance tests for BOF No. 1 and 2 were carried out in May 2019. The final acceptance certificate (FAC) was received thirteen months after contract signing on November 7, 2019. The project milestones are summarised in Table I.

Figure 1 describes the complete solution of the CIP at a BOF [6]. The gas control station was designed to control eight multi hole plugs. The number of plugs could be extended to even 16 lines if required. The number, location, and the configuration of the plugs depend on many parameters such as vessel geometry, heat size, blowing lance design, hot metal chemistry, and steel grades just to name some of the main parameters. The type of gas (argon or nitrogen) and the flow rate are predefined in recipe patterns and supplied for each plug independently. The used recipe would be automatically selected depending on the steel grade chemistry being produced and target values for $[\text{C}]$, $[\text{P}]$ and $[\text{N}]$ are set. Figure 1 displays the core part of the installation from the visualisation of the pulpit, and the data transmitting via ethernet to the control station. Each line is controlled separately and supplied with gas by the rotary joint to each MHP. Additionally, a cross section from a MHP can be seen at the bottom right of Figure 1.

The detailed engineering was done for all three BOFs starting from a defined take-over point for Ar and N₂ to the eight MHPs. Each compact flow control unit was installed close to the corresponding BOF. Additionally, the implementation of basic automation took place simultaneously. Figure 2 shows (a) a section of the converter bottom with one MHP and surrounding bricks during the relining of the vessel, (b) impression of the revamping works at the converter platform, and (c) the installed CIP cabinet for BOF No. 3.

One remarkable challenge was the rotary connection between the mainland platform and the rotating BOF vessel. Figure 3a shows the sketch of the rotary connection to the BOF trunnion and 3b the installed rotary connection.

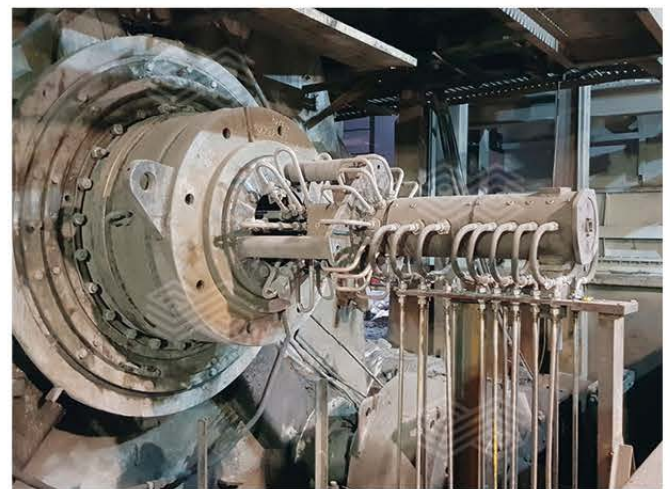
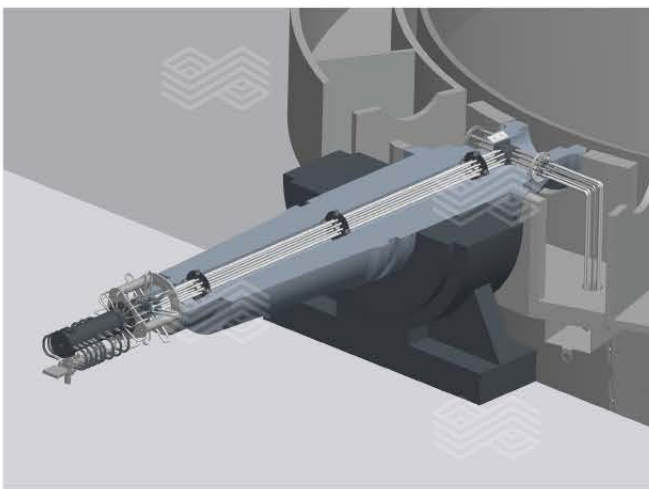
The tailor-made visualisation was an important success factor. Figure 4a demonstrates several key parameters such as target and current flow rate, purging pressure, and type of gas for each MHP. All data is recorded and can be visualised as a trend with purging relevant figures. The histogram shows the actual and set flow and purging pressure for a preselected MHP during a blowing cycle (Figure 4b).

Metallurgical Results

For confidential reasons, metallurgical figures will be not published in detail, but the rapid project realisation and the FAC show indirectly the achievements. The presented performance figures were in the range to be best in class compared with other publications [9–13]. The ongoing process improvements were only possible by customised adaptations of the CIP gas flow programs. However, it must be noted that optimising the metallurgical KPIs runs in contradiction to improving the lifetime of the MHPs [7].

Figure 3.

(a) sketch of the rotary connection through the trunnion and (b) installed rotary connection.

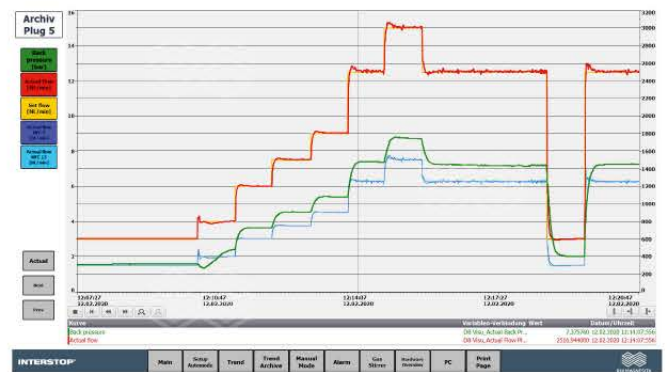
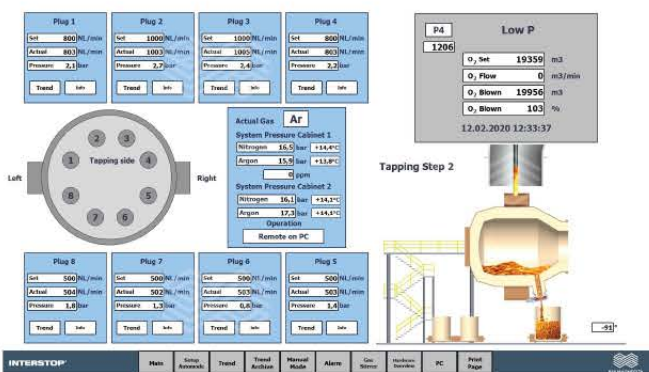


(a)

(b)

Figure 4.

(a) visualisation in the control room and (b) a preselected purging trend during one blowing cycle.



(a)

(b)

Usually higher gas flows lead to improved metallurgical KPIs but also increase the wear rate of the MHPs through erosion. Here, special care must be taken to avoid excessively high gas flows promoting an increased erosion wear mechanism caused by jetting (Figure 5) [8].

CIP also provides additional metallurgical benefits which cannot be achieved without gas purging [14–16]. For example, a very low dephosphorisation ratio can only be achieved by post stirring after the main blowing. This provides the opportunity to produce steel grades with a very low [P] content. Another benefit is the possibility to control the nitrogen content of the steel by selecting the optimised predefined and standardised CIP pattern depending on the requirement. These will match very low or, if required, even very high [N] target levels.

The frequency distributions in Figure 6a and 6b describe the evolution without CIP in 2018, during the performance tests in 2019, and data from January and February 2020. The improvements were significant for the $[C] \times a[O]$ product as well as for the (FeO) content in the slag.

Figure 5.

Depiction of the jetting phenomena.

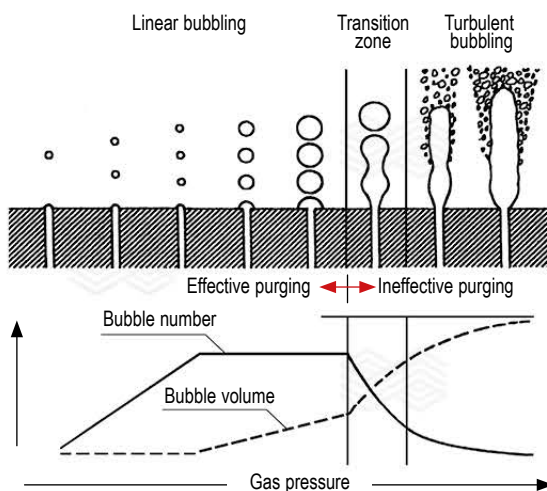
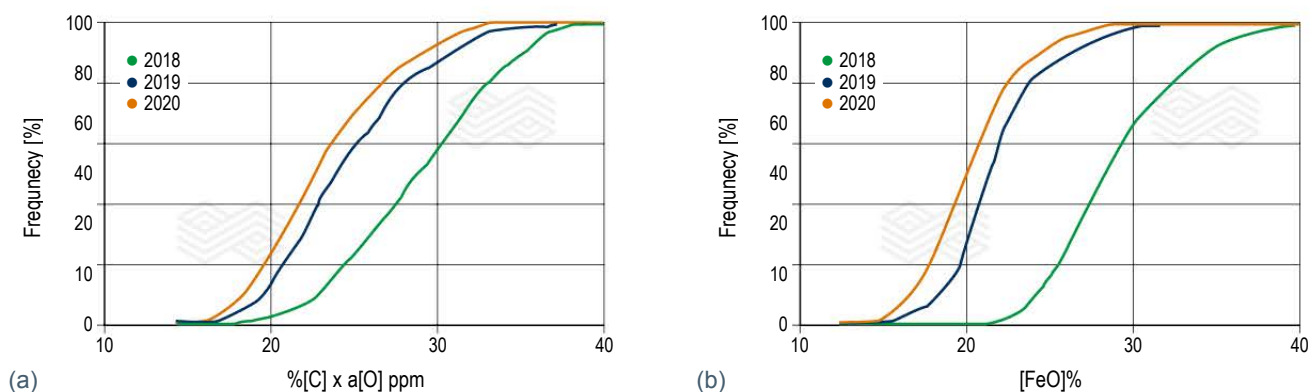


Figure 6.

Frequency distribution of (a) $\%[C] \times a[O]$ in ppm and (b) % (FeO) in 2018, 2019, and 2020.



Conclusion

CIP has set a new standard for steelmaking at Severstal's BOF steelmaking shop and has been integrated within the existing Level 1 and Level 2 automation system. The chosen purging program is automatically selected based on predefined steelmaking parameters. The system is modular in design, which provides many benefits for maintenance and spare part management. Specifically, the regulation system, with high accuracy, functionality, and fast regulation speed is key to generate the benefits. Purging plug clogging and/or deep infiltration caused by hot metal, slag and/or steel is negligible. The CIP was stopped due to safety precautions with high availability at approximately 4000 heats at the beginning of 2020. However, there was still potential for a further lifetime increase as has been shown by periodic measurements of the residual lining thickness by a laser scanner.

Finally, after nearly one year of operation with CIP, the $a[O]$ has been reduced by 21%, the $[C] \times [O]$ product by 29%, and the (FeO) content reduced by 21% compared to activity prior to installation of the CIP in 2018. In addition to these improvements, the steel yield has also been increased since the introduction of CIP. The main cost savings levers were a lower use of deoxidation agents, which is commonly carried out with expensive aluminium. An increased steel yield, due to less (FeO) content in the slag and less consumption of oxygen, highlight the further benefits in addition to the metallurgical benefits such as dephosphorization. CIP is one important milestone to improve the stability of the process and, accordingly, to increase the productivity of the plant [17]. It should also be noted that the introduction of CIP has contributed to a reduction in the CO_2 footprint [18].

Acknowledgment

This remarkable success story was only possible due to the extraordinary close cooperation of all parties in this project, namely Severstal, NSK, and RHI Magnesita. We would like to thank all personnel and management for the trust and support during the project execution, commissioning, and further continuous improvement.

References

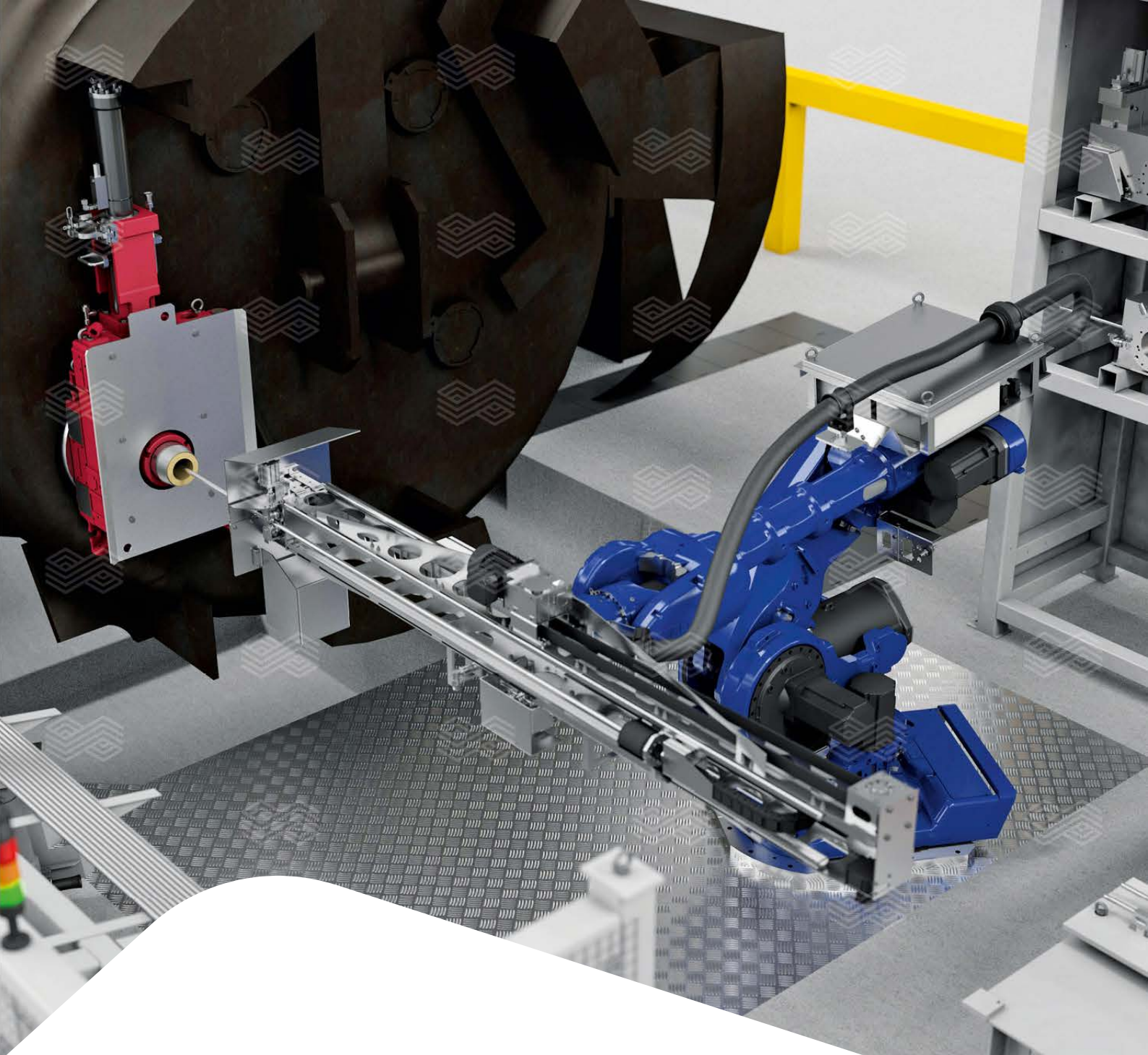
- [1] www.worldsteel.org, Top steelmakers in 2019.
- [2] Krieger, W., Pofnerl, G. and Apfalterer, R. Erzeugung von Stählen mit niedrigem Kohlenstoffgehalt im Bodenspügenden LD-Tiegel. Presented at the Eisenhüttag 1984, Leoben, Austria, 29.05.1984.
- [3] Krieger W., Hubmer, F., Patuzzi, A. and Apfalterer R. LD-Prozeß mit Bodenspülung-Maßnahmen, Möglichkeiten Ergebnisse. *Stahl und Eisen*. 1985, 105, 12, 673–678.
- [4] Hiebler, H. and Krieger, W. Metallurgy of the LD- Process. *BHM*. 1992, 137, 7, 256–262.
- [5] Miller, T.W., Jimenez, J., Sharan, A. and Goldstein, D.A. Making Shaping and Treating of Steel, Chapter 9- Oxygen Steelmaking Processes. AISE Steel Foundation, Pittsburgh, USA, 1998.
- [6] Ehrenguber, R. Excellence in Inert Gas Control Systems for the Steel Industry. *RHI Bulletin*. 2015, 1, 7–15.
- [7] Kirschen, M., Zettl, K.-M. and Ude R. BOF Process Improvements by Enlarged Gas Purging Portfolio from Moderate to Very High Gas Flow Rates. Proceedings of the 8th European Oxygen Steelmaking Conference - EOSC2018, Puglia, Italy, October 2018.
- [8] Steinmetz, E. and Scheller, P.R. Beitrag zu den Strömungsverhältnissen in einer Spülsteinpfanne. *Stahl und Eisen*. 1987, 107, 417–425.
- [9] Schoeman, E., Wagner, A., Ebner, W. and Berger, M. Implementation of Basic Oxygen Furnace Bottom Purging at Mittal Steel Newcastle. *RHI Bulletin*. 2006, 2, 7–11.
- [10] Kollmann, T. and Jandl, C. Basic Oxygen Furnace Benchmarking – Maintenance and Process Considerations. *Stahl und Eisen*. 2013, 12, 37–43.
- [11] Kollmann, T., Jandl, C., Schenk, J., Mizelli, H., Höfer, W., Viertauer, A. and Hiebler, M. Comparison of Basic Oxygen Furnace Bottom Gas Purging Options. *RHI Bulletin*. 2012, 1, 8–15.
- [12] Haider, M. and Kirschen, M. Efficient Bottom Purging for BOF. Proceedings of the 5th International Conference on Refractories at Jamshedpur – ICRJ 2017, Jamshedpur, India, 2017, 55–57.
- [13] Haider, M., Gutschier, G., Schretter, A. and Kirschen, M. BOF Bottom Purging Efficiency and the Impact of Slag Maintenance with a Case Study from Jindal Steel Works in India. *RHI Bulletin*. 2016, 1, 14–19.
- [14] Wünnenberg, K. and Cappel, J. Cost-Saving Operations and Optimization on Metallurgical Reactions in BOF Practice. *Iron and Steel Technology*. 2008, 11, 66–73.
- [15] Bruckhaus, R. and Lachmund, H. Stirring Strategies to meet the Highest Metallurgical Requirements in the BOF Process. *Iron and Steel Technology*. 2007, 11, 44–50.
- [16] Urban, W., Weinberg, M., and Cappel, J. Dephosphorization Strategies and Modeling in Oxygen Steelmaking. *Iron and Steel Technology*. 2015, 4, 91–102.
- [17] Sakar, A., Joshi, H., Schretter, A., Gutschier, G. and Mitterer, T. Efficient Value-Added Steel Production with low mix Maintenance Level at JSW Steel in India. *Bulletin*. 2019, 30–33.
- [18] Kollmann, T., Bundschuh, P., Sann, V., Schenk, J. and Kirschen, M., Gas Purging Benefits in the BOF: A Focus on Material Efficiency and CO₂ Emission Reduction Proceedings of the METEC and 2nd ESTAD2015, 15.-19.06. 2015, Düsseldorf, Germany.

Authors

Sergey G. Zhuravlev, Severstal, Cherepovets, Russia.
 Sergey Razgulyaev, Severstal, Cherepovets, Russia.
 Alexander Papishev, Severstal, Cherepovets, Russia.
 Alexander F. Orlov, NSK, Russia.
 Andreas Viertauer, RHI Magnesita, Vienna, Austria.
 Stanislav Uliitsky, RHI Magnesita Interstop AG, Hünenberg, Switzerland.
 Michael Schacher, RHI Magnesita Interstop AG, Hünenberg, Switzerland.
 Reinhard Ehrenguber, RHI Magnesita Interstop AG, Hünenberg, Switzerland.
 Matthias Scheibmayr, RHI Magnesita Interstop AG, Hünenberg, Switzerland.
 Erich Röllin, RHI Magnesita Interstop AG, Hünenberg, Switzerland.
 Teodor Staicu, RHI Magnesita, Veitsch, Austria.
 Oswin Dolzer, RHI Magnesita, Radenthein, Austria.
 Matthias Stalzer, RHI Magnesita, Vienna, Austria.
 Bernd Trummer, RHI Magnesita, Vienna, Austria.
 Thomas Kollmann, RHI Magnesita, Vienna, Austria.
 Marcus Kirschen, RHI Magnesita, Mülheim-Kärlich, Germany.

Corresponding author: Andreas Viertauer, andreas.viertauer@rhimaginesita.com





Tailor-made ladle-to-mould solutions INTERSTOP Robotics

In order to make steel production safe and economical while maintaining the highest quality standards, we provide our customers with a modular scope of supply, focusing on the core business of systems technology.

For ladle gate systems, INTERSTOP offers solutions in the ladle preparation area and on the CCM floor that allow for manual and robotic operation. The full package contains the latest slide gate technology, fully equipped with casting cylinder and media coupling, all being operated by customised robotic systems.

Curious to find out more details?
Visit rhimagnesia.com/automation-and-robotics

Follow us



RHI MAGNESITA

Aloísio Ribeiro, Anderson Nogueira, Jürgen Schütz, Eduardo Menezes, Rogério Diogo Araújo and Vítor Domiciano

Advanced Technology Package for Blast Furnace Runners Focusing on Operational Safety, Availability, and Refractory Performance

In order to meet the demands of the blast furnace runners related to operational safety, availability, and performance, refractory suppliers are continuously challenged to develop innovative and integrated solutions to fulfil customer needs and requirements. This paper aims to present solutions implemented in the blast furnace runners in South America comparing them to the standard projects and solutions. Easy drying refractory castables based on sol-bonded technology, laser scan measurements for main runner inspections, and monolithic permanent linings were revealed to be the main trends to increase runner availability, enhance refractory performance, and improve operational safety, leading to a new level of operational results.

Introduction

In recent years, the average annual production of hot metal from integrated mills in South America has reached 32 million tonnes, with Brazil accounting for approximately 85–90% of this production, followed by Argentina representing approximately 7% [1]. The major challenges for a safe and effective cost of hot metal production in blast furnaces are closely linked to the tapping practices and the runner projects used in the casthouse. In regards to the blast furnace main runners, the installation of the refractories and their performance play an important role in keeping the stability of the blast furnace production.

Once these parameters are well adjusted, a significant reduction of worker exposure is achieved in the casthouse activities, while also providing suitable conditions for full blast furnace production.

Based on recent developments in South America's blast furnace casthouse refractory projects, this paper will address the major main runner projects in terms of safety, availability, and performance. In order to meet these demands, a systemic assessment of the available technologies will be presented in this work aiming to point out the technological trends for the best practices for blast furnace main runners.

Variables related to blast furnaces' operational conditions and the influence in the main runner refractories' performance have already been covered [2,3] and, therefore, will not be within the scope of this work. Figure 1 presents the different blast furnace runner regions. The main runner experiences the highest thermal load due to the hot metal and slag which intensifies the wear mechanisms mostly related to erosion, corrosion, thermal shock, and oxidation of the refractory working lining. In addition, along its length, the main runner enables the separation of hot metal and slag due to the different densities.

Figure 1.
Regions of blast furnace runners [4].

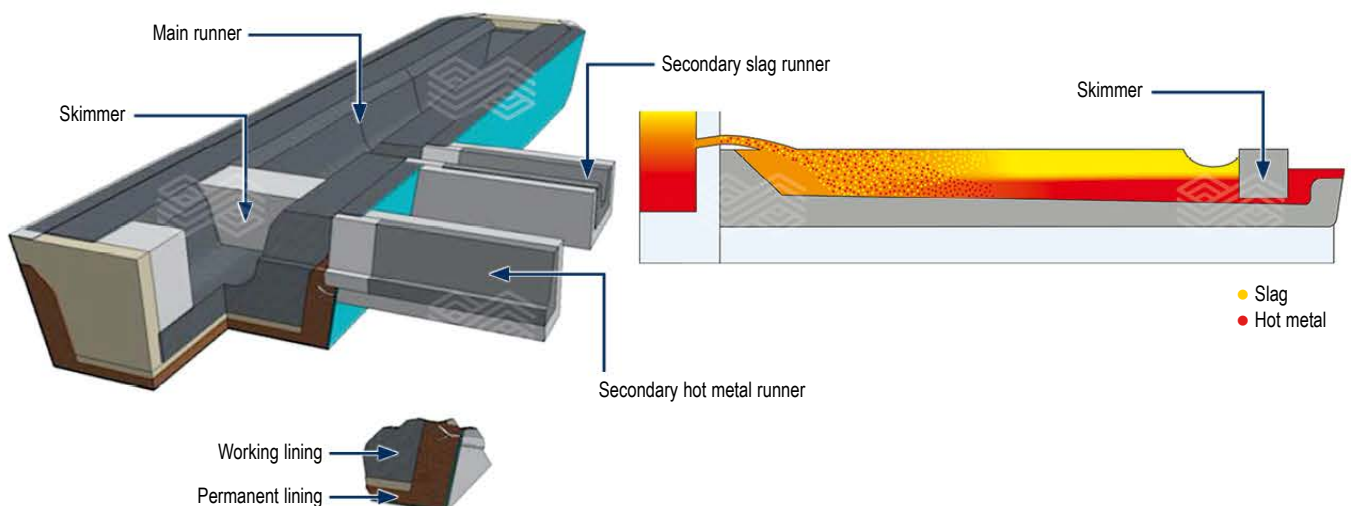


Table I presents the main runner projects, the refractory product technologies, and the campaign expectations for several blast furnaces in South America. In regards to the refractory working lining characteristics, this can be built using a single line castable or it can be cast using zone lining castables (one for the hot metal zone and another for the slag zone).

The skimmer is a dam set up inside the main runner which ensures slag and hot metal separation by the differences in density. The lower opening is known as the throat and only hot metal should pass through. In addition to severe thermomechanical stresses, the main wear mechanisms on the skimmer are erosion in the throat region and corrosion in the upper region due to contact with the slag.

Table I.
Summary of the most relevant main runner projects.

| Blast furnace | | Permanent lining | | | | Working lining | | | |
|-----------------------------------|-----|------------------|-------------------------|-----------------|---|-----------------------|--------------------|--------------------------|------------------|
| Internal volume [m ³] | THs | Metallic shell | External refrigeration* | Insulate lining | Refractory lining | Castable technology** | Characteristics*** | Castable application**** | Campaign [HM kt] |
| 885 | 2 | Yes | No | Brick | 70% Al ₂ O ₃ brick | ULC | SL | P + SHT | 160–180 |
| 885 | 2 | Yes | No | Brick | 70% Al ₂ O ₃ brick | ULC | | P + SHT | 160–180 |
| 3163 | 3 | Yes | ACB | Brick | 70% Al ₂ O ₃ brick | ULC | SL | P + SHT | 90–130 |
| 3051 | 4 | Yes | No | Brick + board | 70% Al ₂ O ₃ and ASC bricks | ULC | SL | PP | 90–130 |
| 1750 | 2 | Yes | No | Brick + board | 70% Al ₂ O ₃ and ASC bricks | ULC | SL | PP | 360–380 |
| 3284 | 2 | Yes | FS | Board | Mullite castable | SBC | SL | PP + SHT | 280–300 |
| 3284 | 2 | Yes | FS | Board | Mullite castable | SBC | SL | PP + SHT | 280–300 |
| 4540 | 4 | Yes | ACB | Brick + board | 70% Al ₂ O ₃ brick | ULC | ZL | PP | 120–140 |
| 1556 | 2 | Yes | ACB | Brick + board | 70% Al ₂ O ₃ brick | ULC | ZL | PP | 340–360 |
| 3617 | 4 | Yes | FS | Brick + board | 70% Al ₂ O ₃ brick | ULC | ZL | PP | 110–130 |
| 1653 | 2 | Yes | No | Brick | 70% Al ₂ O ₃ brick | ULC | ZL | PP | 90–110 |
| 4237 | 4 | Yes | ACB | Brick | 70% Al ₂ O ₃ brick | ULC | ZL | PP | 110–130 |
| 3809 | 4 | Yes | FS | Brick | Al ₂ O ₃ castable | ULC | ZL | PP + DG | 110–130 |
| 1357 | 1 | Yes | ACB | Board | Mullite castable | ULC | ZL | Casting | 115–130 |
| 2610 | 2 | Yes | FAC | Board | Al ₂ O ₃ pre-casting | ULC | ZL | P + SHT | 520–590 |
| 881 | 1 | Yes | ACB | Brick | Fireclay brick | ULC | SL | P + SHT | 90–100 |
| 748 | 1 | | No | Brick | Fireclay brick | HM | SL | Ramming | |

THs: Tapholes; Hm kt: Hot metal kilo tonnes

* ACB: Air circulation box; FS: Free suspended; FAC: Forced air circulation

** ULC: Ultra-low cement; SBC: Sol-bonded castable; HM: Hamming mix

*** SL: Single lining; ZL: Zone lining

**** P: Pumping; PP: Pneumatic pumping; SHT: Shotcrete; DG: Dry gunning

The thermomechanical stresses occur during the main runner operation through a complex expansion–contraction mechanism arising from the heating and cooling cycles, which occur during each tap interval, and mainly along runner drainages, providing significant displacements in the region. In addition to this, during low thermal level events of the blast furnace, the burning of an oxygen lance in the skimmer's throat is a common practice to ensure that the throat remains unobstructed. This procedure leads to severe damage in the skimmer refractory due to oxidation and higher thermal exposure. In this scenario, the goal was to achieve greater structural integrity of the skimmer by using refractory bricks which present higher erosion resistance to hot metal. Figure 2 shows different main runner skimmer projects and the campaign expectations.

Materials and Methods

In order to address the main requirements of blast furnace runners related to safety, availability, and performance, the properties of different refractory castables were laboratory characterised and further validated in the field. For the monolithic permanent lining application, the dilatometry (NETZSCH, heating rate 5 °C/min) of different alumina-silica LC based castables was performed to evaluate the expansion behaviour up to 1400 °C (Figure 3). The physical and mechanical properties were also measured after drying and firing (Table II).

Figure 2.

Characteristics of the main runner skimmer projects.



Casting during the main runner maintenance

Campaign estimate:
80000–120000 hot metal tonnes



Reinforced skimmer using high erosion resistance bricks in the throat region

Campaign estimate:
90000–140000 hot metal tonnes



Preshaped skimmer

Campaign estimate:
140000–400000 hot metal tonnes
(with intermediate repairs)

Table II.

Main properties of the alumina-silica LC refractory castables.

| Main properties | | DIDURIT F55-5-BR | DIDURIT M77-8-BR | DIDURIT B83-6-BR |
|--------------------------|------------------------------------|-------------------|------------------|------------------|
| Main raw materials | | Bauxite, fireclay | Fused mullite | Bauxite |
| Chemical composition [%] | Al ₂ O ₃ | 54.90 | 77.30 | 85.40 |
| | SiO ₂ | 38.00 | 20.60 | 11.20 |
| | CaO | 1.80 | 1.70 | 1.10 |
| | Fe ₂ O ₃ | 1.50 | 0.10 | 0.80 |
| | Na ₂ O+K ₂ O | 0.56 | 0.25 | 0.41 |
| 110 °C/24 h | BD [g/cm ³] | 2.38 | 2.74 | 2.78 |
| | AP [%] | 11.60 | 8.10 | 12.50 |
| | CCS [MPa] | 60.40 | 76.10 | 31.50 |
| | MoR [MPa] | 11.80 | 13.90 | 5.50 |
| | PLC [%] | -0.04 | -0.02 | 0.06 |
| 1200 °C/5 h | BD [g/cm ³] | 2.36 | 2.69 | 2.77 |
| | AP [%] | 18.80 | 16.40 | 17.00 |
| | CCS [MPa] | 66.40 | 84.60 | 86.00 |
| | MoR [MPa] | 13.50 | 9.70 | 22.20 |
| | PLC [%] | -0.17 | 0.11 | -0.06 |
| 1400 °C/5 h | BD [g/cm ³] | 2.35 | 2.68 | 2.74 |
| | AP [%] | 19.10 | 17.00 | 17.90 |
| | CCS [MPa] | 80.40 | 91.60 | 95.20 |
| | MoR [MPa] | 14.90 | 11.10 | 20.20 |
| | PLC [%] | -0.24 | 0.12 | 0.43 |
| HMoR [MPa] – 1200 °C/3 h | | 8.20 | 10.90 | 8.80 |
| HMoR [MPa] – 1400 °C/3 h | | 1.40 | 3.10 | 1.80 |

Finally, the chemical composition was determined using X-ray fluorescence. All field trials presented in this work were carried out in the main runners of Ternium Brazil's blast furnaces (inner volume = 3284 m³, 2 tapholes operating through alternating taps).

The dilatometry results revealed that DIDURIT M77-8-BR (mullite-based) displays a similar thermal expansion to DIDURIT F55-5-BR (bauxite/fireclay-based) in the temperature range of 800–1400 °C. This indicates good dimensional stability for DIDURIT M77-8-BR, though with a higher Al₂O₃ content. On the other hand, when compared to DIDURIT B83-6-BR (bauxite-based; highest Al₂O₃ content), DIDURIT M77-8-BR showed significantly lower thermal expansion, indicating that mullite-based refractory castables may combine lower thermal expansion with good refractoriness for monolithic safety lining applications in blast furnace main runners. Using a standard single line Al₂O₃-SiC-C refractory castable as the working lining, which presents a thermal conductivity varying between 2–3 W/mk [5], the main runner's permanent lining can reach temperatures up to 1300 °C in the turbulent zone at the end of the main runner's campaign. Therefore, a suitable balance between hot mechanical properties and dimension stability is required for a safe and efficient main runner's permanent project. Table II presents the main properties of the different alumina-silica LC (low cement) refractory castables, where DIDURIT M77-8-BR shows higher hot strength combined with lower PLC variation after firing.

Figure 3.
Dilatometry of the alumina-silica LC refractory castables.

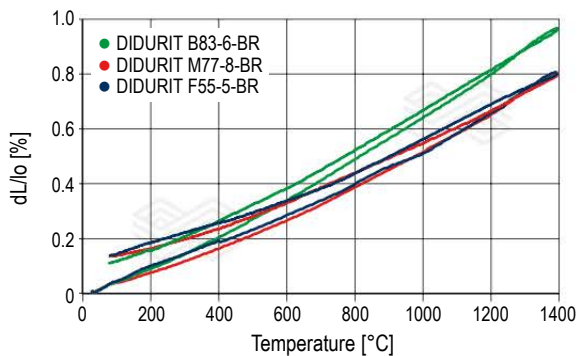
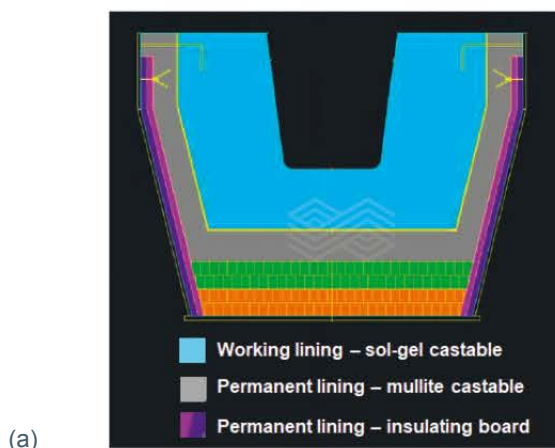


Figure 4.
Main runner's permanent lining, showing (a) designed project and (b) after refractory installation.



Results

Monolithic Permanent Lining

A new main runner project was developed focusing on metallic shell thermal protection and the volumetric stability during the main runners' operation. In this case, an insulating plate layer was installed over the metallic shell followed by a mullite-based refractory castable used as permanent lining replacing the traditional alumina bricks.

After implementing such project improvements, two main runner campaigns achieved a performance of 1.5 million tonnes of hot metal (HM). These results were obtained mainly due to the permanent refractory lining's stability, which showed few vertical cracks after the campaign when compared to the standard project based on medium alumina refractory and insulating bricks (Figure 5).

Historically, conventional brick permanent lining projects have never obtained such a campaign volume in the blast furnaces' main runners at Ternium Brazil. On the contrary, several accidents were registered over the years, some of them caused by the oxidation phenomena occurring in the refractory working lining's cold face due to air passage through the displaced bricks of the permanent lining [6]. When this occurs, a sudden increase in the refractory working lining's wear speed is commonly observed leading to unsafe casthouse operation.

Figure 5.
Monolithic permanent lining after a campaign.



Main Runner’s Working Lining—Sol-Bonded Castables and Preshaped Skimmers

Compared to standard ULC (ultra-low cement) castables, a drastic reduction in the drying/heat-up curve was implemented for the sol-bonded castables (Figure 6). The sol-bonded refractory castable technology demonstrates higher explosion resistance when exposed to fast heating curves due to the higher permeability and absence of the hydraulic phases present in the ULC castables.

The performance of ULC and sol-bonded castable technologies were compared in main runner working lining applications (Figure 7). In both scenarios, a shotcrete repair was carried out during the main runner inspection. The wear speed measured at the end of the campaigns was significantly decreased when using Al₂O₃-SiC-C sol-bonded castables compared to similar ULC castables.

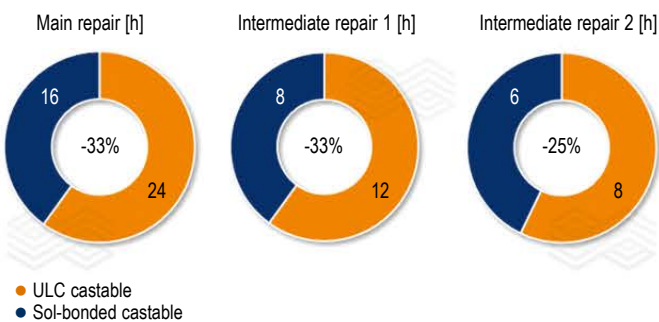
Additionally, in both skimmer projects, the refractory castable installed was identical, however, because the preshaped piece was manufactured under ideal production conditions, the skimmer performance was significantly improved from 120 kilo tonnes to 400 kilo tonnes of hot metal production.

Finally, a significant decrease in specific consumption of the refractory was achieved after implementing this new blast furnace main runner project at Ternium Brazil, which is composed of (1) a mullite-based castable combined with insulating plates in the permanent lining, (2) the sol-bonded Al₂O₃-SiC-C castable as the refractory working lining, and (3) the preshape skimmer using highly erosion resistant bricks. This new combination provided a significant specific consumption reduction (from 0.61 to 0.51 kg/HM tonnes) contributing to increasing the main runner availability.

3D Laser Scan for Refractory Inspection

The 3D laser scan method was implemented for the main runner refractory lining inspection with the aim to eliminate workers’ exposure on site, especially during the tap intervals (“hot inspections”). Essentially, the equipment emits a laser beam from a rotating mirror towards the area to be scanned and all the data is captured and transmitted via wireless LAN. This technique permits rapid and accurate measurements in comparison to the standard procedures (using a manual measuring rod) and is an important and reliable tool to monitor the refractory performance and extend the main runner campaign, while also providing a safer environment in the blast furnace casthouse operations (Figure 8).

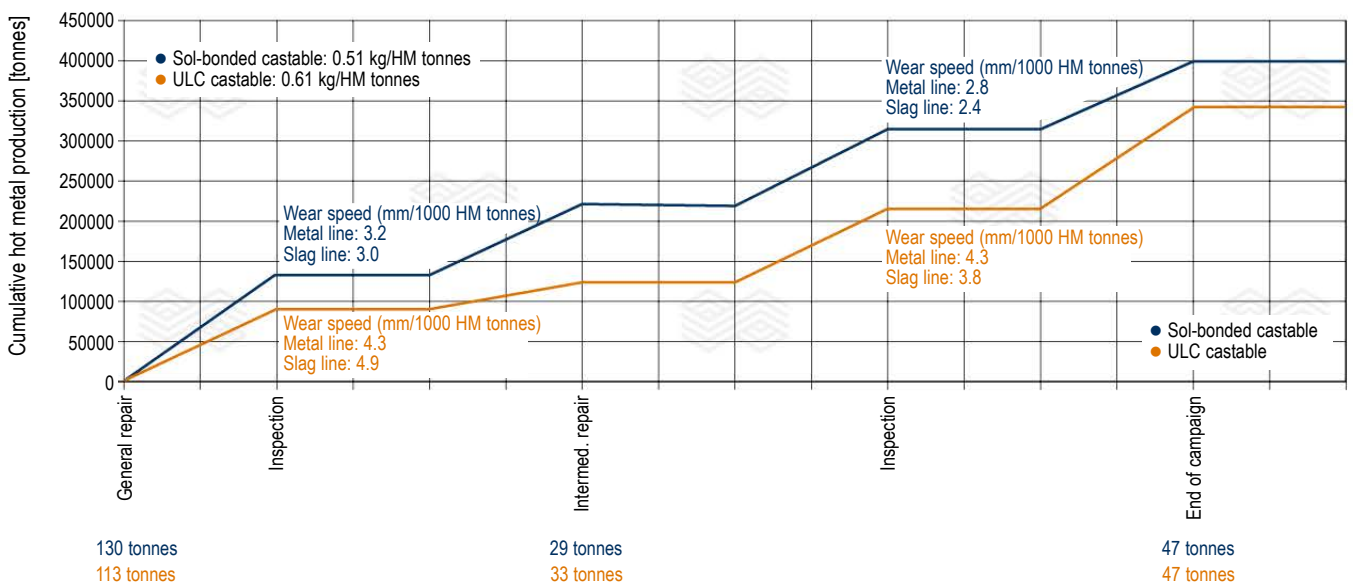
Figure 6. Time spent in the heating curves (h=hours) applied in the main runner refractory maintenance at Ternium Brazil.



Hot Repairs

Though hot repairs are a common practice and carried out in many blast furnace casthouses to extend main runner campaigns, this refractory maintenance activity is an unsafe operation in terms of workers’ exposure as the repair material (refractory castable) is cast over a residual refractory lining at 200–400 °C. Table III shows the differences between the main techniques and products used in hot repairs in blast furnace runners in South America. For these harsh installation conditions, sol-gel dry gunning has proven to be a safer alternative for workers, also mitigating the exposure to high temperatures along the refractory maintenance when compared to traditional methods using cement-bonded castables or ramming mixes.

Figure 7. Main runner campaign performance at Ternium Brazil.



Conclusions

The blast furnace's main runners require continuous improvements in terms of project, refractory technologies, and repairing techniques to fulfil operational requirements related to safety, availability, and refractory performance. For different sections of the main runners, the current trends to improve the main runner's performance are:

- Permanent lining: Replace the conventional alumina brick projects with a monolithic lining using mullite-based castables cast on-site and add an insulating plate layer.
- Working lining: Use of rapid drying refractory castables based on sol-bonded technology to increase the runner's availability, predominantly by decreasing the heat-up curve and the refractory lining wear.
- Hot repairs: Use of dry-gunning sol-bonded castables to improve labour safety during refractory maintenance.
- Runner inspections: Use of 3D laser scan to improve labour safety and to perform accurate measurement of the refractory linings.

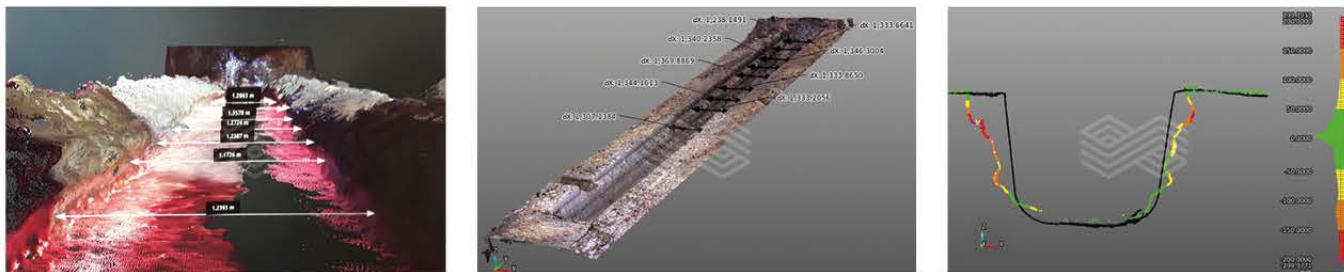
Table III.

Products used for repairs under hot conditions.

| Criteria | Ramming mix | ULC/sol-bonded castable casted | Cement/sol-bonded wet gunning | Cement castable dry gunning | Sol-bonded castable dry gunning |
|---------------------------------------|------------------------|--------------------------------|-------------------------------|-----------------------------|---------------------------------|
| Worker's exposure at high temperature | High | High | Medium | Low | Low |
| Installation | Medium | Medium | Difficult | Easy | Easy |
| Heating curve after installation | Not necessary | Necessary | Not necessary | Not necessary | Not necessary |
| Estimated campaign | Max. 10 kilo tonnes HM | Max. 50 kilo tonnes HM | Max. 45 kilo tonnes HM | Max. 15 kilo tonnes HM | Max. 30 kilo tonnes HM |

Figure 8.

3D laser scan inspection views of the main runners.



References

- [1] Worldsteel Association, Steel Statistical Yearbook 2019 – extended version, Brussels, Belgium.
- [2] Domiciano, V.G., Ribeiro, A.S., Ollmann, A.R., Bassalo, H.C. and Brito, M.A.M. New Robust Main Runner Refractory Castable for Severe Blast Furnace Operating Conditions. Presented at 57th International Colloquium on Refractories, Aachen, Germany, September 2014, 2–4.
- [3] Duarte, A.K., Ollmann, A.R., Reis, G.J., Bassalo, H.C., Brito, M.A. and Domiciano, V.G. Influência dos teores de FeO e MnO da escória no desgaste de refratários de canais de corrida de Altos-Fornos. Presented at 40^o Seminário de Redução de Minério de Ferro e Matérias-Primas, Belo Horizonte, Brazil, September 2010.
- [4] Schütz, J. RHI Magnesita, Technical Marketing, Vienna, Austria, personal communication.
- [5] Ribeiro, A. S. RHI Magnesita, Technical Marketing – Heat Flow Analysis, Brazil, personal communication.
- [6] Nagai, B., Sugiyama, K., Yasuda, N. Deterioration and reliability of trough lining refractories for blast furnaces. *Taikabutsu Overseas*. 7, 3, 24–28.

Authors

Aloísio Simões Ribeiro, RHI Magnesita, Belo Horizonte, Brazil.

Anderson Carvalho Nogueira, Ternium Brasil, Santa Cruz, Brazil.

Jürgen Schütz, RHI Magnesita, Vienna, Austria.

Eduardo Roberto Menezes, RHI Magnesita, Belo Horizonte, Brazil.

Rogério Diogo Araújo, RHI Magnesita, Santa Cruz, Brazil.

Vítor Guarnier Domiciano, RHI Magnesita, Belo Horizonte, Brazil.

Corresponding author: Aloísio Simões Ribeiro, aloisio.ribeiro@rhimagnesita.com



Francisco López, Edmilson Gonzaga, Walter Cassete and Marcelo Santos

Increase of the Internal Volume of an EAF with the Introduction of Hot Heel and Optimisation of the Scrap Melting Process

The ideal design of the EAF refractory profile can lead to meaningful savings in metallic cost, energy consumption and refractory usage, as well as an increase in campaign performance and a marked stability in the meltdown process [1,2]. A specific example from South America is discussed in this paper.

Introduction

The equipment referred to in this paper is an UHP EAF AC furnace with 26 MVA transformer power and a tapping weight of 21 tonnes of steel. This EAF required process adjustments during the campaign due to the loss of the original internal vessel shape, which led to volume variations of the rated capacity, bringing process instability and energy inefficiencies. This present project deals with modifications of the refractory installation profile in order to increase the rated capacity by 33%, as well as introducing the practice of a 6 tonne hot heel, which would have the additional benefit of an extra heat source to speed up the meltdown process and decrease the slag carryover to the steel ladle.

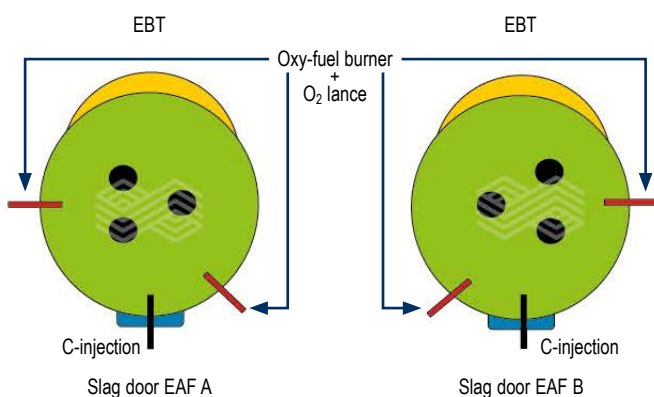
Description of the Plant Facilities

The facility is a full scrap-based silicon-killed (SK) steel mill with a rated capacity of 450000 tonnes of steel per year with the following equipment:

- Electric arc furnace (EAF) with eccentric bottom tapping (EBT), capacity 21 tonnes (Figure 1).
- Ladle furnaces (LF).
- Continuous casting machine (CCM) for squared sections of 120 x 120 mm.

Figure 1.

Layout of oxygen injection and C-injection through slag door.



Description of the Problem

The existing EAF design had a capacity of 25 tonnes and a volume of 3.62 m³. A hot heel was not a common practice and there was a trend of massive slag carryover into the ladle at the end of tapping. The working lining profile was designed to operate over 21 days with an average of 650 heats, using sinter-based MgO-C bricks. The monolithic material on the bottom and banks had a considerable mix thickness (Figure 2).

Repair practice during the campaign was mainly corrective. When the lining reached the middle of the campaign, the initial profile was usually lost, and it was no longer possible to recover. At this point it was necessary to modify the chemical and electric energy parameters with a direct impact on the EAF operating efficiency, such as an increase in power-on and power-off time.

Additionally, the sump burner was retired from operation due to flame rebound caused by the high mix thickness.

Initial Approach for the Solution

In October 2019 a master plan to overcome these drawbacks was discussed with the following goals:

- Increase the EAF volume and initiate the use of a hot heel as routine practice (Figure 3).
- Increase productivity by reducing delays caused by low density scrap (minutes/heat).
- Increase the average tapped heat size (tonne/heat).
- Decrease the number of relinings per year by increasing the EAF campaign life.
- More availability of manpower for other refractory services.
- Decrease the energy consumption (kWh/tonne).
- Decrease the electrodes usage (kg).
- Enable the EAF to receive any type of scrap regardless of the density.

In Figure 4 it is possible to see the comparison between the new and the old profile.

Figure 2.
Original EAF refractory profile.

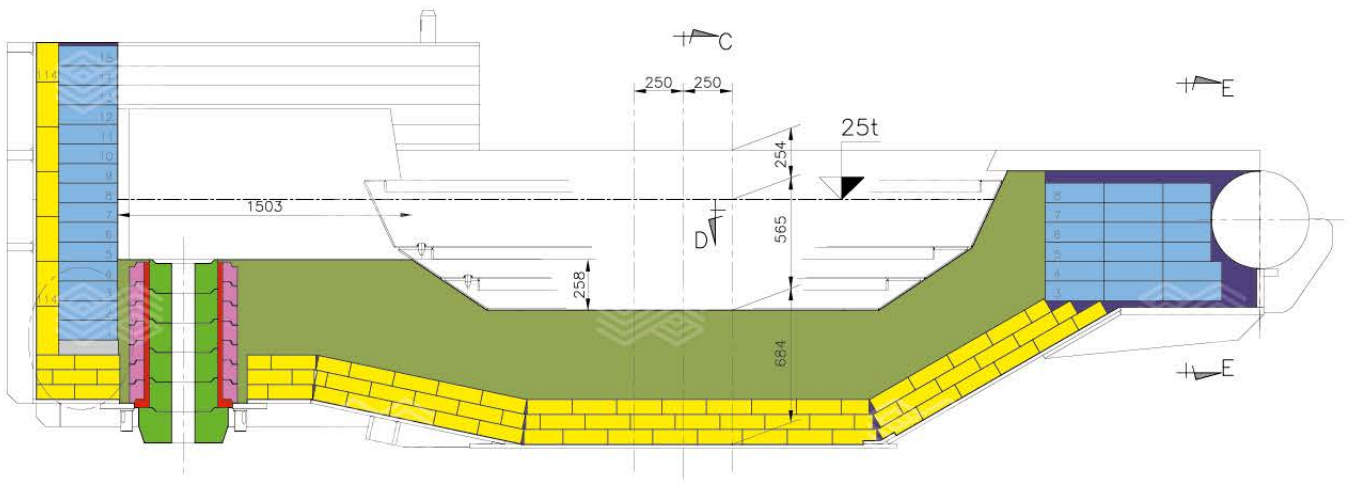


Figure 3.
New EAF profile resulting from the optimisation project.

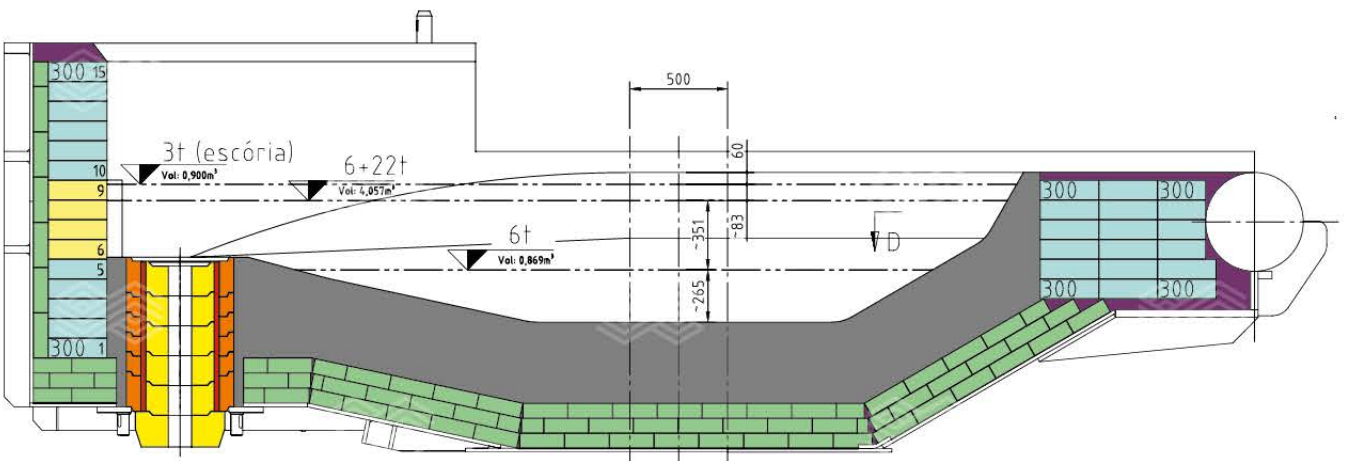
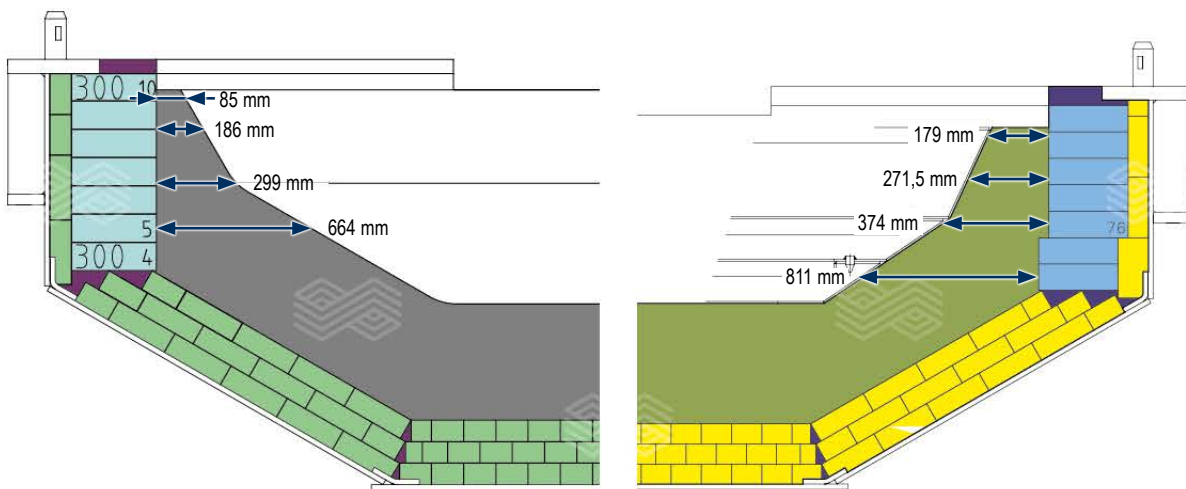


Figure 4.
(a) comparison of the new EAF profile and (b) the original profile.



(a)

(b)

Additionally, a heat transfer simulation was performed according to the bottom wear, comparing the existing and new profile, in order to set a schedule for hot repairs, as shown on Table I. The calculation was 90% accurate, when considering the referenced physical properties of the materials involved. In reality, the outer shell temperatures in the bottom were slightly higher, due to the influence of external temperatures.

Two other actions were taken to ensure full success of this project:

- A schedule was set for the correct inspection and hot repair of the bottom and banks.
- Daily preventive repairs were implemented to reduce the mix thickness at each repair, maintaining the same profile of the bottom and banks.

- The previous action enabled six continuous weeks of operation from the start to the end of each campaign, without modifying the automated meltdown program.
- A simulation of EAF tilting during tapping was performed in order to verify the distance between the steel and the water-cooled panel above the EBT, comparing the degrees with the amount of steel inside the EAF, as shown in Figure 5.

It should be noted that there was an initial safety concern for ongoing operations with this project, due to the reduction of the bottom thickness, however these were resolved.

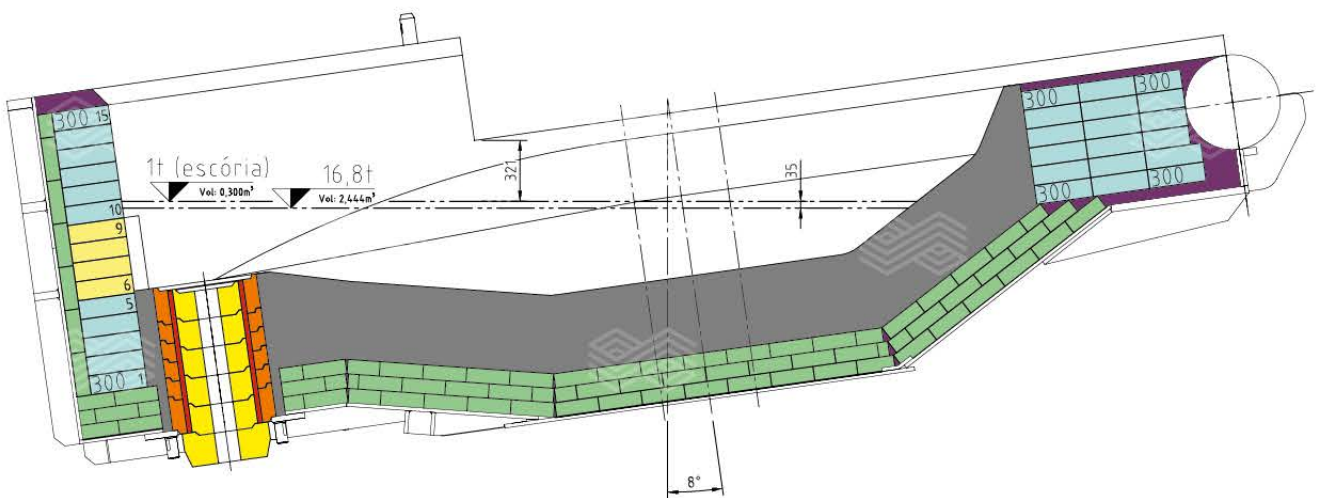
Table I.

Comparison of outer shell temperatures in the bottom depending on wear for existing and new EAF profiles.

| Tracking schedule according to shell temperature | | | | | | |
|--|------|------------------|--------------------|------|------------------|---------------------------|
| Old bottom profile | | | New bottom profile | | | Action |
| Thickness [mm] | Wear | Temperature [°C] | Thickness [mm] | Wear | Temperature [°C] | |
| 683 | 0 | 241 | | | | None |
| 633 | 50 | 253 | 638 | 0 | 252 | None |
| 583 | 100 | 264 | 588 | 50 | 263 | Bottom repair |
| 533 | 150 | 281 | 538 | 100 | 280 | Bottom repair |
| 483 | 200 | 298 | 488 | 150 | 299 | Stop EAF— drain—repair |
| 433 | 250 | 322 | 438 | 200 | 319 | Stop EAF— drain—repair |
| | | | 388 | 250 | 345 | Stop EAF |

Figure 5.

Simulation of EAF tilting during tapping.



Results

The project started in May 2020 in EAF B and in July in EAF A and has resulted in a significant increase in performance with a number of service lifetime records. At least 5 of the 10 initial goals outlined for the project were achieved:

- **Lining performance**

The changes resulted in an outstanding increase in lining performance, with successive records in lifetime until reaching the highest level, with 1275 heats in EAF B in September 2020, as shown on Figure 6.

This is a performance increase of approximately 82% when compared to the initial profile. In this way, it was possible to reduce the number of relinings per year by 50%, enabling more availability of manpower for other refractory services.

It is very important to stress the reduction of impact on the ancillary structure of the steel mill, which can occur during the movement of the EAF shells with the overhead cranes.

- **Heat size**

The internal EAF volume increase enabled a 28-tonne scrap charge for the first heat after relining and 22.6 tonnes in the subsequent heats, maintaining an average 8-tonne hot heel. The new hot heel practice led to the stabilisation of the process keeping the same sill level inside the EAF. This translated into an increase of the tapped heat size in both EAFs, as shown in Figure 7.

- **Power-off due to scrap accommodation**

The use of lower density scrap was enabled, reducing the metallic costs and the power-off due to scrap accommodation. In Figure 8 the reduction of power-off caused by low density scrap can be seen.

Figure 6.
Evolution of EAF lifetime since start-up of the new refractory profile.

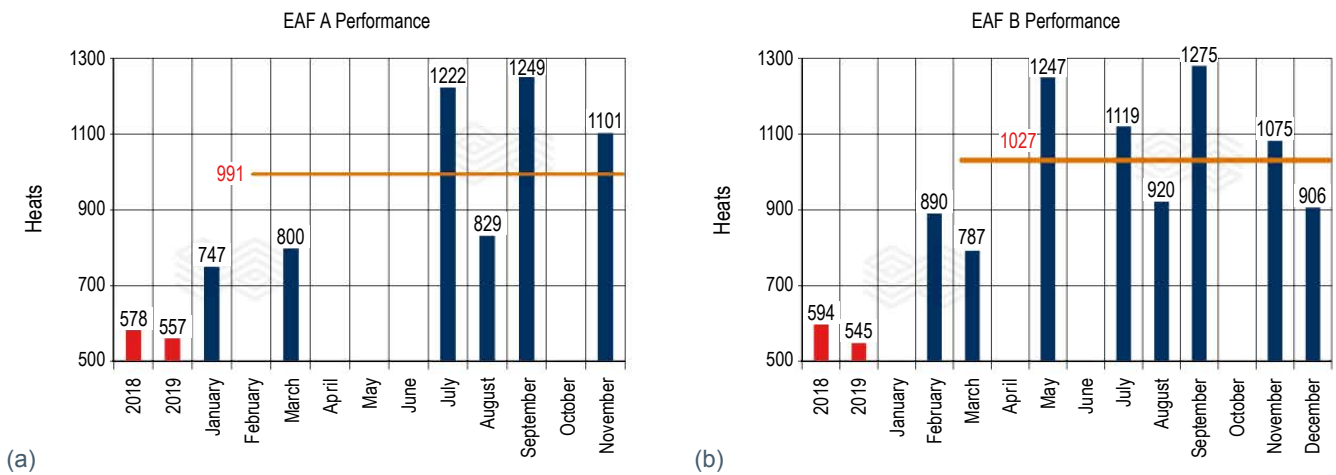


Figure 7.
Evolution of tapped heat size.

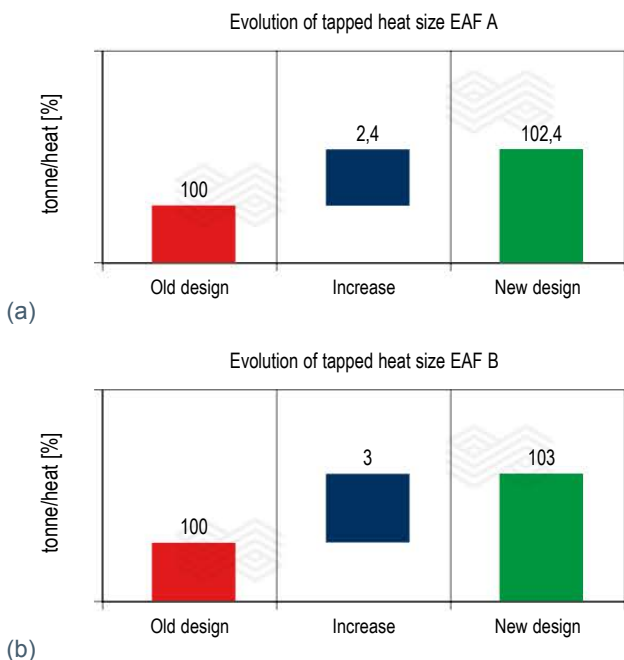
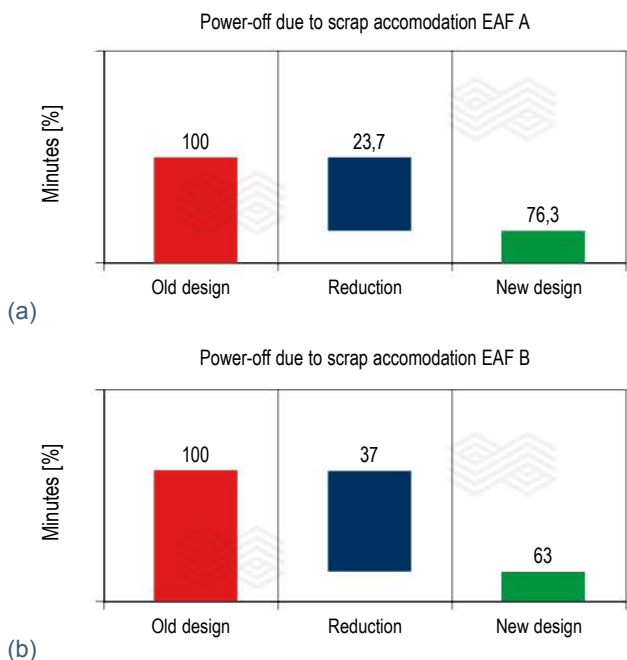


Figure 8.
Evolution of power-off due to scrap accommodation.



- **Total refractory consumption**

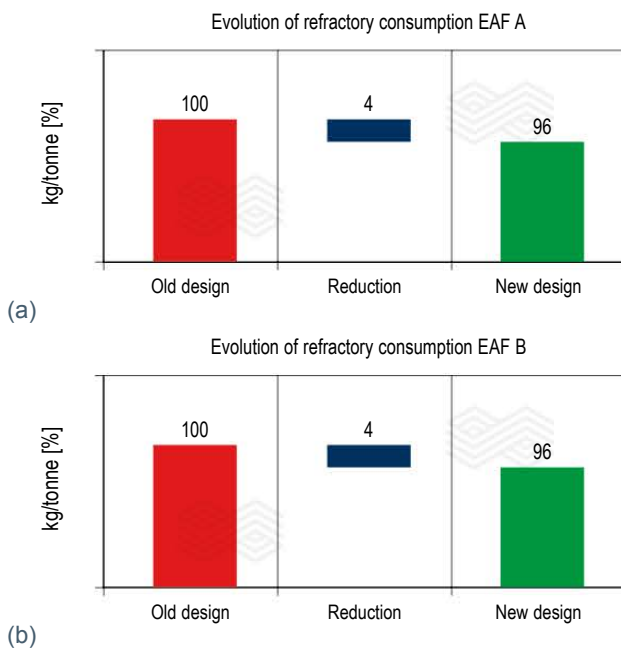
The practice of EAF intermediate repairs to maintain the initial refractory internal shape throughout the campaign was also implemented. These goals were attained with the modification of the bottom and bank profiles during the initial installation and a better zoning of the quality of refractories for the sidewalls. A further reduction of refractory usage could be attained with a hot repair fine tuning during the campaign and refining the tear-out criteria for optimising the remaining thickness at the end of service. In Figure 9 the evolution of the total refractory usage (bricks and mixes) is shown:

Conclusions/Outlook

A very simple approach on the EAF refractory design can lead to meaningful gains in productivity of the steel mill and lining performance. A possibility for reinstalling the sump burner is open, which may add more efficiency in the melt-down process.

Figure 9.

Evolution of total refractory consumption.



References

- [1] Pretorius, E. and Oltmann, H.G. EAF Fundamentals; LWB Refractories, 2001.
 [2] Jones, J.A.T., Bowman, B. and Lefrank, P.A. Electric Furnace Steelmaking on The Making, Shaping and Treating of Steel – 11th Edition; The AISE Steel Foundation, 1998.

Authors

Francisco López, RHI Magnesita, Contagem, Brazil.
 Edmilson Gonzaga, RHI Magnesita, Contagem, Brazil.
 Walter Cassete, RHI Magnesita, Contagem, Brazil.
 Marcelo Santos, RHI Magnesita, Contagem, Brazil.

Corresponding author: Francisco López, Francisco.lopez@rhimagnesita.com





Get access to the new e-tech website

Is your slag optimised for your steel and refractory operations in the steel ladle? Do you waste time doing slag splashing with the wrong slag in the BOF? What about your foamy slag in the EAF?

Play with your calculations for ladle, furnace, stainless, and casting. You can save each scenario and recall it at a later date or view the report in a PDF or Excel file on your smartphone or tablet while on the road.

Curious to find out more details?
Visit etech.rhimagnesita.com

If you have any questions or suggestions, please send a message to etech@rhimagnesita.com or directly to your Sales Manager or Technical Excellence & Solutions Expert.

Follow us



RHI MAGNESITA

Andreas Viertauer, Sumit Sundaram, Ranjeet Kumar Mishra, Andreas Haider, Johannes Wucher, Alexander Ratz, Heiko Dettela, Oswin Dolzer, Mario Hesselberger, Yong Tang, Karim Badr, Prakash Chaudhary, Viral Thakkar and Sanjay Anand

A Success Story for a Close Cooperation with Jindal Shadeed and RHI Magnesita Since 2016

Since spring 2016, RHI Magnesita has had a full line refractory service contract for the entire steel melt shop. This very trustworthy close cooperation is the basis for success and provides the opportunity for continuous improvement. This paper will underline selected refractory applications and describes the remarkable results over the recent years along the steelmaking route from the electric arc furnace (EAF), to the ladles and finally for caster applications.

Introduction

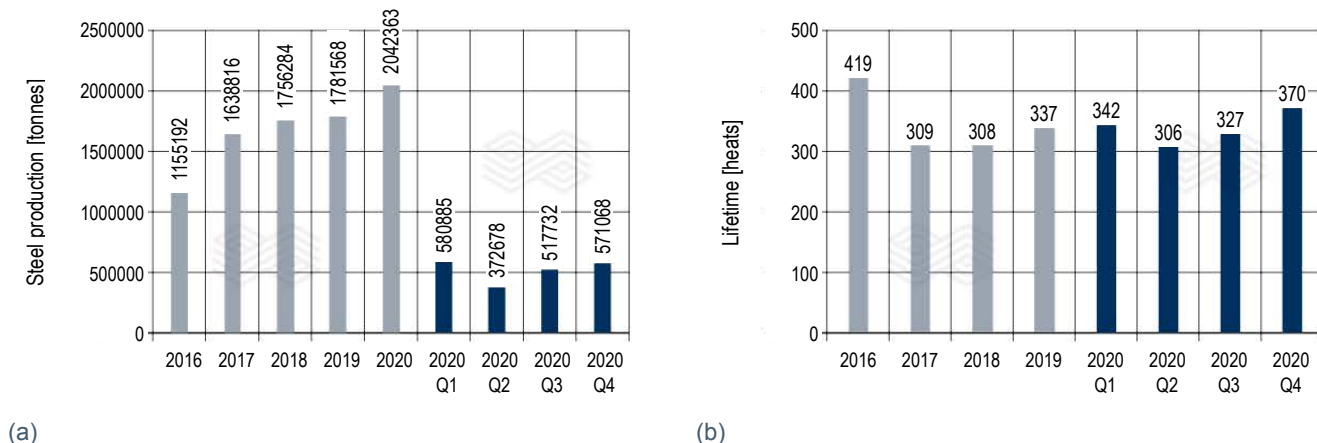
Jindal Steel and Power Ltd (JSPL) has a very long history of steelmaking. Due to the expansion strategy, Shadeed Iron & Steel (SIS) was acquired in 2010 and since then has been part of the global JSPL group and was renamed Jindal Shadeed Iron and Steel Co LLC (JSIS). JSIS is located at the port city of Sohar, (Oman). The EAF steelmaking shop is located close to the direct reduced iron (DRI) plant. The steelmaking shop is equipped with a ladle furnace (LF) with two transfer cars, and additionally two tanks for vacuum degassing (VD) if required. The successful start-up and commissioning with one eight-strand combination casting machine for long products occurred in April 2014 [1]. A second eight-strand combination casting machine has been in operation since December 2018. This boosted the nominal capacity from 2.0 to 2.4 million tonnes of steel per year. The rebar mill completes the plant configuration and the nominal capacity is 1.4 million tonnes annually. Since 2016, RHI Magnesita has been in a close cooperation with a cost per tonne contract with JSIS for the entire melt shop.

Melt Shop

The output of solid steel was, even with the negative impact of COVID-19, a record with 2.04 million tonnes for 2020 (Figure 1a). The main iron source is the direct reduced Iron (DRI) material in addition to other Fe-carriers. The DRI is continuously charged during the meltdown phase. The hot DRI (HDRI) has a temperature up to 650 °C. The HDRI is the main factor for the low specific energy consumption with high productivity. The EAF capacity is one of the largest in the middle east with an average tapping weight of approximately 219 tonnes per heat with a hot heel of approximately 70 tonnes. The average heats per day was 28 for the 4th quarter of 2020. The EAF is equipped with all features which are necessary for modern steelmaking, this includes a high level of automation. Due to the high plant utilisation the time frame for refractory maintenance is very limited, especially for the EAF, which is the bottleneck in the melt shop. The EAF lifetime since 2016 is shown in Figure 1b.

Reliable, constantly improved refractory materials and solutions are one of the key factors for enabling such a high melt shop availability. These constant improvements lead to the best performance of various refractory applications along the steelmaking process route. Some of these records are highlighted in Table I.

Figure 1.
(a) amount of steel production and (b) the EAF lifetime since 2016.



Examples of some refractory applications that support the steel plant productivity are listed below and described in this paper:

- Increased lifetime of the EAF roof.
- Extended lifetime of the eccentric bottom tapping (EBT).
- Ladle refractory performance.
- Tundish refractory improvements and availability.

EAF Roof Lifetime Improvement

The main step forward to increase the lifetime was the newly developed high-alumina material with sol-bonding. Sol-bonding mixes are no-cement castables with a nanotechnology binding system [2]. The nanotechnology binding system comprises of two components, a dry mix and the colloidal silica mixing liquid.

This provides the highest abrasion resistance combined with excellent thermal shock resistance. The current roof configuration is based on three prefabricated segments made with ANKOFORM SBA89CRS-6 and assembled on site into one piece with RUBINIT VK3-TR (Figure 2, Table II). With this configuration lifetimes of up to 2095 heats have been achieved. Currently a trial with an improved grade (ANKOFORM SBA92CRS-6) achieved a record lifetime of 2516 heats with a remaining thickness of 80 mm. Figure 3 shows the roof under hot conditions.

Figure 4 shows the evolution of the lifetime since 2016. The record lifetime of 2516 heats occurred in January 2021 and is not included in Figure 4. Chemical composition, bulk density (BD), apparent porosity (AP), and cold crushing strength (CCS) of the refractory materials used are given in Table II.

Table I.

Best performance figures.

| Facility | Refractory application | Best performance | Unit | Date |
|----------|--|------------------|-------|--------------------|
| EAF | Roof | 2516 | Heats | Jan. 2021 |
| EAF | Eccentric bottom tapping (EBT) | 318 | Heats | Nov. 2020 |
| Ladle | Metal zone | 152 | Heats | Dec. 2020 |
| Ladle | Slag zone | 97 | Heats | Dec. 2020 |
| Ladle | Purging plug | 77 | Heats | Dec. 2020 |
| Ladle | Inner nozzle | 36 | Heats | Oct. 2020 |
| Ladle | Nozzle free-opening index | ~99.7 | % | Calendar year 2020 |
| Tundish | Open casting sequence length (single tundish) | 71 | Heats | Nov. 2020 |
| Tundish | Close casting sequence length (single tundish) | 37 | Heats | Feb. 2020 |

Table II.

Chemical composition and selected physical properties of the refractory grades.

| Grade | Al ₂ O ₃ [wt. %] | MgO [wt. %] | Fe ₂ O ₃ [wt. %] | SiO ₂ [wt. %] | Cr ₂ O ₃ [wt. %] | P ₂ O ₅ [wt. %] | BD [g/cm ³] | AP [vol. %] | CCS [N/mm ²] |
|---------------------|---|----------------|---|-----------------------------|---|--|----------------------------|----------------|-----------------------------|
| ANKOFORM SBA89CRS-6 | 88.6 | | 0.1 | 5.6 | 4.8 | | 3.00 | 18.0 | 80 |
| ANKOFORM SBA92CRS-6 | 91.0 | | 0.1 | 3.4 | 4.8 | | 3.10 | 14.0 | 70 |
| RUBINIT VK3-TR | | 93.0 | 0.2 | 0.6 | 1.9 | 1.3 | | | 30 |

Figure 2.

New EAF roof.



Figure 3.

EAF roof in operation after 1975 heats.



EBT Performance Improvement

Several trials were made with different refractory grades and geometries based on computational fluid dynamics (CFD) calculations to optimise the taphole shape from a cylindrical to CFD optimised design [3,4]. In addition to the geometry change, newly developed refractory grades were also used. Table III shows the chemical composition and properties of one of the refractory materials.

Figure 5 shows the lifetime development since 2017. The performance of the tapholes showed better results although the number of hot repairs with the so called “piping practice” did not change over the years. The main reason for the improved lifetime of 251 heats was the design and grade change. The record lifetime was 318 heats in November 2020.

Secondary Steelmaking—Ladle Lifetime Improvement

After tapping, all heats are treated at the LF. Figure 6a shows the development of the VD treated share since the start-up. The share of VD treated heats varies and reflects the frequent changes of the product mix.

The average treatment time for the VD treatment is 30–40 minutes for closed cast grades and 15–20 minutes for open cast grades. The portion of open cast grades that received a VD treatment was approximately 38% in 2020. The complexity, due to the frequently changing product mix, provides a challenge to the steelmaking operation in general. Figure 6b shows the share of open and closed cast steel grades from 2016 until 2020.

These steel grade groups have different slag chemistries [5]. The open stream steel grades are mainly deoxidised with Si and therefore the slag is CaO-SiO₂ orientated. Closed cast grades are deoxidised with Al and Si and therefore there is an orientation to CaO-Al₂O₃ slags. Figure 7 depicts the ternary diagram for CaO-SiO₂-Al₂O₃ with 10% MgO. The blue dotted points represent slag chemistries from the production period from November 2019 until March 2020 and the orange dotted points represent the slag chemistries from April until November 2020. All samples were taken at the end of the LF treatment. The orientation of the slag chemistries is demonstrated for open (green square) and closed cast grades (red square). These steelmaking conditions are a challenge for the ladle lining configuration.

Table III.

Chemical composition and selected physical properties of an EBT refractory material.

| Grade | MgO [wt. %] | C [wt. %] | Al ₂ O ₃ [wt. %] | Fe ₂ O ₃ [wt. %] | CaO [wt. %] | SiO ₂ [wt. %] | BD [g/cm ³] | AP [vol. %] | CCS [N/mm ²] |
|------------------|----------------|--------------|---|---|----------------|-----------------------------|----------------------------|----------------|-----------------------------|
| ANKERTAP HMC193X | 89.1 | 17.0 | 6.5 | 0.5 | 1.0 | 2.9 | 2.96 | 1.0 | 30 |

Figure 4.

Evolution of the lifetime for the EAF roof since 2016.

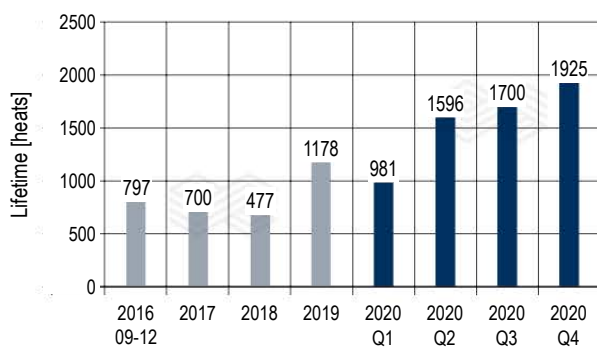
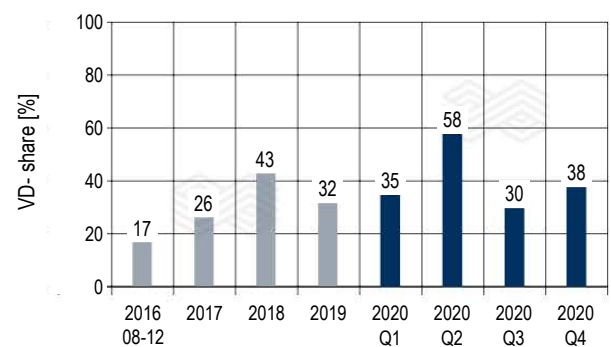


Figure 6.

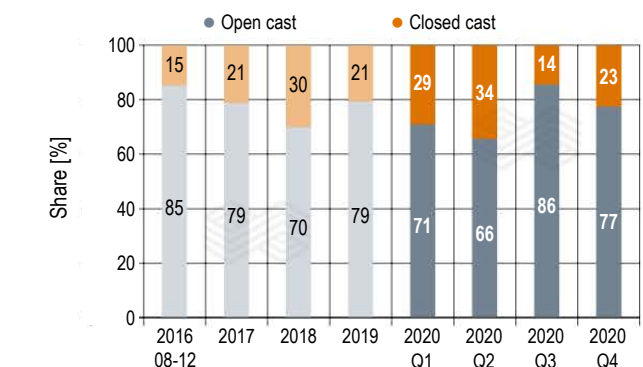
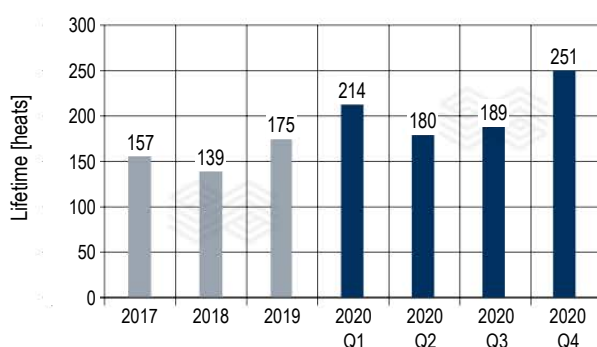
(a) VD share since the start-up and (b) the proportion of open and closed cast grades.



(a)

Figure 5.

Lifetime of the EAF EBT since 2017.



(b)

A MgO enriched doloma is used for the wall metal zone except the transition zone between the slag line and metal zone. Three different MgO-C grades are used to balance the wear rate of the slag line. Above the slag line is the enlarged freeboard area which was necessary for the VD treatment. Alumina castable is used to protect the steel lip ring against steel and slag attack. The bottom lining is comprised of a combination of different refractory materials. The impact area has the main wear ratio of the entire bottom due to the impact of the tapping stream; alumina-magnesia-carbon (AMC) bricks are used here.

To avoid contact reactions, MgO-C bricks are used in the surrounding. The remaining bottom is lined with MgO-enriched doloma. Figure 8a and b show the main wear lining configuration and Table IV describes the chemical composition of the main wear lining refractory materials with selected physical properties.

Figure 7.

CaO-SiO₂-Al₂O₃ ternary system with 10% MgO.

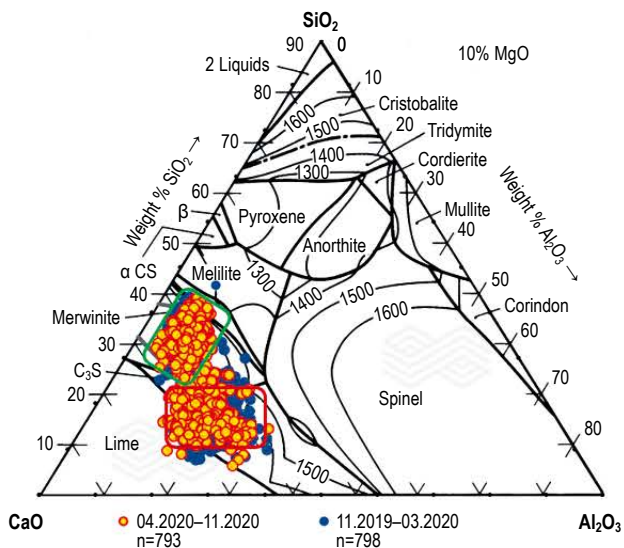


Figure 8.

Current working lining concept; (a) cross section and (b) bottom.

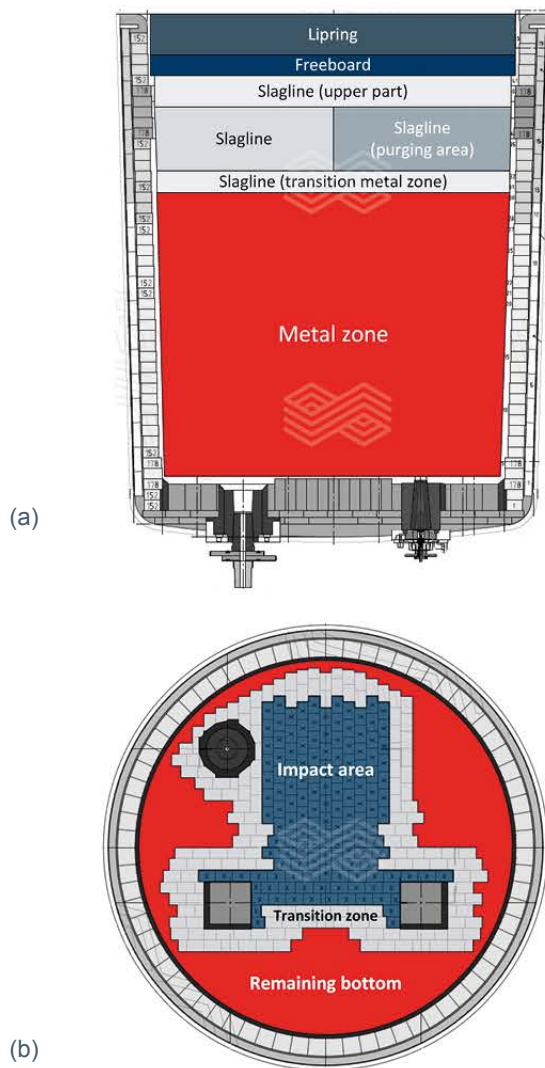


Table IV.

Used grades, chemical composition, bulk density (BD), apparent porosity (AP), and cold crushing strength (CCS).

| Area | Nomenclature | MgO [wt. %] | CaO [wt. %] | Al ₂ O ₃ [wt. %] | Fe ₂ O ₃ [wt. %] | SiO ₂ [wt. %] | C [wt. %] | BD [g/cm ³] | AP [vol. %] | CCS [N/mm ²] |
|---|---|----------------|----------------|---|---|-----------------------------|--------------|----------------------------|----------------|-----------------------------|
| Lip ring | DIDURIT B73-5-IN | - | 2.5 | 73 | 2 | 22 | - | 2.8 | - | - |
| Freeboard | Recycled EAF bricks (different grades) | - | - | - | - | - | - | - | - | - |
| Slag line (upper part) | ANCARBON R CN77D | 95.9 | 1.3 | 0.4 | 0.9 | 1.5 | 14 | 3.04 | 1.5 | 50 |
| Slag line | ANCARBON R CN87D | 96.8 | 1.1 | 0.4 | 0.6 | 1.3 | 14 | 3.05 | 2.0 | 45 |
| Slag line (purging area) | ANCARBON R F1L14 | 97.2 | 1.0 | 0.2 | 0.6 | 0.8 | 14 | 3.01 | 3.0 | 35 |
| Slag line (transition metal zone) | ANCARBON R CN75D | 96 | 1.4 | 0.4 | 0.8 | 1.3 | 10 | 3.10 | 1.5 | 60 |
| Wall (metal zone) | SINDOFORM RF60-3 | 60 | 37 | 0.5 | 0.8 | 0.8 | 3 | 3.02 | - | 100 |
| Bottom (impact area) | ANKO C87AZ | 8 | 0.4 | 87.5 | 0.3 | 1.7 | 7 | 3.25 | 4.5 | 90 |
| Bottom (transition impact zone) | ANCARBON R CN75D | 96 | 1.4 | 0.4 | 0.8 | 1.3 | 10 | 3.10 | 1.5 | 60 |
| Bottom | SINDOFORM RF60-3 | 60 | 37 | 0.5 | 0.8 | 0.8 | 3 | 3.02 | - | 100 |

Figure 9a provides an impression of a newly lined ladle and Figure 9b shows a ladle at the hot inspection stand after 127 heats.

Continuous refractory concept improvements, standardised lining installation, a high number of heats per day caused by high plant utilisation, and an optimised ladle metallurgy are success factors that made it possible to achieve the high ladle lifetime of 135 heats with one intermediate slag line repair (Figure 10). The record lifetime of 152 heats, with a share of 38.5% VD treated heats and a total steel contact of 21047 minutes, was achieved in December 2020. For the purging plugs, the highest achieved lifetime was 77 heats with 6567 purging minutes and 100% purging availability in December 2020.

Casting Improvements

Two eight-strand combi casters are in operation. The product dimensions range from squared 130, 150, to 165 mm and round from 200, 220, 280, 350 to 406 mm. The other differentiation is open versus closed casting depending on the product mix, which varied from 85% for open and 15% for closed casting in 2016 to 77% for open and 23% for closed casting during the 4th quarter of 2020 (Figure 6b). Figure 11 shows the prepared tundish configuration ready for

use. Figure 11a and 11b show the tundish configuration for closed casting and 11c demonstrates the inside of the tundish with starter tubes.

The usual sequence length for open and closed casting is dependent on the steel product mix based on market demand and is not limited in regard to the refractory materials. Figure 12 shows the sequence length which varied for open casting around 18 heats and for closed casting around 8 heats during 2020. The record sequence length for closed casting was 37 heats, which was equivalent to 30 hours and for open casting 71 heats, at 55 hours and 16 minutes.

Figure 9.

(a) newly lined ladle and (b) the working lining in hot condition after 127 heats for the bottom and metal zone, and 72 heats for the slag line.

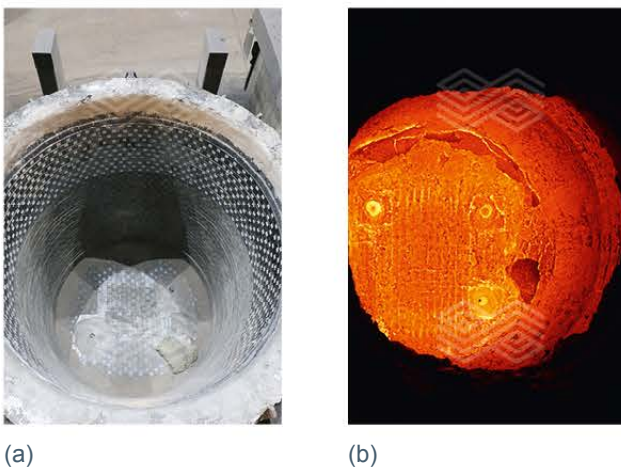


Figure 11.

(a) tundish at the preparation area (b) for closed, and (c) for open casting.



Figure 10.

Development of the ladle lifetime since 2016.

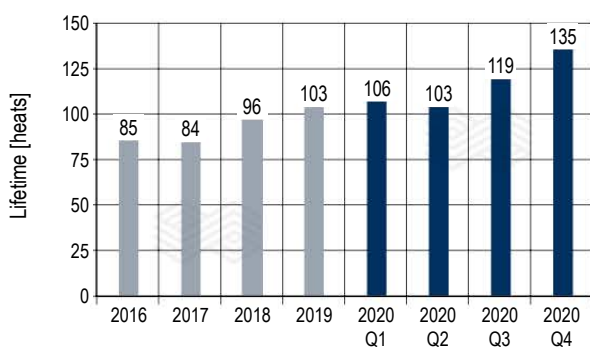
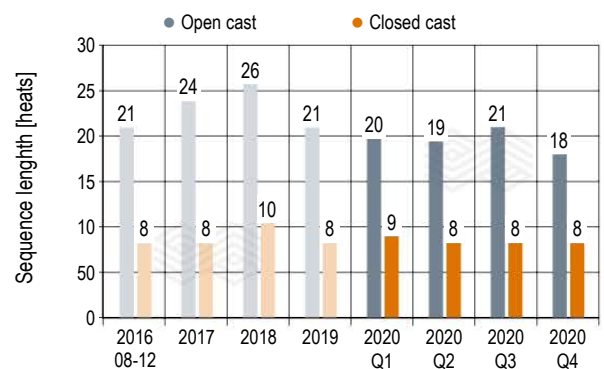


Figure 12.

Overall lifetime performance for open and closed casting since 2016.



For the tundish working lining, a slurry gunning material (ANKERTUN TM10-TR) is used. A scheduled introduction of the cold setting (CS) system (self-hardening (SH) technology [6,7]) was planned for 2020. However, due to the COVID-19 crisis the implementation was postponed to 2021. The main reasons for the conversion to the CS system were lower gas consumption, higher tundish flexibility, lower stress on operators, reduced drying duration, increased tundish flexibility, and reduced stress on the operators. The chemical composition of the slurry gunning and the SH material (ANKERTUN SH20-TR) is provided in the Table V.

New Ladle Shroud Solution

The common ladle shroud has a straight inner diameter. With this design the opening of the slide gate, especially for the second heat from a casting sequence, is only possible if the tip of the shroud is not immersed in the steel. When high-end steel cleanliness is required, the air entrainment should be minimised as much as possible.

Table V.

Main chemical composition and poured density (PD) of the tundish working lining.

| Grade | MgO [wt. %] | CaO [wt. %] | SiO ₂ [wt. %] | Fe ₂ O ₃ [wt. %] | Al ₂ O ₃ [wt. %] | PD [g/cm ³] |
|------------------|----------------|----------------|-----------------------------|---|---|----------------------------|
| ANKERTUN TM10-TR | 89.2 | 3.8 | 5.7 | 0.7 | 0.3 | 1.4 |
| ANKERTUN SH20-TR | 79.5 | 2.5 | 14.8 | 3.0 | 0.2 | 1.9 |

Non immersed opening can lead to an uncontrolled reoxidation of the steel, abnormally high nitrogen pickup, and extended Al and Ca fading. A safe immersed opening, to avoid the so called “back-attack” effect with steel and slide gate filler sand, is only possible with a reversed taper shroud design. This back-attack effect can easily destroy the slide gate mechanism due to the heavy splashes and lead to an unplanned casting sequence break. The first tests with the reverse taper design have been very promising and showed a smooth and safe casting operation. Table VI shows the average composition and bulk density, while Figure 13 shows the different design forms.

Table VI.

Main chemical composition and bulk density of the ladle shroud.

| Grade | Al ₂ O ₃ [wt. %] | SiO ₂ [wt. %] | C [wt. %] | BD [g/cm ³] |
|-------------|---|-----------------------------|--------------|----------------------------|
| DELTEK A721 | 88.6 | 8.8 | 24.3 | 2.65 |

Table VII.

Metering nozzle sleeve and body material composition [8].

| JUSTAL DS8080 | Area | ZrO ₂ [wt. %] | MgO [wt. %] | Al ₂ O ₃ [wt. %] | SiO ₂ [wt. %] | P ₂ O ₅ [wt. %] | BD [g/cm ³] | AP [vol.%] |
|---------------|--------|-----------------------------|----------------|---|-----------------------------|--|----------------------------|---------------|
| ZETTRAL 9515B | Nozzle | 96.0 | 2.3 | | | | 5.2 | 5.0 |
| RESISTAL IN-6 | Body | | | 87.0 | 8.1 | 2.4 | 2.9 | 18.0 |

Open Stream Casting

Since August 2020 the metering nozzle changer advanced system (MNC-AS) has been in operation. The advantages have been a hassle-free operation, simplified handling, and lower maintenance effort. Table VII shows the material composition of the metering nozzle sleeve and body.

Closed Casting

The decision to choose the suitable stopper is mainly dependent on the steel grade chemistry, casting speed, and mould dimension. For an accurate mould level, a multi-radius or pencil nose is in use [9]. DELTEK A112 is used in the stopper body material and DELTEK MA007 is used for the stopper nose. Table VIII shows the chemical composition and physical properties. The submerged nozzles (SN) also have distinct concepts according to the steel grade and mould size to be cast. Table IX shows the chemical composition and selected physical properties for the body, slag band, and seat area.

Figure 13.

(a) conventional straight and (b) reversed taper design for the ladle shroud.



Table VIII.

Chemical composition and physical properties of the stopper.

| Grade | Area | Al ₂ O ₃ [wt. %] | SiO ₂ [wt. %] | MgO [wt. %] | C [wt. %] | LOI [wt. %] | BD [g/cm ³] | AP [vol.%] |
|--------------|------|---|-----------------------------|----------------|--------------|----------------|----------------------------|---------------|
| DELTEK A112 | Body | 89.5 | 6.5 | | 30.0 | 29.0 | 2.5 | 17.0 |
| DELTEK MA007 | Nose | 72.0 | 4.5 | 22.0 | 14.5 | 12.5 | 2.6 | 18.0 |

Table IX.

Chemical composition and physical properties of the submerged nozzle.

| Grade | Area | Al ₂ O ₃ [wt. %] | SiO ₂ [wt. %] | ZrO ₂ +HfO ₂ [wt. %] | MgO [wt. %] | C [wt. %] | LOI [g/cm ³] | BD [vol.%] |
|--------------|-----------|---|-----------------------------|---|----------------|--------------|-----------------------------|---------------|
| DELTEK A716 | Body | 77.8 | 16.6 | | | 23.5 | 22.4 | 2.60 |
| DELTEK Z904T | Slag band | | 0.9 | 92.8 | | 11.4 | 11.8 | 3.95 |
| DELTEK M801 | Seat | | 3.6 | | 92.8 | 13.6 | 13.4 | 2.68 |

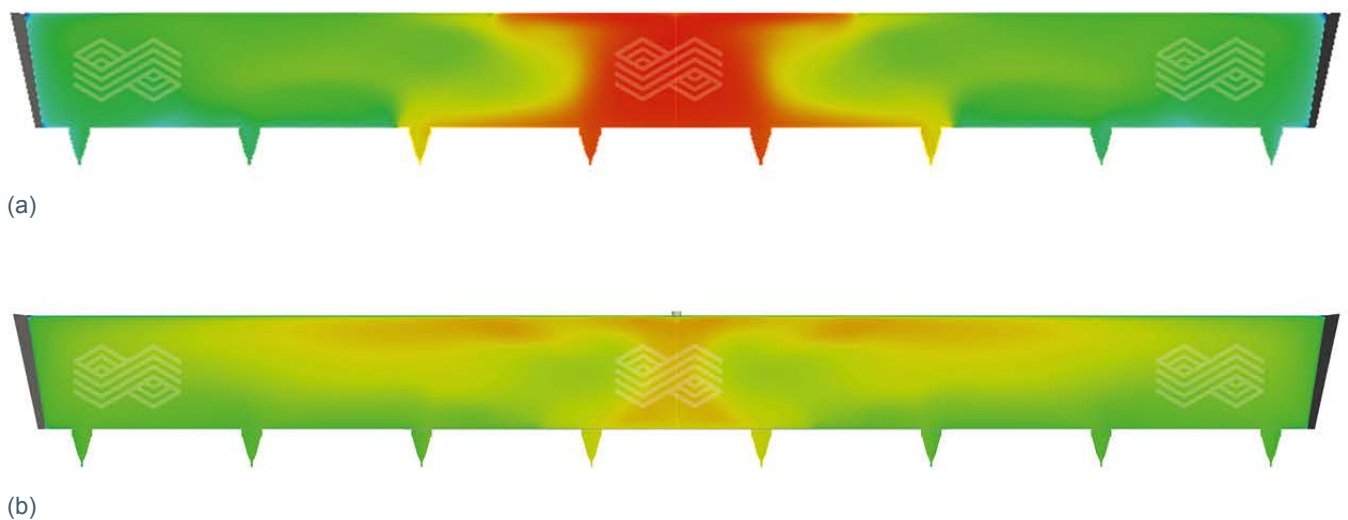
Tundish Furniture

The tundish geometry with eight strands and various mould dimensions is unique. Many tailor-made computational fluid dynamics (CFD) simulations have been carried out in the past years aiming to optimise steel flow distribution among the strands, steel temperature distribution, and inclusion flotation [10,11]. Figure 14 shows a visualisation of the longitudinal cross section from a tundish and the temperature distribution in different colours. It is obvious that the temperature distribution is more uniform with a steel flow modifier (Figure 14a) than without a flow modifier (Figure 14b). Based on the results, industrial tests have been carried out following the simulation results.

Apart from the temperature distribution, the steel flow from the impact area towards the eight strands is illustrated by the CFD simulation velocity vectors. Figure 15a shows the flow velocity on the tundish surface for closed and 15b for open casting. The steel flow velocity intensity (red depicts high intensity while blue depicts low intensity) shows the flow with high velocity magnitude especially in the impact area. This knowledge provides an insight to enable an optimisation of the size and geometry for the tundish furniture for open and closed casting to avoid negative implications, for example open eye formation, high local turbulences, high refractory erosion, and steel cleanliness.

Figure 14.

Tundish cross section with a simulated steel temperature distribution (a) with flow and (b) without flow modifier.



To tackle these above-mentioned potential risks, it is recommended to use a flow distributor. Figure 16a shows the so-called TUNFLOW with the chevron design [12–15] while Figure 16b shows the TUNBOX for open stream casting.

Additional Steps Beyond New Refractory Applications

This paper describes selected success stories for refractory applications along the steelmaking process route. Additional innovative solutions “beyond refractory” recently in execution are:

- Shroud shielded connection (SSC) to avoid air ingress during casting [16,17].
- Electromagnetic level indication (EMLI) ladle slag detection system [18].
- Prefeasibility study for automated process optimisation (APO) ladle [19,20].
- Gunning robot system for EAF [21–23].

Conclusions

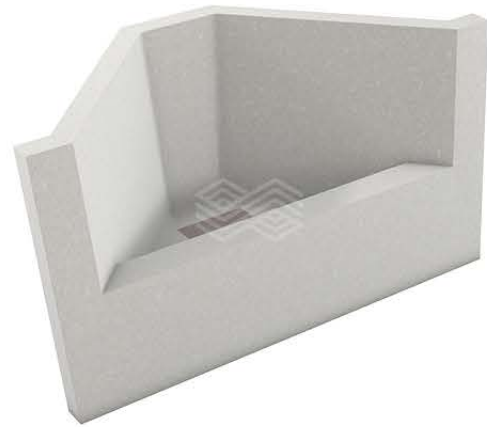
This paper summarises encouraging results for selected refractory products (e.g., EAF roof, EAF EBT, and ladle lining concept), and the various applications for casting solutions. The partnership between JSIS and RHI Magnesita is based on mutual trust, transparency, and willingness for continuous improvement. This relationship is much more than just the refractory business, all are involved in day-to-day activities to facilitate the 24x7 operations of the steel plant. Customer, on-site total refractory management (TRM) team, R&D, production, marketing, and technical excellence are working in coordination to achieve verifiable goals. One of the current ongoing challenge is to reduce the entire refractory consumption by 20% for the melt shop.

Figure 16.

(a) TUNFLOW Chevron with the chevron design for closed and (b) TUNBOX for open stream casting.



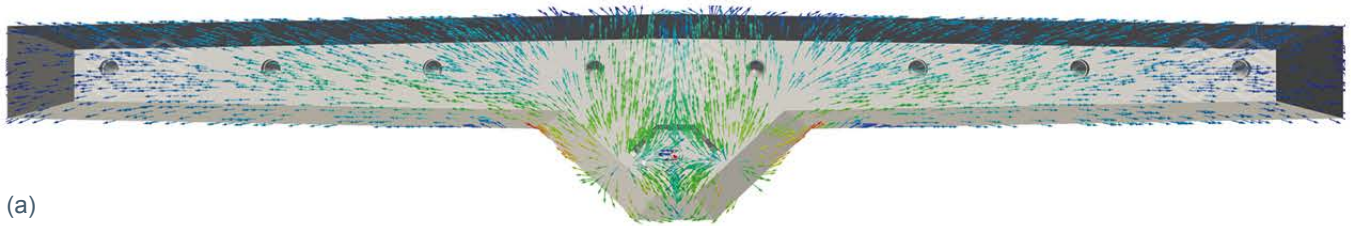
(a)



(b)

Figure 15.

CFD simulation for the impact area (a) closed casting with the TUNFLOW chevron design and (b) open casting with a TUNBOX design.



(a)



(b)

References:

- [1] Homepage www.jindalshadeed.com
- [2] Blajs, M. Preheating of Refractory Linings. *DFFI Verband der Deutschen Feuerfest-Industrie e.V., Steel Meets Refractories, Online Dialogue*, September 8th, 2020, Proceedings.
- [3] Hackl, G., Köhler, S., Fellner, W., Marschall, U., Trummer, B. and Hanna, A. Characterization and Improvement of Steelmaking Process steps Influenced by Refractory Products Using Modelling and Simulation Tools, *RHI Bulletin*. 2017, No. 1, pp. 49–54.
- [4] Bellgardt, B., Köhler, S., Neubauer, B. and Pungersek, R. Taphole Developments for Specific Steel Industry Demands, *RHI Bulletin*. 2015, No. 1, pp. 30–36.
- [5] Brüggmann, C. and Pötschke, J. Contribution to the slagging of MgO in secondary Metallurgical slags. *53rd Int. Colloquium on Refractories*, September 8th and 9th, 2010, Aachen, Germany, pp. 145–149.
- [6] Secklehner, B. A., Casado, M. T., Viertauer, A., Wappel, D. and Brosz, B. Tundish Technology and processes: A New Roadmap. *RHI Bulletin*. 2015, No. 1, pp. 68–77.
- [7] Wappel, D., Petritz, B., Kumar, M., and Freiler, M. Cold Setting Mixes with Higher Preheating Stability. *UNITECR 2019*. October 13th–16th 2019, Yokohama Japan, Proceedings pp. 808–811.
- [8] Jain, N., Barthmann, F. and Ansari, G. RHI Zirkonia Nozzles in Tundish Application. *RHI Bulletin*. 2016, No. 1, pp. 45–50.
- [9] Bauer, C., Rollinger, B., Krumpel, G., Hoad, O., Pascual, J., Rogers, N. and Dösinger, H. Characterization Methods to Investigate Zirconia Phase Transformations in Slag Bands. *RHI Bulletin*. 2016, No. 1, pp. 51–56.
- [10] Hackl, G., Fellner, W., Heinrich, B. and Bühlmann, R. New Slide Gate Water Model Facility. *Bulletin*. 2017, No. 1, pp. 60–63.
- [11] Hackl, G., Heinrich, B., Nitzl, G. and Meurer, D. Characterization of Novel Flow Control Refractories for the Continuous casting Process by Modeling and Simulation. *AISTech 2017*, May 8th–11th 2017, Nashville, Tenn., USA, Proceedings, pp. 1817–1825.
- [12] Hackl, G., Tang, Y., Lukesch, G., Meurer, D., Shivaram, P., Resende, A.D., Impact Zone Solutions for an Improved Flow Performance in the Tundish. *AISTech 2019*, May 6th–9th 2019, Pittsburgh, Pa., USA, Proceedings, pp. 2851–2858.
- [13] Granted patent IN337006B.
- [14] Arth, G., Meurer, D., Tang, Y., Hackl, G. and Petritz, B. Tundish Technology and Processes: Ladle to Mould Systems and Solutions (Part II). *Bulletin*. 2017, No. 1, pp. 64–70.
- [15] Arth, G., Meurer, D., Kappel, M., Loop, P. and Petritz, B. Tundish Technology and Processes: Ladle to Mould Systems and Solutions (Part III). *Bulletin*. 2018, No. 1, pp. 64–70.
- [16] Ehrenguber, R. Excellence in Inert Gas Control Systems for the Steel Industry. *RHI Bulletin*. 2015, No. 1, pp. 7–15.
- [17] Arth, G., Viertauer, A. Hackl, G., Krumpel, G., Petritz, B. and Meurer, D. Tundish Technology and Processes: Ladle to Mould Systems and Solutions (Part I). *RHI Bulletin*. 2016, No. 1, pp. 38–44.
- [18] RHI Magnesita AGELLIS product catalogue.
- [19] Viertauer, A., Lammer, G. and Bloemer, P. Refractory Condition Monitoring and Lifetime Prognosis. *Bulletin*. 2018, No. 1, pp. 42–46.
- [20] Viertauer, A., Mutsam, N., Pernkopf, F., Gantner, A., Grimm, G., Winkler, W., Rössler, R., Lammer, G., Ratz, A. and Persson, M. refractory Lifetime Prognosis for RH Degassers. *Bulletin*. 2020, pp. 36–41.
- [21] Al Emadi, Y., D'Souza, J., Reiterer, R. and Sauer, G. Increased Electric Arc Furnace Availability at Qatar Steel Company Through the Fully Automatic Terminator Gunning Robot. *RHI Bulletin*. 2008, No. 1, pp. 18–21.
- [22] Rom, A. Terminator– the EAF Maintenance Solution, *AISTech 2019*, Pittsburgh, USA, May 2019, Presentation.
- [23] Badr, K. and Hanna, A. Review of EAF Technologies and Refractory Digitalization. *AIST MENA Steel Forum 2020*, November 10th–12th 2020, Virtual Event, Proceedings.

Authors

Andreas Viertauer, RHI Magnesita, Vienna, Austria.

Sumit Sundaram, RHI Magnesita, Sohar, Oman.

Ranjeet Kumar Mishra, RHI Magnesita, Sohar, Oman.

Andreas Haider, RHI Magnesita, Leoben, Austria.

Johannes Wucher, RHI Magnesita, Vienna, Austria.

Alexander Ratz, RHI Magnesita, Vienna, Austria.

Heiko Dettela, RHI Magnesita, Vienna, Austria.

Oswin Dolzer, Veitsch-Radex GmbH & Co OG, Radenthein, Austria.

Mario Hesselberger, RHI Magnesita, Vienna, Austria.

Yong Tang, RHI Magnesita, Leoben, Austria.

Karim Badr, RHI Magnesita, Alexandria, Egypt.

Prakash Chaudhary, JSIS, Sohar, Oman.

Viral Thakkar, JSIS, Sohar, Oman.

Sanjay Anand, JSIS, Sohar, Oman.

Corresponding author: Andreas Viertauer, andreas.viertauer@rhimagresita.com





Valued people building an open, collaborative culture

Do you have what it takes to join a global leader, and the driving force of the refractory industry?

Professionals: Work with us and be your best, alongside the best. At RHI Magnesita, employees are empowered to take responsibility and forge their own career success.

Graduates and Young Professionals: A red-hot start to your career. We are looking for recent graduates and young professionals of technical and business studies.

Internships: If you are a motivated student who wants to gain valuable working experience in an international and innovative working environment, we have internship programs available all over the world.

Theses: Do you have research and development spirit and consider writing your thesis in cooperation with a global leader? We offer support and progress on an individual basis.

Apprentices: Join the driving force of the refractory industry and develop with us. Start your career at RHI Magnesita and become a skilled worker in great demand. We educate in technical and commercial professions.

The size of the company offers all employees numerous opportunities to prove their talents. These talents will be identified and specially promoted with the objective to grow both professionally and personally.

Within RHI Magnesita you can find:

- Multicultural, passionate, and open working environment
- Attractive international career opportunities
- Learning and development at all career levels
- Autonomy in the development of tasks and projects



Test your skills in the world leading refractory company. Discover our current jobs available all over the world: rhimagnesita.com/career



RHI MAGNESITA

Clemens Ebner, Mira-Annika Müller, Thomas Müller, Wilfried Eckstein, Manfred Kappel and Jean-Francois Stenger

Development of a New Raw Material Source for RHI Magnesita's Doloma Products in Europe

RHI Magnesita has been mining valuable raw materials from the mine in Hochfilzen (Austria) for many years. Utilisation of the adjacent highly pure dolomite deposit however was, until recently, not economically feasible. As a result of a thorough reevaluation and extensive raw material research and development it became feasible to cost-efficiently develop this previously unused mining area to produce high-quality sintered doloma. This article provides insight into these developments and describes the rationale behind the significant investment in a new state-of-the-art raw material centre in Austria.

Introduction

RHI Magnesita has been producing doloma-based refractory products in Europe for many decades. The clear focus has been on delivering high-quality products to customers in the steel industry. For these products, the availability of the main raw material, sintered doloma or doloma sinter, is crucial. However, the current main raw material source located in Namur (Belgium) will cease operations in 2021 for ecological and economic reasons and a new high-quality, cost-efficient and eco-friendly raw material source was required. Over the past two years, potential resources around the globe were analysed, tested, evaluated, and eventually the existing mining area in Hochfilzen (Austria) was selected. This article summarises the journey of raw material and product development from this raw material source and highlights considerations for product and raw material quality, sustainability, and ecological responsibility.

The New Hochfilzen Raw Material Centre

RHI Magnesita currently mines raw materials in Hochfilzen, at the nearby Schipfl mountain. Although the focus has not been on dolomite, the tradition-rich site will now become a centre for innovation. The experienced employees at the site performed exploratory drilling and rock analyses together with the research and development team. The high quality of the dolomite found in Hochfilzen was confirmed and was the determining factor in the decision to increase the mining of this raw material in Hochfilzen starting in 2021. The majority of the investment will be allocated to the construction of a state-of-the-art rotary kiln on the plant grounds, which will be used to fire the extracted and crushed dolomite at up to 2000 °C. Starting in 2021, 100000 tonnes of sintered doloma will be produced in Hochfilzen each year.

In order to reduce the impact of the refractory materials transportation on the region and the environment in the future, RHI Magnesita is investing in the conversion from trucks to railway. The majority of sintered doloma from Hochfilzen will be transported by rail to France, where it will be processed further to yield refractory bricks at the plants in Flaumont and Valenciennes. A smaller portion will remain in Hochfilzen and will be converted into high-quality refractory mixes directly on site.

The transportation of the raw material from the mining site at Schipfl mountain to the plant in Hochfilzen will also contribute to decreased freight traffic. In the future, the raw material will be transported underground through an adit extending approximately 1000 m. This will lead to a significant reduction in the level of noise and traffic for the residents of Hochfilzen and the surrounding communities. With these two transportation measures, RHI Magnesita will reduce truck traffic from 12000 trips per year to a maximum of 9500 starting in 2020. Following the completion of the overall project at the end of 2023, the number of trucks per year is expected to drop to 5000.

Raw Material Development: From Laboratory Scale to Industrial Production

As the raw dolomite from Hochfilzen is very pure, with an overall share of impurities below 0.3%, the required specifications for the sinter could not be achieved with a one-step firing process. Laboratory trials conducted in the 1980s achieved the necessary high density only with a cost-intensive two-step firing process. A multinational team of R&D and plant experts began to investigate a cost-efficient method to produce sintered doloma using this resource with the specific target of achieving a one-step firing process, by applying the existing expertise with rotary kilns within the group. Rotary kilns have the significant advantage that almost all grain fractions of the raw material with proper chemical specification can be used and no additional sorting steps need to be employed.

As the first step, a programme for laboratory trials was established with the target to develop sintered doloma which was comparable with available refractory grades on the market with grain densities of 3.15–3.25 g/cm³ and an impurity content between 1.7%–2.2%. During this phase, close cooperation and knowledge exchange occurred between the research centres of Leoben (Austria) and York, (USA) and they provided essential input for the trials.

With this starting point, it was decided to run several trials in the laboratory rotary kiln in York, where different mixes of raw material and sintering additives were tested [1,2]. The results of these tests highlighted the possibility to produce sintered doloma based on a very pure raw material in a one-step firing process using additives in which the grain bulk density and chemical composition of the product were equivalent to standard sintered doloma.

In the next step, the laboratory results were verified by industrial trials in the existing rotary kilns in Hochfilzen and Eskisehir (Turkey). The raw material was beneficiated to a grain size which roughly corresponded to the dimensional needs of the final sinter between 1–10 mm. Thereby, minimising the need to further crush the sinter and leading to lower energy requirements for crushing and maximum hydration resistance [3]. The chemical investigation showed that the total content of impurities could be maintained at a lower level than comparable sintered dolomas while at the same time, high grain bulk density was maintained (Table I).

The SiO₂ content of 0.2% was significantly lower than for comparable grades. In combination with an Al₂O₃ level of 0.4%, the amount of low temperature melting phases in the sintered doloma structure was also very low. Iron oxide, which was adjusted to 0.8–1.0% during the firing process, was predominately found in the periclase crystals, with only small amounts situated in CaO and interstitial phases [1].

This unique structure was a result of well-thought-out kiln settings and intelligent use of additives and further reduces the amount of low temperature melting phases in the entire grain structure (Figure 1b, light grey framing of dark grey periclase crystals) [2].

Mineralogical investigations have shown the advantageous structure of the new sintered doloma to hinder corrosion and hydration. The sinter grains feature a dense outer zone with low porosity which protects the entire grain from surrounding humidity (Figure 2a). This contrasts with the currently used shaft kiln sintered doloma, which shows more pores that are evenly dispersed throughout the whole grain structure (Figure 2b).

The investigation of the different grain size fractions shows that a very homogenous chemical composition can be observed. Iron oxide also displays an even distribution over the grain sizes, which can also be seen in the uniformly dark colour of all grains (Figure 3a). Again, this can be regarded as an advantage over the current standard sintered doloma from a shaft kiln process (Figure 3b).

One of the main issues of sintered doloma is hydration. Therefore, the new sinter was tested in an autoclave under severe conditions (120 °C/100% relative humidity/1.6 bar/ 1 hour) and compared to the behaviour of a standard sintered doloma from a shaft kiln process (Table II).

Table I.

Typical values of the chemical analysis and grain bulk density of different sintered doloma raw materials.

| | Hochfilzen | Europe | US | China |
|---------------------------------------|------------|--------|------|-------|
| Al ₂ O ₃ [wt.%] | 0.4 | 0.4 | 0.4 | 0.4 |
| SiO ₂ [wt.%] | 0.2 | 0.8 | 0.8 | 1.0 |
| Fe ₂ O ₃ [wt.%] | 0.9 | 0.7 | 0.9 | 0.6 |
| Sum of impurities [wt.%] | 1.5 | 1.9 | 2.1 | 2.0 |
| Bulk density [g/cm ³] | 3.20 | 3.18 | 3.25 | 3.25 |

Figure 1.

(a) homogenous microstructure of Hochfilzen sintered doloma and (b) minimal amounts and even distribution of the interstitial phases.

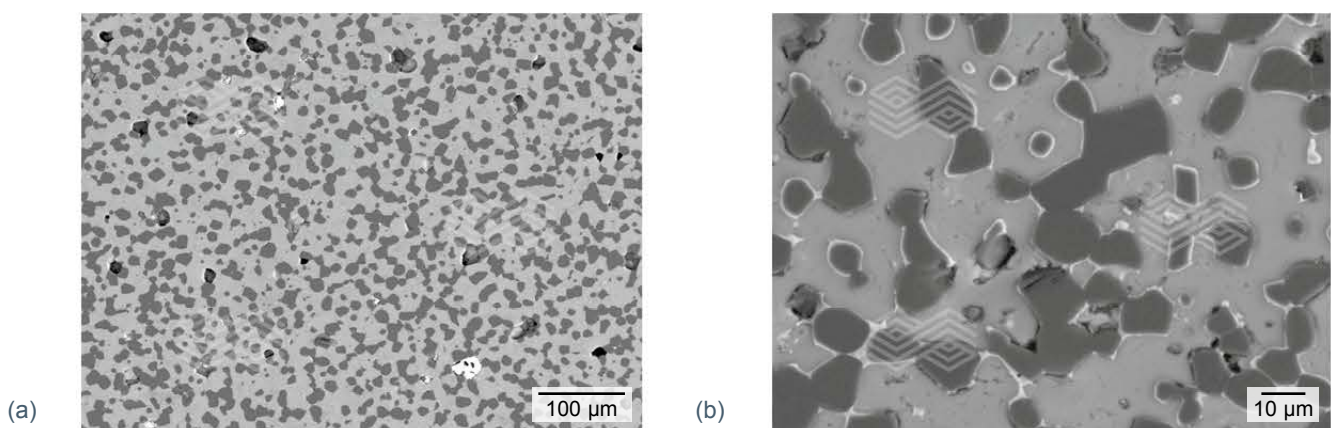


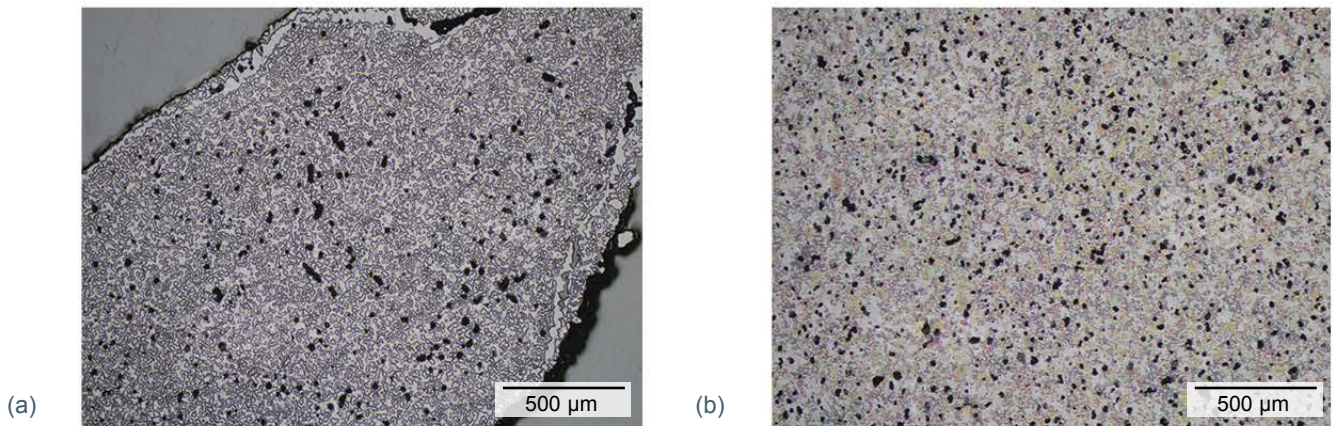
Table II.

Results of the hydration tests.

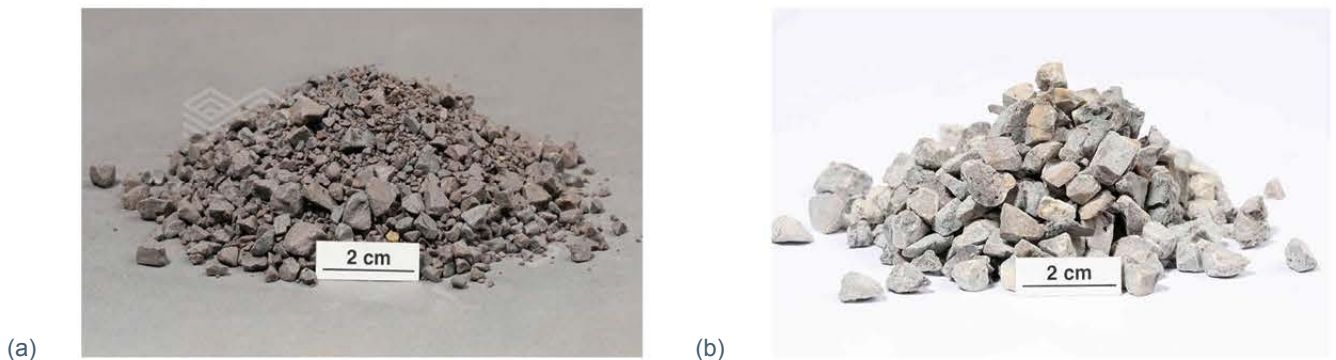
| | European sintered doloma | | Hochfilzen sintered doloma | |
|------------------------------|------------------------------|--|--------------------------------|------------------------------|
| | crushed and sieved 1–5 mm | | uncrushed and sieved 1–5 mm | crushed and sieved 1–5 mm |
| Weight gain [%] | 2.5 | | 0.9 | 1.2 |
| Hydration susceptibility [%] | 16.7 | | 2.1 | 5.1 |

Figure 2.

Photomicrographs of (a) sintered doloma grains from Hochfilzen and (b) for direct comparison the currently used shaft kiln sinter material.

**Figure 3.**

(a) sintered doloma grains from Hochfilzen and (b) the currently used shaft kiln sinter material.



The results show that the new sintered doloma produced in a rotary kiln has a considerably improved resistance to hydration mainly due to the low porosity protective layer but also due to the higher density when compared to the standard doloma sinter [3]. Homogeneous chemical composition and stable properties in a one-step firing process can only be achieved in a rotary kiln and with a feed grain size which closely matches that of the final product requirement. This technique also minimises the overall specific energy consumption for the production process.

Raw Material Testing in Brick Production

Preceded by extensive raw material development and thorough characterisation of the resulting doloma sinter, the materials were transferred to the plants in France, where all grain fractions were prepared completely separate from the standard production. In order to cover the full product range, fired and tempered doloma and magdol bricks were produced in trials at an industrial scale. For mixing, pressing, and firing/tempering, standard procedures were used. Based on experiences with iron-rich sintered doloma from the US obtained in previous trials, extra precautions were taken during firing in order to avoid blockage of the tunnel kiln by deformed bricks. Figure 4a shows severely deformed bricks from the previous trials and the pyramid-like setting pattern for fired doloma bricks used for the initial trials in order to minimise the risk of tipping over and kiln blockage is depicted in Figure 4b.

Despite the raw material's higher iron oxide content when compared to the current European doloma source, no abnormal deformation or firing shrinkage were observed. Physical properties of the produced fired doloma and magdol bricks and tempered doloma bricks were similar to the current standard and, in terms of density and porosity, even superior when compared to the products manufactured

with the current standard material from the shaft kiln process. A special focus was put on hot mechanical property testing, as this enables an estimation of the products' behaviour during application at high temperatures. All physical and chemical properties are summarised in Table III for fired doloma and magdol bricks and in Table IV for tempered doloma bricks.

Table III.

Typical chemical and physical properties of fired doloma and magdol bricks produced with the current standard material and the newly developed sintered doloma from Hochfilzen.

| General information | | | | |
|--|--------------------------|------------------|--------------------------|------------------|
| Product type (brick) | Fired doloma | Fired doloma | Fired magdol | Fired magdol |
| Raw material type | Hochfilzen doloma sinter | Current standard | Hochfilzen doloma sinter | Current standard |
| Chemical analyses | [Wt.%] | [Wt.%] | [Wt.%] | [Wt.%] |
| MgO | 40.1 | 40.2 | 56.5 | 57.7 |
| Al ₂ O ₃ | 0.4 | 0.6 | 0.3 | 0.4 |
| SiO ₂ | 0.2 | 0.9 | 0.3 | 0.8 |
| CaO | 58.3 | 57.7 | 42.0 | 40.4 |
| MnO | 0.1 | 0.1 | 0.1 | 0.1 |
| Fe ₂ O ₃ | 0.9 | 0.5 | 0.8 | 0.6 |
| Physical test results | | | | |
| Bulk density [g/cm ³] | 3.01 | 3.00 | 3.02 | 3.00 |
| Apparent porosity [Vol%] | 11.5 | 12.0 | 11.7 | 12.2 |
| Cold crushing strength [MPa] | 80 | 70 | 70 | 60 |
| Hot modulus of rupture @ 1400 °C [MPa] | 2.3 | 2.3 | 1.9 | 1.7 |
| Hot modulus of rupture @ 1500 °C [MPa] | 1.6 | 1.8 | 1.6 | 1.7 |
| Cold modulus of rupture @ RT [MPa] | 19.3 | 14.5 | 17.0 | 9.5 |
| Creep in compression @1500 °C | | | | |
| T0 [°C] | 1360 | 1330 | 1460 | 1470 |
| Creep after 5 hours [Lin%] | -2.9 | -3.1 | -1.8 | -2.0 |
| Creep after 10 hours [Lin%] | -4.7 | -5.0 | -2.9 | -3.2 |

Figure 4.

(a) deformed brick columns after firing due to another iron-rich raw material in a prior trial and (b) precautionary pyramid-like setting of bricks for the first firing trials with newly developed sinter doloma from Hochfilzen.



Table IV.

Typical chemical and physical properties of tempered doloma bricks produced with the current standard material and the newly developed sintered doloma from Hochfilzen.

| General information | | |
|--|------------------------------|------------------------------|
| Product type (brick) | Tempered resin-bonded doloma | Tempered resin-bonded doloma |
| Raw material type | Hochfilzen doloma sinter | Current standard |
| Chemical analyses | [Wt.%] | [Wt.%] |
| MgO | 42.0 | 41.8 |
| Al ₂ O ₃ | 0.4 | 0.5 |
| SiO ₂ | 0.3 | 0.7 |
| CaO | 56.4 | 56.4 |
| MnO | 0.1 | 0.1 |
| Fe ₂ O ₃ | 0.8 | 0.4 |
| Total carbon content | 4.8 | 5.5 |
| Residual carbon content | 3.1 | 3.2 |
| Physical test results | | |
| Bulk density [g/cm ³] | 2.95 | 2.86 |
| Apparent porosity [Vol%] | 3.9 | 5.6 |
| Cold crushing strength [MPa] | 100 | 87 |
| Bulk density after coking @ 1000 °C [g/cm ³] | 2.87 | 2.79 |
| Apparent porosity after coking @ 1000 °C [Vol%] | 12.8 | 14.8 |
| Cold crushing strength after coking @ 1000 °C [MPa] | 40 | 38 |
| Hot modulus of rupture @ 1400 °C [MPa] | 2.8 | 3.9 |
| Hot modulus of rupture @ 1500 °C [MPa] | 3.1 | 2.7 |
| Cold modulus of rupture @ RT [MPa] | 21.0 | 17.4 |
| Cold modulus of rupture after coking @ 1000 °C [MPa] | 3.9 | 2.0 |

Figure 5.

Different colouring of bricks (light vs. dark brown/black) due to the slightly elevated content of manganese and iron oxide.



The SiO₂ content of the resulting bricks was in the range of 0.2 wt.%, which is considered to be an advantage for slag resistance in application in argon oxygen degassing converters and ladle slag zones. As stated previously, one main difference of the new raw material can be seen in the colour of fired bricks which, due to the slightly elevated content of manganese oxide and the higher iron oxide content, has changed from light brown to dark brown (Figure 5). As the manganese contents in the final products are still very low, the colour difference was only an optical effect and is not relevant to quality or performance.

Comparative mineralogical investigations of fired doloma bricks were conducted to investigate the sintering behaviour and the general structure (Figure 6).

Both photomicrographs reveal strong ceramisation of the doloma grains and low structure porosity. The structure of the brick produced with the newly developed raw material shows significantly less grain porosity, which aligns with raw material analyses and physical brick properties. In terms of slag and hydration resistance this can be regarded as a significant benefit for storage, handling, and performance.

A section of fired and tempered bricks from the industrial trials was provided to customers for testing and has shown at the minimum similar performance as the current products with shaft kiln sintered doloma. RHI Magnesita's product portfolio in Europe not only contains shaped products such as doloma and magdol bricks but is supplemented by a wide range of doloma-based mixes such as standard mixes, special plastic ramming mixes, backfill mixes, and repair mixes as well as EAF hearth mixes. These are mainly used in stainless steel application and initial tests of the newly developed Hochfilzen sintered doloma have shown very promising results, mainly due to the advantages over the current standard sintered doloma. These include:

- High stability of the mixes during production and storage as well as after relining and during operation.
- Reduced requirement for liquid additives for dust suppression and plasticisation.
- Excellent compactibility due to the rounded grain shape.
- Production of mixes in a new state-of-the-art production line situated directly in the sinter plant leading to reduced transportation needs.

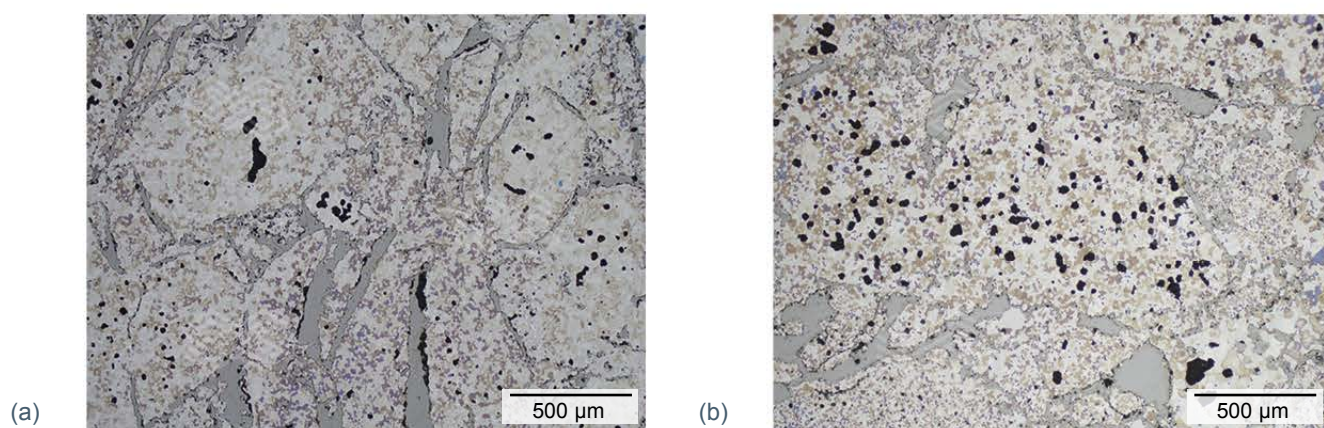
Further tests and field trials are ongoing and the full switch to the new raw material is planned to take place at the end of 2021.

Conclusion

In order to secure a future supply of dead burnt doloma, the raw dolomite from RHI Magnesita's Schipfl mine in Austria was reevaluated by a multinational team of experts from plants and research centres in Austria, the US, and France. The main target was to produce high-purity, high-density dead burnt doloma in a single-step rotary kiln process. In extensive laboratory and industrial trials, the kiln parameters and sintering additives were optimised and the suitability for brick and mix production was confirmed and yielded products which at a minimum display similar physical properties and superior chemical composition when compared to the current standard raw material from shaft kiln processes. This will ensure that RHI Magnesita will be able to supply customers in Europe with high-quality and well-performing doloma products for many more years to come.

Figure 6.

Photomicrographs of (a) fired doloma bricks produced with the newly developed sintered doloma from Hochfilzen and (b) the current standard material.



References

- [1] Duvigneaud, P.-H., Derie, R. and Naessens, G. Influence de l'oxyde de fer sur la croissance des oxydes de calcium et de magnésium dans la dolomite calcinée. *Rev. Int. Hautes Temper. et Refract.* 1972, 9, 313–324.
- [2] Koval, E.J., Messing, G.L. and Bradt, R.C. Effects of Raw Material Properties and Fe_2O_3 Additions on the Sintering of Dolomites. *Ceramics and Composites.* 1984, 63, 2, 274–277.
- [3] Ghosh, A. and Tripathi, H.S. Sintering Behaviour and Hydration Resistance of Reactive Dolomite. *Ceramics International.* 2011, 38, 1315–1318.

Authors

Clemens Ebner, RHI Magnesita, Leoben, Austria.
 Mira-Annika Müller, RHI Magnesita, Leoben, Austria.
 Thomas Müller, RHI Magnesita, Hochfilzen, Austria.
 Manfred Kappel, RHI Magnesita, Leoben, Austria.
 Wilfried Eckstein, RHI Magnesita, Leoben, Austria.
 Jean-Francois Stenger, RHI Magnesita, plant Valenciennes, France.
Corresponding author: Clemens Ebner, clemens.ebner@rhimagnesita.com



bulletin

2021

Copyright notice:

The texts, photographs and graphic design contained in this publication are protected by copyright. Unless indicated otherwise, the related rights of use, especially the rights of reproduction, dissemination, provision and editing, are held exclusively by RHI Magnesita N.V. Usage of this publication shall only be permitted for personal information purposes. Any type of use going beyond that, especially reproduction, editing, other usage or commercial use is subject to explicit prior written approval by RHI Magnesita N.V.

